Examination of Healthy Neuromusculoskeletal Control of the Pectoralis Major Muscle

by

Tea Lulic

A thesis

presented to the University of Waterloo

in fulfillment of the

thesis requirements for the degree of

Doctor of Philosophy

in Kinesiology

Waterloo, Ontario, Canada, 2020

Examining Committee Membership

The following served on the Examining Committee for this thesis. The decision of the Examining Committee is by majority vote.

External Examiner	Dr. Linda McLean Professor, Department of Rehabilitation Sciences University of Ottawa
Supervisor	Dr. Clark Dickerson Professor, Department of Kinesiology University of Waterloo
Internal Members	Dr. Marina Mourtzakis Associate Professor, Department of Kinesiology University of Waterloo
	Dr. Richard Staines Professor, Department of Kinesiology University of Waterloo
Internal-external Member	Dr. Ning Jiang Associate Professor, Department of Systems Design Engineering University of Waterloo

Author's Declaration

I hereby declare that I am the sole author of this thesis. This is a true copy of the thesis, including any required final revisions, as accepted by my examiners.

I understand that my thesis will be made electronically available to the public.

Abstract

The pectoralis major, a large, multipennate muscle, assists in shoulder complex mobility and stability. Although its highly intricate architectural properties allow it to contribute to many upper extremity tasks, its exact role in typical shoulder function is ambiguous. Due to this, the pectoralis major is typically classified as an 'exercise' muscle; its functional relevance to daily and occupational tasks dismissed, and its purpose in arm movements diminished. However, mounting evidence associates direct or indirect injury to this muscle to debilitating long-term arm disability. A more deliberate investigation of its role in typical shoulder function is paramount for developing targeted treatments, exercises, and rehabilitation protocols. Therefore, this dissertation aimed to establish critical foundational knowledge on regional pectoralis major neuromusculoskeletal control in males and females.

Study 1 demonstrates that current electromyographic (EMG) methods misrepresent pectoralis major activation in several tasks and effort levels in healthy males. It proposes a holistic framework, combining high-density surface electromyography (HD-sEMG) and neural decoding. This framework allows for an investigation of the spatial distribution of whole pectoralis major activation, with in-depth insights into its neural and neuromuscular control. In study 2, methodological challenges in EMG acquisition from pectoralis major in females are addressed, demonstrating that HD-sEMG signals in the array overlaying the breast have low amplitudes and high mean power frequency. However, the acquisition of HD-sEMG signals from the top regions of the pectoralis major in females is achievable. Studies 3 and 4 evaluated the activity of the pectoralis major in healthy females. These studies showed predominantly middle sternocostal region involvement in adduction, internal rotation, and extension, while clavicular regions specifically contributed to flexion and horizontal adduction. Further, characterization of pectoralis

major activation in males (Study 5 and 6) revealed lower sternocostal region involvement in tasks requiring adduction, internal rotation, and extension. All three regions assisted in flexion and horizontal adduction. Lastly, study 7 revealed high discharge rates of motor units at low effort levels and reliance on motor unit recruitment to increase force.

Findings from this dissertation have broad implications in fundamental and clinical sciences. First, the scope of this work represents the first transformative step in understanding the role of pectoralis major in typical shoulder function. Second, it addresses several methodological limitations and challenges that currently limit the ability to investigate its intricate control. Lastly, current findings inform surgical procedures involving pectoralis major resection or disinsertion, rehabilitation or exercise protocols aimed at regional pectoralis major recovery, and fundamental studies, aimed at understanding the complexities of shoulder function. This dissertation's outcomes collectively highlight the utility of examining the neuromusculoskeletal control of the pectoralis major and its significance in numerous tasks.

Acknowledgments

This PhD was one of the most thrilling, maddening, and exciting chapters of my life. I vividly remember my initial conversation with Dr. Dickerson regarding the pectoralis major; the conviction I had that this was the knowledge gap I wanted to address; never once stopping to evaluate what exactly I was getting myself into. Now, looking back, I have no regrets, only sadness for the experiments I could not complete due to the pandemic.

I want to thank my mentor, Dr. Clark Dickerson, for taking me under his wing, guiding and supporting me throughout this PhD journey, and not setting limits to the pursuit of knowledge. There was never a doubt in my mind that you were cheering for my success, and I am forever grateful for your friendship and mentorship. I am sorry the pandemic cut this one short and we were not able to complete all the projects we planned to do, but I am confident we will complete these in the future.

I am heavily indebted to our collaborator, Dr. Francesco Negro. Thank you for teaching and helping me throughout this thesis, for all the opportunities you had provided, for your hospitality when I visited Brescia, and for your mentorship and friendship throughout this journey. The guidance, advice, and feedback you have provided me with over these past few years have contributed to tremendous personal and professional growth.

Many thanks to my committee members, Dr. Ning Jiang, Dr. Richard Staines, Dr. Marina Mourtzakis, and Dr. Linda McLean, for their guidance and feedback. I am incredibly grateful to have had such an interdisciplinary committee, with views from different perspectives, which made these projects and the final document stronger.

This journey would not be possible without the support from my colleagues and friends in DIESEL and beyond. Thank you for the supportive chats, comic relief, project help, numerous hours of piloting and collecting with me, and, most importantly, friendship. Many thanks to Craig McDonald for troubleshooting whenever LabView/Vicon software or computer failed. I doubt I would have managed to collect as many participants without your immediate help on these issues. Thank you to Anton Trinh for teaching me LabView and providing me with the skills needed to understand how to program in this “not a matlab” software. Lastly, a special thank you to Dr. Talia Alenabi – for your friendship, support, and willingness to collaborate on some very fascinating projects; and Rachel Whittaker, for the coffees, chats, laughs, and science brainstorming sessions.

I am incredibly lucky to have a close group of friends, that even when I sounded a bit exorbitant in my ideas about the present or future, fully supported me without uttering a word of disapproval. Christy Jones, Demi Gregory, Sam Ehmke, and Valerie Norman-Gerum – this one is for you and for all the females who are still overlooked in research because “subcutaneous tissue” is in the way. Thank you for being my rocks and for giving me a nudge every time I needed it.

I would not be where I am without the unwavering encouragement and support of my mom. Mom, thank you for the unconditional love and understanding throughout this challenging process and for indulging in the world of science, which is not always easy to understand.

Lastly, to my husband, Kacper Kuryllo: I do not have the words to express my gratitude for all you have done for me. Thank you for being my rock, my guiding light, for all the comic relief, science brainstorming sessions, coding lessons, nudges in the right direction, and unconditional love. Also, thank you for reminding me every day that dreams can come true.

As this chapter of my life closes, I am grateful for all the opportunities the University of Waterloo has provided me with and thankful that every day I got to work alongside some of the best minds in academia. More importantly, without DIESEL, these projects would not be possible. I am forever indebted to this amazing team for showing me that those great mountains are worth conquering and that no stone should be left unturned. As I move onto my next steps at the University of Michigan, I hope to make you proud.

Table of Contents

List of Figures

List of Tables

Chapter 1: Introduction

1.1 Motivation

Arm mobility relies on the coordinated activation of multiple muscles within the shoulder complex, with the pectoralis major often contributing. The pectoralis major is a singularly large, multi-functional muscle located on the anterior aspect of the chest. The multiple attachments have a high contribution to arm mobility, specifically in the tasks involving vertical and horizontal adduction, internal rotation, flexion, and extension against resistance. Although the pectoralis major is an acknowledged contributor to arm mobility and stability, it is sometimes characterized as solely crucial in exercise tasks, with scientific and clinical claims going as far as labeling it as not necessary for typical shoulder function (Hoffman and Elliott, 1987; Paterson et al., 2004; David et al., 2012; Mooers et al., 2015; Sanchez et al., 2017). However, these views largely stem from a minimal understanding of the pectoralis major's role in typical shoulder function.

Complications arise in the precise interpretation of the electromyographic (EMG) signals in numerous studies examining the pectoralis major activation using classic EMG. Typically, EMG signals are acquired from the superior regions (i.e., clavicular and superior sternocostal; for examples, see Cram and Kasman, 1998 or Hermens and Freriks, 1997), although electrode location and orientation on the sternocostal region can vary between studies. Inferences regarding its activation and (dys)function are commonly drawn based on these recordings. However, the middle/lower sternocostal and abdominal regions are architecturally divergent (Fung et al., 2009), have independent innervation (Haladaj et al. 2019), attach to a separate tendon (Fung et al. 2009), and assist in arm mobility alongside the superior regions (Paton and Brown, 1994; Brown et al. 2007; Wickham et al. 2004; 2012). These anatomical complexities suggest a problematic mischaracterization of the pectoralis major activation in fundamental and exercise studies.

The lack of recognition of the pectoralis major's importance in typical shoulder function led to the development of surgical procedures that compromise shoulder function and health. These procedures include: (1) breast reconstruction surgeries, which disinsert middle-to-inferior regions of the pectoralis major from its origin to accommodate and support the breast implant, and restore the natural look of the breast (Cemal et al. 2013; Nelson et al. 2018); (2) head and neck reconstruction surgeries following cancer, which disinsert or resect various regions of the pectoralis major (Liu et al. 2001); and (3) surgeries involving the restoration of scapular movement, which use the whole sternocostal region as a transplant to correct for scapular winging (Iceton and Harris, 1987; Post, 1995). In these procedures, it is commonly assumed that other intact shoulder muscles will adapt and compensate for the losses resulting from the pectoralis major disinsertion or resection (Brumback et al. 1992; Clough et al. 2002). However, mounting evidence suggests that resection or disinsertion of the pectoralis major leads to reductions in shoulder strength (~20-26%), range of motion, increased shoulder instability, decreased shoulder stiffness, and consequently, substantial arm disability (de Haan et al. 2007; Moukarbel et al. 2010; Hage et al. 2014; Leonardis et al. 2018; 2019). Ultimately, these deficits negatively affect the ability to return to work, perform functional tasks, and contribute to the development of secondary shoulder pathologies (Ebaugh et al. 2011; Jagsi et al. 2017).

Therefore, this dissertation's primary purpose was to investigate and characterize fundamental pectoralis major activation and neural control using high-density surface electromyography (HD-sEMG) to establish critical foundational knowledge on regional pectoralis major function in healthy cohorts. This dissertation begins with a literature review exploring the following themes: 1) the pectoralis major anatomy, from architecture to function; 2) the pectoralis major activation, including a brief overview on the influence of subcutaneous tissue on EMG

amplitude and frequency spectrum; 3) motor unit overview, including methods to evaluate motor unit recruitment and discharge rate; 4) overview of current methodological limitations evaluating the pectoralis major activation with a summary of the advantages of using HD-sEMG; and 5) an overview of shoulder restrictions following the pectoralis major injury.

Chapter 2: Literature Review

2.1 Pectoralis Major Anatomy

The pectoralis major is a multipennate muscle located on the anterior, superficial aspect of the chest and consists of three regions: the clavicular, sternocostal, and abdominal (Figure 1). It originates from the mid clavicle, sternum, ribs, and the external oblique fascia and converges into a bilaminar tendon, which inserts into the intertubercular groove of the humerus (Wolfe et al., 1992; Fung et al., 2009). The clavicular region spans multiple shoulder joints, including the sternoclavicular and glenohumeral, while the sternocostal and abdominal regions cross the glenohumeral and intercostal joints. The architecture of each fiber region varies, suggesting a versatile and differential function.

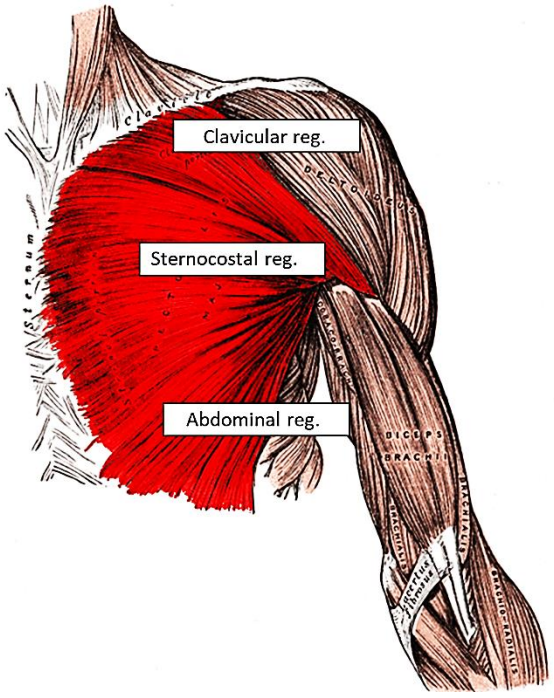

Figure 1: Representation of the typical divisions of the pectoralis major muscle: the clavicular, sternocostal, and abdominal region. Adapted and modified from Gray, 1990.

2.1.1. General description of architectural properties

Mechanically, skeletal muscle generates power, force and produces movement, allowing for the maintenance of functional independence. Architectural properties of the skeletal muscle have considerable effects on force development and production (Narici, 1999), as muscle fibers are arranged relative to the axis of force generation (Huijing, 1992; Lieber, 1992; Roy and Edgerton, 1992). Skeletal muscles are commonly defined based on the physiological (PCSA) or anatomical cross-sectional area (ACSA), muscle fiber pennation angle (PA), and fiber or muscle fascicle length.

The physiological or anatomical cross-sectional area is related to the muscle's functional capability. Both are measured in a plane perpendicular to the muscle fibers or horizontally across the widest part of the muscle belly. Mathematically, PCSA is quantified as the ratio of the muscle volume to fascicle length, multiplied by the cosine of the pennation angle (Wickiewicz et al., 1983; Powell et al., 1984). Several studies demonstrated that ACSA is positively correlated with muscle strength and power (Lieber and Friden, 2000; Masuda et al., 2003; Ikegawa et al., 2008). Further, ACSA is closely related to muscle thickness and muscle volume in the lower (Abe et al., 1997; Miyatani et al., 2002; Ogawa et al., 2012; Franchi et al., 2018) and the upper extremity muscles (Miyatani et al., 2004; Akagi et al., 2010; Yasuda et al., 2010; Takai et al., 2011; Yi et al., 2012). In particular, muscle thickness has a linear relationship with muscle ACSA or muscle volume in the biceps brachii (Miyatani et al., 2004; Akagi et al., 2010), triceps brachii (Miyatami et al., 2004), pectoralis major (Yasuda et al., 2010), supraspinatus (Yi et al., 2012), psoas major (Takai et al., 2011) and vastus lateralis (Franchi et al., 2018).

Pennation angle is closely related to the muscle's cross-sectional area and force output. Morphologically, muscle is divided into parallel and pennate muscles. Muscle fibers either lay

parallel to the muscle's line of action or converge into a tendon at an angle (Gans and de Vree, 1987). Pennation angle is the muscle fibers' angle relative to their attachment to the deep aponeurosis (Fukunaga et al., 1997). Attachment of the muscle fibers at an angle allows for a greater number of muscle fibers to be packed and exert a force on the aponeurosis (Zajac, 1989; Infantolino and Chalis, 2014). Specifically, the larger the pennation angle and muscle volume, the greater the physiological cross-sectional area, and therefore, force-producing capacity.

Fiber length refers to the length of individual muscle fibers and is a determinant of the force-length relationship. Since the individual muscle fibers are challenging to differentiate and experimentally identify, the whole fascicles' length is often quantified. This measurement involves identifying the origin and insertion of the muscle fascicles on the superficial and deep aponeuroses (Franchi et al., 2018). In general, longer fibers have a higher capacity for contractile speed (Abe et al., 2000; Wickiewicz et al., 1984).

2.1.2. Pectoralis major architecture

Architectural properties of the pectoralis major were investigated in cadavers and living humans, albeit in a limited capacity. Studies in cadavers delineated the sternocostal region into multiple partitions, ranging from one to seven (Table 1). In contrast, the clavicular region predominantly consisted of one region, although one study found two partitions within this region (Wickham et al. 2004). In general, the sternocostal region has a larger physiological cross-sectional area, pennation angle, muscle fascicle and tendon length, and volume than the clavicular region (Langenderfer et al. 2004; Fung et al. 2009). Additional studies quantified the pectoralis major muscle thickness in healthy young males pre-training (Yasuda et al., 2010; Mangine et al., 2015, 2018). In one study, the cross-sectional area and muscle thickness were evaluated using resonance magnetic imaging and ultrasound. However, the ultrasound measurements were limited to a single

location - at the mid-clavicle between the third and the fourth costal cartilage [(i.e., mid sternocostal region) Yasuda et al., 2010]. In contrast, Mangine et al. evaluated muscle thickness and cross-sectional area at the second rib (2015, 2018). Differences in protocols and anatomical landmarks resulted in cross-sectional area estimates between 12-87.7 cm^2.

2.1.3. Compartment (partitional) differences in architecture

Muscle compartments or partitions, with apparently differential functions, exist in many animal and human skeletal muscles. Such distinct regions appear in multiple multifunctional shoulder muscles, such as the supraspinatus (Kim et al., 2007), infraspinatus (Fabrizio et al., 2014), subscapularis (Warden et al., 2014), and upper trapezius (Jensen and Westgaard 1995; 1997). This compartmentalization suggests potential distinct mechanical requirements of each muscle partition, enabling force production in multiple directions (Carrasco et al., 1999; Staudenmann et al., 2009).

Four anatomical studies of the pectoralis major muscle demonstrated greater architectural complexity than previously thought (Table 1). These studies showed compartmentalization of the sternocostal and abdominal region into four and three individual compartments (Lewis, 1901; Ashley, 1953; Wickham et al. 2004; Fung et al., 2009), which may have mechanical advantages for complex humeral mobility. In general, the muscle fiber bundle pennation angle and fiber bundle length vary between partitions. The abdominal region has the largest lateral pennation angle compared to the sternocostal and clavicular regions. In contrast, partition three within the sternocostal region has the longest fiber bundle length (Fung et al. 2009). Another study assessed the volume, muscle length, and cross-sectional area of each partition in male cadavers (Wickham et al. 2004). In this study, partition one had the largest volume and cross-sectional area, while partition five had the smallest. Muscle length was the longest for partition five and shortest for

partition one. Collectively, architectural differences between and within regions imply potential differential functional contributions.

Table 1: Mean ± standard deviation of architectural parameters from cadaver studies. PCSA: physiological cross-sectional area; S1-6: sternocostal partitions; C1-2: clavicular partitions

Study	Muscle Regions	Pennation Angle (°)	Fiber Length (mm)	PCSA (cm^2)	Volume (cm^3)
Lewis, 1901	Two: clavicular and sternocostal (segmented: s1-s6)	Not reported	Not reported	Not reported	Not reported
Ashley, 1952	Two: clavicular and sternocostal (segmented: s1-s5)	Not reported	Not reported	Not reported	Not reported
Wolfe et al. 1992	Two: clavicular and sternocostal (segmented: s1-s2)	Not reported	*measures derived from figure Clavicular: ~160 S1: ~175 S2: ~180 S3: ~ 184 S4: ~180 S5: ~160 S6: ~140	Not reported	Not reported
Lee et al. 2000	Two: clavicular and sternocostal (segmented: s1-s2)	Not reported	Not reported	Not reported	Not reported
Langenderfer et al. 2004	Two: clavicular and sternocostal (not segmented)	Clavicular: 17 ± 1 Sternocostal: 25 ± 5	Clavicular: 154 ± 25 Sternocostal: 171 ± 7	Clavicular: 3.07 ± 0.70 Sternocostal: 5.68 ± 0.12	Not reported
Wickham et al. 2004	Two: clavicular (segmented: c1 – c2) and sternocostal (segmented: s1-s4)	N/A	C1: 14.9 C2: 17.1 S1: 17.5 S2: 19.4 S3: 19.2 S4: 20.3	*reported CSA C1: 2.4 C2: 3 S1: 1.6 S2: 1.7 S3: 1.8 S4: 1.3	C1: 36.3 C2: 50.8 S1: 27.3 S2: 33.9 S3: 35.5 S4: 26.6
Holzbaur et al. 2007	One	Not reported	20.2 ± 2.2	15.9 ± 8.3	290 ± 169
Fung et al. 2009	Two: clavicular and sternocostal (segmented: s1-s7)	Overall: 22.7 ± 3.5 Clavicular: 29.4 ± 6.9 Sternal overall: 20.6 ± 2.7 S1: 19.2 ± 5.5 S2: 14.4 ± 5.4 S3: 17.3 ± 2.7 S4: 14.3 ± 3.4 S5: 24.2 ± 5.1 S6: 25.9 ± 9.3 S7: 34.9 ± 11.6	Overall: 16.1 ± 1.1 Clavicular: 15 ± 0.8 Sternal overall: 16.4 ± 1.2 S1: 16.7 ± 1.7 S2: 16.5 ± 1.2 S3: 18.2 ± 1.7 S4: 17.4 ± 2.1 S5: 17.3 ± 1.1 S6: 15.4 ± 2.7 S7: 15.4 ± 1.5	Not reported	Not reported

2.1.4. Moment arms

The length of regional moment arms in the pectoralis major depended on the task and arm posture and was quantified across the range of motion in abduction, flexion, and internal rotation. In adduction, the longest moment arms were quantified in the middle and inferior (i.e., sternocostal) regions between 40° - 60° of arm abduction compared to the clavicular region (Ackland et al. 2008). In contrast, the clavicular region had short moment arms between 0 and 50° of arm abduction. It had a progressively longer abductor (negative) moment arm from 60° to 120° of arm abduction (Ackland et al. 2008). These findings indicate that the middle and inferior regions have a greater mechanical advantage to produce adductor torque than the clavicular region throughout the abduction range of motion.

During flexion in the scapular plane, the superior pectoralis major had the longest flexion moment arm of all three regions (~50 mm), specifically between 50° to 90° of arm abduction, while the middle pectoralis major had a slight flexor moment arm, specifically between 20° to 60° of arm abduction (Ackland et al. 2008). In contrast, the inferior region had an extension (negative) moment arm that increased from 50° to 120° of arm abduction (Ackland et al. 2008). Therefore, the clavicular region has the highest mechanical advantage to flex, while the inferior regions are primarily acting as extensors.

Internal rotation moment arms changed length in both abduction and flexion. During the abduction, the inferior and middle sternocostal regions had longer internal rotation moment arms than the clavicular region, particularly from 30° to 90° of arm abduction (Ackland and Pandy, 2011). During flexion, the middle and inferior pectoralis major had the longest internal rotation moment arms throughout the range of motion (Ackland and Pandy, 2011). A single study evaluated compartmental or partitional moment arms in the anatomical position (Wickham et al. 2004). This

study demonstrated that the second clavicular compartment and first and second sternocostal compartments have the longest flexor and adductor moment arms (Wickham et al. 2004).

2.2. Pectoralis major function

Broadly, pectoralis major assists in vertical and horizontal adduction, flexion, internal rotation, and extension against resistance. Vertical adduction is the movement of the arm downwards, towards the torso in the vertical plane. Horizontal adduction is the movement of the arm across the torso in the horizontal plane. The sternocostal and clavicular regions contribute differentially to arm tasks. Specifically, the sternocostal region assists in vertical/horizontal adduction and internal rotation, while the clavicular region assists in horizontal adduction, internal rotation, and flexion (Jansen et al., 2005; Stegink-Jansen et al., 2011; Leonardis et al. 2017). However, each region's mechanical advantage changes throughout the arm range of motion, as described below in the context of moment arms.

Several studies defined and classified pectoralis major regions as prime movers, synergists, or antagonists and examined their activation alongside other muscles (i.e., latissimus dorsi and deltoid) in several tasks that require pectoralis major activity. For the pectoralis major regions, the prime movers and synergists were defined as regions with an agonist moment arm, although synergists had shorter agonist moment arms (Wickham et al. 2012). The prime movers also had early activations, were active for the duration of the task, and had high EMG amplitudes compared to other regions. A synergist activated after the prime mover and had shorter activation (Brown et al. 2007). Lastly, an antagonist had an antagonist moment arm and typically activated significantly after the prime movers/synergists. In adduction, the sternocostal and abdominal regions of the pectoralis major and all regions of the latissimus dorsi activated early to initiate a task and stayed

active for the duration of the task (Wickham et al. 2012). Therefore, the pectoralis major's sternocostal and abdominal regions acted as prime movers alongside the latissimus dorsi regions (Brown et al. 2007; Wickham et al. 2012). In contrast, the clavicular region and the seventh region of the deltoid acted as synergists in adduction (Wickham et al. 2012). Other deltoid regions acted as antagonists due to their late activation and antagonist moment arms (Wickham et al. 2012). In flexion, the clavicular region activated early, acting as a prime mover with the deltoid (Brown et al. 2007). In comparison, some sternocostal regions activated later and acted as a synergist, except for region four of the pectoralis major, which activated significantly later (Brown et al. 2007). This region acted as an antagonist in flexion. Lastly, in extension, the latissimus dorsi, deltoid, and third region of the pectoralis major activated early and acted as prime movers (Brown et al. 2007).

2.3. Pectoralis major innervation

The pectoralis major receives descending neural input from the lateral (C5-C7) and medial (C8-T1) pectoral nerves, which branch off from the medial and superior trunk of the brachial plexus, respectively. Information regarding regional pectoralis major innervation is currently inconclusive. Some studies report that the medial pectoral nerve innervates the abdominal regions (lower 1/3; Manktelow et al. 1980; Wolfe et al. 1992; Wickham et al. 2004; Haladaj et al. 2019) solely. On the other hand, the lateral pectoral nerve divides into two branches. The superior branch innervates the clavicular region, and the inferior branch innervates the superior and middle sternocostal regions (Wickham et al., 2004; Haladaj et al. 2019). In contrast, other anatomical studies demonstrated that the lateral pectoral nerve supplies the clavicular region, while the medial pectoral nerve innervates the sternocostal region (Tobin, 1985; Gardetto et al., 2003; Macchi et al., 2007). Three pectoral nerves were identified in 15 fresh cadavers (David et al., 2012). This study

demonstrated that the superior pectoral nerve innervates the clavicular region, while the middle and inferior pectoral nerves innervate the sternal and abdominal regions, respectively.

2.4. Investigating pectoralis major activity and neural properties

2.4.1. Pectoralis major activation in males and females

Existent fundamental pectoralis major activation data exists from a limited number of studies, which used classic EMG to record its activation. In males, regional pectoralis major activation depends on the task, and, in some instances, the effort level (Paton and Brown, 1994; Wickham et al., 2004; 2012). Specifically, isometric tasks involving vertical adduction and extension activate the inferior pectoralis major regions at low or high efforts compared to the clavicular, superior, and middle regions (Paton and Brown, 1994). Further, the superior pectoralis major regions (mainly sternocostal) activate highly during horizontal adduction. In contrast, the clavicular regions activate highly during forward flexion, irrespective of the effort level (Paton and Brown, 1994). However, in vertical adduction and flexion, all three regions may also activate to the same magnitude (Wickham et al. 2004). Shoulder muscle activity is spatially dependent. For example, both the clavicular and superior sternocostal regions activated highly in tasks requiring horizontal pulls (McDonald et al. 2012). The clavicular regions are also activated highly in downward pulls (Nadon et al. 2016).

In contrast, information on fundamental pectoralis major activation in females is scarce. In a single study that examined sex-related differences in shoulder muscle activation, differences between males and females emerged in horizontal flexion, whereby males had higher EMG amplitudes than females. In comparison, females had significantly higher EMG amplitudes in horizontal extension and internal rotation (Anders et al. 2004). In Anders et al.'s study, the

horizontal extension, defined as the arm's extension in the horizontal plane from 90° of arm elevation and 0° of the plane of elevation and axial rotation, will be referred to as extension for the remainder of this thesis. However, this study acquired EMG signals from a single pectoralis major location (i.e., the superior sternocostal region), and therefore, the extent of activity in other pectoralis major regions is unknown.

2.4.2. Surrounding shoulder muscle activation

Several studies examined the activity of other shoulder muscles alongside the pectoralis major. The activation and the contribution of these muscles depended on their anatomical moment arms, task, and arm posture. Adduction elicited high activations in the latissimus dorsi and deltoid (Brown et al. 2007; Wickham et al. 2012). In internal rotation, the latissimus dorsi and subscapularis activate highly (Brookham and Dickerson, 2016; McDonald et al. 2017). In flexion and horizontal adduction, the anterior deltoid and the latissimus dorsi have high activations (Brown et al. 2007; Rockwood Jr., 2009). Lastly, in extension, the posterior deltoid and the latissimus dorsi activate highly with the pectoralis major (Ekholm et al. 1978; Rockwood Jr., 2009; Brown et al. 2007).

2.4.3. Tissue effects on sEMG amplitude and frequency: Implications for investigating pectoralis major activity in females

Detection of muscle activity depends on multiple factors, such as the distance between the electrodes and the muscle and the biological tissue content between the two. Depolarized muscle fibers generate an electric field that is spatially spread throughout the tissue and at the skin surface. The nature of this spread depends on the composition and conductivity of the tissue between the bioelectric source and the electrodes. A thorough understanding of the volume conduction must

inform the correct interpretation of the EMG signal, particularly in females. The biological tissue is regarded as a passive, three-dimensional volume conductor (Clark and Plonsey, 1966; Rosenfalck, 1969; Plonsey, 1974; Roeleveld et al., 1997a; Farina et al., 2004b), acting as a temporal low-pass filter (Gath and Stalberg, 1976; Lindstrom and Magnusson, 1977; De Luca, 1979). An inverse power relationship exists between the sEMG amplitude and the motor unit action potential (Ekstedt and Stalberg, 1973; Gath and Stalberg, 1979; Roeleveld et al., 1997a). Specifically, the increase in subcutaneous tissue widens the motor unit action potential (Blok et al., 2002a; Farina et al., 2004b) and decreases its amplitude (Farina et al., 2004b). This reduces the spatial selectivity and removes information on the shapes of motor unit action potentials (Farina and Holobar, 2016).

Studies investigating the effect of tissue thickness on signal amplitude and frequency consistently show reductions in sEMG amplitude and mean power frequency. In general, the amplitude of the EMG signal decays with the inverse of the x-th power of the distance from the source (x = 1.2-1.4) (Ekstedt and Stalberg, 1973; Gath and Stalberg, 1979; Roeleveld et al., 1997; Staudenmann et al., 2010). Overall, high EMG amplitudes are quantified in individuals with lower subcutaneous tissue thickness in multiple muscles (Hemigway et al., 1995; Roeleveld et al., 1997; Farina and Rainoldi, 1999; Farina et al., 2002; Kuiken et al., 2003; Nordaner et al., 2003; Al Harrach et al. 2017). In addition to reductions in sEMG amplitude, mean power frequency is reduced with increases in subcutaneous tissue thickness (Roeleveld et al., 1997; Farina et al., 2002; Staudenmann et al., 2010).

The thickness of the subcutaneous tissue layer and the distance between the sEMG electrode and the muscle influence the relationship between EMG signal amplitude and EMG amplitude cancellation. The sEMG amplitude depends on the net motor unit activity or recruitment

and discharge rate of active motor units. Active motor units closest to the EMG electrode dominate the recorded sEMG signal. As the force level progressively increases and motor units are recruited, the mean power frequency also increases due to higher muscle fiber conduction velocity (Andreassen and Arendt-Nielsen, 1987). Increases in the contraction level amplify the EMG amplitude's cancellation, resulting from the algebraic summation of positive and negative phases of the motor unit action potentials (Keenan et al., 2005).

Additionally, the sEMG detection distance relative to the muscle contraction is ~1-1.5 cm (Fuglevand et al., 1992). However, in instances where large motor units are active, the detection area may increase to ~3.5 cm (Fuglevand et al., 1992). Although largely superficial in males, the pectoralis major muscle is located deep to the breast/subcutaneous tissue in females. The distance between the sEMG electrode and pectoralis major depends on the female's breast anatomy, including breast size and location of the breast tissue distribution. Therefore, the ability to acquire pectoralis major activation in females may depend on breast tissue thickness. For example, in females with low breast tissue, more information regarding the pectoralis major activation may be acquired.

2.5. Motor unit overview

The motor unit consists of the alpha motor neuron located in the ventral horn of the spinal cord, its axon, and muscle fibers that are innervated by the same axon (Sherrington, 1925). The role of motor units is to convert neural input from the central nervous system into the muscle force, which is crucial in the generation of movement (Heckman and Enoka, 2012). Synaptic input arriving from the central nervous system converges onto alpha motor neurons. From here, the synaptic input is converted into trains of action potentials that are relayed from motor neurons to the innervated muscle fibers, eliciting a contraction of all muscle fibers innervated by the motor

unit (Enoka and Duchateau, 2015). The axon of each alpha motor neuron projects as a peripheral or cranial nerve to the target muscle (Enoka and Duchateau, 2015), innervating on average 300 to thousand muscle fibers, depending on the muscle size (Enoka and Fuglevand, 2001). Muscle fibers belonging to a single motor unit are commonly distributed throughout the muscle and intermingle with muscle fibers innervated by other motor neurons. In some muscles, the fibers are confined to discrete neuromuscular compartments, which correspond to the muscle regions innervated by that peripheral nerve.

2.5.1. Motor unit recruitment and discharge rate (Rate coding)

Motor units play a role in force production/control through several different mechanisms. The magnitude of muscle force is dependent on the concurrent motor unit recruitment and modulation of the rate at which motor neurons discharge action potentials (i.e., rate coding or discharge rate; Duchateau et al., 2006). The recruitment of motor units is progressive and occurs according to Henneman's principle (Henneman et al., 1965), whereby motor units are recruited based on size, from smallest to largest. For example, during voluntary contractions, motor units innervating the fewest number of muscle fibers (i.e., the smallest, low threshold motor units) are recruited first. Therefore, the ability to precisely grade force during submaximal contractions depends on the size and the number of low threshold motor units in the muscle.

In contrast, large (high threshold) motor units are recruited when contractions are powerful or rapid (Enoka and Duchateau, 2015). Therefore, at high contractions, the recruitment of motor units increases only if the motor neuron pool's discharge rate is high. Hence, most motor units are recruited during weak (i.e., low force) contractions, with progressively fewer recruited at moderate and high contractions. The motor unit recruitment is modulated by the alpha motor neuron pool's input and output of the alpha motor neuron pool to the muscle fibers (Heckman and Enoka, 2012).

The electrical output generated by the motor unit depends on the rate at which the motor neuron discharges action potentials (Enoka and Duchateau, 2015). Motor unit physiology was examined in multiple shoulder muscles, such as the upper trapezius and biceps. No studies to date, however, evaluated motor unit physiology in pectoralis major.

2.6. Methodological considerations: Advantage of high-density surface electromyography

Global features of muscle activation are commonly investigated using classic, low-spatial resolution or fine wire EMG, while motor unit physiology is evaluated with indwelling EMG. Each of these methods has some inherent limitations in capturing the activation of multifunctional, large muscles such as the pectoralis major. These limitations are briefly discussed below, with an alternative, more objective, non-invasive method presented (i.e., high-density surface electromyography) to evaluate muscle activity and neural decoding concurrently.

The most widely used method to investigate pectoralis major activity is low spatial resolution EMG in bipolar mode. A waveform acquired using classic or fine wire EMG results from active motor units located within the electrode's detection volume. Therefore, this method typically allows for signal acquisition from a small region of the muscle. Global properties of muscle activation are commonly investigated, such as amplitude [e.g., root mean square (RMS)] and power spectral components [e.g., mean and median power frequency]. However, depending on the location of signal acquisition and the number of electrodes, classic EMG methods may not represent the whole muscle's activation, particularly in large muscles, such as the pectoralis major. Also, the detection of regional differences in muscle activation may not occur with this method. The pick-up area of low spatial resolution EMG is relatively small when considering the muscle's size.

Further, multifunctional, compartmentalized muscles exhibit a heterogeneous spatial distribution of EMG amplitude that is dependent on the force level (Holtermann et al. 2005; Holtermann and Roeleveld, 2006; Holtermann et al. 2008) and may also depend on the task. The spatial distribution provides information on the distribution of electrical potential on the skin surface during a muscle contraction, which could be related to motor unit distribution or motor unit recruitment within different compartments (Farina et al. 2008). In addition, the classic EMG cannot be used to identify the neural contribution to muscle activity (Martinez-Valdes et al. 2018), limiting its usefulness in interpreting any changes, differences, or alterations in muscle activation. On the other hand, indwelling EMG, which involves the insertion of electrodes into the muscle, is typically used to examine motor unit physiology. However, this method is invasive, elicits slight discomfort, only allows for the acquisition of EMG signals from a small region of the muscle (i.e., within the indwelling electrode detection area), and only a few motor units can be discriminated from these recordings (Farina and Holobar, 2016).

The more recent development of high-density (multichannel) surface electromyography (HD-sEMG) systems, however, has enabled concurrent investigation of the global features of muscle activation and monitoring of active motor units (Merletti et al. 2008; Holobar et al. 2009; Farina and Holobar, 2016; Negro et al. 2016a). HD-sEMG consists of an array of electrodes spaced close to one another and provides a non-invasive approach to investigate neural and neuromuscular properties in muscles where the insertion of the needles is not desirable (Merletti et al. 2008). Coupled with the decomposition algorithms based on blind source separation (Farina et al. 2004; Holobar et al. 2009; Negro et al. 2016a), HD-sEMG allows for the identification of many concurrently active motor units. The convolutive blind source separation algorithm uses semi-automatic statistical methods to identify motor unit spike trains and extracts information regarding

motor unit discharge rates (Holobar and Zazula, 2007; Farina and Holobar, 2016; Negro et al. 2016a). This algorithm was validated using a two-source method in the abductor digiti minimi and the tibialis anterior (Negro et al. 2016) for a broad range of forces. Further, its accuracy was also validated in animals (Thompson et al. 2018) and healthy or compromised human muscles (Hyngstrom et al. 2018; Martinez-Valdes et al. 2018; Murphy et al. 2018; Perreira et al. 2019; Kapelner et al. 2019; Cogliati et al. 2020; Martinez-Valdes et al. 2020).

HD-sEMG, therefore, combines the main advantages of classic surface and indwelling EMG, capturing muscle activity with a high spatial and temporal resolution, which creates unique opportunities for pectoralis major investigations. Acquisition of EMG signals from the whole muscle in males captures information on pectoralis major activation and neural control, providing unparalleled information on holistic neuromusculoskeletal control of this muscle. Additionally, using HD-sEMG to acquire pectoralis major activation in females has multiple advantages. First, classic sEMG recordings can acquire signals from approximately two independent pectoralis major locations in females prior to breast tissue affecting the signal's quality. In contrast, HD-sEMG provides a tool to capture the activity from multiple, available locations (i.e., whole clavicular, superior, and middle sternocostal regions), breaking new ground in acquiring and characterizing pectoralis major activity in females. Secondly, examining pectoralis major motor unit physiology using indwelling EMG (i.e., needle) in females is challenging, highly invasive, and inadvisable due to the unknown side effects of such methods on breast tissue. With HD-sEMG, therefore, these limitations and challenges are circumvented.

2.7. Overview of shoulder restrictions following pectoralis major injury

Insights into potential functional contributions of pectoralis major regions to arm mobility emerge by evaluating pectoralis major comorbidities. In general, injuries to the pectoralis major

are rare, although the number of cases increased in frequency in the past 20 years (ElMaraghy et al., 2012). The most common activities causing pectoralis major rupture are weightlifting (typically bench press), wrestling, rugby, gymnastics, and boxing (de Castro Pochini et al. 2014; Butt et al. 2015). Injuries to the sternocostal and abdominal regions elicit on average 8% to 40% reduction in vertical or horizontal adduction, internal rotation, extension, or flexion strength, as well as extension range of motion (Pavlik et al. 1998; Schepsis et al. 2000; Hanna et al. 2001; Provencher et al. 2010; de Castro Pochini et al. 2013; Marsh et al., 2020). In case of injuries, surgical repair of the pectoralis major results in recovery of strength (~99%) and functional outcomes (~ 97%) more than conservative treatment (~56%; Bak et al. 2000; Hanna et al. 2001; Cordasco et al. 2017) and is recommended in individuals who are young and active (Provencher et al. 2010). Long-term reductions in vertical adduction strength (~30%) and trends towards reductions in internal rotation strength occur in females who undergo subpectoral breast reconstruction surgery, which involves disinsertion of inferior sternocostal and abdominal regions of the pectoralis major (Leonardis et al. 2019). In addition, these females also have reduced (~30%) shoulder stiffness during vertical adduction (Leonardis et al. 2019). Further, limitations in flexion and extension range of motion exist in individuals whose pectoralis major is used as a pedicled flap to reconstruct the head and neck following cancer (Moukarbel et al. 2010). Additionally, pectoralis major transfers aimed at restoring scapular movement typically result in reductions in adduction strength (Iceton and Harris, 1987; Post, 1995).

2.8 Conclusion

This literature review provides an overview of (1) basic properties of muscle architecture and motor units; (2) a novel method to evaluate the spatial distribution of muscle activity and extract neural properties using HD-sEMG; and (3) pectoralis major architectural properties,

broadly defined function, activation, and injury as it relates to pectoralis major function. The pectoralis major is morphologically complex and is commonly depreciated in typical shoulder function and health. This is partly due to the limited understanding of its contribution and importance in arm mobility. This dissertation addresses several critical methodological challenges that currently prevent deeper insights into the pectoralis major's sophisticated and complex function. Further, it provides an unparalleled characterization of pectoralis major neuromusculoskeletal control in males and females through holistic examinations of global muscle activation and neural decoding, leading to significant biomechanical and neuroscientific advances. Lastly, this dissertation's findings can be used to guide surgical decision-making and rehabilitation strategies following pectoralis major compromise. The purpose of the experiments to follow are twofold: (1) to investigate regional pectoralis major activation in healthy males and females in tasks typically requiring pectoralis major activation; and (2) to investigate the neural control of pectoralis major to understand better the mechanisms behind neural components of mechanical force production within this muscle. Each study's aims and hypotheses are outlined below (Figure 2).

Study 1 examines whether the standard placement of classic EMG electrodes mischaracterizes whole pectoralis major activation. The following hypotheses were made:

Hypothesis 1: The EMG amplitudes in the lower sternocostal region derived with HD-sEMG will be larger compared to EMG amplitudes from upper sternocostal regions derived by classic EMG, specifically in adduction, internal rotation, and extension tasks.

Hypothesis 2: The HD-sEMG and neural decoding approach will provide additional information on neuromuscular and neural properties related to the global EMG activation.

As Study 1 demonstrates, current methods do not capture whole pectoralis major activity. A novel, more holistic framework combining HD-sEMG and neural decoding is proposed for future studies investigating its neuromusculoskeletal control. This framework shows that decomposing HD-sEMG signals into neuromuscular and neural properties can provide additional information regarding the pectoralis major's neuromusculoskeletal control.

Characterization of pectoralis major activity is particularly challenging in females due to the muscle's location with respect to the breast. Currently, the effect of varying breast tissue thickness on HD-sEMG amplitude and mean power frequency is unknown, making it challenging to (1) determine if pectoralis major activation acquisition is feasible in all females and (2) identify the exact location (i.e., row of HD-sEMG array) at which the signal quality substantially declines to the level of inherent noise. Therefore, the purpose of **Study 2** was to inform methods and data analyses in Studies 3 and 4, as well as inform on methodological considerations in any future studies that examine HD-sEMG signals in females. The following hypotheses were made:

Hypothesis 1: Females with the largest breast tissue thickness (i.e.,> 10 cm) will have lower EMG amplitudes across pectoralis major regions than females with low breast tissue thickness.

Hypothesis 2: HD-sEMG mean power frequency will be significantly less in females with large breast tissue thickness than those with low breast tissue thickness.

Studies 3 and **4** build on the findings from Study 2 and focus on characterizing regional pectoralis major activation in females using data only from the superior HD-sEMG array. Currently, no foundational knowledge on regional pectoralis major activation exists in females. However, this knowledge is essential, considering sex-related differences in muscle activity and neural control exist in other muscles (Anders et al. 2004; Bouffard et al. 2019; Cid et al. 2019).

Additionally, establishing typical activation of pectoralis major in females is vital for improving guidelines relating to the prevention of injury, rehabilitation, exercise, and surgical procedures (i.e., breast reconstruction surgeries). The following hypotheses were made:

Hypothesis 1: In adduction 90, adduction 60, apprehension, extension, and internal rotation middle sternocostal region will have higher normalized EMG amplitude than the clavicular and superior sternocostal region.

Hypothesis 2: In flexion, the clavicular region will have higher normalized EMG amplitude than the superior and middle sternocostal region.

Hypothesis 3: In horizontal adduction, clavicular and superior sternocostal regions will have higher EMG amplitude than the middle sternocostal region.

Studies 5 and **6** examines global activation of pectoralis major in males, establishing critical knowledge on regional pectoralis major contribution to a range of tasks. Previous studies characterizing pectoralis major activity using classic EMG captured the activation from a small region of the muscle and directly placed several EMG electrodes on the innervation zones (Paton and Brown, 1994; Brown et al. 2007; Wickham et al. 2004; 2012). The distance of the EMG electrodes overlaying each of the compartments was small (~30 mm as per Paton and Brown, 1994), increasing the possibility of capturing the activation of the surrounding regions. Further, the authors did not investigate pectoralis major activity in internal rotation or abduction 90 with adduction external 90 (i.e., ADDER90). These two tasks are highly relevant, as the pectoralis major is described as an internal rotator alongside subscapularis and latissimus dorsi, while adduction external 90 is typically the task in which the pectoralis major is injured during exercise. Therefore, Studies 5 and 6 aimed to examine the spatial distribution of the whole pectoralis major

activation using HD-sEMG, bypassing some of these limitations. The following hypotheses were made:

Hypothesis 1: In adduction 90, 60, adduction external 90, internal rotation (60 and 90), and extension, lower sternocostal regions will have higher normalized EMG amplitude than clavicular and superior sternocostal regions.

Hypothesis 2: In flexion, the clavicular region will have higher normalized EMG amplitude than superior and lower sternocostal regions.

Hypothesis 3: In horizontal adduction, the clavicular and superior sternocostal regions will have higher normalized EMG amplitude than lower sternocostal regions.

In **Study 7**, neural and neuromuscular control of pectoralis major is for the first time non-invasively explored in males and females, showing atypical motor unit behaviour. Gaining insight into these properties is essential, considering the importance of spinal motor neurons in mechanical force generation. Across Studies 3, 4, 5, and 6, EMG activity either did not change or increased across effort levels. However, the exact mechanisms behind changes in EMG amplitude could not be deciphered. Therefore, this study aimed to complement global EMG findings and elucidate how neural and neuromuscular properties contribute to change in effort level, leading to essential findings on how pectoralis major may modulate force across efforts. The following hypotheses were made:

Hypothesis 1: The discharge rate of motor units will increase with the effort level, indicating reliance on motor unit rate coding to increase the effort level.

Hypothesis 2: Motor unit action potential amplitude will increase with the effort level, indicating the influence of the neuromuscular properties on the sEMG amplitude.

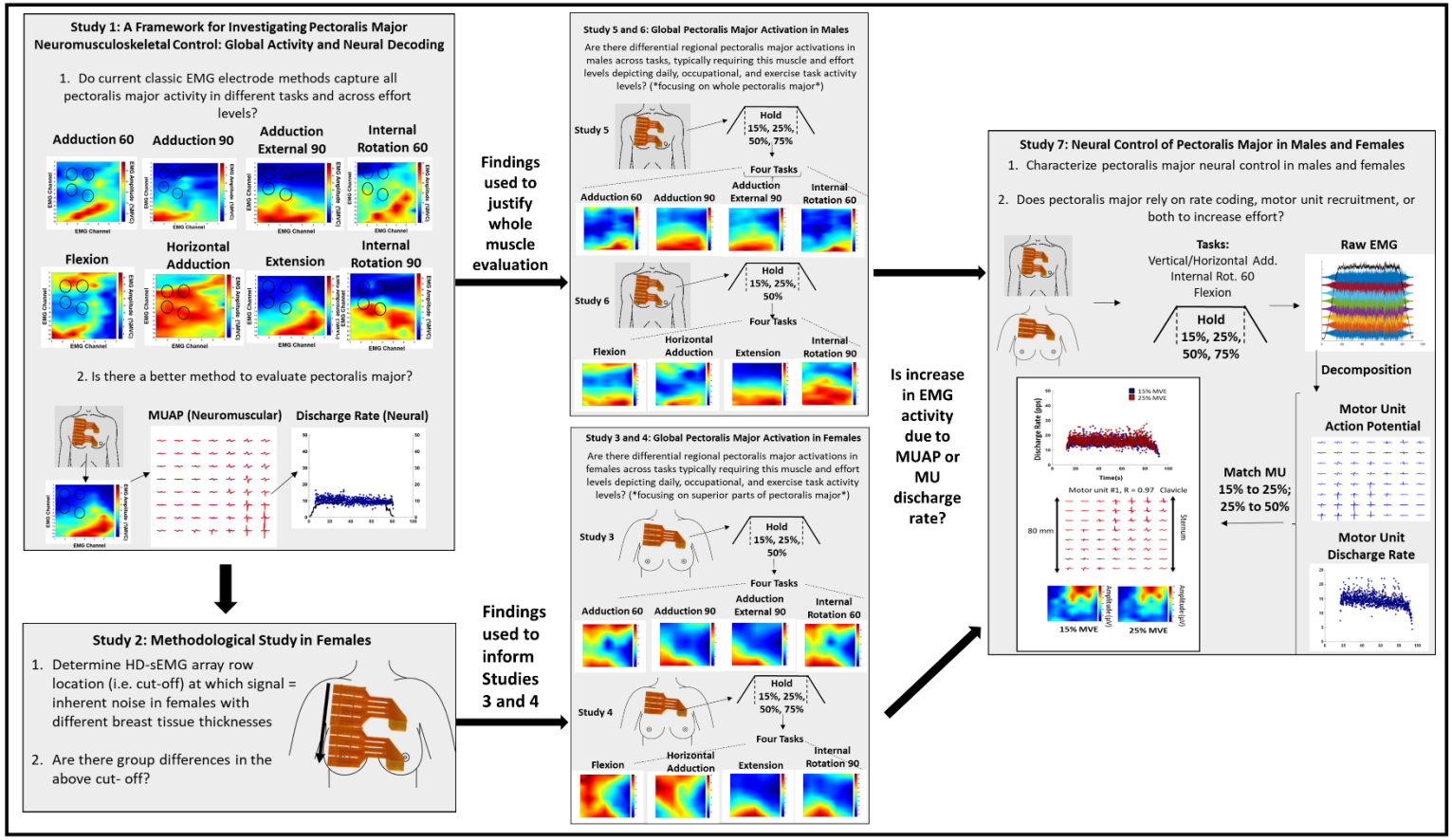

Figure 2: Dissertation experiments. **Study 1** investigated if the current evaluation of EMG activity using classic EMG electrodes underestimates the pectoralis major's activity and proposed a framework to holistically investigate its neuromusculoskeletal control using a combined HD-sEMG and neural decoding approach in healthy males. Black circles on the first set of images indicate the standard location from which the pectoralis major activity is currently investigated. The second set of images shows that acquiring HD-sEMG from the whole muscle can provide more information regarding the global activity and neural and neuromuscular properties. **Study 2** is a methodological study in females, which examined the effect of varying breast tissue thicknesses on HD-sEMG signal amplitude and mean power frequency in healthy females. The findings of Study 2 were used to inform methods in studies 3 and 4. **Studies 3, 4, 5, and 6** investigated fundamental regional pectoralis major activation in healthy females (3 and 4) and males (5 and 6) in eight tasks across multiple effort levels. Lastly, **Study 7** culminated by evaluating pectoralis major neural control (i.e., motor unit physiology) in males and females.

Chapter 3. Framework for investigation of the pectoralis major neuromusculoskeletal control: A combined high-density surface electromyography and neural decoding approach

3.0. Abstract

Pectoralis major assists in several shoulder movements, including humeral vertical and horizontal adduction, flexion, extension, and internal rotation. Despite its involvement in numerous daily, work, and exercise activities, its neuromusculoskeletal control is mostly unknown and understudied. The purpose of this study was to outline knowledge gaps in the current understanding of pectoralis major control, challenges in acquiring relevant quantitative data, and provide a framework to enhance functional pectoralis major knowledge. A novel framework is proposed combining high-density surface electromyography (HD-sEMG) recordings with a neural decoding algorithm. Macroscopic and motor unit level analyses are used to investigate pectoralis major activation and neural control in eight tasks in low (15-25% MVE) and moderate (50% MVE) efforts in healthy males. Virtually derived bipolar EMG amplitudes were quantified for clavicular and upper sternocostal regions, based on common locations used to acquire EMG signals from pectoralis major using classic EMG. HD-sEMG amplitudes from three pectoralis major regions (i.e., clavicular, upper, and lower sternocostal) were compared to virtually derived bipolar EMG amplitudes from the upper sternocostal region to determine if current classic EMG methods mischaracterize pectoralis major activity. Additionally, for the first time, the feasibility of evaluating motor unit physiology in the pectoralis major is presented and explored as an essential method to decipher neural and neuromuscular contributions to the control of pectoralis major. Current findings demonstrate that classic EMG mischaracterizes pectoralis major activation in several tasks and effort levels, highlighting the importance of acquiring signals from multiple pectoralis major regions. Additionally, the proposed framework allows for a holistic

characterization of pectoralis major neuromusculoskeletal control with implications in fundamental, exercise, and clinical sciences.

3.1 Introduction

The pectoralis major fundamentally enables the mobility of the shoulder complex. It originates from the mid clavicle, sternum, true ribs, and external oblique fascia and converges into a bilaminar tendon that inserts into the bicipital groove of the humerus (Wolfe et al. 1992; Fung et al. 2009). It spans multiple joints, including the sternoclavicular, acromioclavicular, glenohumeral, and intercostal joints and is broadly divided into clavicular, sternocostal, and abdominal regions (Fung et al. 2009; Haladaj et al. 2019). Its multipennate architecture assists in several arm movements, including humeral horizontal and vertical adduction, internal rotation, flexion, and extension against resistance. Thus, pectoralis major activation enables a vast array of daily work and exercise activities.

However, neuromusculoskeletal control of pectoralis major is still largely ambiguous, with most of the extant scientific research focusing on its involvement in exercise. Due to the general lack of knowledge on its role in upper extremity mobility, various surgical procedures, biomechanical models, and non-targeted rehabilitation and exercise programs were developed, neglecting pectoralis major regions' key contributions. For example, breast and neck reconstruction surgeries routinely resect or disinsert pectoralis major regions, compromising shoulder health (see Moukarbel et al. 2010; Leonardis et al. 2019; Vidt et al. 2020). Biomechanical models often discount key contributions of abdominal regions (Hogfors et al. 1987; Dickerson et al. 2007; Jastifer et al., 2012; Seth et al., 2019), leading to potentially erroneous ergonomic and clinical solutions. Lastly, non-specific rehabilitation programs developed for breast cancer survivors commonly do not address severely compromised pectoralis major integrity (Hayes et al. 2011; Stout et al. 2012; Vidt et al. 2020). As such, these issues mandate an unraveling of pectoralis major control to enable the development and optimization of surgical procedures, treatments, rehabilitation protocols, and biomechanical models.

Commonly, pectoralis major activation is investigated using low spatial resolution surface electromyography (sEMG) recordings from the clavicular and superior sternocostal regions (Cram and Kasman, 1998; Hermens and Freriks, 1997). These standards neglect to examine the activation of the middle, inferior sternocostal, and abdominal regions. Indeed, only a few studies investigated all regions' activation using classic EMG (Paton and Brown, 1994; Wickham et al. 1998; Brown et al. 2007). These studies demonstrated that the normalized EMG amplitude of regional activation depended on the task and effort level. For instance, exerting low submaximal isometric effort in adduction and extension activated the abdominal region to a greater extent than the clavicular and sternocostal regions. In contrast, the superior sternocostal region activated more during forward flexion (Paton and Brown, 1994). Differential regional activation was attributed to distinct regional neural control.

The amplitude of the interference EMG is dependent on the number of active motor units, their discharge rate, and the amplitude of their motor unit action potentials (MUAPs). Therefore, interference EMG is a combination of the active motor units' central and peripheral properties (Farina et al. 2004). For these reasons, EMG amplitude alone cannot identify the neural contribution to muscle activity (Martinez-Valdes et al. 2018), limiting the usefulness of interpreting any muscle activation alterations. However, this knowledge is essential in studies evaluating training regimens, rehabilitation, or treatment effects, as they may affect neural or neuromuscular control of each region separately. For instance, studies in breast cancer survivors have used mainly classic EMG to characterize pectoralis major activation changes following oncological treatment (Shamley et al. 2007, 2012; Brookham et al. 2018) or exercise protocol (Hagstrom et al. 2017). Although some of these studies showed alterations in EMG amplitude (i.e., increase or decrease) in BCS (Shamley et al. 2007; 2012; Brookham et al. 2018), it is still unknown

whether these changes are due to the disruption in neural or neuromuscular systems, or both. Further, anatomically, the pectoralis major consists of eight independent partitions (Fung et al. 2009). The existence of these partitions suggests that each region may be controlled independently by the central nervous system. Therefore, discernment of this complex behaviour requires a more in-depth and deliberate investigation into neural components of pectoralis major activation.

This paper aims to demonstrate current limitations in acquiring EMG signals from the pectoralis major to provide future directions in investigating pectoralis major neuromusculoskeletal control. This includes showing that: a) classic EMG recordings mischaracterize pectoralis major activation in several tasks; b) high-density sEMG recordings can provide more information regarding the regional activation of the pectoralis major in different tasks; and c) the potential exists for extraction of neuromuscular and neural components from raw EMG signals using high-density surface electromyography (HD-sEMG; Figure 3). The primary hypothesis was that the EMG amplitudes in the lower sternocostal region derived with HD-sEMG would be larger compared to EMG amplitudes from upper sternocostal regions derived by classic EMG, specifically in adduction, internal rotation, and extension tasks. The secondary hypothesis was that the HD-sEMG and neural decoding approach would provide additional information on neuromuscular and neural properties related to the global EMG activation.

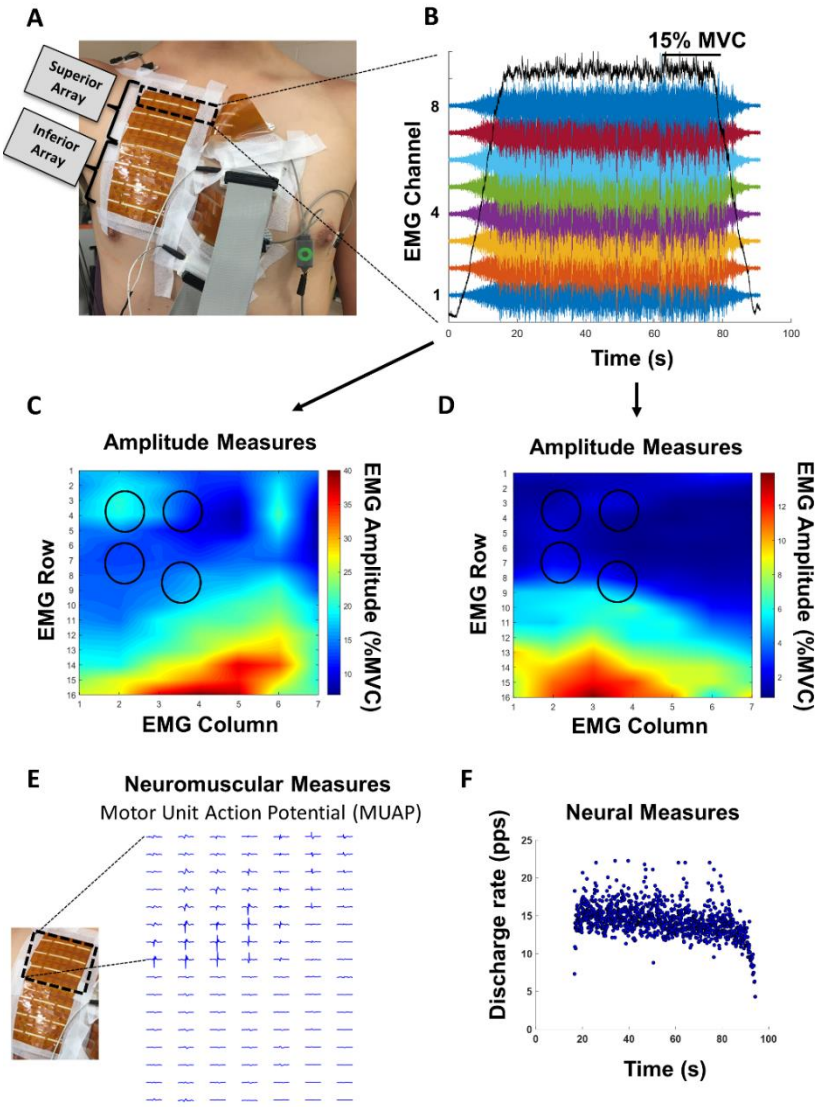

Figure 3: Framework for assessing the pectoralis major neuromusculoskeletal control from the experimental setup, acquisition of HD-sEMG signals to motor unit decomposition. **A:** Two HD-sEMG arrays positioned on the pectoralis major (64 channels in each array). The superior array is the array closest to the clavicle. The inferior array is the second array located right below the superior array. **B:** An example of a trapezoidal ramped effort with eight channels from the superior (i.e., top) HD-sEMG array recorded in a monopolar mode. The Force trace is overlaid in black. **C-D:** Representative spatial maps from a single participant of the pectoralis major activation normalized to the maximal effort in adduction (**C**) and adduction external 90 (**D**) tasks. Black circles on the spatial maps depict the locations of classic EMG electrodes from which signals are commonly acquired. A single electrode in the bipolar configuration is currently placed on the clavicular region, while the second bipolar electrode is placed on the upper sternocostal region (see Cram and Kasman, 1998). **E:** Representative example of the motor unit action potentials from the superior array. **F:** Representative example of motor unit discharge rate in a submaximal effort (15% MVE).

3.2. Methods

3.2.1. Participants

Data presented in this study is from eighteen (25 ± 4.7 years) and ten (25.8 ± 5.3 years) healthy, right-hand dominant, young males collected as a part of two different protocols, respectively, to avoid fatigue during the collection. The chosen sample size was selected using *a priori* power analyses. Sample size calculations were performed in G*Power 3.1 (Universitat Dusseldorf, Dusseldorf, Germany). Sample size calculations indicated that a minimum of 16 participants is required to obtain sufficient power (Cohen, 1988) in both protocols. The effect size chosen ($f^2 = 0.31$) is on the lower end of the observed effect size in previous studies, which reported effect sizes between 0.2 to 0.6 (Paton and Brown, 1994; Brown et al. 2007; Wickham et al. 2004). Males were recruited through word-of-mouth or by posters in kinesiology, engineering, psychology, and student center buildings. The inclusion criteria included healthy right-hand dominant males between 18-40 years old. All recruited males were recreationally active. Participants had no known musculoskeletal, neuromuscular, or neurological disease and no low back pain in the past six months. Each participant provided written informed before the beginning of the study. The study was reviewed and received ethics clearance from the institutional Office of Research Ethics (ORE #31747 and ORE #40849) and conformed to the Declaration of Helsinki.

3.2.2. High-density surface electromyography

Pectoralis major activation was acquired in several tasks in different effort levels using two HD-sEMG arrays, each consisting of 64 electrodes in monopolar mode (interelectrode distance (IED): 1 mm; ELSCH064NM3, OTBioelecttronica, Torino, Italy; Figure 3A). Before applying electrodes, the pectoral area was shaved, cleaned with abrasive paste, and gently cleansed with

water. The electrode arrays were applied on the skin using a 1 mm thick two-sided adhesive foams filled with electroconductive gel. The superior array was placed ~ 2 cm inferior to the clavicle, with the middle of the array located between the sternum and the axilla and parallel to muscle fibers. The inferior array was placed immediately below the superior one. The arrays were fixed with adhesive tape and connected to a 128 channel EMG amplifier (EMGUSB2+, OTBioelecttronica, Torino, Italy). All signals were sampled at 2048 Hz and band-pass filtered with a cut-off frequency between 10-500 Hz with a 12-bit A/D converter (5V dynamic range). Signals were amplified between 100-5000 V/V. One wet reference electrode was wrapped around the participant's right wrist, and a reference electrode was placed on the right clavicle.

3.2.3. Electrocardiography (ECG)

Electrocardiography (ECG) was recorded using silver-silver chloride (Ag-AgCl) disposable electrodes placed over the left chest at six costal level, approximately along the anterior axillary line; and medially at the sternocostalis junction in monopolar mode (Drake and Callaghan, 2006). Before the electrodes' placement, the area overlaying the anatomical landmarks was shaved and cleaned with abrasive gel and water. A reference electrode was placed on the acromion. ECG was collected using a wireless telemetered system (Noraxon Telemyo 2400 T G2 Noraxon, Arizona, USA). Raw signals were band-pass filtered from 10-1000 Hz and differentially amplified with a CMRR > 100dB and an input impedance of 100 MΩ. Analog signals were converted to digital using a 16-bit A/D card with a ±10 V range. The sampling frequency was 1500 Hz.

3.2.4. Force measurement

Raw voltage was acquired concurrently with HD-sEMG and ECG. Participants exerted effort against a custom-built arm-cuff attached to a six-degree of a freedom force transducer (MC3A, AMTI MA, USA) mounted on a robotic arm (Motoman Robotics Division, Yaskawa America, USA). The sampling rate was set to 1500 Hz and amplified (1000x) using VICON Nexus 1.7.1 software.

3.2.5. Experimental protocol

All participants underwent a brief warm-up and training on how to generate maximal voluntary effort (MVE) in different tasks. Following this, participants practiced submaximal efforts against an attachment with visual feedback of their force output provided on a monitor. Next, participants performed two task-specific 5 second MVEs in each task against an arm-cuff while sitting comfortably on a chair with their torso secured with a padded strap. The forearm and upper arm were secured inside a custom-made attachment. Participants performed submaximal and maximal trials in eight tasks: Study 1: a) adduction from 90° of abduction (Figure 4A); b) adduction from 90° of abduction and external rotation (i.e., adduction external 90; Figure 4B); c) adduction from 60° of abduction (Figure 4C); c) internal rotation from 60° of abduction (Figure 4D); and Study 2: a) flexion at 20° of abduction (Figure 4E); b) extension at 20° of abduction (Figure 4F); c) internal rotation from 90° of abduction and 20° of internal rotation (Figure 4G); and d) horizontal adduction from 90° of abduction and 50° of flexion in the transverse plane (Figure 4H). During MVE's performance, participants were verbally encouraged by the investigator. Each MVE was separated by 2 minutes of rest. Maximal MVEs were quantified using a custom-made program in LabVIEW (National Instruments, version 3.1). If the maximal trials

within a task differed by more than 10 N, a third trial was performed to ensure consistency between MVEs. Additionally, off-axis forces were monitored in a custom-made program in LabVIEW (National Instruments, version 3.1). Participants were required to exert an effort of at least 80% in the target direction. If this was not achieved, participants were provided with verbal feedback, and the trial was repeated. For each task, the mean of two task-specific maximal MVE trials was used to scale all submaximal trials (see below).

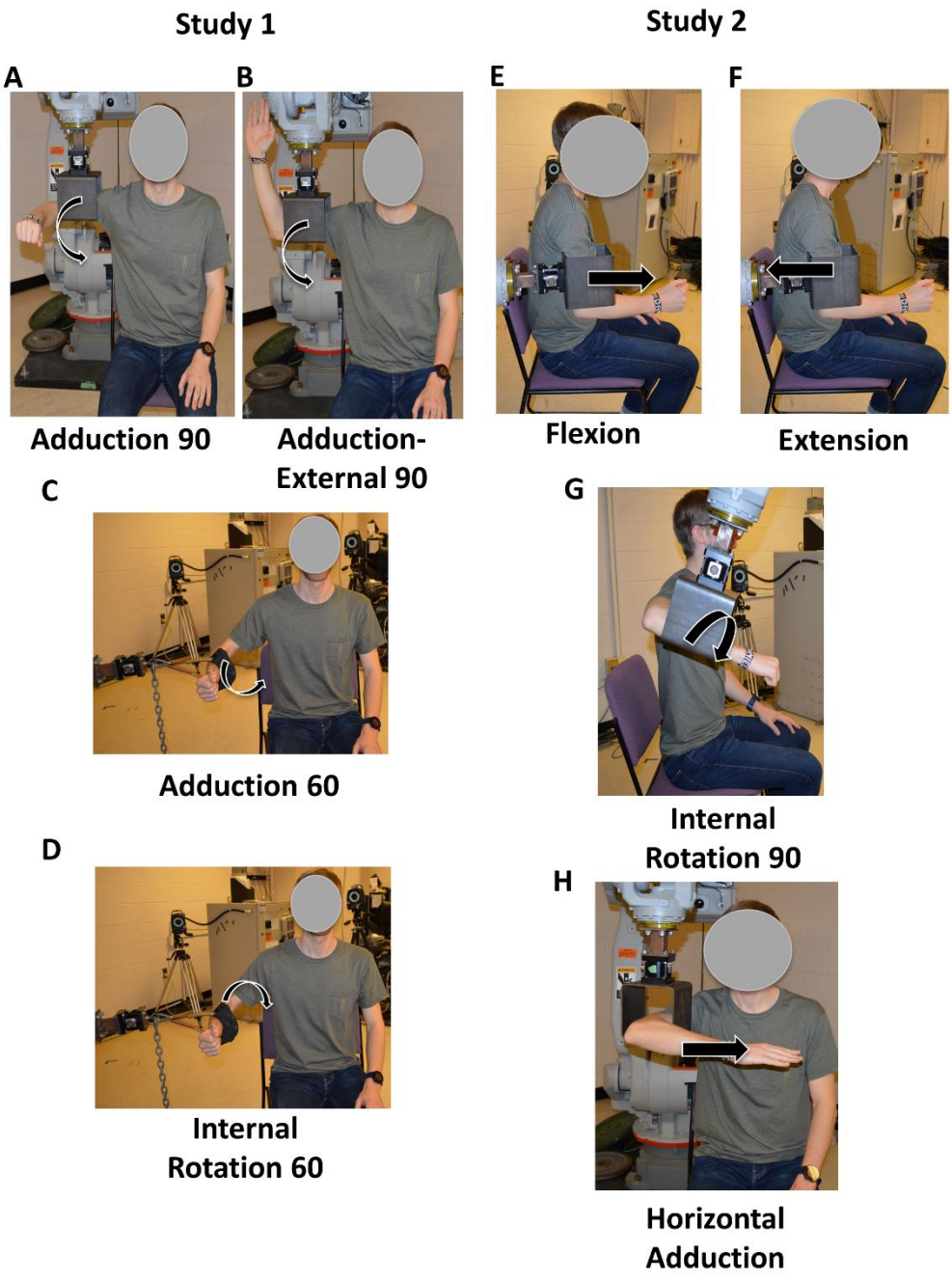

Figure 4: Experimental setup for two studies. Tasks included: Study 1: **A:** adduction from 90° of abduction; **B:** adduction from 90° of abduction and 90° of external rotation (adduction external 90); **C:** adduction from 60° of abduction; **D:** internal rotation from 60° of abduction; Study 2: **E:** flexion at 20° of abduction; **F:** extension at 20° of abduction; **G:** internal rotation from 90° of abduction and 20° of internal rotation; and **H:** horizontal adduction from 90° of abduction and 50° of flexion in the transverse plane.

In each task, participants performed submaximal ramped isometric efforts scaled to 15%, 25%, and 50% of task-specific MVE. Each effort level was performed twice and lasted 60 seconds, 60 seconds, and 30 seconds, respectively, with 3 to 5-minute rest breaks provided between the trials. Participants were encouraged to report feelings of fatigue and the need for longer rest periods. If requested by the participant, longer rest periods were provided. For 15% and 25% MVE, participants ramped at ~2% MVE/s, while at 50% MVE, the ramp was ~3% MVE/s. For each trial, participants were provided with visual feedback (i.e., trapezoid) of the required force output on a monitor and live feedback of the force level they were exerting against the attachment. Tasks were fully randomized between participants, as well as within a participant. Effort levels were randomized within each task, with each submaximal effort performed consecutively within a task.

3.3. Data analysis

3.3.1. HD-sEMG signal processing (Macroscopic level analysis)

Before analyses, all data were visually inspected in a custom-made program in MATLAB (MATLAB 2019b; The Mathworks, Inc.). Tasks and effort levels with low differential EMG activity (i.e., below noise levels) were taken out from further analyses. These included the following tasks and effort levels: adduction external 90 and internal rotation 90 (15% MVE) and extension (15% and 25% MVE).

ECG was removed from monopolar HD-sEMG signals. Due to the differences in sampling frequencies between HD-sEMG and ECG, ECG was first interpolated to 2048 Hz (i.e., HD-sEMG sampling frequency). Following this, HD-sEMG signals were cross-correlated with the ECG, matching the timing of the peak-to-peak amplitude of each heartbeat between two signals. Each trial was visually inspected to ensure the algorithm correctly recognized the ECG peaks. The

precise timing of each ECG peak surrounded by 250-millisecond windows before and after the peak was determined and used to avoid the quantification bias of the root mean square (RMS) amplitude.

HD-sEMG signal processing involved multiple steps. Raw HD-sEMG data were band-pass filtered with a 3rd order Butterworth filter (20-500 Hz), and differential derivation was quantified from right to left (i.e., from right axilla towards the sternum) from the monopolar recordings. RMS was quantified for each differential channel. The resultant force was used as a reference to analyze only the first half of the hold. The most stable part of the resultant force was selected by dividing the signal into 5-second segments and performing the analysis on the one with the lowest coefficient of variation in force. All submaximal data was normalized to maximal trials. For adduction 60 and internal rotation, adduction 90 and adduction external 90, and flexion and extension maximal trials were combined as the arm posture was similar. To quantify the maximum, a mean of 3 seconds of data for each channel was extracted from each maximal trial. Following this, maximal mean value across trials was extracted for each channel, and all submaximal trials were normalized to these values. Hence, each channel within a submaximal trial was normalized to their maximal value achieved during MVEs. Once the data were normalized, the HD-sEMG arrays were divided into clavicular (rows 1-5), upper sternocostal (rows 6-13), and lower sternocostal (rows 14-16) regions, and the mean for each region was quantified (Fung et al. 2009).

3.3.2. Derived bipolar surface electromyography

Derived bipolar sEMG signals were quantified for clavicular and sternocostal regions to compare with HD-sEMG recordings as depicted by four circles in Figures 5 and 6. These signals

were derived from approximate HD-sEMG channels where classic EMG electrodes are typically placed on the pectoralis major.

3.3.3. HD-sEMG decomposition (Motor unit-level analysis)

HD-sEMG signals were decomposed using a convolutive blind source separation algorithm, which was validated in multiple muscles (Negro et al. 2016; Hyngstrom et al. 2018; Martinez-Valdes et al. 2018; Thompson et al. 2018; Murphy et al. 2018; Kapelner et al. 2019; Pereira et al. 2019; Cogliati et al. 2020; Martinez-Valdes et al. 2020). The decomposition precision was determined using the silhouette measure (SIL) that was shown to correlate well with the accuracy in estimating the motor unit discharge patterns (Negro et al. 2016). SIL threshold was set to 0.90, and only those motor unit discharge patterns deemed to have high accuracy were included in the analyses. The individual two-dimensional motor unit action potential profiles were extracted using spike trigger averaging. A motor unit tracking algorithm was implemented to determine if tracking motor units between effort levels within a task is feasible. This algorithm matches motor units with maximally similar motor unit action potential shapes (Martinez-Valdes et al. 2017), based on two-dimensional normalized cross-correlation. The cross-correlation threshold was set to > 0.8. Only motor units that met this threshold at the end with respect to the beginning of the two efforts were considered for further analyses.

3.3.4. Force analysis

Acquired raw voltage data in X, Y, and Z direction was processed for submaximal and maximal trials. Raw voltages were low-pass filtered with a 3rd order Butterworth filter with a cut-off frequency of 15 Hz. Subsequently, they were converted to Newtons using a custom-made

program in MATLAB (MATLAB 2019b; The Mathworks, Inc.). Mean force data in Newtons that matched the most stable part of the force (i.e., HD-sEMG signals analyzed above) was quantified. Force acquired in submaximal trials was then normalized to the mean of the two maximal values quantified in task-specific MVEs. Normalized force data was used to confirm that all participants received the same amount of feedback and exerted 15%, 25%, or 50% MVE during submaximal trials.

3.4. Statistical Analyses

All statistical analyses were performed in SPSS (IBM, version 21). Due to issues with the force feedback, data from all efforts for one participant in flexion were discarded from further analyses. Before statistical comparisons, data were checked for normality and sphericity using the Shapiro-Wilk test and Mauchly's test of sphericity, respectively. Data that were not normally distributed were ln transformed. To compare classic EMG derived upper sternocostal amplitudes to HD-sEMG derived lower sternocostal amplitudes, paired two-tailed t-tests were performed within each effort level in adduction 90, internal rotation 60, adduction external 90, flexion, horizontal adduction, extension, and internal rotation 90. In adduction 60, paired two-tailed t-tests were performed in 15% and 50% MVE, and Wilcoxon Signed rank test in 25% MVE. Further, to clarify if differences between amplitudes existed for three regions, one-way repeated measures ANOVA was performed in the following tasks: extension (50% MVE), adduction 60 (15% MVE), and flexion (15% MVE) with within-subject factor *Region* (clavicular (clav), upper sternocostal (upper stern), lower sternocostal (lower stern). If significant main effects were found, posthoc comparisons with a Dunn-Bonferonni correction were performed between lower sternocostal and clavicular, and lower and upper sternocostal region. Significance was set to $p < 0.05$.

3.5 Results

3.5.1. Macroscopic level analyses (Amplitude)

In general, classic EMG derived amplitudes for the upper sternocostal region were lower than HD-sEMG derived amplitudes for the lower sternocostal region in adduction external 90 at 25% and 50% MVE and adduction 90 and internal rotation 60 at 15% and 25% MVE. When HD-sEMG amplitudes were compared between clavicular, upper, and lower sternocostal regions in extension and adduction 60, it was discovered that lower sternocostal regions activate more than the upper sternocostal regions. Lastly, no differences between classic EMG derived amplitudes and HD-sEMG derived amplitudes were quantified for horizontal adduction and internal rotation 90.

3.5.1.1 Extension

No differences existed between classic EMG derived upper sternocostal region amplitudes and HD-sEMG derived lower sternocostal region amplitudes at 50% MVE ($p = 0.14$). When comparing amplitudes between regions derived from HD-sEMG, a main effect of *Region* existed ($F_{(1.1,10.6)} = 28.1$, $p < 0.0001$; Figure 5A), such that lower sternocostal regions activated 76% more than upper sternocostal ($p < 0.0001$) and 423% more than clavicular region ($p < 0.0001$). Specifically, 9 out of 10 participants showed a propensity for high activation of the lower sternocostal region.

3.5.1.2 Adduction External 90

Normalized HD-sEMG lower sternocostal region amplitudes were statistically higher than upper sternocostal derived amplitudes (Figure 5B). Specifically, at 25% MVE, lower sternocostal

regions had 34% higher amplitude than upper sternocostal classic EMG derived amplitudes ($p < 0.001$). Similarly, at 50% MVE, HD-sEMG lower sternocostal region amplitudes were 13% higher than upper sternocostal classic EMG derived amplitudes ($p = 0.03$). In general, high activity in the lower sternocostal regions was quantified in 15 out of 18 participants at 25% MVE and 50% MVE.

3.5.1.3 Adduction 90

Normalized HD-sEMG lower sternocostal region amplitudes were statistically higher than classic EMG derived amplitudes (Figure 5C). Specifically, at 15% MVE, lower sternocostal region HD-sEMG amplitudes were 45% higher than upper sternocostal classic EMG derived amplitudes ($p < 0.001$), while at 25% MVE, lower sternocostal regions quantified from HD-sEMG had 23% higher amplitude than upper sternocostal classic EMG derived amplitudes ($p = 0.003$). At 50% MVE, no statistical differences between HD-sEMG lower sternocostal region amplitudes and upper sternocostal classic EMG derived amplitudes existed ($p = 0.5$). However, out of 18 participants, 12 showed a propensity for a greater lower sternocostal region activation in this effort.

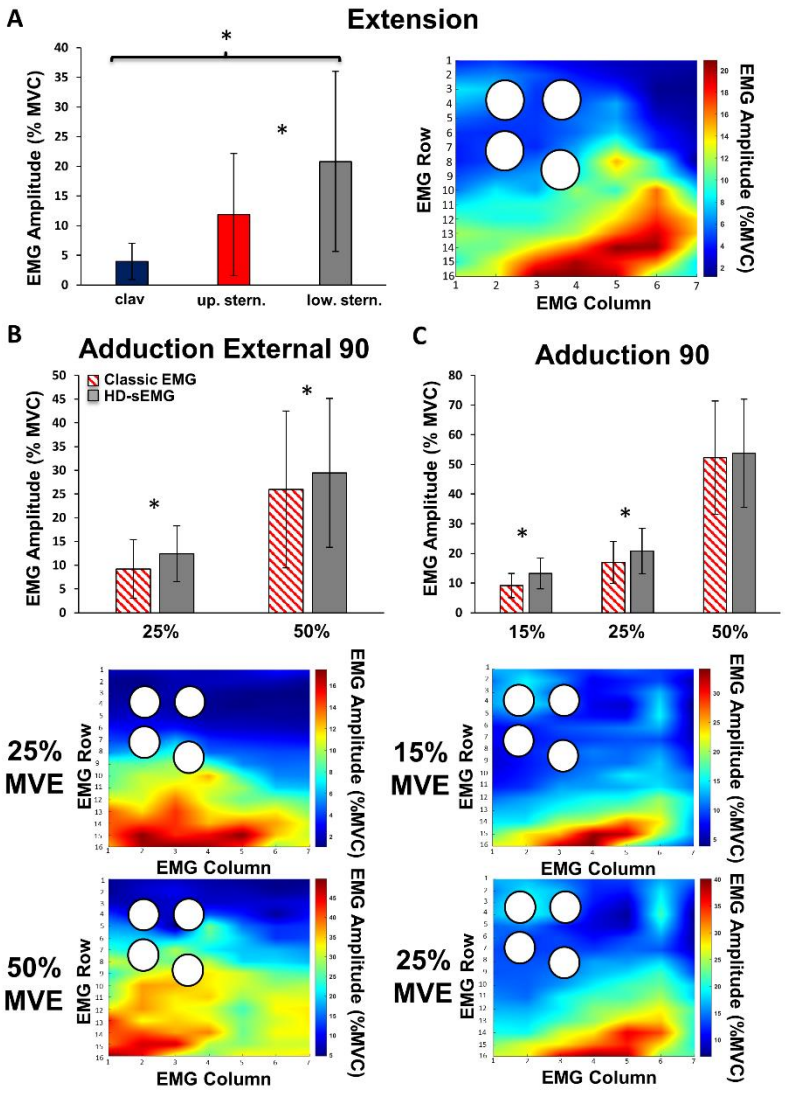

Figure 5: Mean normalized regional pectoralis major activation with standard deviations in different tasks and effort levels quantified using classic EMG or HD-sEMG paired with a representative spatial map of an example effort. **A:** Mean normalized regional pectoralis major activation in extension (HD-sEMG derived amplitudes). The lower sternocostal region activated more than the clavicular and the upper sternocostal region. A representative spatial map from a single participant shows high activation of the lower sternocostal region at 50% MVE. **B:** Comparison of classic EMG derived upper sternocostal region amplitudes with HD-sEMG derived lower sternocostal region amplitudes in adduction external 90. HD-sEMG derived amplitudes were higher in 25% and 50% MVE. Representative spatial maps from a single participant show high activation of the lower sternocostal regions in both efforts. **C:** Comparison of classic EMG derived upper sternocostal amplitudes with HD-sEMG derived lower sternocostal region amplitudes in adduction 90. HD-sEMG derived amplitudes were higher at 15% and 25% MVE, but not at 50% MVE. Representative spatial maps from a single participant show high activations of the lower sternocostal regions at 15% and 25% MVE. White circles on the spatial maps depict commonly acquired classic EMG signals from the clavicular and upper sternocostal regions. Significant differences between regions or two techniques are denoted with an asterisk (*).

3.5.1.4 Internal Rotation 60

HD-sEMG derived lower sternocostal region amplitudes were statistically higher than upper sternocostal classic EMG derived amplitudes at 15% (29%; $p < 0.001$) and 25% MVE (16%; $p = 0.03$; Figure 6A), but not at 50% MVE ($p = 0.054$). However, at 50% MVE, 10 out of 18 participants showed a propensity for a greater lower sternocostal region activation.

3.5.1.5 Adduction 60

HD-sEMG derived lower sternocostal region amplitudes were not statistically higher than upper sternocostal classic EMG derived amplitudes at 15% ($p = 0.108$) and 25% MVE ($p = 0.67$; Figure 6B). At 50% MVE, classic EMG derived sternocostal region amplitudes were 17% higher than HD-sEMG derived lower sternocostal region amplitudes ($p = 0.008$).

The interpretation of regional activation differed between the two techniques. Using classic EMG, no differences existed between clavicular and sternocostal region activity at 15% MVE ($p = 0.59$). However, comparisons of clavicular, upper, and lower sternocostal region EMG amplitudes using HD-sEMG yielded a main effect of *Region* ($F_{(1.1,19.2)} = 5.01$, $p = 0.033$). Planned comparisons showed that lower sternocostal region had higher EMG amplitudes than upper sternocostal region ($p < 0.0001$; Figure 6B), but not clavicular region ($p = 0.92$).

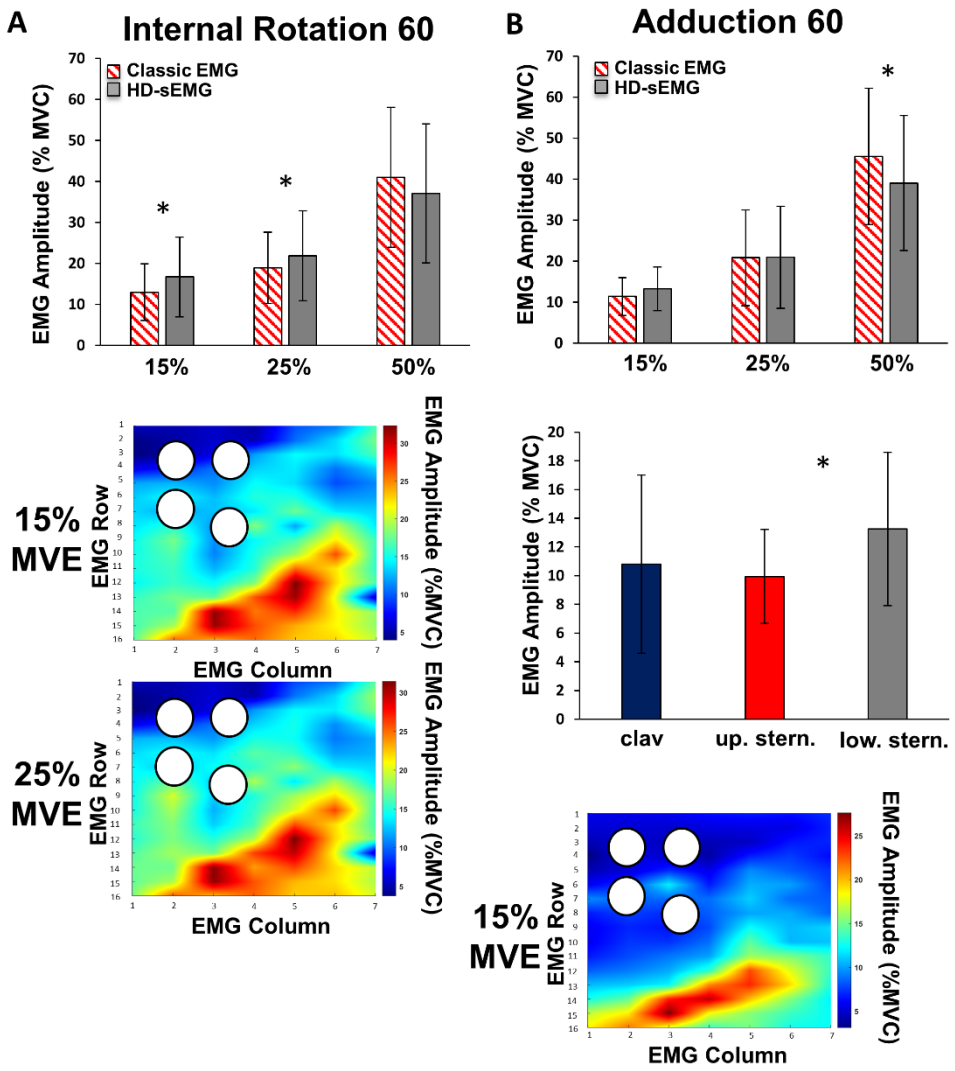

Figure 6: Mean normalized regional pectoralis major activation with standard deviations in different tasks and effort levels quantified using classic EMG or HD-sEMG paired with a representative spatial map of an example effort. **A:** Comparison of classic EMG derived upper sternocostal amplitudes with HD-sEMG derived lower sternocostal region amplitudes in internal rotation 60. HD-sEMG derived amplitudes were higher at 15% and 25% MVE, but not 50% MVE. Representative spatial maps from a single participant show high activations of the lower sternocostal regions at 15% and 25% MVE. **B:** Comparison of classic EMG derived upper sternocostal amplitudes with HD-sEMG derived lower sternocostal region amplitudes in adduction 60. Classic EMG derived amplitudes were higher at 50% MVE (top panel). Upon closer examination, the lower sternocostal regions activated more than upper sternocostal regions at 15% MVE when quantified with HD-sEMG (middle panel). Representative spatial map from a single participant at 15% MVE shows high activations of the lower sternocostal regions at these two effort levels (bottom panel). White circles on the spatial maps depict commonly acquired classic EMG signals from the clavicular and upper sternocostal regions. Significant differences between regions or two techniques are denoted with an asterisk (*).

3.5.1.6 Flexion

Classic EMG derived amplitudes were not different than HD-sEMG derived amplitudes at 15% ($p = 0.24$), 25% ($p = 0.81$), or 50% MVE ($p = 0.39$).

3.5.1.7 Internal Rotation 90

No statistically significant differences existed between classic EMG derived sternocostal region amplitudes and HD-sEMG derived lower sternocostal region amplitudes at 25% ($p = 0.58$) or 50% MVE (0.98).

3.5.1.8 Horizontal Adduction

Classic EMG derived amplitudes were not different than HD-sEMG derived amplitudes at 15% ($p = 0.73$), 25% ($p = 0.36$), or 50% MVE ($p = 0.76$).

3.5.2 Motor unit level analyses

The decomposition of HD-sEMG signals was possible in multiple participants. Specifically, pairing HD-sEMG with neural decoding could extract motor unit discharge patterns with SIL value greater than the selected threshold of 0.9, particularly at low efforts (i.e., 15 or 25% MVE). The majority of motor units successfully decomposed were in the clavicular and upper sternocostal regions (i.e., superior array). The decomposition's success depended on the task, as the motor unit yield was highest in adduction at 60 and 90, internal rotation at 60, flexion, and horizontal adduction.

The possibility to detect multiple motor units within or across efforts is presented in Figures 7 and 8. The topographical map of activation in adduction at 60 depicted in Figure 7, for instance,

shows three motor units with distinct topographical signatures. All three motor units are located near the sternum, with two motor units (2 and 3) close to the sternoclavicular joint. Additionally, finding several motor units with different topographies within different low effort levels is also feasible (Figure 8). Figure 8 also shows the widespread activity of these motor units between regions. Lastly, it is also possible to implement motor unit matching (or tracking) between low effort levels (Figure 9), allowing for an investigation into how motor units in pectoralis major contribute to an increase in effort. For example, in Figure 9, two motor units are shown in horizontal adduction. In both examples, the motor unit discharge rate did not change between effort levels.

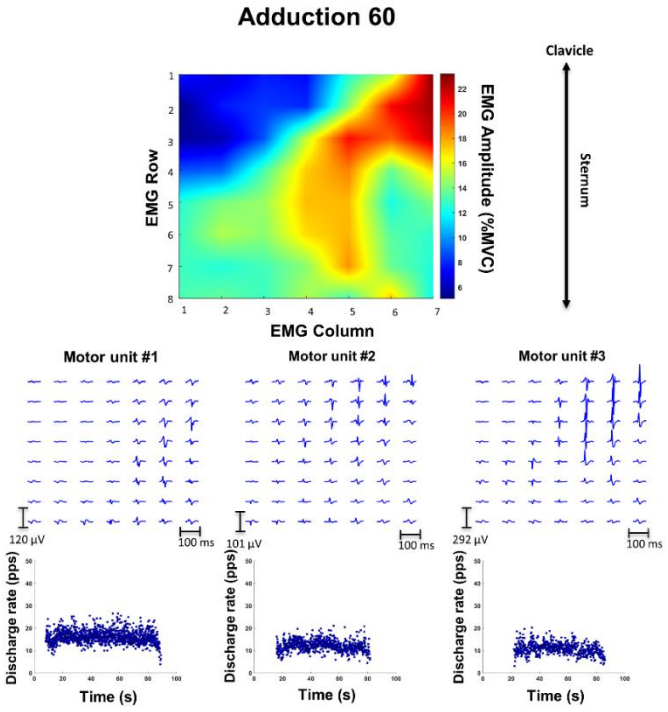

Figure 7: Spatial map of pectoralis major activation in the superior array in a single trial from a single participant in adduction 60 at 15% MVE with depictions of 2D motor unit action potential topographical distributions and motor unit discharge rates related to the motor unit. **A:** Spatial map from the superior array shows high activity in the clavicular region spreading upper sternocostal region. **B:** Examples of motor unit action potentials and discharge rates from superior array related to the spatial activation map decomposed using a convolutive blind source separation algorithm. These figures show a confined spatial distribution of motor unit action potentials without differences in the discharge rate.

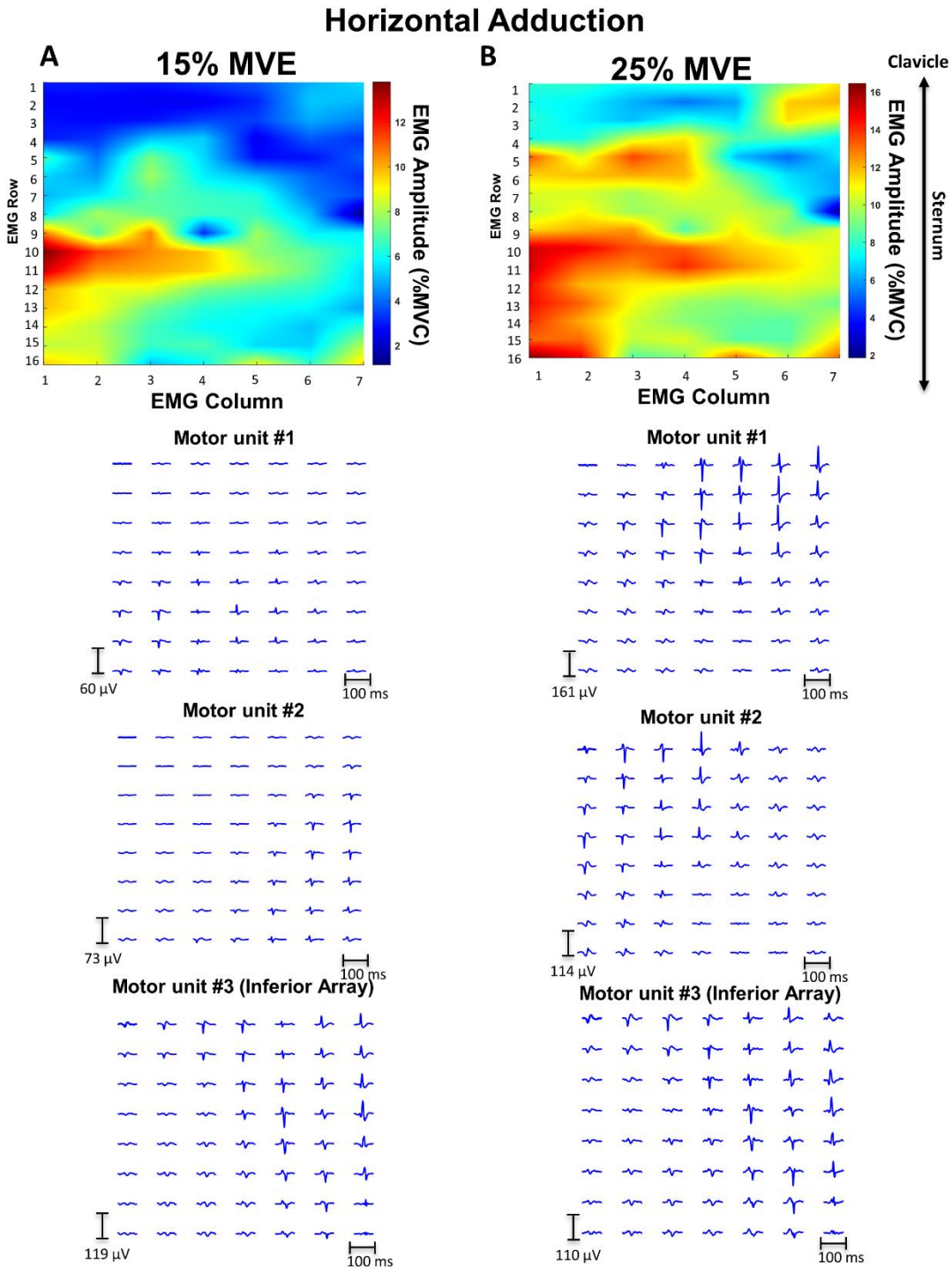

Figure 8: Spatial map of pectoralis major activation in the superior and inferior array in a single trial from a single participant in horizontal adduction at 15% MVE (**A**) and 25% MVE (**B**) with a depiction of 2D motor unit action potential topographical distributions related to the two effort levels. Motor unit action potential topographical distributions are spread throughout the whole muscle at 15% and 25% MVE.

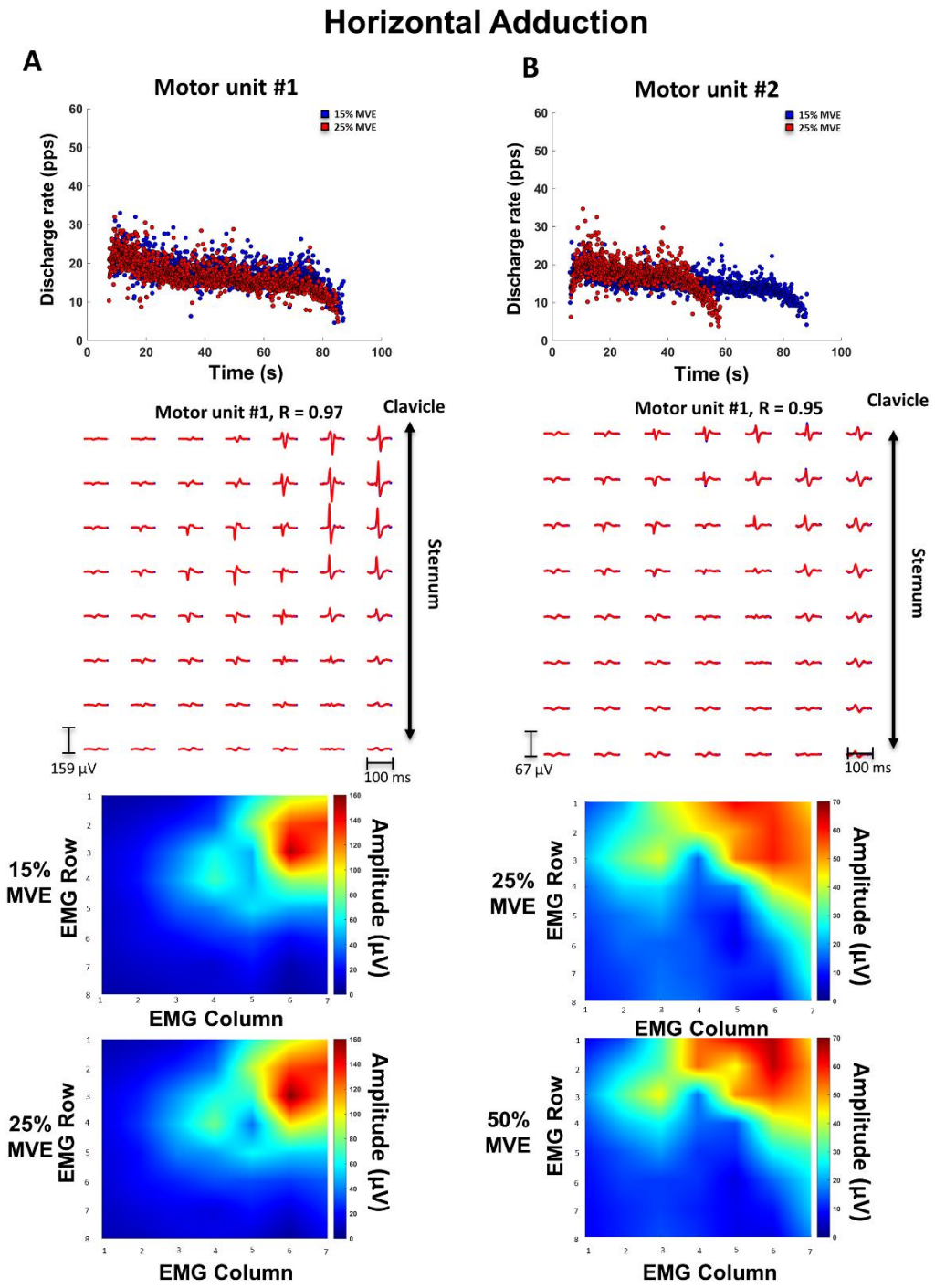

Figure 9: An example of a motor unit matching between 15% and 25% MVE (**A**) and 25% and 50% MVE (**B**) in horizontal adduction from a single participant. Motor units in both matched trials show no change in discharge rate despite the increase in effort level. These two motor units had a cross-correlation of 0.97 and 0.95 in (A) and (B). A representative motor unit action potential spatial maps for each effort level from a single participant are depicted at the bottom, showing the location and the spread of motor unit action potentials.

3.6. Discussion

This study demonstrates that pectoralis major activation is mischaracterized using standard classic EMG acquisition methods in several tasks, which rely on pectoralis major activation. Additionally, pairing HD-sEMG recordings with neural decoding provides important, complementary information on neural control aspects contributing to this activation. Therefore, a holistic framework is proposed to increase knowledge and understanding of the neuromusculoskeletal control of pectoralis major and its role in shoulder health.

3.6.1. Investigating pectoralis major activation using high-density surface electromyography

Characterization of regional pectoralis major control is not trivial, as its activation is highly dependent on the task and effort level. While several seminal EMG studies in male participants emphasized the importance of lower sternocostal regions in several arm tasks (Paton and Brown, 1994; Wickham et al. 1998; Brown et al. 2007), the acquisition of sEMG signals from these regions did not gain momentum in the scientific community. Indeed, many studies investigating pectoralis major activity still acquire sEMG signals from the clavicular and upper sternocostal regions, while some record solely from a single location (typically sternocostal; for examples, see: Schwartz et al. 2017; Dicus et al. 2018; MacLean et al. 2019; Leonardis et al. 2020; Quittman et al. 2020; Alizadeh et al. 2020). However, present findings demonstrate that the acquisition of EMG signals from two common sEMG locations mischaracterizes pectoralis major activation in at least five out of the eight tasks studied. Additionally, even at effort levels where no significant differences exist between derived bipolar and HD-sEMG amplitudes, such as at 50% MVE in adduction 90 and internal rotation at 60, multiple participants activate the lower sternocostal more than the upper

sternocostal regions. This suggests that in some tasks, high inter-subject variability in pectoralis major activation exists. These variations may be due to architectural differences in pectoralis major between individuals (Haladaj et al. 2019). Therefore, to mitigate these mischaracterizations and capture the whole muscle's activity, sEMG should also be acquired from lower sternocostal regions.

In some instances, sampling from small muscle regions can lead to misestimations in pectoralis major activity. For example, in adduction 60, comparisons between clavicular and upper sternocostal regions at 15% MVE revealed no differences in activation with either classic EMG or HD-sEMG method. However, when the whole muscle activity was quantified with HD-sEMG, subtle differences between the upper and lower sternocostal regions emerged in support of previous reports (Paton and Brown, 1994). Differences in activation between these two regions would not be revealed if sampled only from two superior locations. Similarly, in extension, differences between upper sternocostal (classic EMG) and lower sternocostal (HD-sEMG) amplitudes did not exist. However, the acquisition of EMG from lower sternocostal regions revealed substantially larger amplitudes than the upper sternocostal region and underestimated regional pectoralis major activation. Indeed, mechanically, lower sternocostal regions are essential in this task (Wolfe et al. 1992). Therefore, these two examples reinforce the importance of acquiring signals from multiple pectoralis major regions to avoid mischaracterizing their behaviour and function.

Indeed, several anatomical and clinical studies have alluded to the importance of lower sternocostal regions in these tasks. Architecturally, lower sternocostal regions have greater lateral pennation angles, shorter fiber bundle lengths (Fung et al. 2009), and larger adductor moment arms (Ackland et al. 2008) than the upper sternocostal and clavicular regions. As the pectoralis major

consists of a bilaminar tendon, lower sternocostal regions attach to an independent (*i.e.*, posterior) tendon. In contrast, the clavicular and upper sternocostal regions attach to the anterior tendon (Fung et al. 2009). Additionally, lower sternocostal regions also receive independent innervation by the medial pectoral nerve, while the lateral pectoral nerve branches to innervate the clavicular and upper sternocostal regions (Wickham et al. 2004; Haladaj et al. 2019).

The role of pectoralis major in arm mobility is often revealed in clinical case scenarios. For example, direct or indirect injuries to the pectoralis major contribute to substantial reductions in adduction (vertical and horizontal), internal rotation, flexion, and extension strength and inability to perform tasks (Schepsis et al., 2000; Bak et al. 2000; Provencher et al., 2010; Marsh et al., 2020). Additionally, surgical procedures that resect or disinsert pectoralis major regions elicit substantial long-term deficits in adduction, internal rotation, flexion, and extension (Leonardis et al. 2019; Mourkarbel et al. 2010; Vidt et al. 2020).

3.6.2. The importance of investigating neural and neuromuscular properties of motor units

The acquisition of whole pectoralis major activity with HD-sEMG has additional advantages in increasing knowledge on this muscle's intricate control. Pairing HD-sEMG with neural decoding can be used to gain otherwise unavailable insights into motor units' neural and neuromuscular properties in pectoralis major. In the present study, motor units with different motor unit action potential signatures were quantified across multiple tasks. For example, in horizontal adduction, the distribution of motor unit action potentials was spread throughout all muscle regions. In other tasks, such as adduction 60, motor unit action potential distribution was more confined to the muscle's specific regions. These observations suggest a potentially differential topographical spread of motor unit activations within pectoralis major regions in different tasks.

Knowledge of topographical information of motor unit action potentials in healthy individuals is essential to delineate neuromuscular or neural deficits in clinical populations. For example, the spatial distribution of motor unit action potentials can be used to determine the location and number of necessary detection points on pectoralis major for improved control of myoelectric prostheses (Kapelner et al. 2019) or rehabilitation protocols using functional electrical stimulation. Further, one of the major challenges in characterizing pectoralis major function is in its multipennate architecture. Hence, topographical distribution of motor unit action potentials may be used to estimate muscle fiber length and orientations across regions, as was demonstrated for complex facial musculature (Lapatki et al. 2006). Pectoralis major also has at least two known innervation zones (Barbero et al. 2010; Mancebo et al. 2019), which can be identified by extracting individual motor unit action potentials from HD-sEMG signals, but not from classic, low-spatial resolution EMG.

Identification of motor unit discharge rates in conjunction with neuromuscular information could be leveraged for multiple applications. For example, investigating the change in motor unit discharge rate between effort levels may be used to study the generation and control of force in this muscle. Additionally, neural decoding can be used to develop novel upper extremity neuromechanical models for estimating mechanical function from motor unit decoding, such as those recently developed and tested for the lower limb (Sartori et al. 2017). The development of such models is particularly important in cases where raw EMG data cannot be acquired from the lower sternocostal regions, such as in females. In these cases, decoded motor neuron activity from the clavicular and upper sternocostal regions, for example, could be used to predict neuromusculoskeletal control of lower sternocostal regions, as well as augment currently available shoulder biomechanical models (Dickerson et al. 2007).

3.7 Limitations

This study had some limitations. The study included only young males, and therefore, findings may not transfer to females, aging, or clinical population. The setup did not have an arm brace to fix the elbow into 90° of flexion. However, the investigators observed all trials to ensure posture maintenance, and in cases when this did not occur, the trial was repeated. Crosstalk from the surrounding muscles, such as the pectoralis minor, serratus anterior, external obliques, or intercostal muscles, may have influenced the patterns of regional activation quantified in this study. Attempts were made to minimize the degree of crosstalk by sampling EMG from many closely spaced electrodes (10 mm interelectrode distance) and quantifying differential derivation in the post-processing steps. Challenges existed in acquiring HD-sEMG signals from the whole abdominal region, specifically below the nipple and approximately over the floating ribs. This was due to the design of the HD-sEMG arrays, which were not produced to accommodate the curvature of the chest. Lastly, it is known that the pectoralis major consists of at least two innervation zones (Barbero et al. 2012; Mancebo et al. 2019). Due to the challenges in quantifying the innervation zones from motor unit action potentials, the exact location of the innervation zones was challenging to determine. Therefore, this study quantified the mean normalized EMG amplitudes across innervation zones, which may have influenced the findings.

3.8 Conclusions

This paper proposes a new framework for investigating neuromusculoskeletal control of pectoralis major by combining HD-sEMG with neural decoding. The framework showed: 1) limitations in using low-spatial resolution sEMG recordings to draw inferences regarding pectoralis major activation; 2) improved characterization of pectoralis major activation using high-density sEMG recordings; and 3) ability to decode HD-sEMG into neural and neuromuscular constituents, providing a more holistic representation of pectoralis major neuromusculoskeletal

function. This approach has broad implications in an emergent fundamental understanding of arm function. It can be particularly useful to investigate alterations in neural processes in clinical populations with compromised pectoralis major integrity. Additionally, improvements in pectoralis major EMG acquisition methods may lead to better characterizations of pectoralis major's activity and, therefore, an increase in understanding the pectoralis major's function in shoulder health.

Chapter 4: Characterization of the effects of breast tissue on the amplitude and frequency spectrum of high-density electromyography signals from pectoralis major in healthy females

4.0. Abstract

Pectoralis major is essential in the performance of functional tasks. However, evaluating its electromyographic (EMG) activity in females is challenging due to the breast tissue. While EMG amplitude and mean power frequency (MNF) decrease with an increase in subcutaneous tissue, no existing data evaluated the effect of breast tissue on the EMG signal. Due to this, it is difficult to determine the cut-off point at which the estimation of EMG amplitude is no longer advisable, particularly as it pertains to the high-density EMG (HD-sEMG) in this cohort. This study's aim was twofold: (1) to determine the location at which amplitude and MNF significantly decline and if differences in this location exist between three groups with different breast tissue thicknesses; and (2) to provide guidelines for investigating pectoralis major activity in females. Twenty healthy, right-hand dominant females (22.4 ± 2.2 years) were divided into three groups based on breast tissue thickness: Cup A (<7 cm); cup B (7 to 10 cm); and Cup C/D/DD (>10 cm). Pectoralis major activity was acquired using two HD-sEMG arrays in two tasks: adduction 60 and adduction 90, at two effort levels: 25% and 50% scaled to the task-specific maximal voluntary effort (MVE). The root mean square was quantified at baseline and in the hold phase of the task for each HD-sEMG channel. MNF was quantified for the hold phase of the task for each HD-sEMG channel. Subsequently, mean amplitude and MNF across seven channels for each row were quantified, and the pectoralis major was divided into four regions: clavicular, first, second, and third sternocostal. MNF increased in the inferior array, irrespective of the group. The location (i.e., HD-sEMG row) at which MNF increased was ~ row 8-11, depending on the group. EMG amplitude was not different between groups for any region or effort level in adduction 60 (all p >

0.05). In contrast, in adduction 90, EMG amplitudes were ~191% higher in Cup A ($p = 0.046$) and ~400% higher in Cup B ($p = 0.032$) in second sternocostal region in comparison to Cup C/D/DD at 50% MVE. In contrast, EMG amplitudes were higher only in Cup B in comparison to Cup C/D/DD at 25% MVE (~187%; $p = 0.022$). Current findings indicate that HD-sEMG signals acquired from the inferior array have low, inconsistent amplitudes and high mean power frequency. Therefore, the acquisition of EMG from this location is not advisable in females.

4.1. Introduction

Pectoralis major plays a fundamental role in humeral mobility, stability, and overall shoulder health. However, in females, an overlying, non-evenly distributed breast tissue layer complicates the evaluation of pectoralis major activation using surface electromyography (sEMG). During a muscle contraction, electrical signals are low-pass filtered and attenuated as they pass through the medium of subcutaneous and connective tissue (Gath and Stalberg, 1977; Lindstrom and Magnusson, 1977; Lowery et al., 2002; Farina et al., 2004; De Luca, 1979; Fuglevand et al., 1992; Al Harrach et al., 2017). Therefore, the greater the distance between the recording electrode and the activated muscle, the larger the filtering and attenuation of the EMG signal, due to the change in the shape of motor unit action potentials (Farina and Holobar, 2016). Indeed, lower sEMG amplitudes were quantified in individuals with larger subcutaneous tissue thickness in upper trapezius (Nordaner et al., 2003), multifidus, iliocostalis (Hemingway et al., 1995), and biceps brachii (Al Harrach et al., 2017).

In females, the thickness, distribution, and composition of breast tissue changes from superior to inferior regions of the pectoralis major, making it challenging to acquire consistent signals across all regions. For instance, the size, the composition, and the distribution of the breast tissue vary between females (Coltman et al. 2018). However, the acquisition of sEMG signals from multiple pectoralis major regions is essential in fully characterizing its activity. It has differential activation dependent on the task and, in some instances, effort level (Paton and Brown, 1994; Wickham et al., 2004). The ability to acquire pectoralis major activity in females and the exact location at which EMG signals can no longer be acquired may be influenced by cup size and breast tissue distribution overlying the muscle. No existing data evaluate breast tissue's effect on the EMG signal, increasing the difficulty in determining the cut-off point (or location). The estimation of

EMG amplitude is no longer advisable, particularly as it pertains to the high-density surface electromyography (HD-sEMG). Therefore, characterizing the effect of cup size on EMG amplitude and mean power frequency is a prerequisite for evaluating the feasibility of assessing pectoralis major activation in a female cohort. The purpose of this study was to determine the location (i.e., channel row) at which the HD-sEMG signal significantly declines in amplitude and mean power frequency (MNF) and determine if group differences (i.e., based on cup size) exist. This study aimed to provide guidelines for investigating pectoralis major activity in females across broad breast tissue thicknesses (i.e., cup sizes) for different scenarios. The primary hypothesis was that females with the largest breast tissue thickness (i.e. > 10 cm) will have lower EMG amplitudes across pectoralis major regions than females with low breast tissue thickness. The secondary hypothesis was that HD-sEMG mean power frequency will be significantly less in females with large breast tissue thickness than those with low breast tissue thickness.

4.2. Methods

4.2.1. Participants

Twenty healthy, right-hand dominant females (22.4 ± 2.2 years; weight: 61.7 ± 4.7 kg; height: 164.3 ± 7.5 cm) participated in this study. Participants were recruited by word-of-mouth or using posters advertising the kinesiology, psychology, engineering, and student center building study. The inclusion criteria included healthy young (between 18-40 years old), right-hand dominant females. Females who underwent breast reconstruction or augmentation surgeries were not included in the study. All recruited females were recreationally active. Participants reported no history of musculoskeletal injury to the right arm, back, or low back pain in the past six months and no neurological disease presence. Additionally, none of the participants showed positive signs

of impingement, as determined by Apley's Scratch and Hawkin's test. This study was reviewed and received ethics clearance from the institutional office of research ethics.

Before the beginning of the study, investigators collected anthropometric data. The participant's ribcage and chest circumference were measured using a measuring tape. Ribcage circumference involved measuring around the ribcage, just under the breasts, in the area where the bra band is located. Chest circumference was measured starting from the fullest part of the participant's bust, with measuring tape wrapped around under armpits. During breast circumference measurements, extra care was taken not to compress the breast tissue. Additionally, participants were asked to self-report their band and cup size (Table 2). All participants wore a normal bra (i.e., no sports bra) to allow for placement of the HD-sEMG arrays over the muscle without compressing the breast tissue.

Table 2: Anthropometric and self-reported measurements for each participant.

Participant number	Ribcage circumference (cm)	Chest circumference (cm)	Breast thickness (cm; objective measurement)	Self-reported cup and band size
S001	74.3	86.5	12.2	34C
S002	79.6	86.6	7	34A
S003	78.3	86	7.7	36C
S004	87	103.5	16.5	32D
S005	80	96	16	34D
S006	79.4	83.5	4.1	32B
S007	77	90.6	13.6	32DD
S008	82.5	89.4	6.9	34B
S009	85.1	94.1	9	34B
S010	77	90.2	13.2	34C
S011	84.8	94	9.2	36D
S012	81	86.2	5.2	32B
S013	81.5	90.3	8.8	32A
S014	87.2	93.5	6.3	34B
S015	73.7	89	15.3	32B
S016	78.7	81.9	3.2	32B
S017	84	87.2	3.2	34B
S018	80.9	89.6	8.7	32DD
S019	80.4	96.3	15.9	28A

4.2.2. High-density surface electromyography

High-density surface electromyography was acquired from pectoralis major in two tasks at two effort levels. Two HD-sEMG arrays consisting of 64 electrodes each (ELSCH064NM3, OTBioelecttronica, Torino, Italy) recorded pectoralis major activation in monopolar mode (Figure 10A). Arrays consisted of electrodes in an 8 by 8 matrix with an inter-electrode distance of 10 mm. Before applying the arrays, the pectoral area was cleaned with abrasive paste and water to reduce impedance. The electrode arrays were applied on the skin using 1 mm thick two-sided adhesive foam with holes filled with an electroconductive gel that corresponds to the electrode surface. The superior HD-sEMG electrode was placed ~2 cm inferior to the clavicle, with ~15% mediolateral

distance from the sternum. The second HD-sEMG electrode array was placed directly below the superior one (i.e., touching the first array). The arrays were fixed with adhesive tape and connected to a 128 channel EMG amplifier (EMGUSB2+, OTBioelecttronica, Torino, Italy). One wet reference electrode was wrapped around the participant's right wrist, and a reference electrode was placed on the right clavicle. All signals were bandpass filtered with cut off frequency between 10 – 500 Hz and sampled at 2048 Hz with a 12-bit A/D converter (5V dynamic range). HD-sEMG signals were amplified by a factor between 100-5000 V/V depending on the task, effort level, and participant. The saturation level for 128 channels was monitored online by OTBioLab software (OTBioelecttronica, Torino, Italy). In case more than ten channels were saturated during task performance, the trial was terminated, gain adjusted, and the trial repeated.

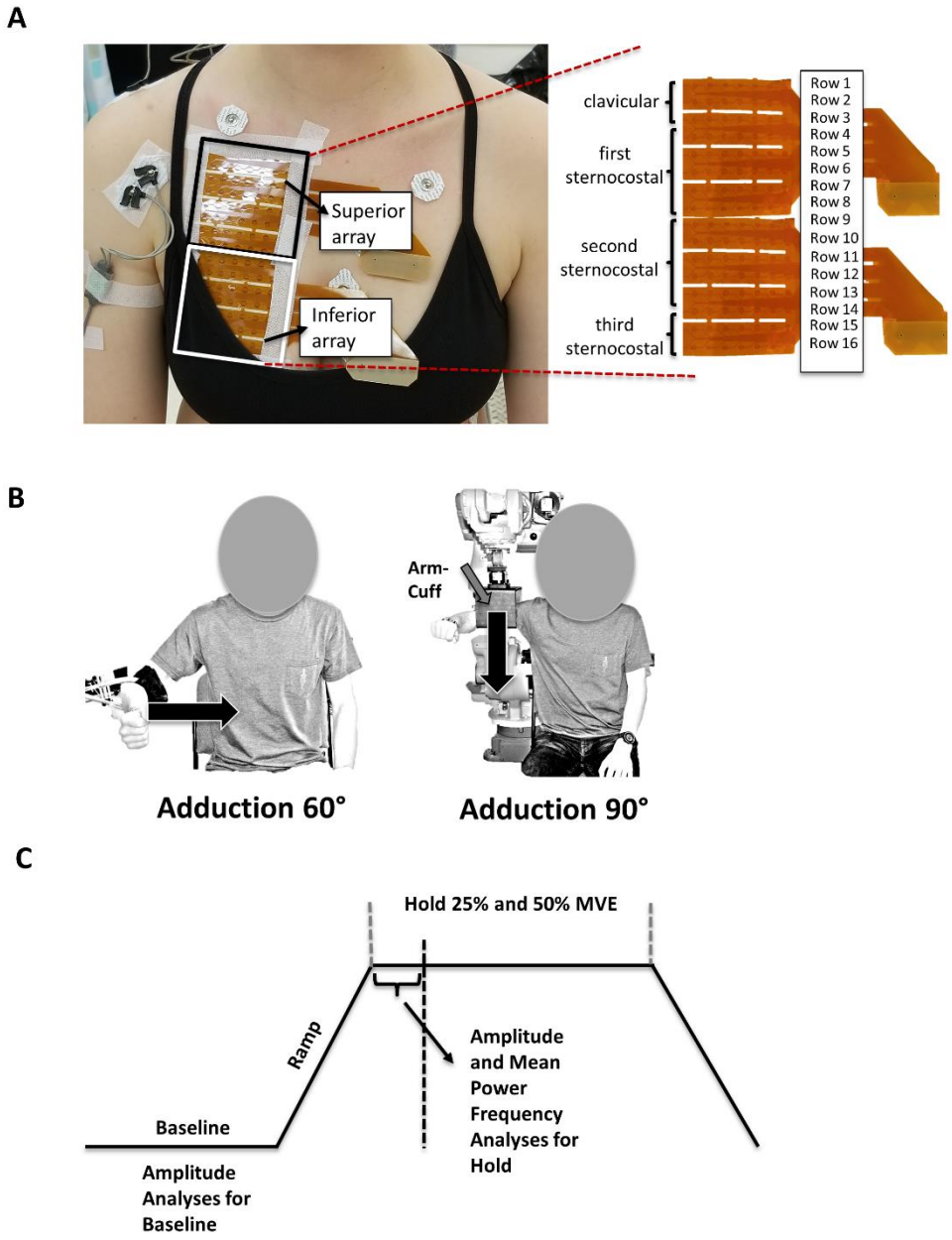

Figure 10: Schematic of experimental setup and protocol. **A:** Two 64 channel high-density surface electromyography arrays were placed on the breast overlying the pectoralis major. The top array represents the superior array, while the bottom array represents the inferior array. Each array consists of 64 channels (a total of 16 rows for two HD-sEMG arrays). Arrays were divided into pectoralis major regions, with rows 1-3 representing clavicular; 4-8 representing first sternocostal; 9-13 representing second sternocostal; and 14-16 representing a third sternocostal region. **B:** Participants performed submaximal efforts in two tasks: adduction at 60 (left) and adduction at 90 (right). **C:** Participants performed ramped submaximal tasks at 25% and 50% MVE. Amplitude measures were quantified from the baseline and hold. Mean power frequency was quantified in the hold phase.

4.2.3. Force measurement

The raw voltage from the transducer was acquired simultaneously with HD-sEMG as participants exerted effort against a custom-built arm-cuff attached to a six-degree of a freedom force transducer (MC3A, AMTI MA, USA) mounted on a robotic arm (Motoman Robotics Division, Yaskawa America, USA). The sampling rate was set to 1500 Hz and amplified (1000x) using VICON Nexus 1.7.1 software.

4.2.4. Electrocardiography measurement (ECG)

Concurrently with HD-sEMG measures, electrocardiography (ECG) was acquired for each participant using silver-silver chloride (Ag-AgCl) disposable electrodes in a monopolar configuration. Three electrodes were placed over the left chest at the 6^{th} costal level, approximately along the anterior axillary line, and medially at the sternocostalis junction (Drake and Callaghan, 2006). Before the placement of the electrodes, the area was shaved and cleaned with abrasive gel and water. A reference electrode was placed on the right acromion. ECG was collected using a wireless telemetered system (Noraxon Telemyo 2400 T G2 Noraxon, Arizona, USA). Raw signals were band-pass filtered from 10-1000 Hz and differentially amplified with a CMRR > 100dB and an input impedance of 100 MΩ. Analog signals were converted to digital using a 16-bit A/D card with a ±10 V range. The sampling frequency was 1500 Hz.

4.2.5. Experimental protocol

Experimental protocol included a performance of task-specific maximal voluntary efforts (MVE) and isometric ramped submaximal trials in two tasks at two effort levels. Before the experimental protocol, all participants underwent a brief warm-up and training on how to elicit MVE, after which they practiced submaximal efforts against the arm cuff with real-time visual

force feedback provided on a monitor. This training served to precondition the muscle-tendon unit (Maganaris et al., 2002). Following this, participants performed two task-specific 5-second MVEs in the following tasks: a) adduction from 60° of humeral abduction, and b) adduction from 90° of humeral abduction (Figure 10B). During MVE's performance, participants were verbally encouraged by the investigators. Each MVE was separated by 2 minutes of rest. Maximal MVE values were quantified using a custom-made program in LabVIEW (National Instruments, version 3.1). For each task, the mean of two MVE trials was used to scale all submaximal trials within that task.

Participants performed submaximal ramped isometric efforts scaled to 25% and 50% task-specific MVE. Each effort level was performed twice and lasted 60 and 30 seconds, respectively, with 3 to 5-minute rest breaks implemented between the trials. Participants were encouraged to report feelings of fatigue and the need for longer rest periods. The submaximal trial included rest at the beginning of the trial, a ramp-up, hold, and ramp down (Figure 10C). The rate of the ramp was ~2% MVE/s for 25% MVE and ~3% MVE/s for 50% MVE. For each trial, participants were provided with visual feedback of the required force output on a monitor and live feedback of the level of force exerted to enable matching. Tasks and effort levels were fully randomized between participants, while each effort level was repeated twice consecutively.

4.3 Data Analysis

4.3.1. Breast tissue thickness (Anthropometrics)

Breast tissue thickness was quantified by taking the difference between chest and ribcage circumference. This measurement was then used to divide the sample into three groups: Cup A

(breast tissue thickness: less than 7 cm); cup B (breast tissue thickness: between 7 to 10 cm); and Cup C/D/DD (breast tissue thickness: more than 10 cm).

4.3.2. High-density surface electromyography signal processing

Signal processing involved multiple stages. Before any analyses, all 128 HD-sEMG channels were inspected for artifacts using a custom-made MATLAB program (MATLAB 2019b; Mathworks, Inc.). Channel was tagged and removed if it contained movement artifacts, was saturated, or had insufficient skin contact (i.e., no signal detected). These channels were subsequently interpolated in data analyses. One participant's data could not be used due to the technical issues with HD-sEMG signal acquisition, and hence, their data were excluded from further analyses. Following visual inspection of the signals, acquired ECG was interpolated to 2048 Hz. The HD-sEMG signals in submaximal trials were cross-correlated with the ECG data to match the timing of the peak amplitude of each heartbeat. Each trial was visually inspected to ensure the heart rate peaks were correctly recognized by the algorithm (Figure 11A). The precise timing of each ECG peak surrounded by 250-millisecond windows before and after the peak was determined and used to avoid the quantification bias of the root mean square (RMS) amplitude and mean power frequency (MNF). Raw HD-sEMG data were band-pass filtered with a 3rd order Butterworth filter (20-500 Hz), and differential derivation was quantified from left to right (i.e., from axilla towards sternum). RMS and MNF were quantified for each differential channel, as described below.

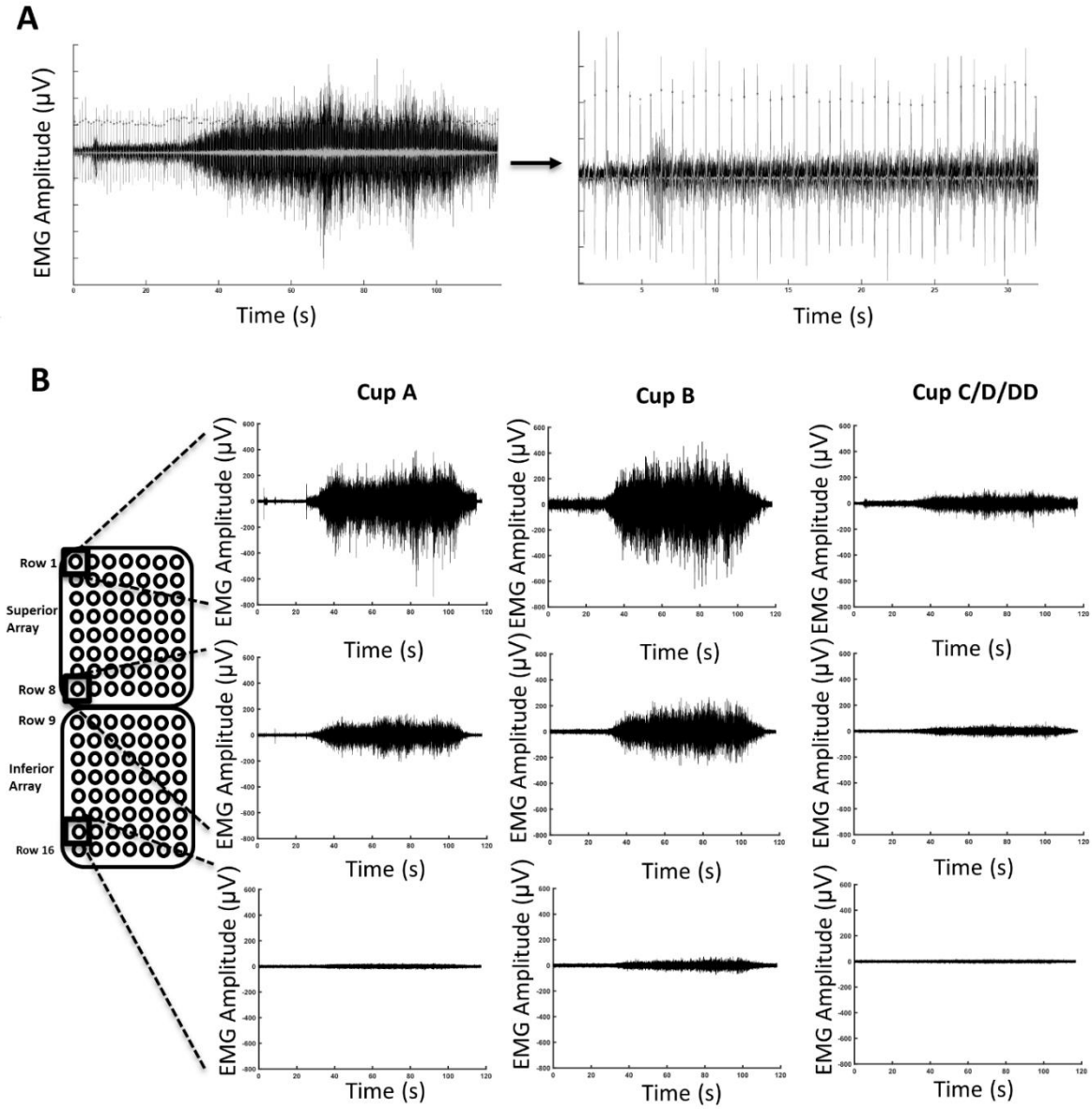

Figure 11: Example of ECG removal and differential EMG amplitudes for each group across the two high-density surface electromyography arrays. **A:** Electrocardiography measures were interpolated to 2048 Hz to match HD-sEMG sampling frequency. The HD-sEMG submaximal signals were cross-correlated with the ECG to match the timing of the peak amplitude of each heartbeat (figure on the left). Each trial was visually inspected to ensure the heart rate peaks were correctly recognized by the algorithm (figure on the right). **B:** Example of differential HD-sEMG signals from the first and fiftieth channel of the superior array and forty-third channel of the inferior array for one participant in each of the three groups (all data to scale). Reductions in raw EMG amplitude can be observed from superior to an inferior array and between groups, particularly Cup A/Cup B, in comparison to Cup C/D/DD. Note the lack of EMG signal in the inferior array.

4.3.3. HD-sEMG amplitude

Amplitude analyses involved quantifying two measures: 3-second amplitude of the signal at the baseline (i.e., before ramp-up) and 3-second amplitude of the signal in the hold phase (Figure 10C). For the hold phase, the resultant force was used to focus on the first quarter of the hold (Figure 10C). In both baseline and hold phase, the most stable part was selected by dividing the resultant force into 3-second segments and performing EMG analyses on the segment with the lowest coefficient of variation in force.

A thresholding technique was used to determine if the hold's EMG signal was larger than the baseline. The signal amplitude within the hold phase had to be two times greater than the baseline. The difference between EMG amplitude at baseline and hold was quantified for each channel to determine if the hold phase's amplitude is larger than two times the baseline noise, yielding 112 data points across two arrays. Mean across seven channels within each row was then quantified for each trial and effort level within each task, yielding a total of 16 amplitude measures corresponding to 16 rows across two HD-sEMG arrays. Subsequently, each trial was divided into clavicular (rows 1-3), first sternocostal (rows 4-8), second sternocostal (rows 9 – 13), and third sternocostal (rows 14-16) region (Figure 10A). The overall division of the pectoralis major signals into the clavicular and sternocostal region was based on the landmarks from Fung et al. 2009. The sternocostal region's subsequent divisions into three parts were performed to divide the first and second array. The mean of the two trials within each effort level and the task was determined for each region.

4.3.4. Mean power frequency

Mean power frequency was quantified on the same 3 seconds of data as the EMG amplitude in the hold phase. Mean power frequency was quantified using Welch's power spectral density estimate. Segments were windowed with a rectangular non-overlapping window. Following this, the mean of the mean power frequency measure for each row of the HD-sEMG array was determined.

4.3.5. Mean power frequency cut-off for HD-sEMG arrays

The mean power frequency values were closely examined for each cup group to determine the exact row of channels at which MNF was consistent. A changepoint statistic was implemented in a custom-made program in MATLAB on the standard deviation within each group to determine the statistically significant point of this change. The changepoint statistic determines the location at which the signal changes abruptly.

4.3.6. Mean power frequency as a cut-off for individual data

Similarly to the above, the statistical changepoint was applied to individual data within an effort, task, and group. This was performed to determine if the statistical changepoint method can be used on individual data. This may be of importance in clinical cohorts, where analyses of individual data may be necessary. The output for each participant was compared to the statistical changepoint detected in the group data. Success was judged if the statistical changepoint location determined within an individual matched that of the group level location plus/minus an additional row.

4.4. Statistical Analyses

The changepoint statistic was applied to the standard deviation of the mean power frequency for each group and each participant, task, and effort level to determine the significant changes in MNF of the signal across rows. This statistic determines the point at which the mean power frequency standard deviation changes significantly between the rows of channels. Group differences in EMG amplitude were tested. A non-parametric Kruskal Wallis test was used to determine differences in amplitude between *Groups* (Cup A, Cup B, Cup C/D/DD) for each *Region* (clavicular, first, second, and third sternocostal). If significant differences between groups existed, the Mann-Whitney U test with Dunn-Bonferonni correction was used as a post-doc to determine between which group significant differences existed. Significance was set to $p < 0.05$.

4.5. Results

4.5.1. Mean power frequency (Group and individual levels)

In general, mean power frequency had a consistent pattern across the rows in the superior array but changed significantly in the inferior array. In the superior array, the range of mean power frequencies was between 57 to 87 Hz for adduction 60 and 63 to 119 Hz for adduction 90 at both efforts. In the inferior array, mean power frequency increased in adduction 60 and adduction 90. As determined by the changepoint statistic, the cut-off depended on the task and cup group but was similar between effort levels (Table 3; Figures 12A-D denoted by arrows). For Cup A, mean power frequency statistically increased after row 9 (i.e., inferior array; middle sternocostal region) in both tasks and effort levels (denoted by arrows in Figure 12). In Cup B, mean power frequency statistically increased after row 11 (i.e., inferior array; middle sternocostal region). In contrast, in cup C/D/DD, mean power frequency increased after row 8 (last row of the superior array) and 9

(first row of an inferior array) at 25% and 50% MVE, respectively (denoted by arrows in Figure 12).

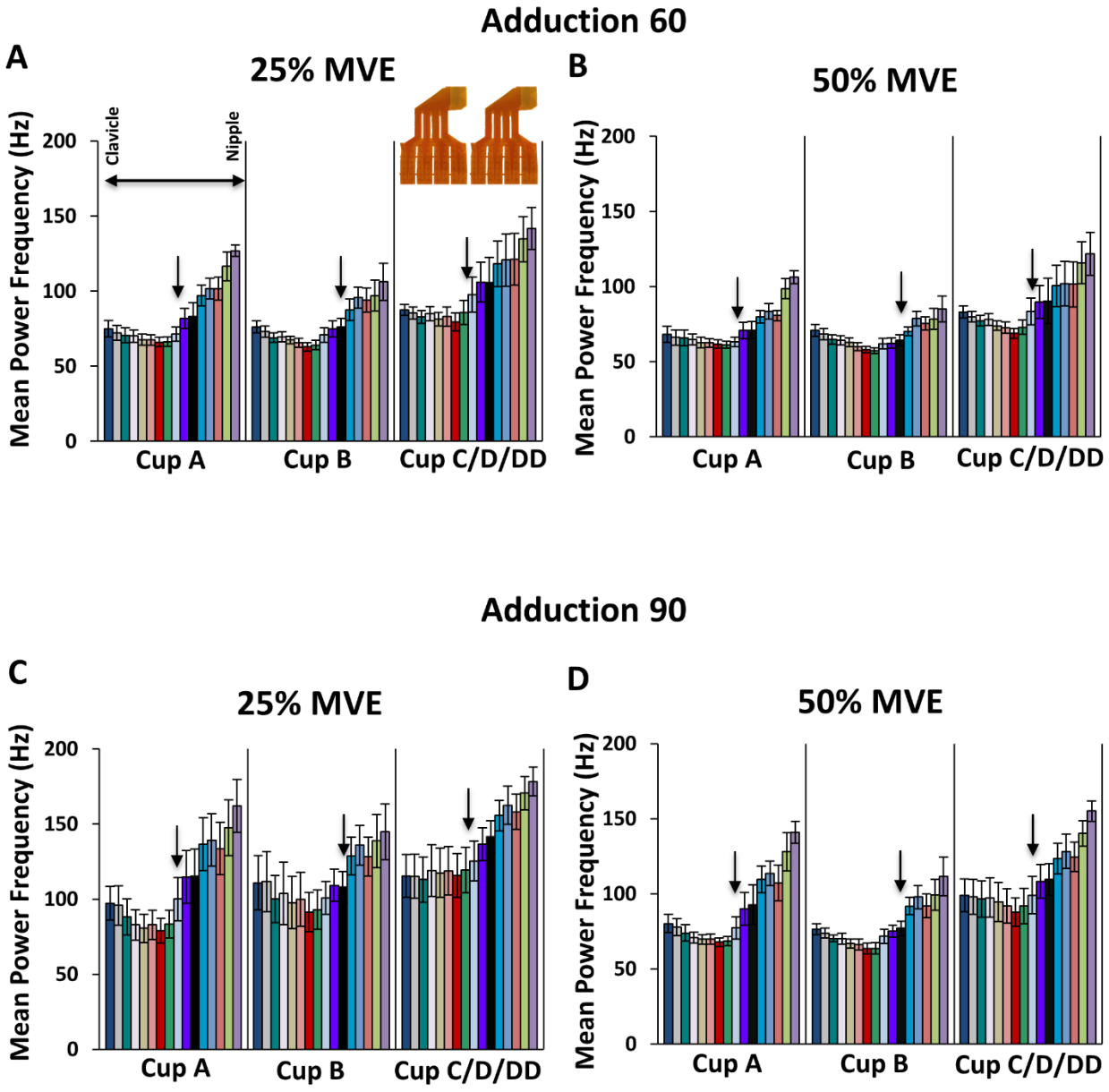

Figure 12: Mean power frequency in adduction 60 (**A** and **B**) and adduction 90 (**C** and **D**) at 25% and 50% MVE across three groups for each row of HD-sEMG superior and inferior array. The first row for each group is closest to the clavicle, while the last row is closest to the nipple. Mean power frequency is constant within the superior array irrespective of the group, task, and effort level. However, mean power frequency increases in an inferior array in all groups, tasks, and efforts. Arrows within each group depict the row at which statistical changepoint detected significant changes in mean power frequency.

Table 3: Group-level analyses in mean power frequency for each task, effort level, and group. The table depicts the cut-off row for EMG measurement as determined by the changepoint statistic for each task, effort level, and group. MNF: mean power frequency. Rows 1 through 8: superior array; rows 9 through 16: inferior array.

Task	Effort Level	Group	MNF row number cut-off (last accepted)
ADD60	25%	Cup A	9
		Cup B	11
		Cup C/D/DD	8
ADD60	50%	Cup A	9
		Cup B	11
		Cup C/D/DD	9
ADD90	25%	Cup A	9
		Cup B	11
		Cup C/D/DD	8
ADD90	50%	Cup A	9
		Cup B	11
		Cup C/D/DD	9

In addition to group-level analyses, statistical changepoints identified were similar between group and individual level analyses if the mean power frequency values followed a similar pattern across the two arrays (Figure 13). This pattern was defined as the mean power frequency between 50 to 100 Hz in the superior array (rows 1 through 8) and an increase in mean power frequency (more than ~100 Hz) in the inferior array (Supplementary Figure 1). In a few individuals, however, the statistical changepoint detected on the individual level did not match that of the group (see Figure 13D, participant 1). The mean power frequency in these participants was high (typically MNF > 100 Hz) in the first several rows of the superior array. In such cases, raw EMG data should be more thoroughly inspected to determine the source of the data's noise and usability.

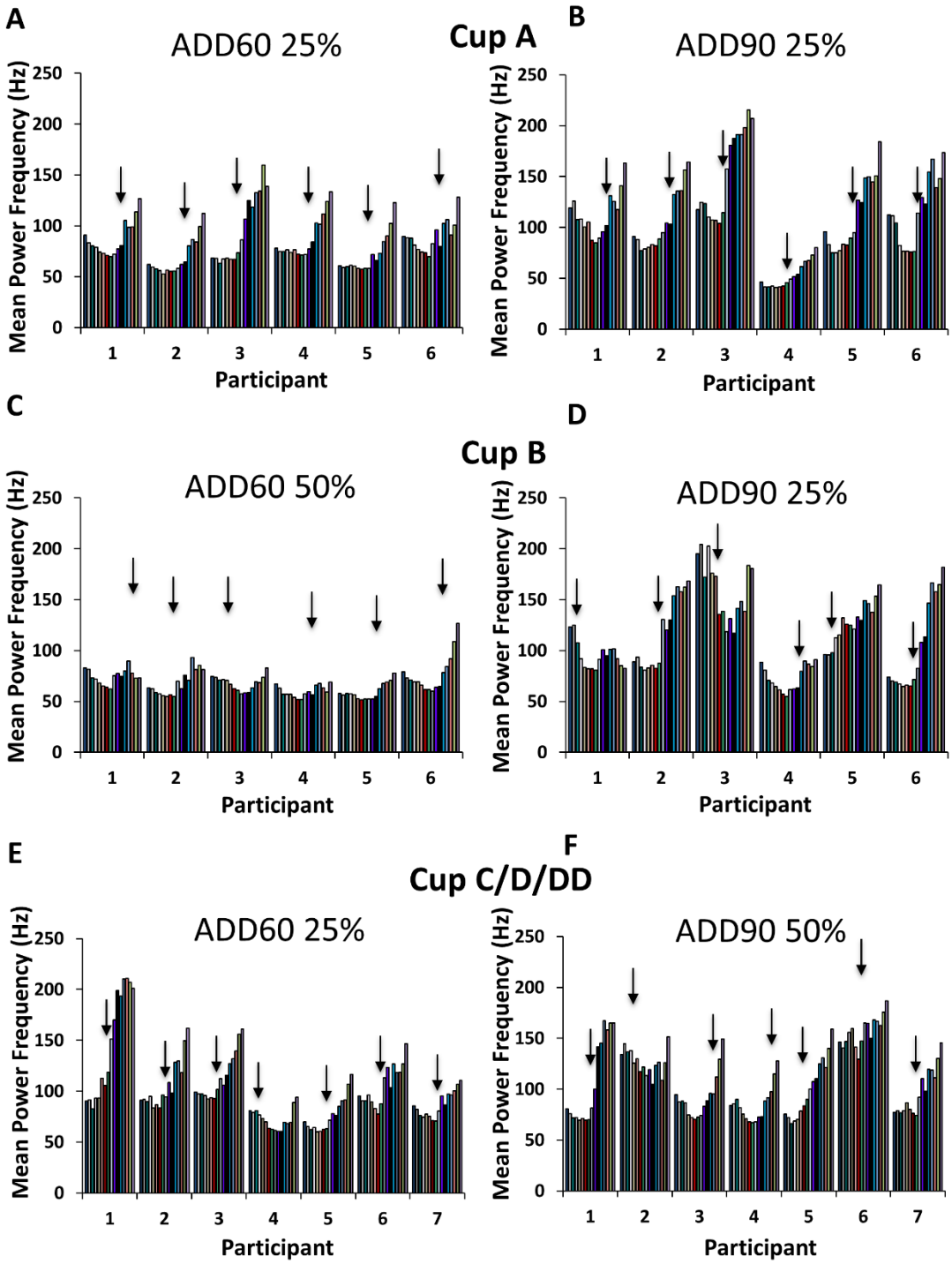

Figure 13: Mean individual mean power frequency examples for each group for a specific task and effort level. Arrows indicate the row at which the statistical changepoint detected significant mean power frequency changes within an individual. Please note interindividual variability in mean power frequency and statistical changepoint location.

4.5.2. Group differences in EMG amplitude

No differences in EMG amplitude existed between groups at 25% or 50% MVE in adduction at 60° task (all $p > 0.05$; Figure 14A). In adduction at 90°, differences between groups for second sternocostal region existed at 25% MVE ($p = 0.047$) and 50% MVE ($p = 0.045$), but not other regions (all $p > 0.05$; Figure 14B). Second sternocostal region amplitudes were 187% higher in Cup B group than Cup C/D/DD group at both 25% MVE ($p = 0.022$) and ~400% higher at 50% MVE ($p = 0.032$). Further, second sternocostal region amplitudes were also ~191% higher in Cup A than Cup C/D/DD ($p = 0.046$) at 50% MVE.

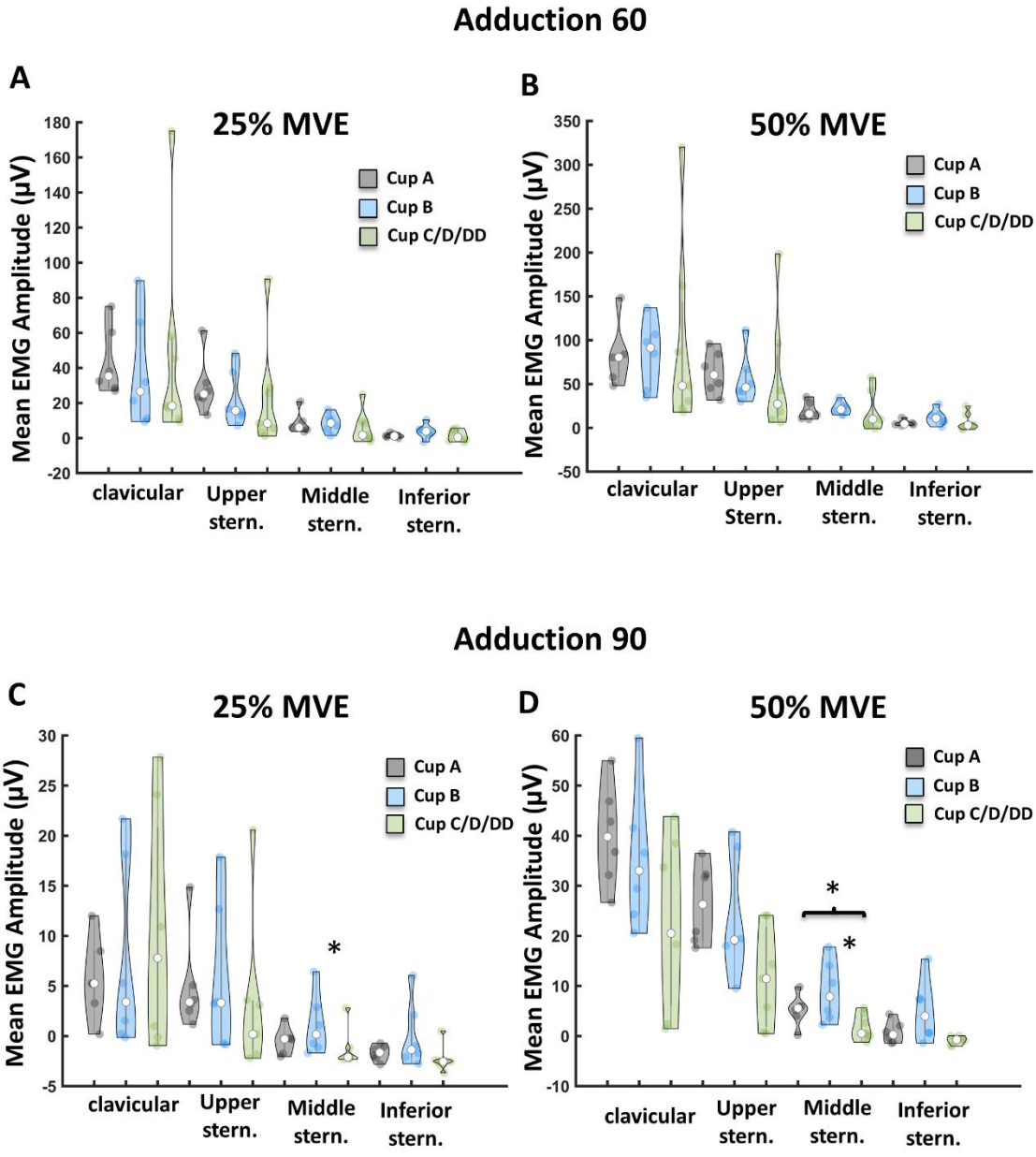

Figure 14: Violin plots for EMG amplitude with individual scatter points for each pectoralis major region across groups, tasks, and effort levels. **A** and **B**: No significant differences between groups exist in EMG amplitude in the four regions at two efforts in adduction 60. **C** and **D**: In adduction 90, differences between groups emerged for the middle sternocostal region. Significant differences are denoted by an asterisk (*). Negative amplitude values indicate a larger inherent noise than the EMG signal. Cup A: gray; Cup B: blue; Cup C/D/DD: green. White circles in the middle of violin plots denote median.

4.6. Discussion

This is the first study to evaluate breast tissue's influence on HD-sEMG amplitude and mean power frequency and provide evidence-based guidelines for recording and characterizing pectoralis major activation in females using HD-sEMG. Further, it confirms the feasibility of detecting HD-sEMG amplitudes from a superior HD-sEMG array, irrespective of the cup size.

4.6.1. Increase in mean power frequency in inferior HD-sEMG array

Stable mean power frequency existed in the superior array, but a progressive increase in HD-sEMG mean power frequency occurred in the inferior array. This finding contrasts with previous research, which demonstrated declines in mean power frequency with increases in subcutaneous tissue thickness (Farina et al. 2002b; Cescon et al. 2008; Minetto et al. 2013). It is possible that despite thick subcutaneous tissue overlying the muscles in these studies, the EMG signal, although low in amplitude, remained higher than the level of internal noise. In the present study, visual inspection of the EMG amplitude in the inferior array confirmed the lack of EMG signal and a substantial increase in internal noise, particularly in the bottom parts of the inferior array (see Figure 11). Therefore, the estimate of the mean power frequency in the inferior array is not of the EMG signal but internal noise.

Commonly, high mean power frequency was attributed to increases in muscle fiber conduction velocity (Andreassen and Arendt-Nielsen, 1987), motor unit recruitment, and differences in muscle fiber type (von Tscharner and Nigg, 2008). However, EMG spectral properties do not provide information regarding motor unit recruitment or muscle fiber type (Farina, 2008). Additionally, pectoralis major regions consist of predominantly Type II fibers

(Johnson et al., 1973; Srinivasan et al., 2007). Therefore, increases in mean power frequency in the inferior array are not likely due to the regional differences in muscle fiber type.

Quantification of mean power frequency across HD-sEMG arrays overlaying the pectoralis major in females may be used to determine the location (i.e., row of channels) at which characterization and evaluation of the EMG signal amplitude is no longer advisable. This applies across cup size groups, as the mean power frequency remained consistent across rows 1 through 8, following which it increased from rows 9 through 16, irrespective of the group. Therefore, caution is recommended when interpreting HD-sEMG signals acquired after row 8. Since the bulk of the breast tissue underlies the inferior HD-sEMG array, changes in this array's mean power frequency are expected. The breast tissue thickness progressively increases from top to bottom of the inferior array, increasing the distance between the HD-sEMG electrodes and the pectoralis major, thus filtering and attenuating the HD-sEMG signals (Farina and Holobar, 2016).

Additionally, some interindividual variability in mean power frequency values existed within each group (see Supplementary Figure 2). These differences may be due to the variability in breast tissue composition, which is influenced by body mass index, hormones, and age (Page and Steele, 1999; Vandeweyer and Hertens, 2002; Boyd et al., 2009; Coltman et al., 2018). Previous studies also demonstrated that some females have a large proportion of fibroglandular breast tissue, while others primarily contain adipose tissue (Brisson et al. 1984; Graham et al. 1995). All these factors may also influence the EMG power spectrum and may have contributed to interindividual differences in the current sample of females.

4.6.2. Group differences in amplitude

In general, the HD-sEMG amplitudes acquired from the superior HD-sEMG array were comparable across thickness groups and were not higher in Cup A as hypothesized. Differences in amplitude between groups only existed in adduction 90 at 25% and 50% MVE in the second sternocostal region. The EMG amplitude was higher in Cup B at 25% MVE, and Cup A and B compared to C/D/DD at 50% MVE. Mechanisms for these differences are unclear, as adduction 60 demonstrated no differences. Group differences in adduction 90 may be due to breast tissue composition or re-distribution of breast tissue, which is common between activities in healthy females (Gibson et al. 2019). Alternatively, it is plausible that intersubject differences in activation patterns contributed to the differences quantified between the groups in this task. For example, some participants may have activated the clavicular or upper sternocostal more than middle and inferior sternocostal regions, as well as other muscles surrounding the shoulder complex.

4.7. Limitations

Several considerations delimit the study findings. Gross anthropometric measurements were used to quantify breast tissue thickness, limiting volumetric resolution. The ultrasound machine limitations hindered the ability to quantify breast tissue thickness in all females. These limitations included inability to pair the ultrasound system with the motion tracking system to quantify the exact orientation and location of the linear transducer with respect to the sternum in post-processing steps; inability to quantify the breast tissue thickness at several locations of the breast due to the equipment limitations in adjusting the image depth to visualize the muscle fibers, particularly at the level of the nipple; and lastly, the low ultrasound image quality, hampering the ability to precisely determine the boundaries of skin and breast tissue, as well as breast tissue and

muscle fibers. Further, skin thickness or breast tissue composition was not quantified in the current study, although these measures may influence signal characteristics (Al Harrach et al. 2017). Additionally, crosstalk from the surrounding muscles, such as the pectoralis minor, serratus anterior, external obliques, or intercostal muscles, may have influenced the patterns of regional activation quantified in this study. Attempts were made to minimize the degree of crosstalk by sampling EMG from many closely spaced electrodes (10 mm interelectrode distance) and quantifying differential derivation in the post-processing steps. Finally, this study acquired signals from healthy, young females, and hence, the results do not apply to the aging population, as the female breast changes with age (Brown et al. 1999).

4.8. Conclusions and future directions

Examining pectoralis major activation in females is challenging due to the overlying breast tissue and compounded by individual differences in breast tissue thickness and variations in the composition of this tissue overlying the muscle. Females are commonly excluded from research evaluating pectoralis major activation due to the overlying breast tissue. In the present study, HD-sEMG signals acquired at the level of the inferior array had low, inconsistent amplitudes and demonstrated a substantial increase in mean power frequency irrespective of the group in comparison to the superior array. Therefore, the acquisition of HD-sEMG signals from superior to middle regions of the pectoralis major is feasible in females, irrespective of the breast size. Additionally, a novel method is proposed (i.e., changepoint statistic) to determine the cut-off point or location at which acquisition and interpretation of the EMG signal is not advisable. This method can be applied to individual or group level mean power frequency data to determine the location at which evaluation and quantification of HD-sEMG signals are not advisable.

Chapter 5: Differential regional pectoralis major activation indicates functional diversity in healthy females

5.0 Abstract

Pectoralis major activation fundamentally enables numerous tasks. Despite its importance in arm mobility, regional pectoralis major activation in females is unknown, leading to ineffective recommendations for rehabilitation, as well as surgical decisions that biomechanically compromise shoulder health. Knowledge of regional pectoralis major activations is, therefore, crucial to inform these decisions. Regional pectoralis major activation was acquired in twenty females (22.4 ± 2.2 years) in four isometric tasks: adduction from 90° or 60° of arm abduction; adduction at 90° of abduction with 90° external rotation; and internal rotation from 60° of abduction; at three submaximal efforts: 15%, 25%, and 50% scaled to individual task-specific maximal voluntary effort. High-density surface electromyography (HD-sEMG) was used to acquire the activation of clavicular, superior, and middle sternocostal regions. Normalized regional mean root mean square amplitudes were quantified for each region. Activity between regions across effort levels was compared within each of the tasks. Differences in regional activations were dependent on the task and effort level. The clavicular and middle sternocostal region had higher EMG amplitudes than the superior sternocostal region (10-16%) in internal rotation, irrespective of the effort level. The clavicular region had higher EMG amplitudes than both sternocostal regions in adduction 60 at 15% (~19%) and 25% MVE (~17%). Middle sternocostal regions were more active than clavicular (~15%) and superior sternocostal (~22%) region at 15% MVE in adduction 90, than superior sternocostal at 25% (~15%) and 50% (~8%) MVE in adduction 90, and across all efforts in adduction external 90 (~12-44%). Lastly, in adduction 60, all three regions activated to the same magnitude at 50% MVE. These findings provide novel concepts regarding fundamental control capacities while also informing rehabilitation strategies.

5.1 Introduction

Anatomically intricate pectoralis major enables arm mobility in multiple directions facilitating various daily, work, and exercise tasks. It assists in humeral horizontal and vertical adduction, flexion, internal rotation, and extension against resistance. Anatomical findings differentiate pectoralis major into three anatomically distinct regions: clavicular, sternocostal, and abdominal (Lewis, 1901; Ashley, 1952; Wolfe et al., 1992; Fung et al., 2009). Sternocostal regions also subdivide into four anatomically divergent partitions (Fung et al. 2009), indicating possible functional differentiation (Paton and Brown, 1994).

Pectoralis major's extensive blood supply often motivates surgical harvesting as a myocutaneous flap, allowing resected regions to serve as surrogates to aid in breast reconstruction (Cemal et al., 2013; Nelson et al., 2018). These surgeries typically fail to consider the biomechanical consequences of regional disinsertion on shoulder health, focusing on cosmetic outcomes. However, long-term functional limitations such as reductions in strength, range of motion, and changes in pectoralis major material properties are frequently reported in females who underwent these surgeries (de Haan et al., 2007; Forthomme et al., 2010; Leonardis et al., 2019). As females comprise most breast reconstruction recipients, this establishes the undeniable importance of delineating regional pectoralis major contribution in tasks necessitating its activation in females.

Regional pectoralis major activation in females is unknown, as females are commonly excluded from studies evaluating pectoralis major activity due to the challenges in surface electromyography (sEMG) acquisition. However, several studies in males demonstrated that the magnitude of partitional activation depends on the task performed and effort level (Paton and Brown, 1994; Wickham et al., 2004; Wickham and Brown, 2012). For example, during adduction

at low efforts, localized activity was quantified in abdominal partitions, increasing recruitment of additional partitions at high efforts (70% MVE; Paton and Brown, 1994). Currently, it is unknown if differences in regional pectoralis major activity exist in females.

While the characterization of muscle activity using classic EMG provides some information regarding the regional activity, it is limited to sampling from a small region of the muscle and does not allow for evaluation of this activity across all accessible areas of the pectoralis major. As inferior regions are inaccessible due to the breast tissue, the acquisition of EMG signals from available locations of the pectoralis major is essential in females. High-density surface electromyography (HD-sEMG) consists of an array of electrodes. It can be used to circumvent classic EMG limitations, as it allows for sampling of muscle activity from multiple regions of the muscle simultaneously, providing high temporal and spatial resolution (Merletti et al. 2010). Therefore, this study's purpose was to characterize the pectoralis major's spatial activity using HD-sEMG in healthy, young females during low-to-moderate submaximal isometric efforts in four arm tasks. The primary hypothesis was that the middle sternocostal regions will have higher normalized EMG activity than superior sternocostal and clavicular regions in all tasks studied.

5.2 Methods

5.2.1. Participants

Twenty healthy, right-hand dominant, young females participated (22.4 ± 2.2 years; Table 4). The chosen sample size was selected using *a priori* power analyses. Sample size calculations in G*Power 3.1 (Universitat Dusseldorf, Dusseldorf, Germany) indicated that a minimum of 16 participants is required to obtain sufficient power (Cohen, 1988). The effect size chosen ($f^2 = 0.31$) is on the lower end of the observed effect size in previous studies, which reported effect sizes

between 0.2 to 0.6 (Paton and Brown, 1994; Brown et al. 2007; Wickham et al. 2004). Females were recruited using word-of-mouth and posters advertising the study in the kinesiology, engineering, psychology, and student center buildings. All recruited females were recreationally active. The inclusion criteria included healthy young (between 18-40 years old), right-hand dominant females. Females who underwent breast reconstruction or augmentation surgeries were not included in the study. All participants were free from musculoskeletal or neurological injuries in the right arm or low back pain in the past six months. Additionally, no participants tested positive for signs of impingement, as determined by Hawkin's impingement and Apley's Scratch test. All participants wore a normal bra (i.e., no sports bra) to allow electrode placement over the muscle without compressing the electrodes. Participants were instructed by the investigator not to consume any caffeinated drinks the morning of the session and drink plenty of water the day before the session. All participants refrained from engaging in strenuous physical activity for 24 hours before the session. This study received ethics clearance by the institutional office of research ethics, and all participants provided informed consent.

Initially, anthropometric measurements were collected, including height, weight, rib cage and chest circumference, clavicle, and sternum length (Table 4). Rib cage circumference was measured using a measuring tape wrapped around the rib cage, just under the breasts, in the area where the bra band is located. In contrast, chest circumference was measured starting from the fullest part of the participant's bust, with measuring tape wrapped under the axilla. Clavicle length was measured from the acromion to the sternal notch, while the sternal length was measured from the sternal notch to the palpated xiphoid process. The clavicular and sternal length were used to scale the normalized EMG data to account for differences in pectoralis major size.

Table 4: Participant demographics and anthropometric measurements (± standard deviation) for nineteen participants included in this study's analyses.

Age (years)	22.4 ± 2.3
Height (cm)	164.4 ± 7.7
Weight (kg)	62 ± 4.6
Chest circumference (cm)	90.2 ± 5.1
Ribcage circumference (cm)	80.6 ± 3.8
Breast tissue thickness at the nipple (cm)	9.5 ± 4.4
Clavicle length (cm)	15.3 ± 1.6
Sternum length (cm)	20.6 ± 2.2

5.2.2. High-density surface electromyography

HD-sEMG was acquired from a pectoralis major using two arrays in monopolar mode (ELSCH064NM3, OTBioelecttronica, Torino, Italy; Figure 15A). Each array consisted of sixty-four channels in an 8 by 8 matrix with a 10 mm inter-electrode distance. The arrays were fixed with adhesive tape and connected to a 128-channel EMG amplifier (EMGUSB2+, OTBioelecttronica, Torino, Italy). Before applying the electrodes, the pectoral area was cleaned with abrasive paste and gently cleansed with water. The electrode holes were filed with electroconductive gel, and the arrays were applied on the skin using 1 mm thick two-sided adhesive foam. The superior array was placed ~ 2 cm inferior to the clavicle, with the middle of the array located between the sternum and the axilla and parallel to muscle fibers. The inferior array was placed immediately below the superior one. All EMG signals were bandpass filtered with a cut-off frequency between 10 – 500 Hz and sampled at 2048 Hz with a 12-bit A/D converter (5V dynamic range). HD-sEMG signals were amplified by a factor between 100-5000 V/V, depending on the task and effort level. One wet reference band was wrapped around the participant's right wrist, while one reference electrode was placed on the right clavicle.

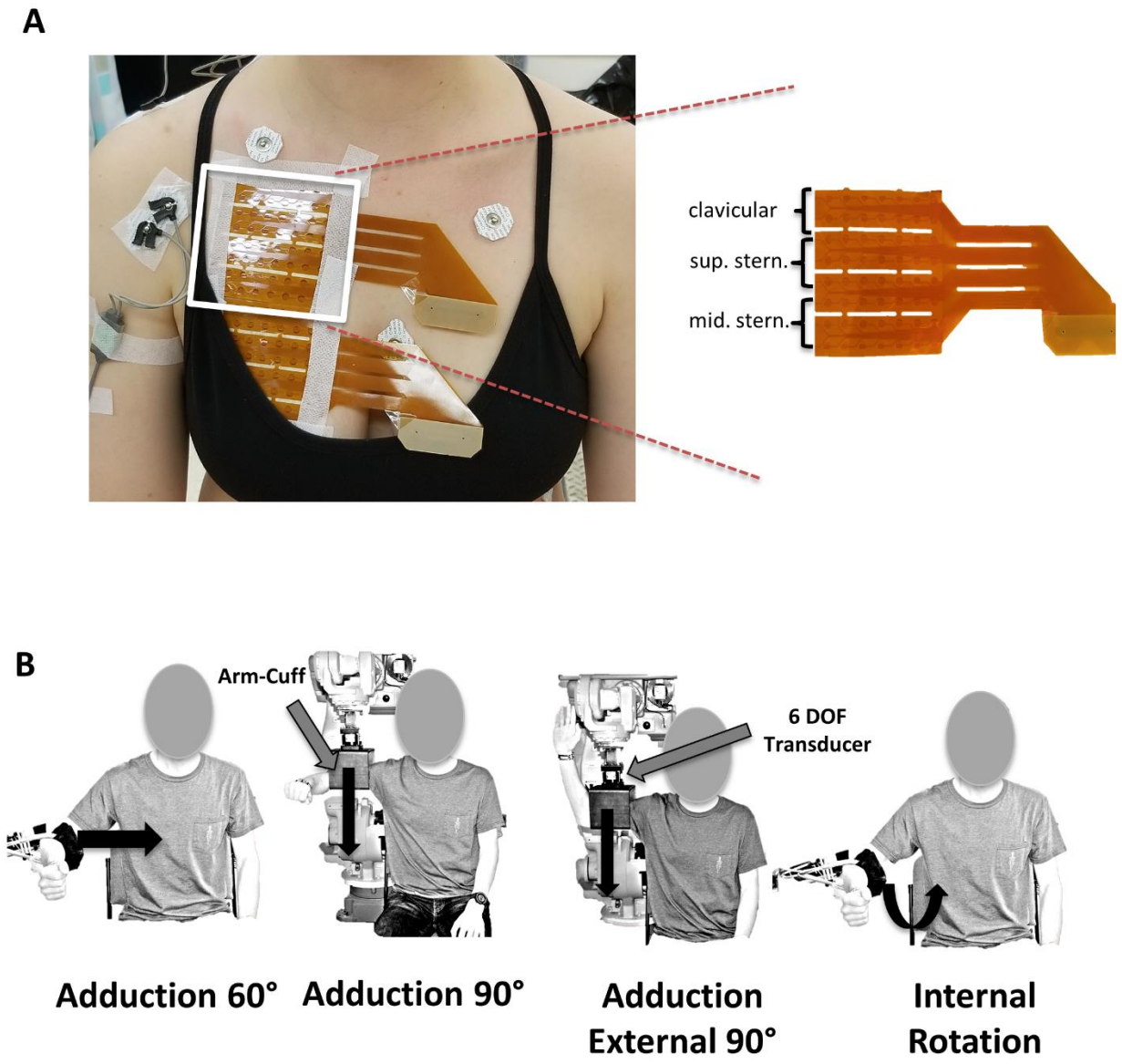

Figure 15: Location of HD-sEMG arrays and schematic of tasks investigated. **A:** Two HD-sEMG 64-channel arrays were fixed over the pectoralis major. The white square indicates a superior HD-sEMG array, which was used for analyses. Superior HD-sEMG was used for analyses divided into regions: rows 1 to 2 clavicular; 3 to 5 superior sternocostal; and 6 to 8 middle sternocostal. **B:** Tasks included adduction from 60° of abduction (ADD60), which required pulling towards the torso; adduction from 90° of abduction (ADD90), which involved pushing downwards; adduction from 90° of abduction and 90° of external rotation (ER90), which involved pushing downwards; and internal rotation from 60° of abduction (IR60), which involved medially rotating the forearm towards the torso. Black arrows indicate the direction of effort. The figure also displays the arm-cuff and the location of the six-degree-of-freedom transducer.

5.2.3. Force measurement

The raw voltage of exerted effort was acquired concurrently with the HD-sEMG signals. Participants exerted effort against a custom-built arm cuff attached to a six-degree-of-freedom transducer (MC3A, AMTI MA, USA) mounted on a robotic arm (Figure 15B; Motoman Robotics Division, Yaskawa America, USA). The sampling rate was 1500 Hz and amplified (1000x) using VICON Nexus 1.7.1 software.

5.2.4. Electrocardiography (ECG)

Electrocardiography (ECG) was acquired concurrently with HD-sEMG to eliminate the heart rate contamination in post-processing steps. ECG was recorded using silver-silver chloride (Ag-AgCl) disposable electrodes in a monopolar configuration. Three electrodes were placed over the left chest at the 6^{th} costal level, approximately along the anterior axillary line, and medially at the sternocostalis junction (Drake and Callaghan, 2006). ECG was collected using a wireless telemetered system (Noraxon Telemyo 2400 T G2 Noraxon, Arizona, USA). Raw signals were band-pass filtered from 10-1000 Hz and differentially amplified with a CMRR > 100dB and an input impedance of 100 MΩ. Analog signals were converted to digital using a 16-bit A/D card with a ±10 V range. The sampling frequency was 1500 Hz.

5.2.5. Additional shoulder muscle monitoring

The activity of six additional shoulder muscles was acquired and monitored concurrently with HD-sEMG. Upper trapezius, latissimus dorsi, deltoid (anterior, middle, and posterior), and infraspinatus activity was collected. sEMG activity was recorded using silver-silver chloride (Ag-AgCl) disposable electrodes with a 1 cm diameter and a fixed inter-electrode spacing of 2 cm in a

bipolar configuration. Before the electrode placement, the area overlying the muscle belly was shaved and cleansed with abrasive gel and water. Placement of the sEMG electrodes was confirmed with palpation while the participant exerted a low, submaximal contraction of the muscle in positions described in Supplementary Table 1 (Cram and Kasman, 1998; Kelly et al., 1996). The reference electrode was placed on the acromion. sEMG was collected using a wireless telemetered system (Noraxon Telemyo 2400 T G2 Noraxon, Arizona, USA). Raw signals were band-pass filtered from 10-1000 Hz and differentially amplified with a CMRR > 100dB and an input impedance of 100 MΩ. Analog signals were converted to digital using a 16-bit A/D card with a ±10 V range. The sampling frequency was 1500 Hz.

5.2.6. Experimental protocol

Participants performed task-specific maximal voluntary efforts (MVE) and isometric ramped submaximal trials in four tasks at three effort levels. Before the experimental protocol, all participants underwent a brief warm-up and training on how to elicit MVE, after which they practiced submaximal efforts against the arm cuff with real-time visual force feedback provided on a monitor. This training served to precondition the muscle-tendon unit (Maganaris et al., 2002) and familiarize the participant with the task. The participant sat on a chair with an upright torso with the trunk secured using a padded strap throughout all trials. The arm was secured in the cuff to minimize movement during task performance. Participants performed two 5-second task-specific MVEs in the following isometric tasks (Figure 15B): a) adduction (ADD60) and b) internal rotation (IR60) from 60° of arm abduction; c) adduction from 90° of arm abduction (ADD90); and d) adduction from 90° of arm abduction and 90° of arm external rotation (adduction external 90; ADDER90). While the majority of occupational and daily tasks rely on a combination

of arm postures and exertion directions, the tasks and effort levels chosen reflect tasks which are typically evaluated following pectoralis major compromise (see Brookham et al. 2018; Brookham et al. 2018; Leonardis et al. 2019; Lipps et al. 2019). During MVE's performance, participants were verbally encouraged by the investigators. Each MVE was separated by 2 minutes of rest. Maximal MVE values were quantified using a custom-made program in LabVIEW (National Instruments, version 3.1). The mean of two maximal task-specific MVEs was used to scale all submaximal trials within each task. During MVE performance, the off-axis forces were monitored in LabVIEW, such that at least 80% of the effort generated had to be directed in the target direction. If this was not achieved, the participant was provided with verbal feedback on the task-specific effort direction, and the trial was repeated. Additionally, if two maxima generated in MVE trials differed by more than 10 Newtons, a third trial was performed to ensure consistency between MVEs.

Participants performed three submaximal ramped isometric efforts at 15%, 25%, and 50% of the task-specific MVE. These submaximal effort levels reflect muscle activation levels required in many occupational and daily tasks. Each effort level was performed twice and lasted 60, 60, and 30 seconds, respectively, with rest breaks provided between the trials. Participants were encouraged to report feelings of fatigue and the need for longer rest periods. If requested by the participant, longer rest periods were provided. Participants ramped-up at ~2% MVE/s, maintained the effort level, and then ramped down at ~2% MVE/s. Tasks were fully randomized between participants, as well as within a participant. Effort levels were randomized within each task, with each submaximal effort performed consecutively within a task. Participants received visual feedback of the required force output on a monitor and live feedback of each trial's exerted effort level.

5.3. Data Analysis

5.3.1. HD-sEMG signal processing (Amplitude)

For all participants, HD-sEMG data analyses focused on the superior array due to the effect of breast tissue on HD-sEMG amplitude and mean power frequency in the inferior array, quantified in Chapter 4. Any trials with motion artifact, low skin-electrode contact, or substantial saturation were removed from further analyses (~1.5% of total trials). Technical issues related to signal acquisition contaminated data from one participant across tasks and one participant in two tasks, prompting their removal from analysis for these tasks. Before processing HD-sEMG, acquired ECG was used to remove heart rate contamination from monopolar HD-sEMG signals. ECG was interpolated to 2048 Hz, and the HD-sEMG signals were cross-correlated with the heart rate data to match the timing of each heartbeat's peak amplitude. Each trial was visually inspected to make sure the algorithm correctly recognized the ECG peaks. The precise timing of each ECG peak surrounded by 250-millisecond windows before and after the peak was determined and used to avoid the quantification bias of the root mean square (RMS) amplitude.

Raw HD-sEMG data were band-pass filtered with a 3rd order Butterworth filter (20-500 Hz), and the differential derivation was quantified from left to right (i.e., from axilla towards sternum). RMS was quantified for each differential channel. The resultant force was used to focus on the first half of the hold. The most stable part of the hold was selected by dividing the resultant force into 5-second segments and performing EMG analyses on the force segment with the lowest coefficient of variation. Maximal trials were combined for adduction and internal rotation at 60° and adduction tasks at 90° as these were performed at the same arm posture. For each HD-sEMG channel within MVE, the mean of a 3-second window surrounding the maximal force was extracted. Subsequently, each channel's maximal value across four MVE trials was extracted,

following which each channel in a submaximal trial was normalized to the channel-specific maximal value. Following EMG normalization, spatial scaling was applied for each participant to account for differences in pectoralis major size. Each participant's normalized EMG amplitudes were scaled to the participant with the largest pectoralis major. The largest pectoralis major was determined based on sternal and clavicular length measurements. Following normalization, the superior HD-sEMG array was divided into clavicular (rows 1-2), superior sternocostal (rows 3-5), and middle sternocostal (rows 6-8) region. Subsequently, the mean for each region across all channels was quantified (Figure 15A). The regional divisions in the HD-sEMG array were based on the anatomical description of each region's location (Fung et al., 2009). Subsequently, the regional mean of the two trials within each task and effort level was quantified.

5.3.2. Force

Raw voltage data acquired in submaximal and maximal trials was processed. Raw voltages were filtered using a 3rd order low-pass Butterworth filter with a cut-off frequency of 15 Hz and converted to Newtons using a custom-made program in MATLAB 2019b. Mean force data in Newtons that matched the most stable part of the force (i.e., HD-sEMG signals were analyzed above) was quantified. Force acquired in submaximal trials was then normalized to the mean of the two maximal values quantified in task-specific MVEs. Normalized force data was used to confirm that all participants received the same amount of feedback and exerted 15%, 25%, or 50% MVE during submaximal trials.

5.3.3. Bipolar surface electromyography

Bipolar EMG data in task-specific maximal MVE and submaximal trials were processed. All sEMG data was band-pass filtered with a 2nd order Butterworth filter (30-500 Hz), and RMS was quantified. MVE and submaximal trials were processed using the same methods and for the same force segment for HD-sEMG. For submaximal trials, this included a mean of a 5-second segment with the lowest coefficient of variation in force. Maximal trials were combined for adduction and internal rotation at 60° and adduction tasks at 90° as these were performed at the same arm posture. The mean of a 3-second window surrounding the maximal force was extracted, following which maximal value across four trials was quantified. Submaximal trials were then normalized to muscle-specific maxima. sEMG was normalized to task-specific MVEs to not underestimate EMG activity by normalizing to standard MVEs (Maciukiewicz et al. 2019). Mean across 5 seconds of normalized RMS data was quantified for each submaximal trial. Subsequently, the mean of two task-specific submaximal trials was quantified.

5.4. Statistical Analyses

All statistical analyses were performed in SPSS (IBM, version 21). Before any comparisons, the data were checked for normality and sphericity using the Shapiro-Wilk test and Mauchly's test of sphericity, respectively. Data in all tasks were not normally distributed and were ln transformed. Two-way repeated-measures analysis of variance (ANOVA) examined mean normalized EMG amplitude for each task with within-subject factors *Region* (clavicular, superior, and middle sternocostal) and *Effort* (15, 25, 50% MVE). If significant interactions between *Region* and *Effort* were found, planned comparisons with Dunn-Bonferonni correction were performed. EMG amplitudes quantified for additional shoulder muscles were ranked from highest to lowest

activity based on each task's activation level. They were used to determine which additional shoulder muscles contributed highly to the task. Partial eta-squared (ηp^2) examined the effect sizes related to significant differences. ηp^2 less than 0.06 was deemed as "small," 0.07-0.14 as "moderate," and greater than 0.14 as "large" (Cohen, 1969). The significance level was set to $p < 0.05$.

5.5 Results

In general, middle sternocostal regions activated more than superior sternocostal and clavicular regions in adduction with external rotation at all effort levels (ADDER90; Figure 16C). In internal rotation, the clavicular and middle activated more than the superior sternocostal regions across effort levels (Figure 16D). Additionally, differential regional activation existed in adduction at 60° and 90° of abduction and depended on the effort level (Figure 16A and 16B). All participants received the same amount of feedback across tasks and effort levels (Table 5).

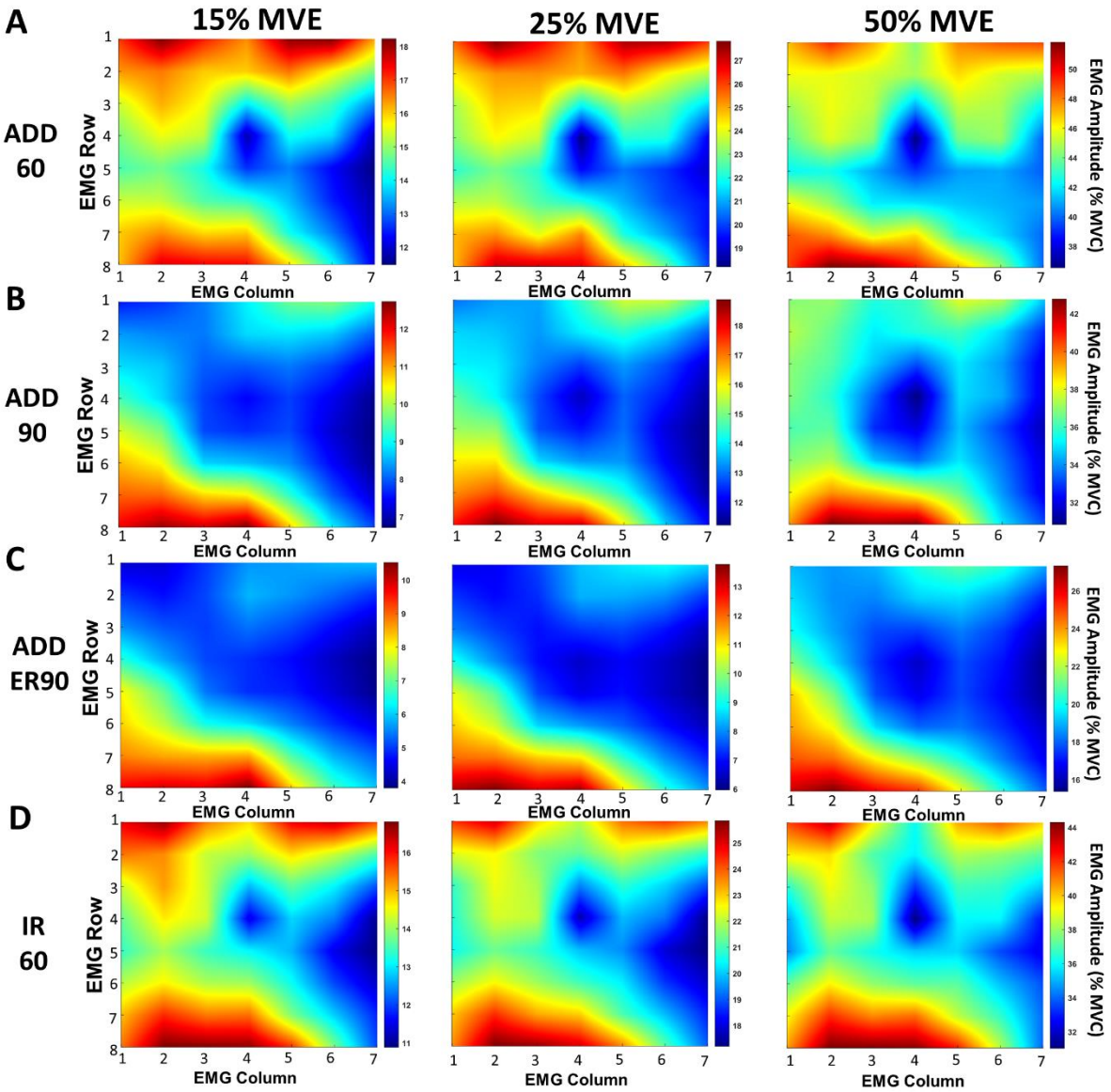

Figure 16: Scaled mean normalized (%MVC) spatial topographical maps for each task and effort level across the whole sample. **A:** Scaled mean normalized topographical maps for 15%, 25%, and 50% MVE in isometric adduction from 60° of abduction. Note the high activations of the clavicular and the middle sternocostal regions at low effort levels. **B:** Scaled mean normalized topographical maps for 15%, 25%, and 50% MVE in isometric adduction from 90° of abduction. Note the high activations of the middle sternocostal regions at low effort levels, with increases in the clavicular region's activation as effort increases. **C:** Scaled mean normalized topographical maps for 15%, 25%, and 50% MVE in isometric adduction from 90° of abduction and 90° external rotation. Note the high activations of the middle sternocostal regions irrespective of the effort level. **D:** Scaled mean normalized topographical maps for 15%, 25%, and 50% MVE in isometric internal rotation. Note the high activation of the clavicular and the middle sternocostal regions irrespective of the effort level. Blue colour indicates low activation. Red colour indicates high activations.

Table 5: Mean force (N) and mean %MVE ± standard deviation achieved for each task and effort level.

Task	Effort Level	Mean Force (N)	Mean %MVE
Adduction 60	15%	30 ± 6.4	15.7 ± 1.2
	25%	49.3 ± 10.7	25.8 ± 1.5
	50%	95.4 ± 19.5	50.3 ± 5
	100%	187.9 ± 42.8	-
Adduction 90	15%	24.6 ± 6.2	14.9 ± 1.3
	25%	40.9 ± 10.3	24.9 ± 2.5
	50%	83.7 ± 18.4	51.1 ± 1.8
	100%	163 ± 34.9	-
Internal Rotation	15%	22.7 ± 6.4	15.8 ± 1.2
	25%	37.4 ± 10.2	26.1 ± 2.7
	50%	75.6 ± 19.9	52.8 ± 6.5
	100%	145.3 ± 43	-
Adduction External 90	15%	24.2 ± 6.7	14.5 ± 2.3
	25%	41.4 ± 9	24.9 ± 2
	50%	84.5 ± 16.6	51 ± 1.7
	100%	165.4 ± 30.6	-

5.5.1. Adduction at 60° of abduction

Region by Effort interaction existed in adduction 60° ($F_{(2.4, 41.2)} = 10.09$, $p < 0.0001$, $\eta p^2 = 0.37$; Figure 17A). Compared to the superior sternocostal region, the EMG amplitude was 19% higher in the clavicular at 15% MVE ($p < 0.0001$). Similarly, at 25% MVE, the EMG amplitude was 16% higher in the clavicular ($p < 0.0001$) than in the superior sternocostal region. At 50% MVE, the EMG amplitude was similar between regions (all $p > 0.025$).

Along with the pectoralis major, additional shoulder muscles contributed to the performance of this task. Specifically, the middle and posterior deltoid and upper trapezius activated at 15% MVE between 16-17% MVC (Figure 18A). At 25% and 50% MVE, latissimus dorsi, posterior, and middle deltoid activated between 25-27% MVC at 25% MVE and 50-54% MVC at 50% MVE (Figure 18A; Supplementary Table 2).

5.5.2. Adduction at 90° of abduction

Region by Effort interaction existed in adduction from 90° ($F_{(2.4, 43.9)} = 3.6$, $p = 0.027$, $\eta p^2 = 0.16$; Figure 17B). Middle sternocostal activated 15% more than clavicular and 22% more than superior sternocostal region at 15% MVE (mid. stern > clav, $p = 0.024$; mid. stern > sup. stern, $p < 0.001$). At 25% MVE, the middle sternocostal amplitude was 15% higher than superior sternocostal ($p = 0.001$), but not different than the clavicular region ($p = 0.04$). Lastly, at 50% MVE, EMG amplitudes in the middle sternocostal region were 8% higher than the superior sternocostal region ($p = 0.012$), but not different than the clavicular region ($p = 0.21$).

At 15% MVE, the upper trapezius activated with pectoralis major (~22% MVC), while at 25% MVE, both upper trapezius and middle deltoid activated between 17-18% MVC (Figure 18B). At 50% MVE, anterior deltoid, latissimus dorsi, and middle deltoid activated between 34-36% MVC (Figure 18B; Supplementary Table 2).

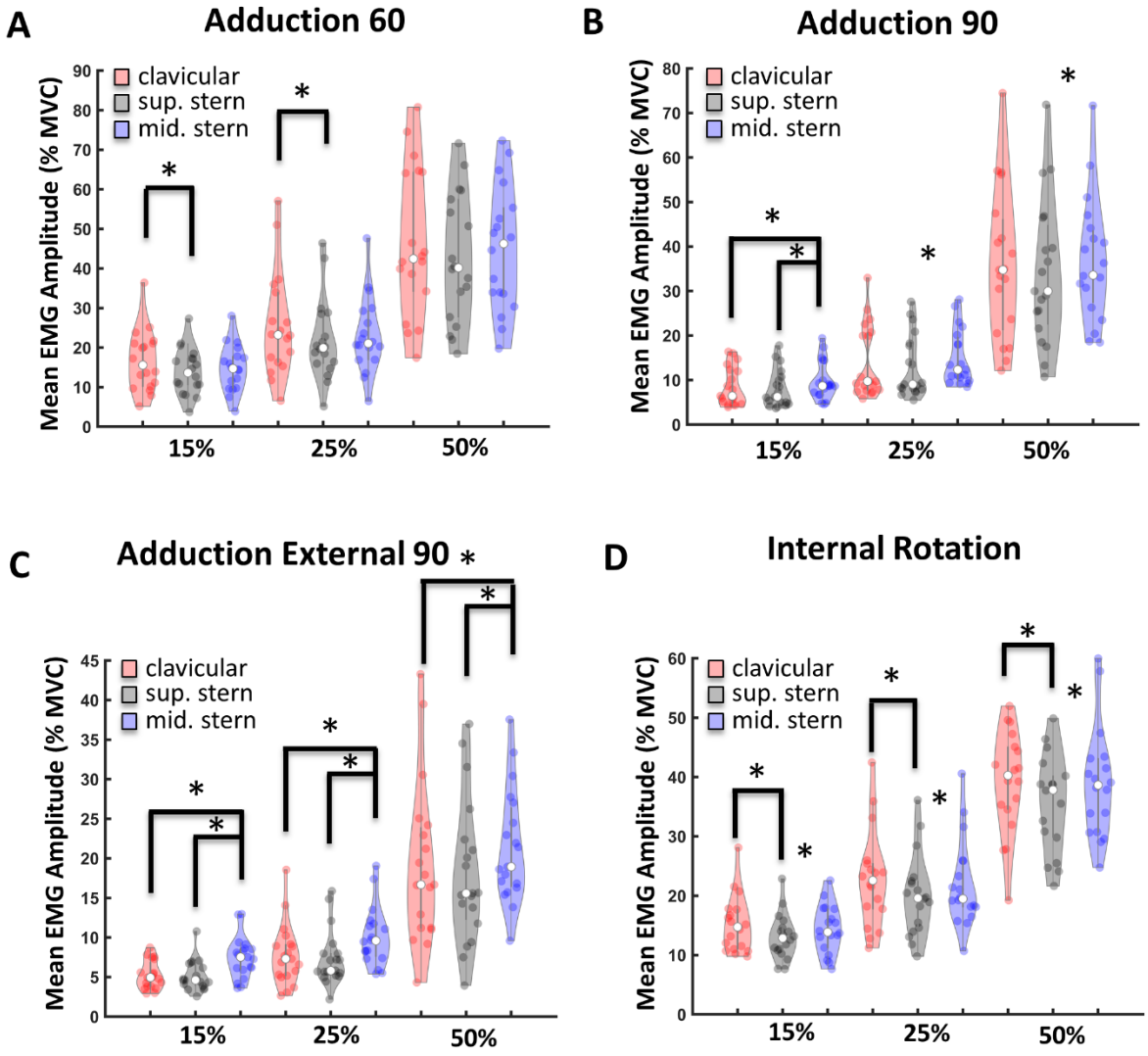

Figure 17: Mean normalized EMG amplitude violin graphs with individual scatter data for clavicular, superior, and middle sternocostal regions across 15%, 25%, and 50% MVE for each task. Each region is denoted in different shades: clavicular region: red; superior sternocostal region (sup. stern): grey; middle sternocostal region (mid. stern): purple. White dots in the middle of each violin plot are medians. **A:** Isometric adduction at 60° abduction (ADD60). The clavicular region activated more than superior sternocostal at 15% and 25% MVE. **B:** Isometric adduction at 90° abduction (ADD90). The middle sternocostal region activated more than the clavicular and superior sternocostal region at 15% MVE. At 25% and 50% MVE, the middle sternocostal region activated more than superior sternocostal region **C:** Isometric adduction at 90° of abduction and 90° external rotation (ADDER90). The middle sternocostal region activated more than clavicular and middle sternocostal irrespective of the effort level. **D:** Isometric internal rotation (IR60). Clavicular and middle sternocostal regions were more active than the superior sternocostal region regardless of the effort level. Asterisk (*) denotes significant differences between regions.

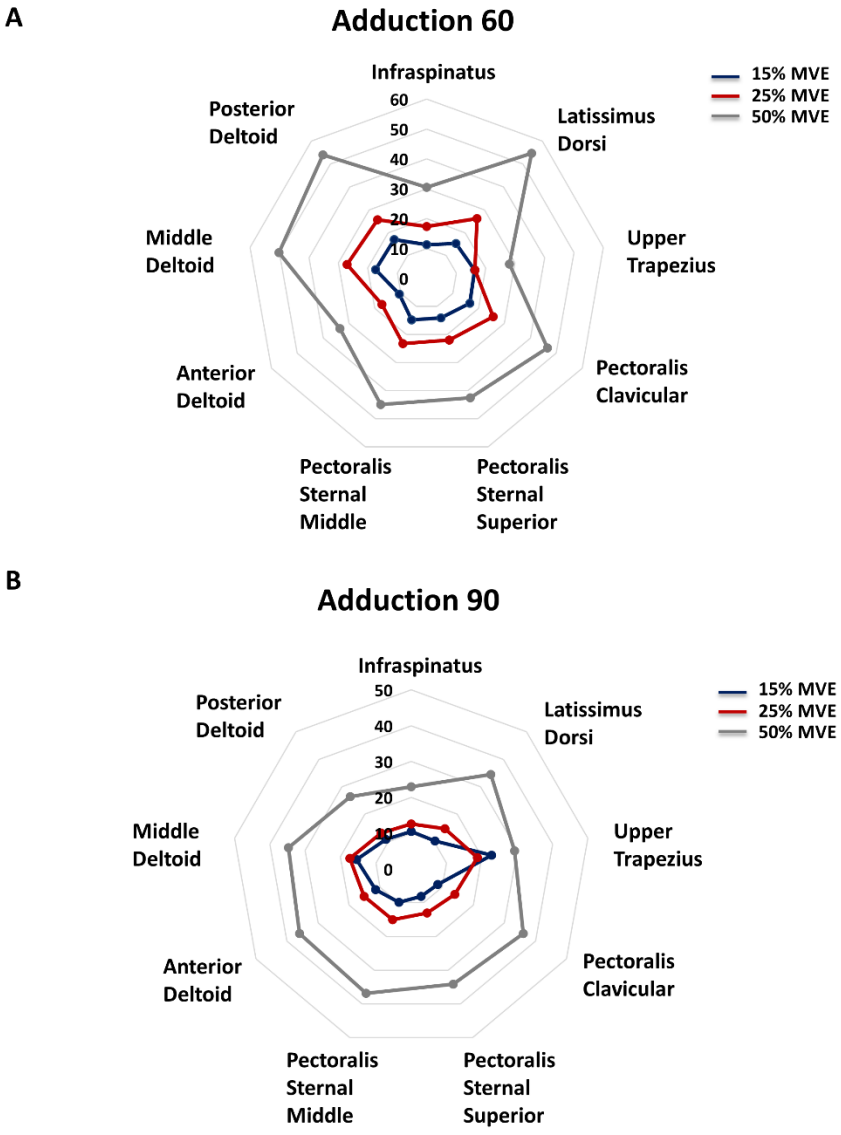

Figure 18: Polar plots depicting mean activation for infraspinatus, latissimus dorsi, upper trapezius, anterior, middle, and posterior deltoid alongside pectoralis major regions in adduction 60 (**A**) and adduction 90 (**B**). Each coloured line depicts the effort level: blue: 15% MVE; red: 25% MVE; and 50% MVE: grey. The magnitude of activation is represented on the Y-axis, with each additional inner circle representing an increase in 10% MVC.

5.5.3. Adduction at 90° of abduction and 90° of external rotation (Adduction external 90)

Region by Effort interaction existed while adducting in adduction external 90 task ($F_{(1.8, 32.7)} = 4.1$, $p = 0.028$, $\eta p^2 = 0.18$; Figure 17C). At 15% MVE, middle sternocostal had 42% and 44% higher amplitudes than clavicular and superior sternocostal regions, respectively (mid. stern > clav, $p < 0.001$; mid. stern > sup. stern, $p < 0.001$). At 25% MVE, the amplitudes were 29% and 37% higher in the middle sternocostal than the clavicular and the superior sternocostal region, respectively (mid. stern > clav, $p = 0.001$; mid. stern > sup. stern, $p < 0.001$). High activity in the middle sternocostal region remained at moderate effort (i.e. 50% MVE; mid. stern > clav:12%, $p = 0.007$; mid. stern > sup. stern: 19%, $p < 0.001$).

At 15% MVE, upper trapezius activated highly (22% MVC). As the effort increased to 25% MVE, infraspinatus (23% MVC), latissimus dorsi (20% MVC), and upper trapezius (22% MVC) had high activations. At 50% MVE, infraspinatus (42% MVC), latissimus dorsi (42% MVC), middle (39% MVC), and posterior deltoid (40% MVC) had high activity (Figure 19A; Supplementary Table 2).

5.5.4. Internal rotation

In internal rotation, *Region by Effort* interaction existed ($F_{(2.5, 43.1)} = 4.77$, $p = 0.008$, $\eta p^2 = 0.21$; Figure 17D). At 15% MVE, both the clavicular (16%, $p < 0.001$) and middle sternocostal regions (9%, $p = 0.020$) activated more than the superior sternocostal region. Similarly, at 25% MVE, both also activated more than the superior sternocostal region ($p = 0.001$; clav by 14%; $p = 0.007$; mid. stern by 10%). In moderate efforts, both clavicular ($p = 0.013$) and middle sternocostal region ($p = 0.007$) activated 10% more than the superior sternocostal region.

At 15% MVE, the upper trapezius activated ~15% MVC to assist the pectoralis major (Figure 19B; Supplementary Table 2). In contrast, at 25% and 50% MVE, the highest activity was quantified in latissimus dorsi (18-38% MVC), middle (16-33% MVC), and posterior deltoid (17%-32% MVC).

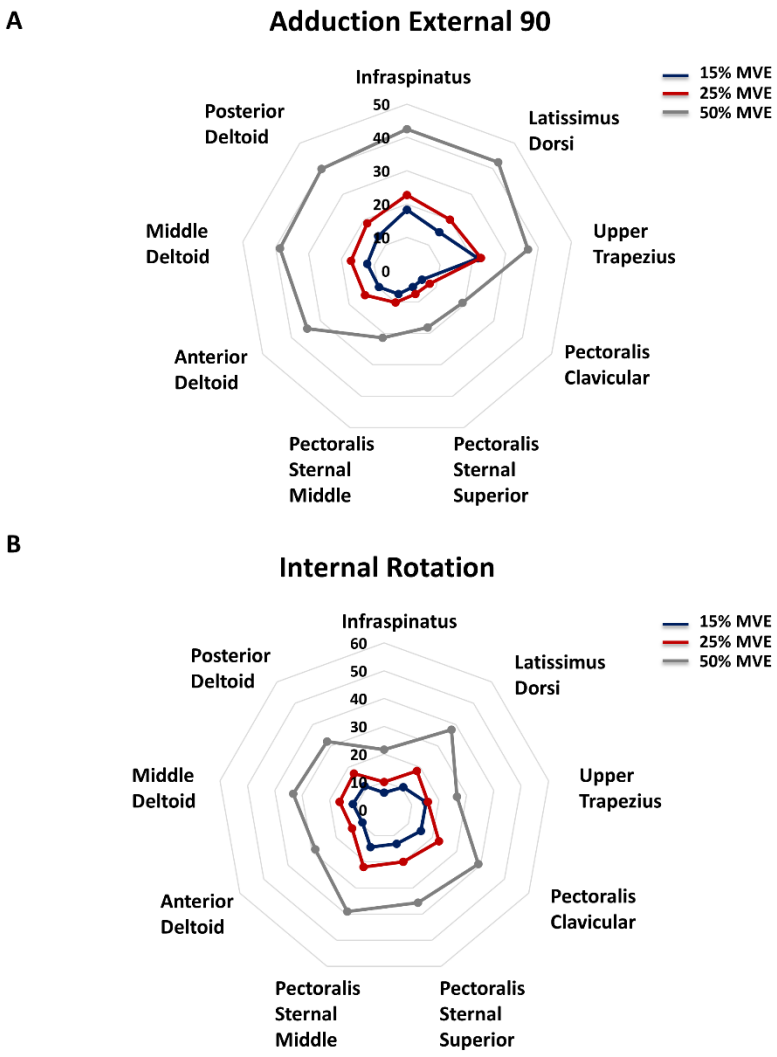

Figure 19: Polar plots depicting mean activation for infraspinatus, latissimus dorsi, upper trapezius, anterior, middle, and posterior deltoid alongside pectoralis major regions in adduction external 90 (**A**) and internal rotation (**B**). Each coloured line depicts the effort level: blue: 15% MVE; red: 25% MVE; and 50% MVE: grey. The magnitude of activation is represented on the Y-axis, with each additional inner circle representing an increase in 10% MVC.

5.6. Discussion

Differential regional pectoralis major activation emerged across tasks and effort levels, indicating complex task and effort interactions. The clavicular and middle sternocostal regions activated highly in tasks without external rotation. In contrast, in the task with external rotation, the middle sternocostal region activated more than the other two regions at all effort levels, indicating a specialized role.

Regional contributions to internal rotation are unclear. While some studies demonstrated clavicular region involvement in this task (Wolfe et al., 1992; Stegink-Jansen et al., 2011), reduced internal rotation strength occurred following an injury to the sternocostal regions (Schepsis et al., 2000; Provencher et al., 2010; Leonardis et al., 2019; Marsh et al., 2020). However, anatomical studies suggest that both regions may support internal rotation moment (Ackland and Pandy, 2011). Although both regions can internally rotate the arm, the clavicular region has two-to-three times shorter internal rotation moment arm than the sternocostal, with the longest internal rotation moment arm in the sternocostal region at 30-60° of abduction (Ackland and Pandy, 2011). Additionally, at 60° of abduction, the clavicular region has an abductor moment arm (Ackland et al., 2008). Correspondingly, the clavicular and middle sternocostal regions had similar EMG amplitudes in this task, reflecting dual contributions to isometric internal rotation effort and postural maintenance of arm abduction.

In isometric adduction, arm posture, and the required effort level dictated regional activations. Adductor moment arm lengths vary by region and within each region, by arm abduction angle (Ackland et al., 2008). Specifically, the clavicular region has a larger abductor moment at 90° than 60° of abduction when the arm is not externally rotated. In comparison, sternocostal regions have longer adductor moment at 60° than 90° of abduction (Ackland et al.,

2008). Accordingly, the clavicular region activated to maintain arm abduction, while the middle sternocostal regions generated complementary isometric adduction. Differences between these tasks emerged in spatial activity changes with increasing effort. At 50% MVE in 60° of abduction, higher relative EMG amplitudes occurred in the superior and middle sternocostal region. In contrast, higher effort in 90° of abduction produced high activations in the middle sternocostal region. This may result from the greater adduction leverage of the sternocostal regions in 60° of abduction, while the clavicular region has more leverage at 90° of abduction (Ackland et al., 2008).

In adduction with external rotation, middle sternocostal regions had higher EMG amplitudes than the clavicular and superior sternocostal region. Relatively greater EMG amplitudes were previously quantified in the sternocostal in comparison to the clavicular region in isometric and dynamic tasks involving similar postures (Nadon et al. 2016; MacLean et al. 2019). In contrast, no such regional differences existed in stiffness in a similar task in males (Leonardis et al. 2017), suggesting equivalent regional contributions. Differences between studies may be due to sex-related differences. The clavicular region is more passively stretched than the sternocostal region in this arm posture (Leonardis et al. 2017), although both regions experience ~33% strains (Stegnik-Jansen et al., 2011). It is unknown, however, if differences in strain exist between sternocostal partitions.

5.6.1. Implications for surgical disinsertion or injury to pectoralis major regions

The clavicular and superior/middle sternocostal regions were essential in maintaining submaximal efforts in internal rotation and adduction tasks. Accordingly, injury to the sternocostal regions may reduce the ability to maintain isometric submaximal adduction efforts at 90° of abduction and external rotation, prompting increased compensatory activation by other adductors, such as latissimus dorsi and external rotator muscles (Chopp-Hurley et al., 2016). Further, such

injury may significantly affect the performance of vertical adduction without external rotation in low efforts. Supportingly, individuals who underwent subpectoral breast reconstruction involving sternocostal disinsertion could not maintain shoulder joint stiffness at 10% MVE in the submaximal vertical adduction torque task (Leonardis et al., 2019). Reductions in vertical adduction strength also existed in a subpectoral reconstruction group (Leonardis et al., 2019) and breast cancer survivors following radiation (Lipps et al., 2019).

5.6.2. Evidence of partitional activation in pectoralis major regions

Lower EMG amplitudes emerged in the superior compared to the middle sternocostal region for multiple tasks, suggesting potential functional differentiation between sternocostal partitions. Data on partitional sternocostal moment arms are lacking. A single study demonstrates variations in partitional adduction moment arms when the upper extremity is at 20° of abduction in the frontal plane (Brown et al., 2007). However, adduction moment arms throughout the range of motion were not evaluated, and internal rotation moment arms were not defined. Distinct anatomical differences in sternocostal muscle fiber bundles (Brown et al., 2007; Fung et al. 2009) suggest possible functional differences between partitions. The largest differences between superior and middle sternocostal fibers exist in the lateral pennation angle, with superior fibers exhibiting greater pennation angles than middle sternocostal fibers (Fung et al., 2009). While it is plausible that lower EMG amplitudes in superior partitions resulted from possible innervation zone proximity, lower EMG amplitudes would be more prominent laterally (i.e., towards the axilla) as defined previously (Mancebo et al., 2019). Further, higher EMG amplitudes in superior fibers occurred for moderate effort levels. The present results provide preliminary evidence for partitional functional differentiation.

5.7. Limitations

Methodological limitations accompany this study. Previous studies in males quantified higher activations in the inferior sternocostal and abdominal partitions, particularly in tasks requiring isometric adduction (Paton and Brown, 1994). While these regions may also highly activate in females, their recording was infeasible due to the overlying breast tissue. Secondly, the study included only young females, and therefore, findings may not transfer to other cohorts. Finally, present results likely do not reflect muscular activations in unstudied tasks, including horizontal adduction, flexion, and extension against resistance.

Additionally, crosstalk from the surrounding muscles, such as the pectoralis minor, serratus anterior, external obliques, or intercostal muscles, may have influenced the patterns of regional activation quantified in this study. Attempts were made to minimize the degree of crosstalk by sampling EMG from many closely spaced electrodes (10 mm interelectrode distance) and quantifying differential derivation in the post-processing steps. Lastly, it is known that at least one innervation zone is located within the superior region of the pectoralis major (Mancebo et al. 2019). Due to the challenges in quantifying the innervation zones from motor unit action potentials, the exact location of these innervation zones was challenging to determine. Therefore, this study quantified the mean normalized EMG amplitudes across the innervation zones, which may have influenced the findings.

5.8. Conclusions

This study provides unprecedented evidence for differential regional pectoralis major activation in females and regional activation dependency on the task performed and effort level required. Specifically, present findings indicate localized activation of the middle sternocostal regions in tasks requiring adduction with external rotation irrespective of the effort level. In

contrast, both clavicular and middle sternocostal regions activate in tasks involving internal rotation and adduction without external rotation. These novel findings may be used to inform surgical interventions which resect pectoralis major regions or rehabilitation protocols aimed at pectoralis major recovery following compromise.

Chapter 6: Task and effort level influence regional pectoralis major activation in healthy females: A high-density electromyography study

6.0 Abstract

Pectoralis major activation fundamentally enables commonly performed tasks. Despite important contributions to arm mobility, ambiguity exists regarding its regional activation in females. Knowledge of regional activation is critical for the development of targeted rehabilitation protocols in compromised populations. This study quantified regional pectoralis major activation in low-to-moderate ramped isometric efforts in nine young, healthy females in four arm tasks: a) extension; b) flexion; c) horizontal adduction; and d) internal rotation; at four effort levels: 15%, 25%, 50%, and 75% scaled to the individual task-specific maximal voluntary effort (MVE). High-density surface electromyography from clavicular, superior, and middle sternocostal regions was used to compute the regional mean root mean square amplitudes (normalized to maxima). Middle sternocostal regions had higher EMG amplitudes than clavicular and superior sternocostal regions in extension (all $p < 0.001$) and internal rotation ($p < 0.0001$) across all effort levels. In horizontal adduction, clavicular had 22% and 19% higher EMG amplitudes, respectively, than middle sternocostal region at 15% MVE ($p = 0.018$) and 25% MVE ($p = 0.019$). Additionally, clavicular region had 14% higher EMG amplitudes than superior sternocostal region at 25% MVE ($p = 0.017$). All three regions had similar EMG amplitudes at 50% and 75% MVE (all $p > 0.025$). In flexion, clavicular region had higher EMG amplitudes at 15% MVE ($p = 0.022$) and 25% MVE ($p = 0.005$) than other two regions. At 50% and 75% MVE, all three regions displayed similar EMG amplitudes (all $p > 0.025$). Present findings indicate differential regional pectoralis major activation, providing foundational knowledge regarding fundamental activation and informing surgical and rehabilitation interventions.

6.1 Introduction

Arm movement requires simultaneous activation of multiple shoulder muscles. One of these muscles is the pectoralis major, which contributes to humeral mobility and overall shoulder stability. Remarkably, it also allows for the mobility of the sternoclavicular, acromioclavicular, and indirectly, scapulothoracic joints. Comprised of at least three anatomically distinct regions (Ashley, 1952; Fung et al. 2009; Lewis 1901; Wolfe et al. 1992), pectoralis major activation assists in humeral horizontal and vertical adduction, flexion, internal rotation, and extension against resistance. Indeed, its multipennate architecture permits for variation in regional moment arms throughout the range of motion (Ackland et al. 2008; Ackland and Pandy, 2011), shifting regional activations based on the arm posture (Paton and Brown, 1994; Wickham et al. 2004; Wickham and Brown, 2012). However, these mechanical contributions and functional divisions are even more sophisticated. The most recent anatomical evidence suggests the presence of multiple partitions within sternocostal and abdominal regions (Fung et al. 2009), which may activate differentially depending on the arm posture, effort level, and task performed.

Despite its multifunctional role, pectoralis major regions are commonly resected and used as donor tissues in various surgical interventions involving head, neck, or breast reconstruction and restoring functional limitations in other shoulder muscles. These surgical procedures rarely consider the biomechanical consequences of pectoralis major disinsertion. Several studies investigating the effects of pectoralis major resection showed reduced arm strength (Steinmann and Wood, 2003; de Haan et al. 2007; Leonardis et al. 2019), restrictions in mobility (Steinmann and Wood, 2003), and changes in pectoralis major material properties (Leonardis et al. 2019).

Data on regional pectoralis major activation in females is lacking. However, information regarding regional pectoralis major activation in females is essential to resolve the

pathophysiology of functional limitations in compromised populations and develop improved surgical procedures. A limited understanding of regional activation in females motivates precise examination of regional pectoralis major activation and function using advanced techniques. High-density surface electromyography (HD-sEMG), consisting of an array of electrodes, can capture the whole muscle's EMG activation, enabling quantification of the spatial distribution of muscle activity. As the acquisition of EMG signals from pectoralis major in females is limited to the superior to middle regions, the possibility to acquire EMG signals from available muscle locations is essential. Therefore, the present study aimed to characterize regional pectoralis major activation in low, moderate, and high ramped isometric efforts in healthy, young females in four arm tasks. The range of effort levels and arm tasks chosen in this study reflect a range of muscular responses and focus on the tasks which require pectoralis major activation. The primary hypothesis was that the middle sternocostal region will have higher normalized EMG than the superior sternocostal and clavicular region in internal rotation 90 and extension. Further, in flexion, it was hypothesized that the clavicular region will have higher normalized EMG amplitudes than the superior and middle sternocostal regions. Lastly, in horizontal adduction, it was hypothesized that clavicular and superior sternocostal regions will have higher normalized EMG amplitudes than middle sternocostal regions.

6.2 Methods

6.2.1. Participants

Nine healthy, right-hand dominant young females (24.5 ± 3.1 years; height: 165 ± 3.5 cm; weight: 61 ± 8.9 kg; Table 6) participated. The chosen sample size was selected using *a priori* power analyses. Sample size calculations in G*Power 3.1 (Universitat Dusseldorf, Dusseldorf, Germany) indicated that a minimum of 16 participants is required to obtain sufficient power (Cohen, 1988). The effect size chosen ($f^2 = 0.31$) is on the lower end of the observed effect size in

previous studies, which reported effect sizes between 0.2 to 0.6 (Paton and Brown, 1994; Brown et al. 2007; Wickham et al. 2004). The actual sample did not satisfy the quantified *a priori* sample as collections were halted due to the Canadian government's lockdown measures due to the COVID-19 pandemic. Females were recruited using word-of-mouth and posters advertising the study in the kinesiology, engineering, psychology, and student center buildings. All recruited females were recreationally active. The inclusion criteria included healthy young (between 18-40 years old), right-hand dominant females. Females who underwent breast reconstruction or augmentation surgeries were not included in the study. Participants reported no history of musculoskeletal or neurological injuries in the right arm or low back and had no back pain in the past six months. No participants tested positive for signs of impingement, as screened with Hawkin's impingement and Apley's Scratch test. Participants did not engage in strenuous physical activity at least 24 hours before the session. Participants were instructed by the investigator not to consume any caffeinated drinks the morning of the session and drink plenty of water the day before the session. All participants wore a normal bra (i.e., no sports bra) to mitigate breast tissue compression and allow placement of HD-sEMG arrays over the pectoralis major. This study was reviewed and received ethics clearance from the Institutional Research Ethics (ORE #31747) and conformed with the Declaration of Helsinki.

Before the experimental protocol, height, weight, rib cage, chest circumference, clavicle, and sternum length were measured. Rib cage circumference involved measurements around the rib cage, just under the breasts, in the area where the bra band is located. Chest circumference was measured starting from the fullest part of the participant's bust, with measuring tape wrapped around under the axilla. Clavicle length was measured from acromion to sternal notch, while the sternal length was measured from the sternal notch to the palpated xiphoid process. The clavicular

and sternal length were used to scale the normalized EMG data to account for differences in pectoralis major size.

Table 6: Participant demographics and anthropometric measurements (± standard deviation).

Age (years)	24.5 ± 3.1
Height (cm)	165 ± 3.5
Weight (kg)	61 ± 8.9
Chest circumference (cm)	87.9 ± 7
Ribcage circumference (cm)	77.2 ± 8
Clavicle length (cm)	16.3 ± 1.2
Sternum length (cm)	19.6 ± 1.5

6.2.2. High-density surface electromyography

Two HD-sEMG arrays consisting of 64 electrodes in an 8 by 8 matrix with a 10 mm inter-electrode distance were used to acquire EMG from pectoralis major in monopolar mode (ELSCH064NM3, OTBioelecttronica, Torino, Italy; Figure 20A). The superior array was placed ~2 cm inferior to the clavicle, with the middle of the array located between the sternum and the axilla, parallel to the muscle fibers. The inferior array was placed directly below the superior array. The arrays were fixed with adhesive tape and connected to a 128 channel EMG amplifier (EMGUSB2+, OTBioelecttronica, Torino, Italy). Before applying the electrodes, the skin overlying the pectoralis major was cleaned with abrasive paste and water. The electrode holes were filled with electroconductive gel, and the arrays were applied on the skin using a 1 mm thick two-sided adhesive foam. All EMG signals were bandpass filtered with a cut-off frequency between 10 – 500 Hz and sampled at 2048 Hz with a 12-bit A/D converter (5V dynamic range). HD-sEMG signals were amplified by a factor between 100-5000 V/V and depended on the task, participant, and effort level. Saturation of the HD-sEMG signal was visually monitored during the collection using OTBioLab software (OTBioelecttronica, Torino, Italy). If more than ten channels were saturated during the trial, the collection of the trial was stopped, the gain was adjusted, and the

trial was repeated. One wet reference electrode was wrapped around the participant's right wrist, while a reference electrode was placed on the right clavicle.

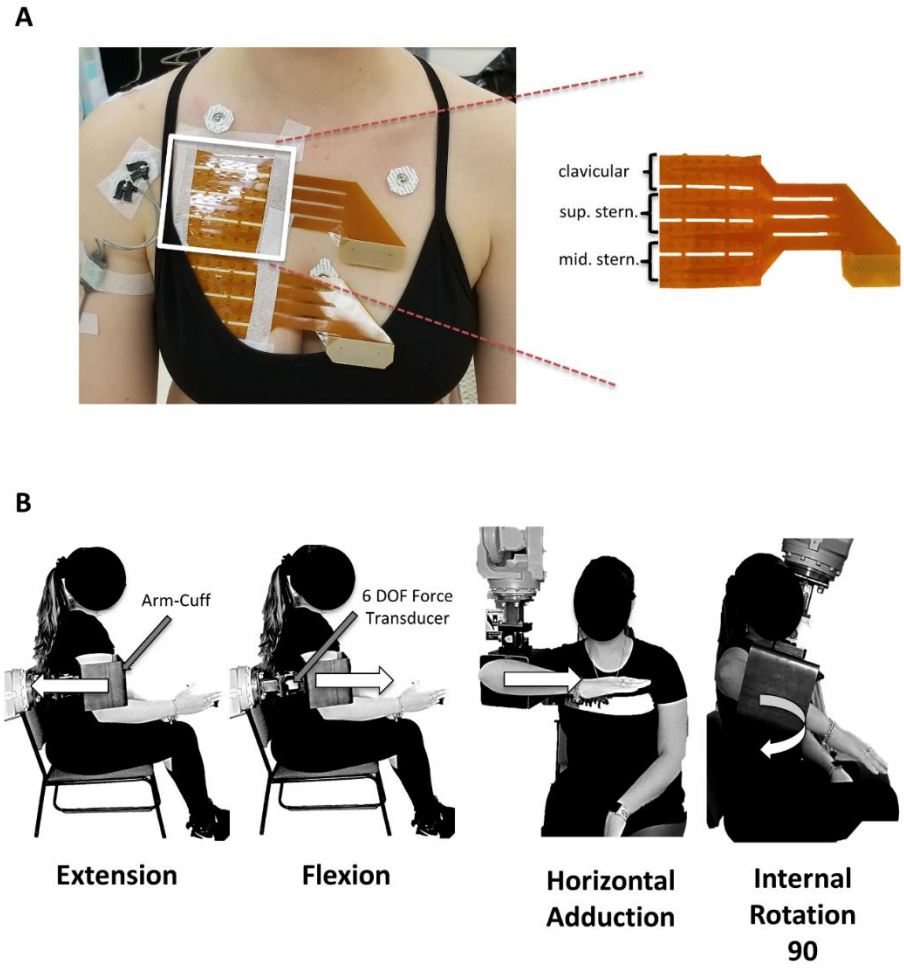

Figure 20: Figure depicting the location of superior and inferior HD-sEMG arrays overlaying the pectoralis major and a schematic of an experimental setup. **A:** Two HD-sEMG 64-channel arrays were fixed on the pectoralis major. The white square indicates a superior HD-sEMG array, which was used for analyses. The superior array was divided into regions: rows 1-2 clavicular; 3-5 superior sternocostal; and 6 to 8 middle sternocostal. **B:** Tasks included: a) extension from 20° of abduction (EXT); b) flexion from 20° of abduction (FLEX); c) horizontal adduction from 90° of abduction and 50° of flexion in the transverse plane (HORADD), and d) internal rotation from 90° of abduction and 20° of internal rotation (IR90).

6.2.3.Force measurement

Raw voltage in X, Y, and Z directions were acquired concurrently with the HD-sEMG signals. Participants exerted effort against a custom-built arm-cuff attached to a 6 degree of a freedom force transducer (MC3A, AMTI MA, USA) mounted on a robotic arm (Figure 20B; Motoman Robotics Division, Yaskawa America, USA). The force transducer's sampling rate was set to 1500 Hz and amplified (1000x) using VICON Nexus 1.7.1 software.

6.2.4. Electrocardiography measurement (ECG)

Electrocardiography (ECG) was acquired concurrently with HD-sEMG using silver-silver chloride (Ag-AgCl) disposable electrodes in a monopolar configuration. The purpose of ECG collection was to eliminate heart rate contamination in post-processing steps without distorting the EMG signals. Three electrodes were placed over the left chest at the 6^{th} costal level, approximately along the anterior axillary line, and medially at the sternocostalis junction (Drake and Callaghan, 2006). Before the placement of electrodes, the area was cleaned with abrasive gel and water. ECG was collected using a wireless telemetered system (Noraxon Telemyo 2400 T G2 Noraxon, Arizona, USA). Raw signals were band-pass filtered from 10-1000 Hz and differentially amplified with a CMRR > 100dB and an input impedance of 100 MΩ. Analog signals were converted to digital using a 16-bit A/D card with a ±10 V range. The sampling frequency was 1500 Hz.

6.2.5. Additional shoulder muscle monitoring

The activity of six additional shoulder muscles was recorded and monitored using bipolar sEMG. Upper trapezius, latissimus dorsi, infraspinatus, anterior, middle, and posterior deltoid activity was monitored in the background. sEMG activity was recorded using silver-silver chloride

(Ag-AgCl) disposable electrodes with a 1 cm diameter and a fixed inter-electrode spacing of 2 cm in a bipolar configuration. Before the electrode placement, the area overlying the muscle belly was shaved and cleaned with abrasive gel and water. Placement of the sEMG electrodes was confirmed with palpation while the participant exerted a low, submaximal contraction of the muscle in positions described in Supplementary Table 1 (Cram and Kasman, 1998; Kelly et al., 1996). A reference electrode was placed on the acromion. sEMG was collected using a wireless telemetered system (Noraxon Telemyo 2400 T G2 Noraxon, Arizona, USA). Raw signals were band-pass filtered from 10-1000 Hz and differentially amplified with a CMRR > 100dB and an input impedance of 100 MΩ. Analog signals were converted to digital using a 16-bit A/D card with a ±10 V range. The sampling frequency was 1500 Hz.

6.2.6. Experimental protocol

During the experimental protocol, participants performed task-specific maximal voluntary efforts (MVE) and submaximal ramped isometric trials in four tasks at three effort levels. All participants underwent a brief warm-up and training on how to generate maximal voluntary effort (MVE) and ramped submaximal isometric tasks. This training served to familiarize the participant with each of the tasks and precondition the muscle-tendon unit (Maganaris et al., 2002). Submaximal tasks were performed against the arm-cuff with visual feedback of the participant's force output provided on a monitor. The participant was comfortably sitting on a chair with an upright torso secured using a padded strap throughout all trials. Following practice, participants performed two trials of task-specific 5-second MVEs in four tasks (Figure 20B): a) extension from 20° of abduction (EXT); b) flexion from 20° of abduction (FLEX); c) horizontal adduction from 90° of abduction and 50° of flexion in the transverse plane (HORADD), and d) internal rotation

from 90° of abduction and 20° of internal rotation (IR90). These tasks were chosen as they reflect tasks that typically require the activation of the pectoralis major and are involved in many daily, work, and athletic activities. During MVE performance, participants were verbally encouraged by the investigators. Each MVE was separated by 2 minutes of rest. Maximal MVE values were quantified using a custom-made program in LabVIEW (National Instruments, version 3.1). For each task, the mean of two task-specific MVE trials was used to scale all submaximal trials within that task. During MVE performance, the off-axis forces were controlled in the LabVIEW program, such that participants were required to achieve above 80% exertion of effort in a specific axis. If unsuccessful in meeting this criterion, the participant was provided with verbal feedback, and the trial was repeated. Additionally, if two maxima generated in MVE trials differed by more than 10 Newtons, a third trial was performed to ensure consistency between MVEs.

Participants performed submaximal ramped isometric tasks for each task, scaled to 15, 25, 50, and 75% MVE according to the task-specific maxima defined above. These effort levels were chosen to reflect approximate submaximal muscle activation levels required in daily, occupational, and athletic activities. Tasks and effort levels were completely randomized between and within participants, while each trial within an effort was performed twice consecutively. Each trial lasted 60 seconds for 15% and 25%, 30 seconds for 50%, and 10 seconds for 75%. Three to five-minute rest breaks interposed trials, with more time allocated if requested by the participant. Participants were encouraged to report feelings of fatigue and the need for longer rest periods. For 15% and 25% MVE, participants slowly ramped up at ~2% MVE/s, held the effort, and then ramped down at ~2% MVE/s. At 50% MVE, participants ramped up and down at ~3% MVE/s, while at 75% MVE, the ramp was set to ~5% MVE/s. During each trial, visual feedback of the required effort

and live feedback of the effort level they were exerting against an arm cuff were displayed on a monitor.

6.3. Data Analysis

6.3.1. HD-sEMG signal processing

Before analyses, HD-sEMG signals for each channel were inspected for artifacts using a custom-made MATLAB program (MATLAB 2019b; Mathworks, Inc.). Channel was tagged and removed if it contained movement artifacts, was saturated, or had insufficient skin contact (i.e., no signal detected). These channels were subsequently interpolated in data analyses. Further, the differential amplitude of HD-sEMG signals across channels was below inherent noise levels in extension and internal rotation at 15% MVE across all participants, prompting the removal of this effort level from further analyses for these tasks. Lastly, any trials with substantial saturation, artifacts, or low electrode-skin contact were removed from further analyses (~1.2% of the trials).

Data analyses focused on the superior array for all participants due to the effect of breast tissue on HD-sEMG amplitude and mean power frequency in the inferior array. Before signal processing, ECG was used to eliminate heart rate contamination from monopolar HD-sEMG signals. ECG was interpolated to 2048 Hz, and the HD-sEMG signals were cross-correlated with the heart rate data to match the timing of each heartbeat's peak amplitude. Each trial was visually inspected to make sure the algorithm correctly recognized the ECG peaks. The precise timing of each ECG peak surrounded by 250-millisecond windows before and after the peak was determined and used to avoid quantifying the root mean square (RMS) amplitude in these segments.

Raw HD-sEMG data were band-pass filtered with a 3rd order Butterworth filter (20-500 Hz), and the differential derivation was quantified from left to right (i.e., from axilla towards sternum). The root mean square (RMS) was quantified for each differential channel. The resultant

force was used as a reference to analyze only the first half of the hold. The most stable part of the resultant force was selected by dividing the force signal into 5-second segments and performing the analyses on the one with the lowest coefficient of variation. All submaximal data were normalized to maximal trials. Maximal trials were combined for flexion and extension as the arm posture was the same. For each HD-sEMG channel within MVE, a 3-second mean window surrounding the maximal force was extracted. Subsequently, the maximal mean value was quantified for each channel. Following this, each channel within a submaximal trial was normalized to the channel and task-specific maximal value. Following EMG normalization, spatial scaling was applied for each participant to account for differences in pectoralis major size. Normalized EMG amplitude was defined in an individual pectoral system by scaling each individual's EMG data to the participant whose clavicle and the sternal length was the longest. Following scaling, the superior HD-sEMG array was divided into clavicular (rows 1-2), superior sternocostal (rows 3-5), and middle sternocostal (rows 6-8) regions, and the mean for each region was quantified. This division was based on the regional anatomical descriptions defined by (Fung et al., 2009). Subsequently, the regional mean of the two trials within each task and effort level was quantified.

6.3.2.Force

Raw voltage data collected in submaximal and maximal trials was low pass filtered using a 3rd order Butterworth filter with a cut-off frequency of 15 Hz and converted to Newtons using a custom-made program in MATLAB. The mean force that matched the most stable part of the resultant force (i.e., same as for HD-sEMG analyses) was quantified for all submaximal trials and normalized to the task-specific MVE. Normalized force data was used to confirm that all

participants received the same amount of feedback and exerted 15%, 25%, or 50% MVE during submaximal trials.

6.3.3. Bipolar surface electromyography

Bipolar sEMG data for additional shoulder muscles in task-specific maximal MVEs and submaximal trials were analyzed. All sEMG data was band-pass filtered with a 2nd order Butterworth filter (30-500 Hz), and RMS of the signal was quantified across the whole submaximal and maximal trial. Subsequently, RMS for each muscle in the submaximal trial was quantified for the same force segment as for HD-sEMG (i.e., a 5-second segment with the lowest coefficient of variation in force). In maximal trials, the mean of a 3-second window surrounding the maximal force was extracted. Maximal trials were combined for flexion and extension, as these were performed in the same arm posture. Submaximal trials were then normalized to posture specific maxima for each muscle. RMS was normalized to task-specific MVEs to not underestimate EMG activity by normalizing to standard MVEs (Maciukiewicz et al. 2019). Subsequently, the mean for each muscle for each effort level and the task was quantified.

6.4. Statistical Analyses

All statistical analyses were performed in SPSS (IBM, version 21). Before any comparisons, the data were checked for normality and sphericity using the Shapiro-Wilk test and Mauchly's test of sphericity, respectively. Data across all tasks were not normally distributed and were, therefore, ln transformed. Two-way repeated-measures analysis of variance (ANOVA) was performed on EMG amplitude in flexion and horizontal adduction with within-subject factor *Region* (clavicular, superior sternocostal, middle sternocostal) and *Effort* (15%, 25%, 50%, 75%

MVE). Similarly, for extension and internal rotation, two-way repeated-measures ANOVA was performed on EMG amplitudes with within-subject factor *Region* (clavicular, superior sternocostal, middle sternocostal) and *Effort* (25%, 50%, 75% MVE). If significant interactions between *Region* and *Effort* emerged, planned comparisons with Dunn-Bonferonni correction were performed to determine significant differences between regions within an effort level. EMG amplitudes quantified for additional shoulder muscles were ranked from highest to lowest activity based on the activation level for each task. They were used to determine which additional shoulder muscles contributed highly to the task. Partial eta-squared (ηp^2) defined the effect size of the significant differences in EMG parameters. With ηp^2 less than 0.06 deemed "small," 0.07-0.14 "moderate," and greater than 0.14 "large" (Cohen, 1969). Significance was set to $p < 0.05$.

6.5 Results

Generally, middle sternocostal regions activated more than superior sternocostal and clavicular regions in extension and internal rotation. Regional activation depended on the effort level in horizontal adduction and flexion. All participants received the same amount of feedback across tasks and effort levels (Table 7).

Table 7: Mean force in Newtons and as a percent of MVE (± standard deviation) for all tasks and effort levels.

Task	Effort Level	Mean Force (N)	Mean %MVE
Flexion	15%	19.9 ± 6	13.8 ± 2.8
	25%	34.3 ± 9.1	23.7 ± 3.05
	50%	71.8 ± 17.8	49.8 ± 4.01
	100%	143.6 ± 32.3	-
Horizontal Adduction	15%	24.8 ± 7.8	15.3 ± 2.04
	25%	40.9 ± 11.5	25.4 ± 1.81
	50%	81.4 ± 21.2	50.8 ± 2.28
	100%	159.4 ± 38.9	-
Internal Rotation	15%	15 ± 4.8	14.7 ± 2.32
	25%	26.3 ± 7.4	25.8 ± 2.8
	50%	54.2 ± 14.2	53.5 ± 6.2
	100%	103.8 ± 33.2	-
Extension	15%	24.5 ± 6.12	16.1 ± 2.4
	25%	39.4 ± 10.6	25.9 ± 4.5
	50%	81.1 ± 19.7	53.4 ± 8.8
	100%	152.7 ± 35.9	-

6.5.1. Flexion

Region by Effort interaction existed for flexion ($F_{(1.7,14.1)} = 12.2$, $p = 0.001$, $\eta p^2 = 0.6$; Figure 21A). Clavicular region had 22% and 21% higher EMG amplitudes, respectively, than superior sternocostal region at 15% and 25% MVE (15% MVE: $p = 0.022$, 7 out of 9 participants; 25% MVE: $p = 0.005$; 9 out of 9 participants). In contrast, EMG amplitudes were not significantly different between the clavicular and middle sternocostal region at either effort (all $p > 0.025$). At 50% and 75% MVE all three regions had similar EMG amplitudes (all $p > 0.025$).

Along with the pectoralis major, additional shoulder muscles displayed high activity. Specifically, at 15% MVE, anterior and middle deltoid, infraspinatus, and upper trapezius were highly activated (~17-20% MVC; Figure 22A; Supplementary Table 3). At 25% and 50% MVE, anterior deltoid, infraspinatus, and middle deltoid had high activity (25% MVE: ~29% MVC; 50% MVE: 47-57% MVC; Figure 22A), while at 75% MVE, high activity was quantified for anterior

(~78% MVC) and middle deltoid (~72% MVC), infraspinatus (~67% MVC), and upper trapezius (~64% MVC).

6.5.2. Horizontal adduction

Region by Effort interaction existed for horizontal adduction ($F_{(6,48)} = 28.37$, $p < 0.0001$, $\eta p^2 = 0.78$; Figure 21B). Clavicular region activated 22% more than middle sternocostal region at 15% MVE ($p = 0.018$; 8 out of 9 participants). Additionally, clavicular region activated 14% more than superior sternocostal region at 25% MVE ($p = 0.017$; 8 out of 9 participants), as well as 19% more than middle sternocostal region ($p = 0.019$; 7 out of 9 participants). At 50% and 75% MVE all three regions had similar EMG amplitudes (all $p > 0.025$).

Additional shoulder muscles are activated highly in horizontal adduction. At 15% MVE, middle deltoid (~28% MVC), upper trapezius (~25% MVC), and infraspinatus (~26% MVC; Figure 22B; Supplementary Table 3) had the highest activation. At 25% MVE, upper trapezius (~29% MVC), middle (~30% MVC), and posterior deltoid (~29% MVC) were highly activated alongside pectoralis major, while at 50% MVE, upper trapezius (~48% MVC) had high activation. At 75% MVE, the upper trapezius had the highest activity (~62% MVC).

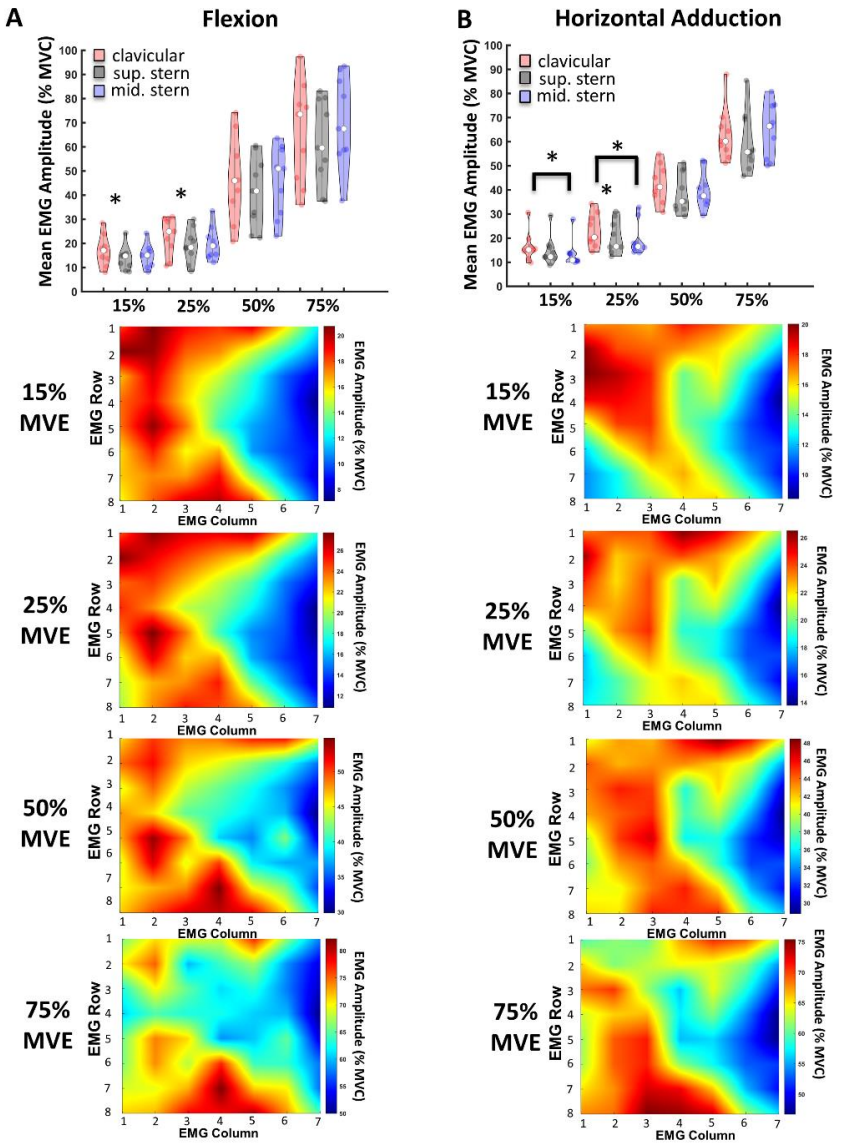

Figure 21: Mean normalized EMG amplitude violin graphs with individual scatter data for clavicular, superior, and middle sternocostal regions with mean normalized (%MVC) spatial topographical maps across the whole sample in 15%, 25%, 50%, and 75% MVE in flexion and horizontal adduction. In violin graphs, each region is denoted in different shades: clavicular region: red; superior sternocostal region (sup. stern): grey; middle sternocostal region (mid. stern): purple. White dots in the middle of each violin plot are medians. In topographical maps, the red colour indicates high activation, while the blue colour indicated low activation. Asterisk (*) denotes significant differences between regions. **A:** Flexion. The clavicular region activated more than superior sternocostal in 15% and 25% MVE. All three regions activated the same in 50% and 75% MVE. **B:** Horizontal adduction. The clavicular region had higher EMG amplitudes than the middle sternocostal at 15% MVE. At 25% MVE, the clavicular region had higher EMG amplitudes than superior and middle sternocostal. At 50% and 75% MVE, all three regions had similar EMG amplitudes.

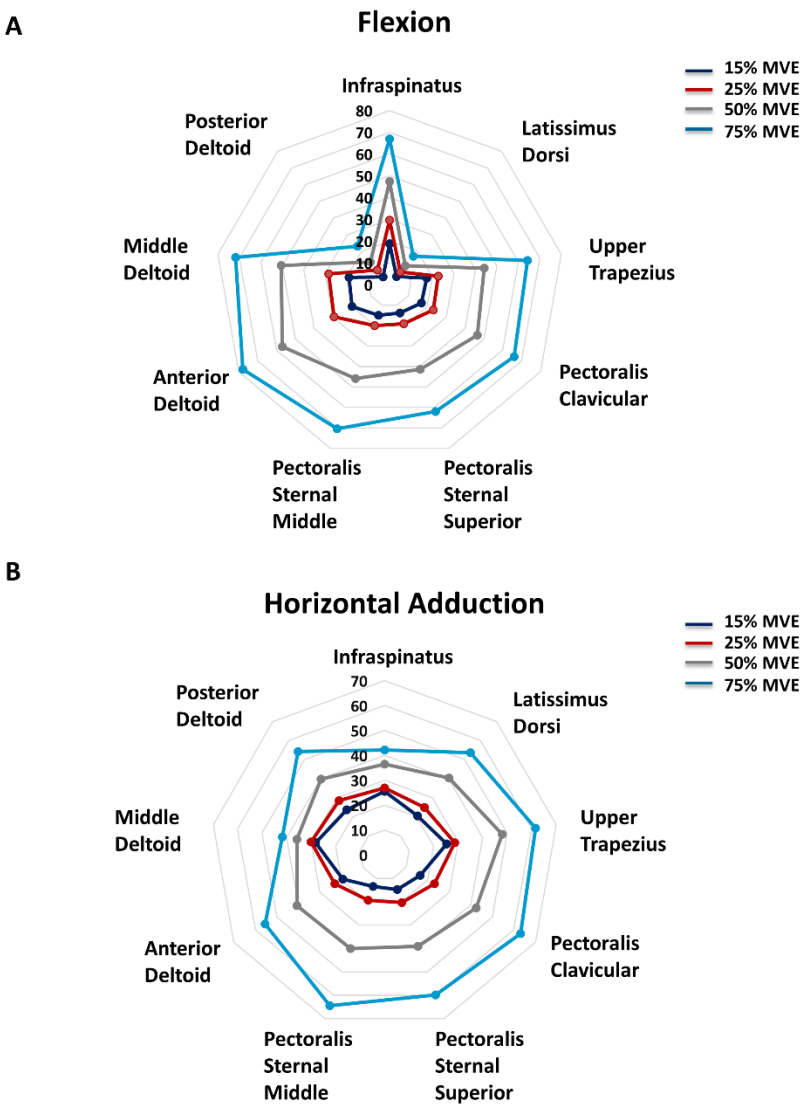

Figure 22: Polar plots depicting mean activation for infraspinatus, latissimus dorsi, upper trapezius, anterior, middle, and posterior deltoid alongside pectoralis major regions in flexion and horizontal adduction. Each coloured line depicts the effort level: blue: 15% MVE; red: 25% MVE; and 50% MVE: grey; and 75% MVE: teal. The magnitude of activation is represented on the Y-axis, with each additional inner circle representing an increase in 10% MVC.

6.5.3. Extension

Region by Effort interaction existed ($F_{(1.77,14.1)} = 12.6$, $p = 0.001$, $\eta p^2 = 0.61$; Figure 23A). At 25% MVE, middle sternocostal region EMG amplitude was ~2 times higher than the clavicular region ($p < 0.001$; 8 out of 9 participants) and superior sternocostal region ($p < 0.001$; 9 out of 9 participants). At 50% MVE, EMG amplitudes were 78% and 81% greater in middle sternocostal region than clavicular ($p = 0.001$; 8 out of 9 participants) and superior sternocostal ($p < 0.001$; 9 out of 9 participants). At 75% MVE, EMG amplitudes remained high in the middle sternocostal in comparison to clavicular (60%; $p = 0.004$; 8 out of 9 participants) and superior sternocostal region (69%; $p < 0.001$; 9 out of 9 participants). Clavicular and superior sternocostal region activated to the same degree in all efforts (all $p > 0.025$).

Additional shoulder muscles also activated highly alongside pectoralis major in this task. Specifically, latissimus dorsi and posterior deltoid displayed high activations at 25% MVE (~20% MVC), 50% MVE (~44% MVC), and 75% MVE (~72-78% MVC; Figure 24A; Supplementary Table 3).

6.5.4. Internal rotation

A main effect of *Region* ($F_{(2,16)} = 166$, $p < 0.0001$, $\eta p^2 = 0.95$; Figure 23B) and *Effort* ($F_{(2,16)} = 24.6$, $p < 0.0001$, $\eta p^2 = 0.75$) existed for internal rotation. Middle sternocostal region had higher EMG amplitudes than clavicular (14%; $p = 0.002$; 8 out of 9 participants) and superior sternocostal region (24%; $p < 0.001$; 9 out of 9 participants). No differences existed between clavicular and superior sternocostal regions ($p > 0.025$).

Additional shoulder muscles displayed high activations in this task. At 25% MVE, all six muscles activated ~20-25% MVC (Figure 24B; Supplementary Table 3). At 50% MVE,

infraspinatus had the highest activation (~54% MVC), while at 75% MVE, latissimus dorsi displayed the highest activity (~73% MVC).

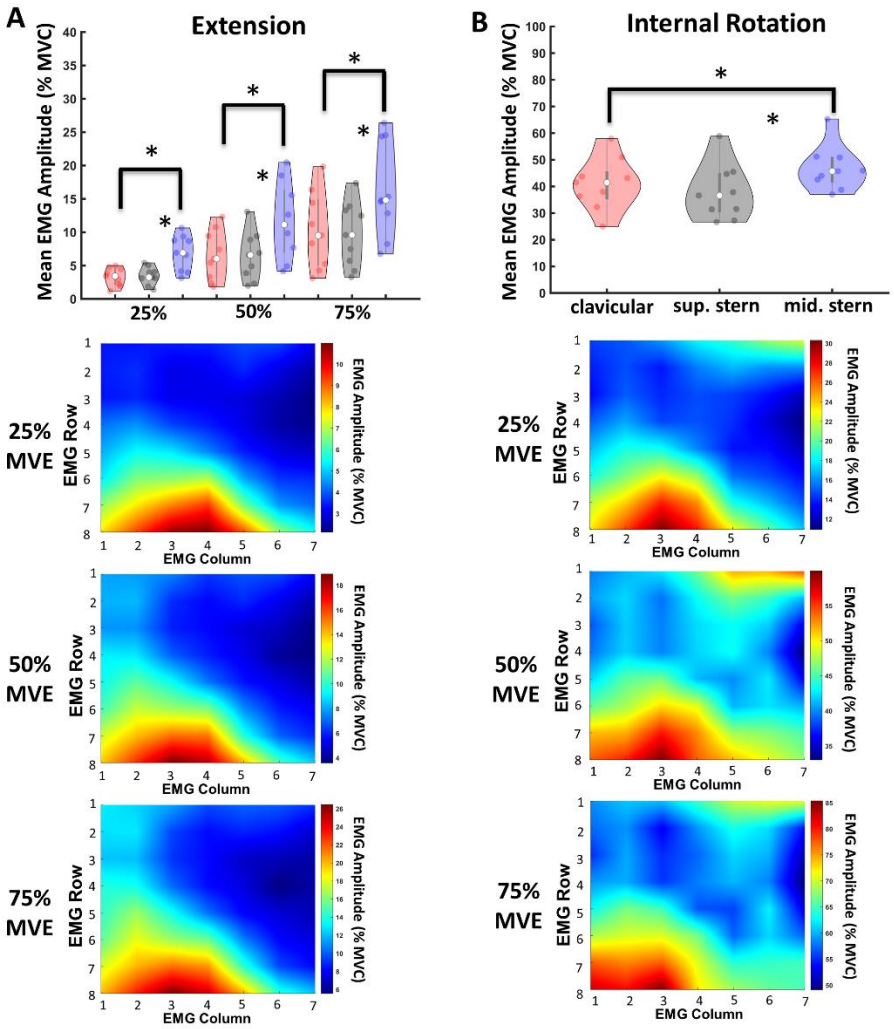

Figure 23: Mean normalized EMG amplitude violin graphs with individual scatter data for clavicular, superior, and middle sternocostal regions with mean normalized (%MVC) spatial topographical maps across the whole sample in 25%, 50%, and 75% MVE in extension and internal rotation. Each region is denoted in a different colour in violin graphs: clavicular region: red; superior sternocostal region (sup. stern): grey; middle sternocostal region (mid. stern): purple. White dots in the middle of each violin plot depict medians. In topographical maps, red colour indicates high activation, while blue indicated low activation. Asterisk (*) denotes significant differences between regions. **A:** Extension. Middle sternocostal regions had higher EMG amplitudes than clavicular and superior sternocostal region, across all efforts. **B:** Internal rotation. The middle sternocostal region had higher EMG amplitudes than clavicular and superior sternocostal regions.

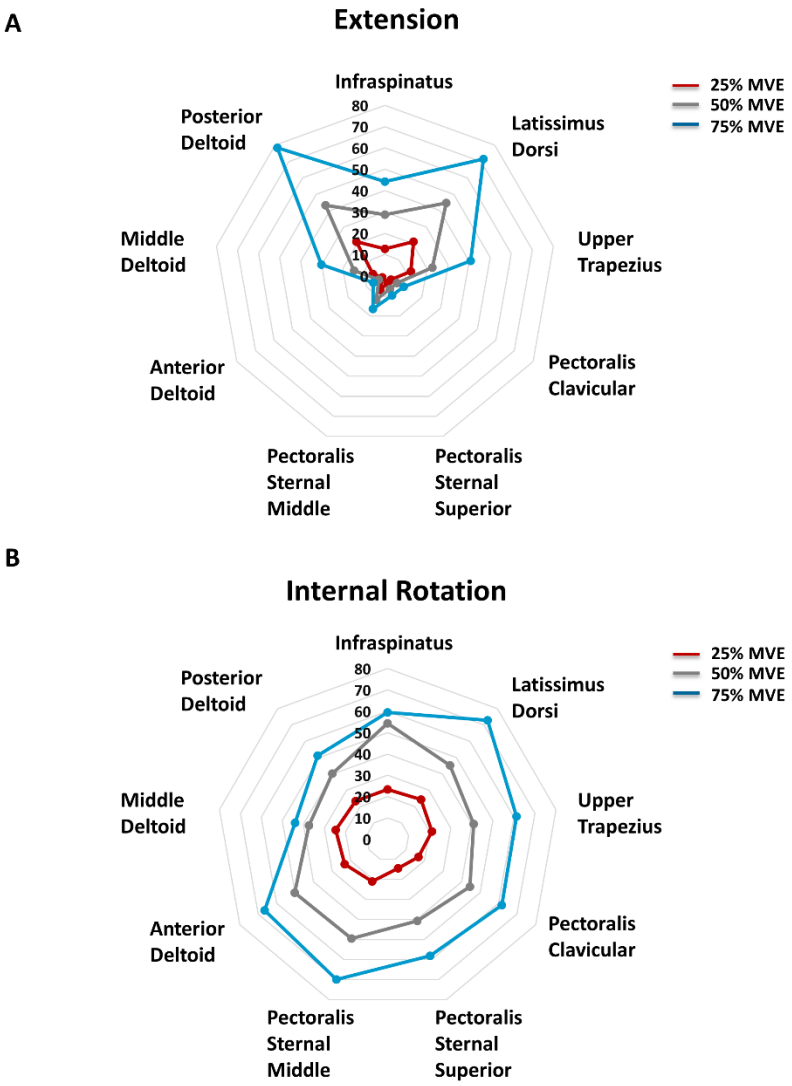

Figure 24: Polar plots depicting mean activation for infraspinatus, latissimus dorsi, upper trapezius, anterior, middle, and posterior deltoid alongside pectoralis major regions in extension and internal rotation. Each coloured line depicts the effort level: blue: red: 25% MVE; and 50% MVE: grey; and 75% MVE: teal. The magnitude of activation is represented on the Y-axis, with each additional inner circle representing an increase in 10% MVC.

6.6. Discussion

This is the first study to provide novel evidence of differential regional pectoralis major activation in healthy females. Regional pectoralis major activity differed between the tasks evaluated and, in some tasks, such as horizontal adduction and flexion, depended on the effort level. Specifically, maintaining low effort elicited higher EMG amplitudes in the clavicular region in both flexion and horizontal adduction, while EMG amplitudes increased in other regions at moderate-to-high efforts. In contrast, middle sternocostal regions activated highly compared to clavicular and superior sternocostal regions in internal rotation and extension across all effort levels.

Effort level dictated which pectoralis major regions had higher EMG amplitudes in isometric flexion. In the present study, middle sternocostal and clavicular regions had similar EMG amplitudes, suggesting equivalent involvement. In contrast, high activation of the clavicular region was previously quantified in males in the same task (Paton and Brown, 1994). The disparity between the studies may lay in the location of EMG electrode placement or sex-related differences in regional pectoralis major activation. Anatomically, the clavicular and middle sternocostal regions are architecturally distinct. The clavicular region has shorter fiber bundle lengths but greater medial and lateral pennation angles than the middle sternocostal region (Brown et al. 2007; Fung et al. 2009).

Further, in flexion, regional moment arm lengths also differ, such that the clavicular region has longer flexor moment arms than the superior sternocostal region (Ackland et al., 2008). Additionally, at 20° of abduction, the clavicular region may also act as an abductor (Ackland et al. 2008). Therefore, the clavicular region may activate to maintain arm in abduction, while the middle sternocostal region activates to generate and sustain flexion at low efforts. Increased contribution

of middle sternocostal regions was particularly evident at moderate and high efforts. While absolute EMG amplitudes increased in all three regions, the relative increase was greater in the middle sternocostal regions (from 25% to 50% MVE: 128%, from 25% to 75% MVE: 251%). This is especially important to consider in the context of daily tasks, such as carrying and holding a heavy grocery bag, which requires sustained moderate efforts.

Similar to flexion, effort level dictated which pectoralis major regions had higher EMG amplitudes in horizontal adduction. Pectoralis major has a large horizontal adduction moment arm when the arm is at 90° of abduction (Kuechle et al. 1997; Bassett et al. 1990). Supportingly, clavicular and superior sternocostal regions had similar EMG amplitudes at 15% MVE, while EMG amplitudes were higher in clavicular than other regions at 25% MVE. Higher EMG amplitudes (Paton and Brown, 1994; McDonald et al. 2012) and greater stiffness (Leonardis et al. 2017) were previously quantified in clavicular compared to the sternocostal region at low efforts in this task. Additionally, in the present study, an increased contribution of sternocostal regions was evident in moderate and high efforts, such that relative EMG amplitudes in the superior and middle sternocostal regions substantially increased. Increased activation of sternocostal regions at high efforts was previously quantified in males in a similar task (Paton and Brown, 1994). Thus, despite the clavicular region's architectural and mechanical advantages for this task, the sternocostal regions act to maintain performance in moderate and high efforts.

In contrast to horizontal adduction and flexion, a more localized activation specific to middle sternocostal regions occurred in internal rotation and extension tasks. While both clavicular and sternocostal regions contribute to internal rotation (Wolfe et al. 1992; Provencher et al. 2010; Stegnik-Jansen et al. 2011; Leonardis et al. 2019; Marsh et al. 2020), sternocostal regions also have a mechanical advantage in extension against resistance (Paton and Brown, 1994; Brown et

al. 2007; Stegnik-Jansen et al. 2011). Internal rotation moment arms decrease with arm abduction for all regions (Ackland and Pandy, 2011). When the arm is at 90° of abduction, the estimated length of internal rotation moment arms for clavicular and sternocostal regions is ~1.7 mm and ~6.4 mm, respectively (Ackland and Pandy, 2011). Therefore, sternocostal regions have a greater mechanical advantage than the clavicular region to assist in internal rotation in this arm posture. In extension, increased fiber lengthening in the lower sternocostal regions occurs when extending the arm from neutral to 30° of extension (Wolfe et al. 1992). Lower sternocostal regions are more likely to assist in extension against resistance, mainly when the arm is at 20° of abduction. Higher EMG amplitudes in the lower sternocostal regions, irrespective of the effort level, were quantified in males (Paton and Brown, 1994; Brown et al. 2007). Plausibly, lower sternocostal regions may also be highly engaged in this task in females, but their recording in the current study was infeasible due to the overlying breast tissue.

6.6.1. Existence of partition specific activation in the sternocostal region

Present findings indicate a specialized role of the middle sternocostal regions in comparison to the superior sternocostal regions. Architecturally, the superior sternocostal region has greater medial and lateral muscle fiber pennation angles than the middle sternocostal region (Fung et al. 2009). Further, an average of five to six nerves branching from the brachial plexus as a lateral pectoral nerve innervate different muscle fiber bundles within the sternocostal region (Manktelow et al. 1980; Haladaj et al. 2019), indicating the possibility for differential regional innervation. Due to the architectural differences, middle sternocostal regions may have a greater advantage in isometric internal rotation and extension. This preliminary evidence suggests possible differences in functionality between the two sternocostal regions and should be probed further.

6.6.2. Implications of findings to clinical cases

Collectively, clavicular and sternocostal fiber regions demonstrated fundamental utility in horizontal adduction, flexion, extension, and internal rotation. Correspondingly, injury to the sternocostal regions may reduce the ability to maintain moderate-to-high efforts in horizontal adduction and flexion while also reducing the capability to maintain effort in extension and internal rotation. Additionally, an intact clavicular region may be sufficient to maintain low horizontal adduction and flexion effort, as suggested previously (Leonardis et al. 2019). However, maintaining moderate-to-high efforts required in some athletic activities and specific daily tasks, such as lifting a heavy grocery bag, may be compromised, prompting compensatory activations of other shoulder muscles. Reductions in internal rotation and extension strength were evident in females who underwent subpectoral breast reconstruction surgery (de Haan et al., 2007; Leonardis et al. 2019), although the maintenance of effort in these tasks is yet to be examined.

6.7. Limitations

Inherent methodological limitations accompany this work. HD-sEMG could not be acquired from all regions of the pectoralis major due to the overlying breast tissue. Higher EMG amplitudes were previously quantified in inferior pectoralis major in male participants in isometric extension (Paton and Brown, 1994). Plausibly, this region may also highly activate in females. Future studies may consider using fine-wire EMG to investigate these regions. Secondly, only young females were recruited for this study, limiting the findings to other age groups. Finally, a subset of tasks was assessed, resulting in potential difficulty in transferring insights to other tasks.

Additionally, crosstalk from the surrounding muscles, such as the pectoralis minor, serratus anterior, external obliques, or intercostal muscles, may have influenced the patterns of regional

activation quantified in this study. Attempts were made to minimize the degree of crosstalk by sampling EMG from many closely spaced electrodes (10 mm interelectrode distance) and quantifying differential derivation in the post-processing steps. Lastly, it is known that at least one innervation zone is located within the superior region of the pectoralis major (Mancebo et al. 2019). Due to the challenges in quantifying the innervation zones from motor unit action potentials, the exact location of these innervation zones was challenging to determine. Therefore, this study quantified the mean normalized EMG amplitudes across the innervation zones, which may have influenced the findings.

6.8. Conclusions

This investigation provides the most comprehensive electromyographic evaluation of pectoralis major activation in healthy females across a subset of tasks and effort levels, providing novel data regarding regional pectoralis major activation in this cohort. The regional activity of pectoralis major in females depends on the task and effort level. It reinforces the need to consider the full complexity of regional pectoralis major activation in healthy and compromised populations. This knowledge is particularly crucial in evaluating pectoralis major damage, exercise, and surgical interventions involving the disinsertion of specific pectoralis major regions.

Chapter 7: Divergent regional pectoralis major activation in adduction and internal rotation in healthy males: A high-density electromyography study

7.0. Abstract

Pectoralis major assists in numerous daily tasks, although its regional activation and functional importance to typical shoulder function remain ambiguous. Lack of knowledge on its contributions has led to mischaracterizations in its activation in fundamental, exercise, and clinical research. Increased knowledge of regional pectoralis major activation is critical in understanding its role in shoulder control and improving current practices in acquiring its activation. The present study explored regional pectoralis major activation in four isometric tasks in healthy males. Two high-density surface electromyography arrays captured regional activation in four tasks: adduction at 90° of arm abduction and 90° of the external arm rotation (i.e., adduction external 90); adduction at 60° of arm abduction; and internal humeral rotation at 60° of abduction at four effort levels: 15%, 25%, 50%, and 75% scaled to task-specific maxima acquired in maximal voluntary efforts (MVE). At 15% and 25% MVE, lower sternocostal regions activated between 14-31% more than upper sternocostal regions in internal rotation and adduction 60. In contrast, at 50% and 75% MVE, all regions activated equally in these tasks (all $p > 0.025$). In adduction 90, lower sternocostal regions activated more than the upper sternocostal (~20-39%) at 15%, 25%, 50% MVE, and clavicular (~23-56%) regions across all effort levels. Similarly, in adduction external 90, the lower sternocostal region activated 51% more than the clavicular and 26% more than the upper sternocostal region, irrespective of the effort level. Current findings reveal that lower sternocostal regions activate highly in adduction and internal rotation tasks, necessitating their surveillance to describe pectoralis major function adequately.

7.1. Introduction

Pectoralis major activation enables the performance of numerous functional tasks. This multipennate muscle crosses at least three shoulder joints – sternoclavicular, acromioclavicular, and glenohumeral. It consists of three distinct regions: clavicular, sternocostal, and abdominal (Ashley, 1952; Fung et al., 2009; Lewis 1901; Wolfe et al., 1992), with more recent anatomical studies describing four and three partitions within the sternocostal and abdominal regions, respectively (Fung et al. 2009). Due to its architecture, the pectoralis major is multifunctional and assists in humeral vertical and horizontal adduction, flexion, internal rotation, and extension against resistance.

Commonly, pectoralis major activation is evaluated using classic, low-spatial resolution surface electromyography (sEMG) in bipolar derivation, such that EMG is acquired from clavicular and/or sternocostal regions. The number of electrodes and the location of sEMG electrode placement differs between studies, as some acquired EMG from clavicular and superior sternocostal regions (for example, see: Lauver et al. 2015; MacLean et al. 2019; Ho et al. 2019; Leonardis et al. 2020), while others only evaluated activity from a single pectoralis major location (usually sternocostal; for example see: Schwartz et al. 2017; Dicus et al. 2018; Quittmann et al. 2020; Alizadeh et al. 2020). Therefore, no consensus exists on classic sEMG electrode placement, resulting in conflicting and highly variable findings on pectoralis major activation across studies. Further, assessment of middle/inferior sternocostal and abdominal region activation is often neglected, despite their functional importance and anatomical divergence from superior regions. Indeed, only several studies characterized activation of these regions (Paton and Brown, 1994; Glass and Armstrong, 1997; Wickham et al. 2004; Brown et al. 2007; Muyor et al. 2019). However, even in these studies, the location and orientation of sEMG electrode placement varied.

Collectively, considerable variability in sEMG electrode location and orientation increases the difficulty in interpreting and drawing inferences regarding pectoralis major contribution in different tasks.

Recording pectoralis major activation using classic EMG is not trivial. Multi-functional muscles such as pectoralis major do not activate homogeneously. Their activity is highly dependent on the arm posture, task, and effort level (Paton and Brown, 1994; Wickham et al. 2004; Brown et al. 2007; Holtermann et al. 2008; Farina et al. 2008; Watanabe et al. 2012). Additionally, at least two known innervation zones exist in pectoralis major (Barbero et al. 2012; Mancebo et al. 2019). As such, EMG amplitude quantified using classic EMG is dependent on the location of the EMG electrodes and provides limited information on the activation of the whole muscle.

High-density surface electromyography (HD-sEMG), consisting of an array of electrodes, enables the acquisition of EMG signals from the whole muscle, allowing for quantification of spatial distribution in muscle activity. A single study to date evaluated pectoralis major activation using HD-sEMG during a bench press (Mancebo et al. 2019), demonstrating a large deviation in the spatial distribution of activity within pectoralis major regions in this exercise. Therefore, characterizing the spatial distribution of muscle activity within pectoralis major using HD-sEMG may provide greater insight into pectoralis major contribution in different tasks, role in fundamental shoulder function, and differences in regional activation across tasks. This knowledge can then be leveraged for more informed EMG electrode placement and improved characterization of pectoralis major changes following exercise training, treatment, or rehabilitation. Therefore, this study aimed to characterize regional pectoralis major spatial distribution at low to high efforts in four submaximal isometric tasks in healthy males. The tasks in this study reflect tasks in which pectoralis major activation is necessary. In contrast, different effort levels reflect a wide range of

muscular responses required in the performance of daily, occupational, and exercise tasks. The primary hypothesis was that the lower sternocostal regions will have higher normalized EMG amplitudes than superior sternocostal and clavicular regions across all tasks studied.

7.2. Methods

7.2.1. Participants

Nineteen healthy, right-hand dominant males (25 ± 4.7 years; weight: 75.3 ± 8.1 kg; height: 173.5 ± 5 cm; Table 8) participated. The chosen sample size was selected using *a priori* power analyses. Sample size calculations in G*Power 3.1 (Universitat Dusseldorf, Dusseldorf, Germany) indicated that a minimum of 16 participants is required to obtain sufficient power (Cohen, 1988). The effect size chosen ($f^2 = 0.31$) is on the lower end of the observed effect size in previous studies, which reported effect sizes between 0.2 to 0.6 (Paton and Brown, 1994; Brown et al. 2007; Wickham et al. 2004). Males were recruited using word-of-mouth or posters advertising the study in the kinesiology, engineering, psychology, and student center buildings. The inclusion criteria included healthy right-hand dominant, young males (between 18 and 40 years old). All males recruited were recreationally active. Participants did not engage in strenuous physical activity at least 24 hours before the session. Participants were instructed by the investigator not to consume any caffeinated drinks the morning of the session and drink plenty of water the day before the session. All participants reported no history of musculoskeletal injury to the right arm or back and no back pain in the past six months or the presence of neurological disease. Further, no participants displayed positive signs of impingement, as screened with Appley's Scratch and Hawkin's impingement tests. This study was reviewed and received ethics clearance from the Institutional Office of Research Ethics and conformed to the Declaration of Helsinki.

When participants arrived at the laboratory, their height, weight, rib cage, chest circumference, clavicle, and sternal length were measured. The chest was measured starting from the fullest part of the participant's bust, with measuring tape wrapped around under the axilla. Rib cage circumference involved measuring around the rib cage, just beneath the fullest part of the participant's bust. Next, the clavicular length was measured from the acromion to the sternal notch, while the sternal length was measured from the sternal notch to the palpated xiphoid process.

Table 8: Participant demographics and anthropometric measurements (± standard deviation).

Age (years)	25 ± 4.7
Height (cm)	173.5 ± 8.1
Weight (kg)	75.3 ± 8.1
Chest circumference (cm)	99.7 ± 7.8
Ribcage circumference (cm)	94.7 ± 7.2
Breast tissue thickness at the nipple (cm)	4.9 ± 2.4
Clavicle length (cm)	17.2 ± 1.7
Sternum length (cm)	18.8 ± 2.1

7.2.2. High-density surface electromyography

Two 64-channel high-density surface electromyography (HD-sEMG) arrays in the monopolar mode were used to acquire regional pectoralis major activation (ELSCH064NM3, OTBioelecttronica, Torino, Italy; Figure 25A). Electrode arrays consisted of channels in an 8 by 8 matrix with a 10 mm inter-electrode distance. Before applying the electrodes, the skin overlying the pectoralis major was shaved if necessary and cleaned with abrasive paste and water to reduce impedance. Two HD-sEMG arrays were applied on the skin using a 1 mm thick two-sided adhesive foam with holes filled with electroconductive gel. The superior array was placed ~ 2 cm inferior to the clavicle. The middle of the array was positioned between the sternum and the axilla, parallel to the muscle fibers. The inferior array was placed directly below the superior array with no space in between the two arrays. The arrays were fixed with adhesive tape and connected to a 128

channel EMG amplifier (EMGUSB2+, OTBioelecttronica, Torino, Italy). All EMG signals were bandpass filtered with a cut-off frequency between 10 – 500 Hz and sampled at 2048 Hz with a 12-bit A/D converter (5V dynamic range). HD-sEMG signals were amplified by a factor between 100-5000 V/V depending on the task, effort level, and participant. The level of saturation was monitored online. If more than 5% of the channels were saturated during the trial, the trial was immediately terminated, gain adjusted, and the trial repeated. One wet reference band was wrapped around the participant's right wrist, while a reference electrode was placed on the right clavicle.

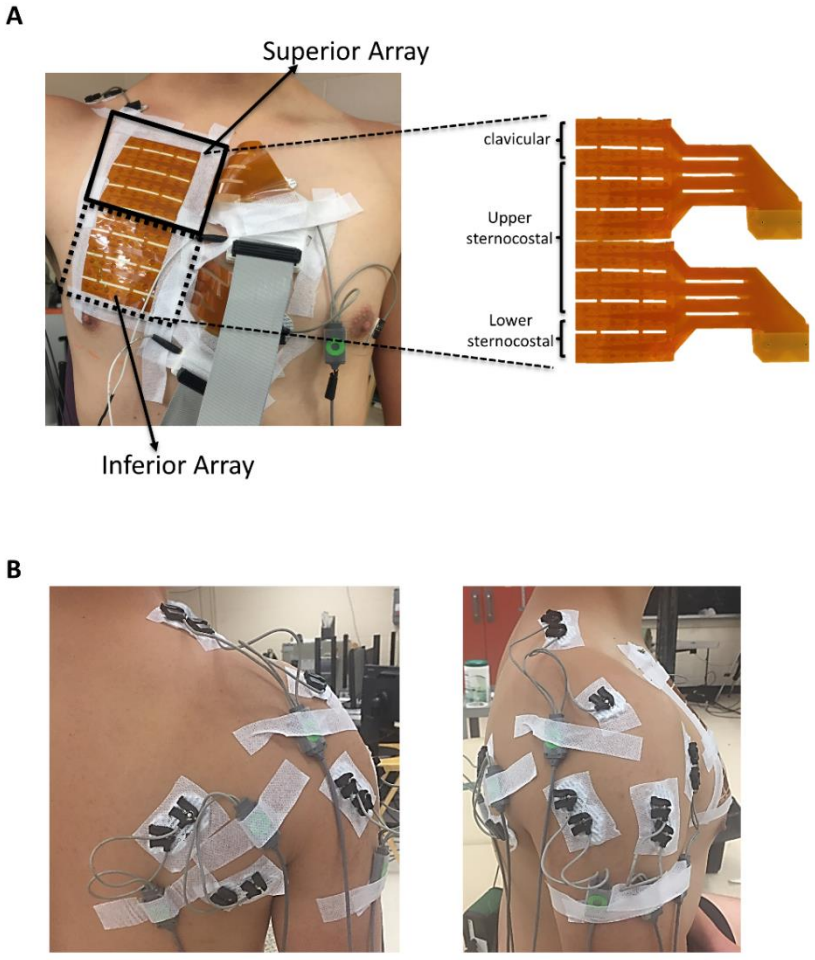

Figure 25: HD-sEMG array and bipolar sEMG electrode location. **A:** Two 64 channel high-density arrays were placed overlying the pectoralis major muscle (128 channels total). **B:** Additional shoulder muscles were collected using bipolar sEMG.

7.2.3. Force measurement

Raw voltage was acquired concurrently with HD-sEMG while participants exerted effort against an arm cuff. The custom-made arm cuff was attached to a six-degree-of-freedom (6-DOF) force transducer (MC3A, AMTI MA, USA) mounted on a robotic arm (Figure 26; Motoman Robotics Division, Yaskawa America, USA). Force was sampled at 1500 Hz and amplified (1000x) using VICON Nexus 1.7.1 software.

7.2.4. Electrocardiography measurement (ECG)

Electrocardiography (ECG) was collected with HD-sEMG and force measures. ECG was captured using silver-silver chloride (Ag-AgCl) disposable electrodes in a monopolar configuration. Before the placement of electrodes, the area was shaved and cleaned with abrasive gel and water. Three electrodes were placed over the left chest at the 6^{th} costal level, approximately along the anterior axillary line, and medially at the sternocostalis junction (Drake and Callaghan, 2006). ECG was collected using a wireless telemetered system (Noraxon Telemyo 2400 T G2 Noraxon, Arizona, USA). Raw signals were band-pass filtered between 10-1000 Hz and differentially amplified with a CMRR > 100dB and an input impedance of 100 MΩ. Analog signals were converted to digital using a 16-bit A/D card with a ±10 V range. The sampling frequency was 1500 Hz.

7.2.5. Additional shoulder muscle monitoring

The activity of six additional shoulder muscles was concurrently recorded with HD-sEMG, ECG, and force. Upper trapezius, latissimus dorsi, deltoid (anterior, middle, and posterior), and infraspinatus activity was monitored in the background (Figure 25B). sEMG activity was recorded

using silver-silver chloride (Ag-AgCl) disposable electrodes with a 1 cm diameter and a fixed inter-electrode spacing of 2 cm in a bipolar configuration. Before the placement of the electrodes, the area overlying the muscle belly was shaved and cleaned with abrasive gel and water. Placement of the sEMG electrodes was confirmed with palpation while the participant exerted a low, submaximal contraction of the muscle in positions described in Supplementary Table 1 (Kelly et al., 1996; Cram and Kasman, 1998). A reference electrode was placed on the acromion. sEMG was collected using a wireless telemetered system (Noraxon Telemyo 2400 T G2 Noraxon, Arizona, USA). Raw signals were band-pass filtered from 10-1000 Hz and differentially amplified with a CMRR > 100dB and an input impedance of 100 MΩ. Analog signals were converted to digital using a 16-bit A/D card with a ±10 V range. The sampling frequency was 1500 Hz.

7.2.6. Experimental protocol

Experimental protocol included the performance of several maximal voluntary efforts (MVE) and isometric ramped submaximal trials in four tasks at four effort levels. All participants underwent a brief warm-up and training on how to generate MVE in different tasks. Following this, participants practiced exerting an effort against an arm-cuff with visual feedback of their force provided on a monitor. This training served to precondition the muscle-tendon unit (Maganaris et al., 2002) and familiarize the participant with the submaximal task. The participant sat on a chair with the torso secured to the chair by a padded strap for all trials. Additionally, the arm was secured in the arm-cuff to mitigate any arm movement during the task performance. Following training and familiarization, participants performed two 5-second task-specific MVEs in the following isometric tasks (Figure 26): a) adduction (ADD60; Figure 26A) and b) internal rotation (IR60; Figure 26B) from 60° of arm abduction; c) adduction from 90° of arm abduction (ADD90; Figure

26C); and d) adduction from 90° of arm abduction and 90° of arm external rotation (ER90; Figure 26D). During MVE performance, participants were verbally encouraged by the investigator. Each MVE was separated by 2 minutes of rest. Maximal MVEs were quantified using a custom-made program in LabVIEW (National Instruments, version 3.1). For each task, the mean of two maximal task-specific MVE trials was used to scale all analogous submaximal trials. During MVE performance, off-axis forces were monitored in the LabVIEW program, such that participants were required to achieve above 80% of the total effort along the intended transducer axis. If this was not accomplished, participants received verbal feedback, and the trial was repeated. Additionally, if the second MVE trial was different from the first by 10 Newtons, the MVE trial was repeated to ensure consistency between MVEs.

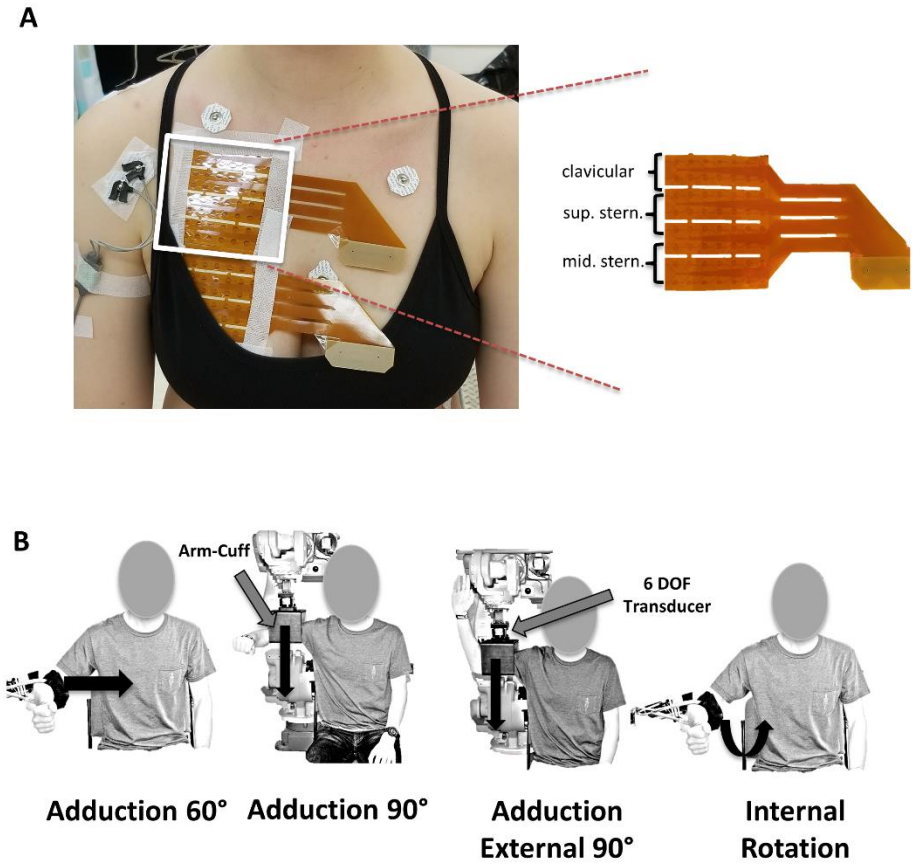

Figure 26: Experimental protocol. Participants performed four tasks: **A**: adduction from 60° of abduction (ADD60); **B**: adduction from 90° of abduction (ADD90); **C**: adduction from 90° of abduction and 90° of external rotation (ADDER90); **D**: internal rotation from 60° of abduction (IR60).

For each task, participants performed submaximal ramped isometric efforts scaled to task-specific MVE. The effort levels included: 15%, 25%, 50%, and 75% MVE. Participants performed each effort level twice, and trials lasted 60, 60, 30, and 10 seconds, respectively, with three to five-minute rest breaks between the trials, with more time allocated if requested by the participant. Participants were encouraged to report feelings of fatigue and the need for longer rest periods. At 15% and 25% MVE, participants ramped up at ~2% MVE/s, held the effort, and then ramped down at ~2% MVE/s. At 50% MVE, participants ramped at ~3% MVE/s, while at 75% MVE, participants ramped at ~5% MVE/s. Tasks were fully randomized between participants, as well as within a participant. Effort levels were randomized within each task, with each submaximal effort performed consecutively within a task. Intratrial visual feedback provided on a monitor displayed the required effort level and live feedback of the exerted effort against the arm-cuff.

7.3. Data Analysis

7.3.1. HD-sEMG signal processing

Pre-processing steps in data analysis involved visual inspection of the raw HD-sEMG data and removal of heart rate from the monopolar HD-sEMG signals. Before signal processing, raw HD-sEMG data was inspected for any artifacts or channel saturation in a custom-made program in MATLAB (MATLAB 2019b; Mathworks Inc.). Channels that saturated or had artifacts were tagged and removed. Subsequently, values for those channels were interpolated. Next, acquired ECG was used to remove heart rate contamination from monopolar HD-sEMG signals. ECG was interpolated to 2048 Hz, and the HD-sEMG signals were cross-correlated with the heart rate data to match the timing of each heartbeat's peak amplitude. Each trial was visually inspected to make sure the algorithm correctly recognized the ECG peaks. The precise timing of each ECG peak

surrounded by 250-millisecond windows before and after the peak was determined and used to avoid the quantification bias of the root mean square (RMS) amplitude.

Raw HD-sEMG data were band-pass filtered with a 3rd order Butterworth filter (20-500 Hz), and the differential derivation was quantified from left to right (i.e., from axilla towards sternum). RMS was quantified for each differential channel. Following this, the resultant force was used to focus on the first half of the hold. The most stable part of the hold was selected by dividing the resultant force into 5-second segments and performing EMG analyses on the force segment with the lowest coefficient of variation. All submaximal data were normalized to maximal trials. Maximal trials were combined for adduction, and internal rotation at 60° and adduction tasks at 90° as these tasks were performed at the same arm posture and direction. For each HD-sEMG channel within MVE, the mean window of the 3-second data segment surrounding the maximal force achieved was extracted. Following this, each channel's maximal value within posture-specific MVEs was extracted, and each channel within a submaximal trial was normalized to the channel-specific maximal value within two tasks. Following EMG normalization, spatial scaling was applied for each participant to account for differences in pectoralis major size. Normalized EMG amplitude was defined in an individual pectoral system by scaling each participant's EMG data to the participant whose clavicle and the sternal length was the longest. Normalized scaled data was then divided into clavicular (rows 1-3), upper sternocostal (rows 4-13), and lower sternocostal (rows 13-16) regions. This division was based on an anatomical description of regional locations (Fung et al., 2009). Subsequently, the regional mean of the two trials within each task and effort level was quantified.

7.3.2. Force

Raw voltage data obtained in submaximal and maximal trials were processed in a custom-made program in MATLAB. First, the raw voltage was converted to Newtons and filtered using a 3rd order low-pass Butterworth filter with a cut-off frequency of 15 Hz. The mean force that matched the most stable part of the resultant force (i.e., same as for HD-sEMG analyses) was quantified for all submaximal trials and normalized to the task-specific MVE. Normalized force data was used to confirm that all participants received the same amount of feedback and exerted 15%, 25%, or 50% MVE during submaximal trials.

7.3.3. Bipolar surface electromyography

Bipolar EMG data in task-specific maximal MVEs and submaximal trials were processed. Before analyses, sEMG data were visually inspected for any artifacts using a custom-made MATLAB program. Subsequently, all sEMG data was band-pass filtered with a 2nd order Butterworth filter (30-500 Hz), and RMS was quantified. The mean 5-second RMS for each muscle was quantified for the same force segment as for HD-sEMG submaximal trials. Similarly, for MVEs, the mean of a 3-second window surrounding the maximal force was extracted and matched the same window used to extract maxima in HD-sEMG. Maximal trials were combined for adduction 60, and internal rotation and adduction 90, and adduction external 90 as these tasks were performed in the same arm posture. Subsequently, maximal value across posture-specific MVEs was quantified, and submaximal trials were normalized to the muscle-specific maxima.

7.3.4. Data removal

Data from one participant had to be removed due to the technical issues with the acquisition of HD-sEMG signals. Additionally, the amplitude of HD-sEMG signals across channels was low (i.e., below inherent noise levels) in adduction external 90 at 15% MVE across all participants, prompting the removal of this effort level from further analyses. Further, several participants experienced fatigue in 75% MVE effort during the ramping, prompting the removal of two participants in adduction 60° task and four participants from adduction at 90° task. Lastly, ~1% of the trials were removed due to artifacts, saturation, or low electrode-skin contact.

7.4. Statistical Analyses

All statistical analyses were performed using SPSS (IBM, version 21). Before any comparisons, the data were checked for normality and sphericity using the Shapiro-Wilk test and Mauchly's test of sphericity, respectively. Not normally distributed data were ln transformed. Two-way repeated-measures analysis of variance (ANOVA) was performed on EMG amplitude in adduction at 60°, adduction 90°, and internal rotation with within-subject factors *Region* (clavicular, upper, and lower sternocostal) and *Effort* (15%, 25%, 50%, 75% MVE). Similarly, for adduction external 90, two-way repeated-measures ANOVA was performed on EMG amplitudes with within-subject factor *Region* (clavicular, upper and lower sternocostal) and *Effort* (25%, 50%, 75% MVE). If significant interactions between *Region* and *Effort* existed, planned comparisons with Dunn-Bonferonni correction were performed to determine significant differences. EMG amplitudes quantified for additional shoulder muscles were ranked from highest to lowest activity based on the activation level for each task. They were used to determine which additional shoulder muscles contributed highly to the task. Partial eta-squared (ηp^2) assessed the effect size of the

significant differences in EMG amplitudes. ηp^2 less than 0.06 was deemed as "small," 0.07-0.14 as "moderate," and greater than 0.14 as "large" (Cohen, 1969). Significance was $p < 0.05$.

7.5. Results

Generally, lower sternocostal regions had higher EMG amplitudes across all effort levels in tasks when the arm was at 90° of elevation, and for low effort levels (i.e., 15% and 25% MVE) in tasks when the arm was at low elevations (i.e., 60° of abduction). All three regions activated similarly in moderate and high effort levels (i.e., 50% and 75% MVE) when the arm was at 60° of abduction. All participants received the same amount of feedback across tasks and effort levels (Table 9).

Table 9: Mean force in Newtons and as a percent of MVE (± standard deviation) for all tasks and effort levels.

Task	Effort Level	Mean Force (N)	Mean %MVE
Adduction 60	15%	45.6 ± 4.8	15.6 ± 1.1
	25%	75.2 ± 8.5	25.7 ± 1.8
	50%	151.9 ± 17.2	51.8 ± 2.4
	75%	228.5 ± 28.4	77.9 ± 3
	100%	293.8 ± 39.5	-
Adduction 90	15%	47 ± 14.5	15.9 ± 1.8
	25%	76.7 ± 21.6	26 ± 1.8
	50%	151.2 ± 42.8	50 ± 2.6
	75%	228.6 ± 63.4	77 ± 5
	100%	295 ± 82.9	-
Internal Rotation	15%	41.8 ± 10.3	16 ± 2.8
	25%	69.1 ± 18.2	26.1 ± 1.4
	50%	138.5 ± 37.1	52.3 ± 1.8
	75%	207.5 ± 58.1	78 ± 2.2
	100%	258.5 ± 72.7	-
Adduction External 90	15%	40.8 ± 9.4	14.8 ± 1.5
	25%	68.5 ± 14.7	24.9 ± 1.6
	50%	139.7 ± 30.5	50.7 ± 3.1
	75%	208.1 ± 46.3	75.4 ± 3.8
	100%	274 ± 59.9	-

7.5.1. Internal rotation

During internal rotation, a significant *Region by Effort* interaction existed ($F_{(2.1,37)} = 5.1$, $p = 0.009$, $\eta p^2 = 0.23$; Figure 27A). Specifically, lower sternocostal region activated 30% more than the upper sternocostal region at 15% MVE ($p < 0.0001$; 15 out of 18 participants) and 21% more at 25% MVE ($p = 0.001$; 14 out of 18 participants). At 50% MVE and 75% MVE all three regions activated to the same magnitude (all $p > 0.025$).

Several additional shoulder muscles were activated alongside the pectoralis major. Specifically, at 15% MVE, the latissimus dorsi and upper trapezius were highly activated, while at 25%, 50%, and 75% MVE, high activations were quantified only in the latissimus dorsi (Supplementary Table 4; Figure 28A).

7.5.2. Adduction from 60° of abduction

A significant *Region by Effort* interaction existed ($F_{(2.1,32)} = 12.5$, $p < 0.0001$, $\eta p^2 = 0.45$; Figure 27B). Specifically, lower sternocostal region activated 25% more than upper sternocostal region at 15% MVE ($p = 0.003$; 10 out of 16 participants) and 14% more at 25% MVE ($p = 0.004$; 9 out of 14 participants), but not at 50% MVE ($p = 0.92$) or 75% MVE ($p = 0.49$). Clavicular and upper sternocostal region, and clavicular and lower sternocostal region activated similarly across all efforts (all $p > 0.025$).

Additional shoulder muscles had high activations in this task. Latissimus dorsi and middle deltoid had high activations across all efforts (Supplementary Table 4; Figure 28B). At 50% MVE and 75% MVE, the posterior deltoid also had high activity.

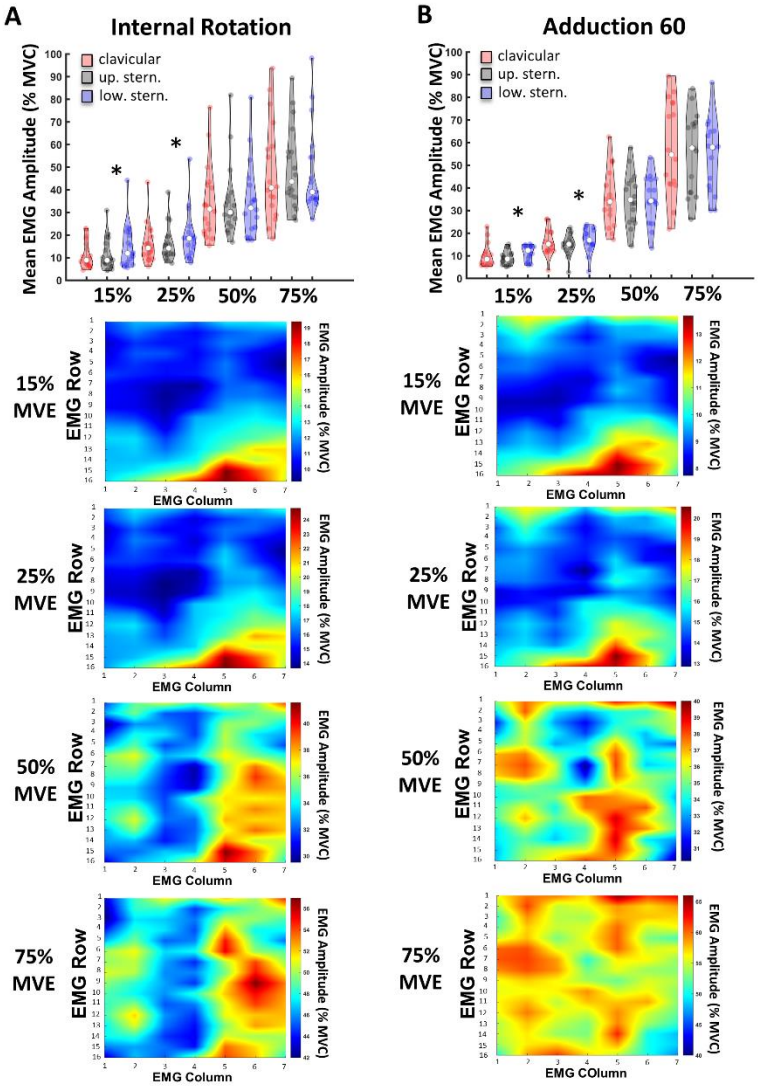

Figure 27: Scaled mean normalized EMG amplitude violin graphs with individual scatter data for clavicular, upper, and lower sternocostal regions with mean normalized (%MVC) spatial topographical maps across the whole sample in 15%, 25%, 50%, and 75% MVE in internal rotation and adduction from 60° of arm abduction. Each region is denoted in a different colour in violin graphs: clavicular region: red; upper sternocostal region (up. stern): grey; lower sternocostal region (low. stern): purple. White dots in the middle of each violin plot are medians. In topographical maps, the red colour indicates high activation, while the blue colour indicates low activation. Asterisk (*) denotes significant differences between regions. **A:** Internal rotation. The lower sternocostal region activated more than the upper sternocostal at 15% and 25% MVE. All three regions activated the same in 50% and 75% MVE. **B:** Adduction 60°. The lower sternocostal region had higher EMG amplitudes than the upper sternocostal at 15% and 25% MVE. At 50% and 75% MVE, all three regions had similar EMG amplitudes.

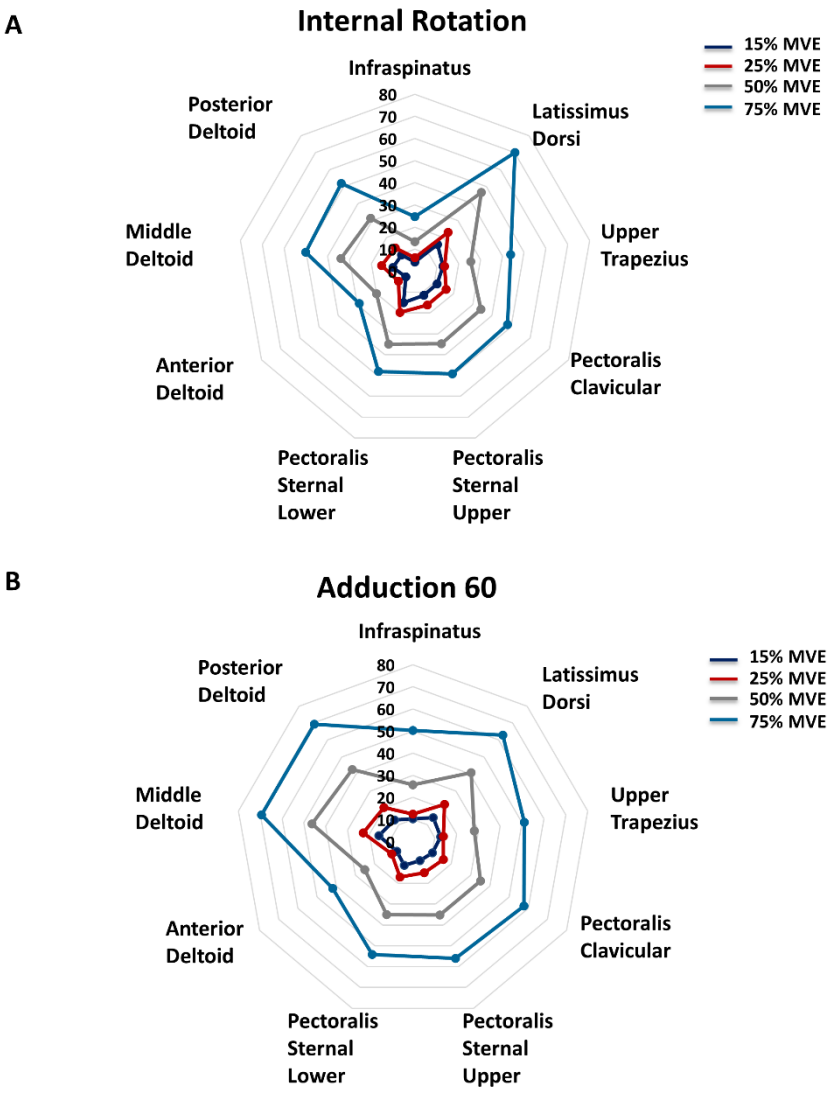

Figure 28: Polar plots depicting mean activation for infraspinatus, latissimus dorsi, upper trapezius, anterior, middle, and posterior deltoid alongside pectoralis major regions in internal rotation and adduction 60. Each coloured line depicts the effort level: blue: 15% MVE; red: 25% MVE; 50% MVE: grey; and 75% MVE: teal. The magnitude of activation is represented on the Y-axis, with each additional inner circle representing an increase in 10% MVC.

7.5.3. Adduction from 90° of abduction

A significant *Region by Effort* effect emerged ($F_{(2.6,34.9)} = 6.2$, $p = 0.002$, $\eta p^2 = 0.32$; Figure 29A). Specifically, the lower sternocostal region activated 56% more than clavicular in 15% MVE ($p = 0.002$; 13 out of 14 participants), 37% more at 25% MVE ($p = 0.016$; 12 out of 14 participants), 44% more at 50% MVE ($p < 0.001$; 12 out of 14 participants) and 23% more at 75% MVE ($p = 0.01$; 11 out of 14 participants). Further, lower sternocostal region also activated 39% more than the upper sternocostal region at 15% MVE ($p < 0.0001$; 13 out of 14 participants), 28% more at 25% MVE ($p = 0.002$; 12 out of 14 participants), and 20% more at 50% MVE ($p = 0.006$; 11 out of 14 participants), but similarly at 75% MVE ($p = 0.15$). Additionally, upper sternocostal region activated 21% more than clavicular at 50% MVE ($p = 0.004$) and 15% more at 75% MVE ($p = 0.008$), but not at 15% MVE ($p = 0.04$) or 25% MVE ($p = 0.11$).

Other shoulder muscles had high activations. At 15% MVE, the upper trapezius was highly active (~19% MVC), while at 25% MVE, latissimus dorsi (14% MVC), upper trapezius (14% MVC), anterior (15% MVC), and middle deltoid (15% MVC) all displayed high activations (Figure 30A; Supplementary Table 4). At 50% and 75% MVE, latissimus dorsi (53% MVC) and anterior deltoid (54% MVC) had high activations.

7.5.4. Adduction from 90° of abduction and external rotation

Significant main effects of *Region* ($F_{(2,34)} = 93.7$, $p < 0.0001$, $\eta p^2 = 0.84$) and *Effort* ($F_{(1.1,18.8)} = 17.9$, $p < 0.0001$, $\eta p^2 = 0.51$; Figure 29B) existed. Specifically, lower sternocostal region activated 51% more than clavicular ($p < 0.001$; 14 out of 18 participants) and 26% more than the upper sternocostal region ($p < 0.001$; 15 out of 18 participants). Additionally, upper sternocostal region activated 20% more than the clavicular region ($p < 0.001$; 12 out of 18

participants). EMG amplitude increased with effort level, such that EMG amplitudes were 332% higher at 50% MVE in comparison to 15% MVE and 71% higher in comparison to 25% MVE (all $p < 0.001$). Additionally, EMG amplitudes were 72% higher at 25% MVE in comparison to 15% MVE ($p < 0.001$).

Other shoulder muscles had high activations in this task. Specifically, infraspinatus and upper trapezius had high activations at 25% MVE (~21-23% MVC; Figure 30B; Supplementary Table 4). At 50% MVE, infraspinatus, latissimus dorsi, anterior, and middle deltoid had high activity (~41-43% MVC). Lastly, at 75% MVE, latissimus dorsi and infraspinatus had high activity (~67% - 75% MVC).

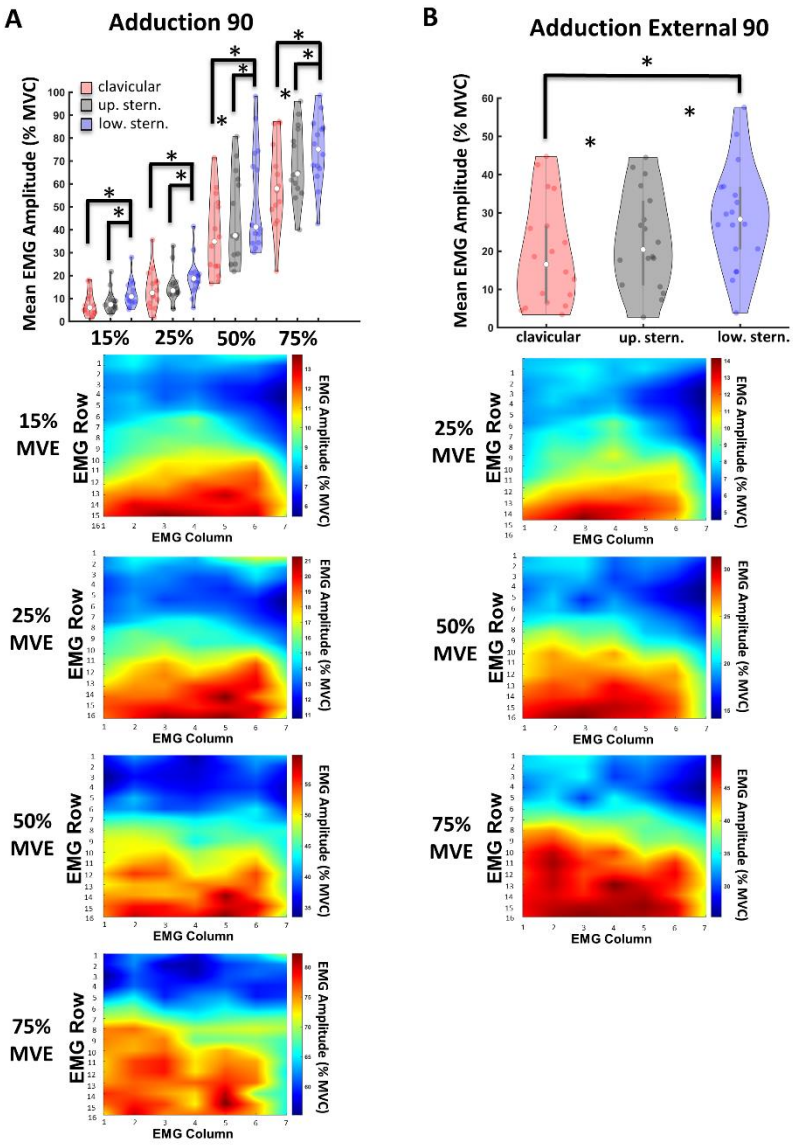

Figure 29: Scaled mean normalized EMG amplitude violin graphs with individual scatter data for clavicular, upper, and lower regions with mean normalized (%MVC) spatial topographical maps across the whole sample in15%, 25%, 50%, and 75% MVE in adduction at 90°, and 15%, 25%, and 50% MVE in adduction external 90. Each region is denoted in a different colour in violin graphs: clavicular region: red; upper sternocostal region (up. stern): grey; lower sternocostal region (low. stern): purple. White dots in the middle of each violin plot are medians. In topographical maps, the red colour indicates high activation, while the blue colour indicates low activation. Asterisk (*) denotes significant differences between regions. **A:** Adduction from 90° (ADD90). The lower sternocostal region activated more than upper sternocostal and clavicular regions at all effort levels. Further, the upper sternocostal activated more than the clavicular region at 50% and 75% MVE. **B:** Adduction external 90. The lower sternocostal region had higher EMG amplitudes than the upper sternocostal and clavicular regions.

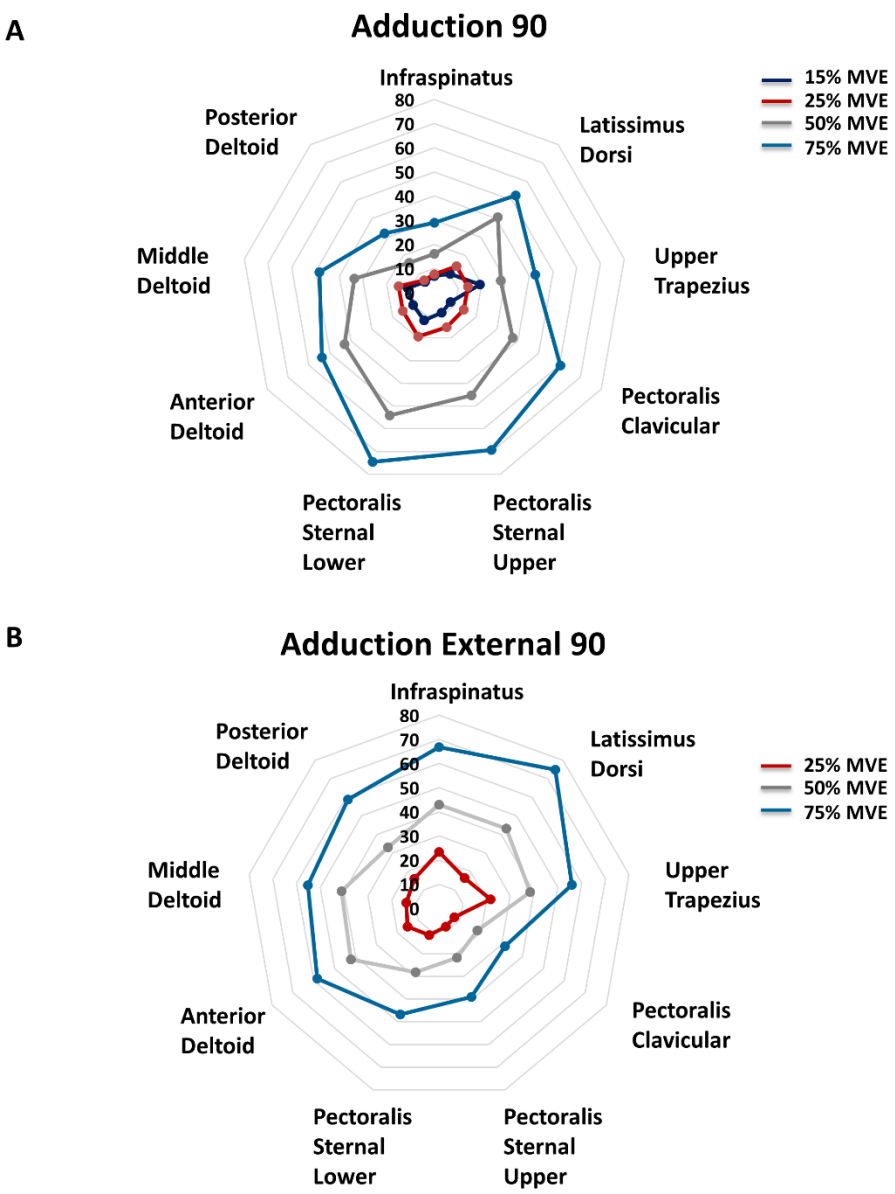

Figure 30: Polar plots depicting mean activation for infraspinatus, latissimus dorsi, upper trapezius, anterior, middle, and posterior deltoid alongside pectoralis major regions in adduction 90 and adduction external 90. Each coloured line depicts the effort level: blue: 15% MVE; red: 25% MVE; 50% MVE: grey; and 75% MVE: teal. The magnitude of activation is represented on the Y-axis, with each additional inner circle representing an increase in 10% MVC.

7.6 Discussion

7.6.1. The importance of lower sternocostal regions in adduction and internal rotation at low efforts

Lower sternocostal regions demonstrated functional relevance during adduction and internal rotation tasks. In the present study, localized lower sternocostal region activation occurred at low efforts in internal rotation and adduction 60 and in adduction tasks when the arm was elevated to 90°. These findings support the hypothesis of functionally distinct lower sternocostal region activation in specific tasks and effort levels. Similar localized activation was reported in adduction at low efforts (Paton and Brown, 1994). In a single previous study, the sternocostal region had greater stiffness than clavicular in adduction at 30% MVE, but not at 15% MVE (Leonardis et al. 2017). Findings from that study suggested greater involvement of the sternocostal region at moderate than low effort levels. When adduction was performed with the arm externally rotated, regional differences in stiffness disappeared (Leonardis et al. 2017), indicating potentially equivalent contributions of the two regions in this task. However, since shear wave velocities were examined only from the clavicular and middle sternocostal regions, no corresponding lower sternocostal region information exists.

The lower sternocostal region's muscle fiber bundles have greater lateral pennation angles compared to the clavicular and the superior sternocostal regions (Fung et al. 2009; Brown et al. 2007). Therefore, their primary action facilitates tasks requiring downward (i.e., vertical and horizontal adduction) and inward (i.e., internal rotation) effort requirements. Correspondingly, lower sternocostal regions have greater adduction and internal rotation moment arms than upper sternocostal and clavicular regions, particularly at 60° and 90° of abduction (Ackland et al. 2008;

Ackland and Pandy, 2011). The lower sternocostal regions also have independent innervation (Manktelow et al. 1980; Haladaj et al. 2019), an independent tendon attachment (Wolfe et al. 1992; Fung et al. 2009), and vascular supply (Manktelow et al. 1980). This evidence collectively suggests a functional distinction between the lower sternocostal, clavicular, and upper sternocostal regions.

7.6.2. The influence of moderate and high efforts on regional activation

In moderate and high efforts, the entire pectoralis major activated during adduction and internal rotation at 60°. Increasing the effort level while adducting the arm from 60° of abduction contributes to a dispersion of activity across multiple regions, although the bulk of the activation is in the inferior sternocostal and abdominal regions (Paton and Brown, 1994; Brown et al., 2007). These contrasting findings are not surprising, considering the current study acquired activity from the whole muscle, while previous work recorded from localized muscle sites (see Paton and Brown, 1994 for electrode placement). Previous work examined short bursts of pectoralis major activation at 70-75% MVE, while the present study required maintaining an effort for a longer period. Increased activity in the clavicular region may be due to its role in controlling the sternoclavicular and acromioclavicular joints. Therefore, some participants may have increased the activation of this region to stiffen the joints for more precise modulation of effort (Osu et al. 2002). On the other hand, upper sternocostal regions also have adduction and internal rotation moment arms (Ackland et al. 2008; Ackland and Pandy, 2011), and therefore, can contribute to these types of tasks.

The lower sternocostal region activity remains high in adduction at 90° with or without external rotation. The localized activity of these regions at high efforts was previously noted in a similar arm posture (Paton and Brown, 1994; Brown et al. 2007). However, some activity also occurred in the upper sternocostal regions. In general, the pectoralis major and latissimus dorsi

activate together to maintain adduction in this arm posture, with preferential recruitment of the lower pectoralis major regions (Brown et al. 2007). At rest, both the clavicular and upper sternocostal regions have high stiffness when the arm is at 90° of elevation (Leonardis et al. 2017). External rotation of the arm increases stiffness in both regions, possibly due to the stretch experienced by all three regions as the arm is externally rotated (Leonardis et al. 2017). Therefore, lateral pennation angles of the lower sternocostal region likely increase more than in other regions, increasing adduction contributions. Supportingly, the clavicular region has a large abductor moment arm at 90° of arm elevation, while the lower sternocostal region acts as an adductor (Ackland et al. 2008).

7.6.3. Practical implications

Present findings suggest that injuries to the lower sternocostal region may compromise the ability to adduct and internally rotate the arm, prompting compensatory activation in other adductors and internal rotators, such as the latissimus dorsi and subscapularis. Reductions in adduction and internal rotation strength occur in individuals with compromised abdominal and sternocostal regions (Schepsis et al., 2000; Provencher et al., 2010; Leonardis et al., 2019; Lipps et al., 2019; Marsh et al., 2020). Additionally, the incidence rate of pectoralis major ruptures increases when the arm is abducted and externally rotated (i.e., adduction external 90; Bak et al. 2000). Lastly, the inability to maintain shoulder stiffness in vertical adduction is also present in individuals who had subpectoral breast reconstruction (Leonardis et al. 2019).

In addition to the clinical implications above, current findings provide information regarding the characterization of pectoralis major activation. As the lower sternocostal region activity was high across all tasks and efforts, it is recommended that the activation of these regions is acquired and evaluated in future studies involving adduction and internal rotation tasks. The

surface EMG placements should also avoid known innervation zones (Barbero et al. 2012; Mancebo et al. 2019). Further, high interindividual variability in regional pectoralis major activation emphasizes the importance of acquiring EMG signals from all three regions to limit mischaracterizations of its overall activation, particularly in tasks at low arm elevations. These variations may arise from multiple sources, including architectural differences between individuals (Haladaj et al. 2019), functional uses of pectoralis major in daily activities, or sport-specific adaptations. Activities such as weightlifting or bodybuilding and sports requiring adduction and internal rotation (i.e., racquet sports) may promote utilization of the lower sternocostal regions more than other activities. The activation of all pectoralis major regions should also be considered in exercise training regimens, as exercise-induced changes in regional activity may depend on the direction and task.

7.7. Limitations

This study had some limitations. The study included only young males, and therefore, findings may not transfer to other cohorts. These tasks likely do not reflect muscle activation in other tasks, such as horizontal adduction, flexion, and extension against resistance. The setup did not include an arm brace to fix the elbow into 90° of flexion. However, the investigators observed all trials to ensure posture maintenance, and in cases when this did not occur, the trial was repeated. Additionally, crosstalk from the surrounding muscles, such as the pectoralis minor, serratus anterior, external obliques, or intercostal muscles, may have influenced the patterns of regional activation quantified in this study. Attempts were made to minimize the degree of crosstalk by sampling EMG from many closely spaced electrodes (10 mm interelectrode distance) and quantifying differential derivation in the post-processing steps. Challenges existed in acquiring HD-sEMG signals from the parts located directly underneath the nipple and approximately over

the floating ribs. This was mainly due to the HD-sEMG arrays, which were not produced to accommodate the curvature of the chest. Lastly, it is known that the pectoralis major consists of at least two innervation zones (Barbero et al. 2012; Mancebo et al. 2019). Due to the challenges in quantifying innervation zones from motor unit action potentials, the exact location of the innervation zones was challenging to determine. Therefore, this study quantified the mean normalized EMG amplitudes across innervation zones, which may have influenced the findings.

7.8. Conclusions

Mounting evidence, including present findings, promote focusing future research on functional implications of the lower sternocostal regions in fundamental arm function. This is especially important considering these regions likely contribute across effort levels in adduction and internal rotation tasks. Specifically, these tasks appear in numerous daily activities, such as reaching and lowering, carrying a grocery bag, combing; occupational tasks, such as painting; or exercise activities, such as tennis and squash. Additionally, these regions are more prone to injury in occupational and exercise tasks that involve eccentric contractions with heavy loads (Wolfe et al. 1992; Bak et al. 2000; Fung et al. 2009). Therefore, distinct regional activations in these tasks reinforce the importance of acquiring EMG signals from all pectoralis major regions, including the lower sternocostal region.

Chapter 8: The task influences regional pectoralis major activity in healthy males

8.0. Abstract

Pectoralis major is an architecturally complex muscle that assists in multi-functional task performance and supports arm movement over a wide range of motion. Although its function is broadly defined, very little knowledge exists on how its regions activate and contribute to arm task performance. Limited understanding of its regional activation has led to a largely simplified view of its function and role in shoulder mobility and stability. In turn, this has led to inaccurate inferences on its activation in daily, exercise, and occupational tasks and the development of surgical procedures undervaluing its purpose in shoulder health. Therefore, to circumvent these, the present study explored regional pectoralis major activation in healthy males in isometric tasks. Two high-density surface electromyography (HD-sEMG) arrays acquired regional (clavicular, upper, and lower sternocostal) pectoralis major activity in four tasks, which typically require the activation of the pectoralis major: flexion, horizontal adduction, internal rotation, and extension, at three effort levels: 15%, 25%, and 50% scaled to participant's maxima obtained in maximal voluntary efforts. Regional normalized root mean square EMG amplitudes were quantified and compared within each task as a function of effort level. All three regions had similar normalized EMG amplitudes in flexion and horizontal adduction, irrespective of the effort level. In extension, EMG amplitudes in the lower sternocostal region were 83% higher than in the upper sternocostal ($p = 0.001$) and 376% higher than in the clavicular region ($p = 0.001$), while upper sternocostal region had 159% higher EMG amplitudes than clavicular region ($p = 0.002$). In internal rotation, lower sternocostal region had 49% higher EMG amplitudes than clavicular region ($p = 0.012$). This study demonstrated for the first time that all three regions of the pectoralis major assist in

flexion and horizontal adduction. In contrast, lower sternocostal regions have a specialized role in tasks involving internal rotation and extension.

8.1. Introduction

Pectoralis major assists in the performance of numerous daily tasks. This multi-functional muscle consists of three distinct regions: clavicular, sternocostal, and abdominal, that join to insert into a bilaminar tendon (Lewis 1901; Ashley, 1952; Wolfe et al., 1992; Fung et al., 2009). The sternocostal and abdominal regions divide into additional partitions hypothesized to have divergent mechanical contributions to humeral mobility (Paton and Brown, 1994; Wickham et al. 2004; Brown et al. 2007; Fung et al. 2009). The role of each pectoralis major region is broadly described. The clavicular region assists in flexion, horizontal adduction, and internal rotation, the sternocostal in vertical and horizontal adduction, as well as flexion, and the abdominal in vertical adduction and extension.

Despite holistically identified regional contributions, pectoralis major activation and role in typical shoulder function is mostly unknown and understudied. It is commonly not considered necessary in functional task performance despite its multifunctional role (David et al. 2012; Hage et al. 2014). Hence, its regions are commonly resected and used as a myocutaneous flap in the neck and head reconstruction surgeries following cancer or injury (Liu et al. 2001) in the repair of anterosuperior rotator cuff tears (Gavriildis et al. 2009; Philipp et al. 2017; Kany, 2020), or the treatment of serratus anterior dysfunction (Sanchez et al. 2017). However, mounting evidence shows decreased shoulder function with damage to the pectoralis major. For example, reductions in strength and range of motion in flexion and extension, respectively, occurred in individuals following neck reconstruction surgeries (Moukarbel et al. 2010). Studies evaluating pectoralis major activity commonly acquire surface electromyography (sEMG) from slightly different locations of the sternocostal region, resulting in variable and conflicting findings even for the same tasks. Considering the presence of multiple partitions within sternocostal regions (Paton and

Brown, 1994; Fung et al. 2009) and the presence of at least two innervation zones (Barbero et al. 2012; Mancebo et al. 2019), selection of the exact location of electromyographic (EMG) recording from the sternocostal region is not trivial. Additionally, abdominal region activation is rarely acquired and reported, despite its distinct contributions to vertical adduction and extension (Wolfe et al. 1992; Paton and Brown, 1994; Ackland et al. 2008; Fung et al. 2009; Stegink-Jansen et al. 2011), and its hypothesized role in other tasks, such as flexion and horizontal adduction (Brown et al. 2007).

Limited seminal studies investigated regional activation of pectoralis major in different tasks and effort levels. Reported classic, low-spatial resolution sEMG data reflected a dependency of pectoralis major region activation on task, and sometimes effort level (Paton and Brown, 1994; Brown et al. 2007). The setup included multiple electrodes located medially (i.e., towards the sternum; see Paton and Brown, 1994). However, classic EMG methods provide limited information on the activation of the whole muscle, excluding the possibility of evaluating the spatial distribution of activity across a muscle. In contrast, high-density surface electromyography (HD-sEMG), consisting of an array of electrodes, enables multiple recordings from the whole muscle and construction of spatial distributions of muscle activity. This information elucidates the localization or distribution of muscle activity across regions, clarifying how regions of the pectoralis major activation may contribute variously to different tasks. Therefore, the present study characterized regional pectoralis major activation in low to moderate efforts during four submaximal isometric tasks in healthy males. The primary hypothesis was that the lower sternocostal regions will have higher normalized EMG amplitudes than superior sternocostal and clavicular regions in extension and internal rotation 90. Further, it was hypothesized that in flexion, the clavicular region will have higher normalized EMG amplitudes than other regions. Lastly, in

horizontal adduction, it was hypothesized that clavicular and superior sternocostal regions will have higher normalized EMG amplitude than lower sternocostal regions.

8.2. Methods

8.2.1 Participants

Ten healthy, right-hand dominant males participated (25.8 ± 5.3 years; weight: 71.3 ± 10.5 kg; height: 173.07 ± 6.67 cm; Table 10). The chosen sample size was selected using *a priori* power analyses. Sample size calculations in G*Power 3.1 (Universitat Dusseldorf, Dusseldorf, Germany) indicated that a minimum of 16 participants is required to obtain sufficient power (Cohen, 1988). The effect size chosen ($f^2 = 0.31$) is on the lower end of the observed effect size in previous studies, which reported effect sizes between 0.2 to 0.6 (Paton and Brown, 1994; Brown et al. 2007; Wickham et al. 2004). The actual sample did not satisfy the quantified *a priori* sample as collections were halted due to the Canadian government's lockdown measures due to the COVID-19 pandemic. Males were recruited using word-of-mouth or posters advertising the study in the kinesiology, engineering, psychology, and student center buildings. The inclusion criteria included healthy right-hand dominant, young males (between 18 and 40 years old). All males recruited were recreationally active. Participants reported no history of musculoskeletal injuries to the right arm or low back, including low back pain in the past six months and no neurological disease presence. All participants tested negative for signs of impingement, as screened with Hawkin's impingement and Apley's Scratch test. Participants did not engage in strenuous physical activity at least 24 hours before the session. This study was reviewed and received ethics clearance from the institutional office of research ethics and conformed to the Declaration of Helsinki.

Before the experimental protocol, stature, body weight, rib cage circumference, chest circumference, clavicle, and sternum length were measured. Rib cage circumference was measured around the rib cage, just under the nipple. Chest circumference was measured starting from the fullest part of the participant's chest (i.e., nipple area), with measuring tape wrapped around under the axilla. Clavicle length was measured from acromion to sternal notch, while the sternal length was measured from the sternal notch to the palpated xiphoid process.

Table 10: Participant demographics and anthropometric measurements (± standard deviation).

Age (years)	25.8 ± 5.3
Height (cm)	173
Weight (kg)	71.3 ± 10.5
Chest circumference (cm)	93.8 ± 8.3
Ribcage circumference (cm)	89.1 ± 8.5
Breast tissue thickness at the nipple (cm)	4.7 ± 2.3
Clavicle length (cm)	17.7 ± 2.3
Sternum length (cm)	17.5 ± 1.9

8.2.2. High-density surface electromyography

Pectoralis major activity was acquired using two 64-channel high-density surface electromyography (HD-sEMG) arrays in monopolar mode (ELSCH064NM3, OTBioelecttronica, Torino, Italy; Figure 31A). Each array consisted of electrodes in an 8 by 8 matrix with a 10 mm inter-electrode distance. Before applying the electrodes, the pectoral area was shaved, cleaned with abrasive paste and water to reduce impedance. The HD-sEMG arrays were applied on the skin using 1 mm thick two-sided adhesive foam with holes filled with electroconductive gel. The superior array was placed ~ 2 cm inferior to the clavicle with the midline of the array located between the sternum and the axilla and parallel to muscle fibers. The inferior array was placed directly below the superior array. The arrays were fixed with adhesive tape and connected to a 128 channel EMG amplifier (EMGUSB2+, OTBioelecttronica, Torino, Italy). All HD-sEMG signals

were bandpass filtered with a cut-off frequency between 10 – 500 Hz and sampled at 2048 Hz with a 12-bit A/D converter (5V dynamic range). HD-sEMG signals were amplified by a factor between 100-5000 V/V depending on the task, effort level, and participant. Saturation of HD-sEMG signals was monitored online in the OTBioLab software, and if saturation occurred in more than ten channels, the trial was terminated, gain adjusted, and trial repeated. One wet reference band was wrapped around the participant's right wrist, while a reference electrode was placed on the right clavicle.

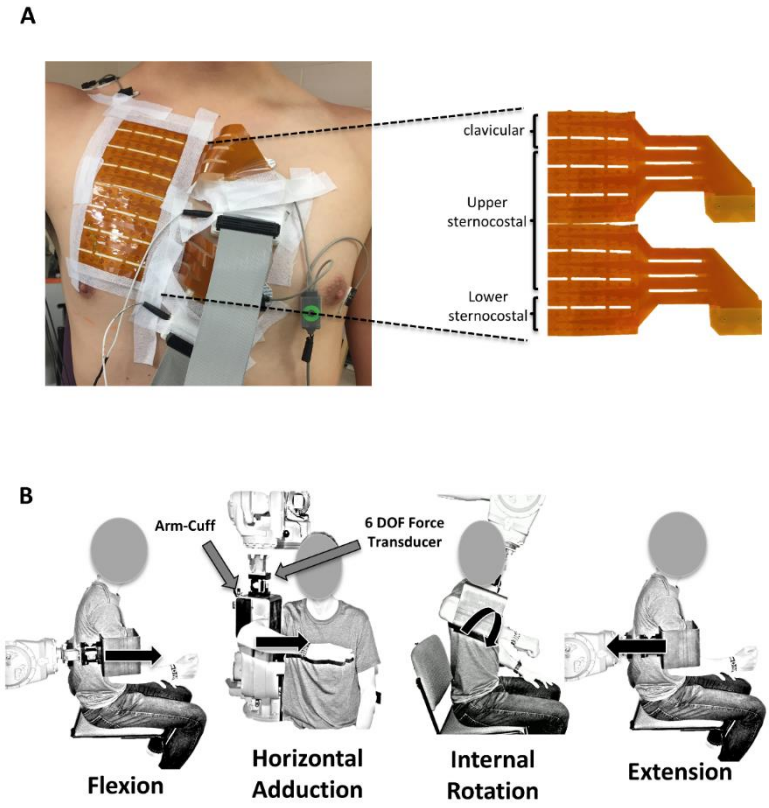

Figure 31: HD-sEMG array location and experimental setup. **A:** Two 64 channel high-density arrays were placed over the pectoralis major muscle (128 channels total). **B:** Participants performed four tasks: flexion, horizontal adduction; internal rotation; and extension against a six-degrees-of-freedom MSA-6 transducer attached to a robotic arm.

8.2.3. Force measurement

An effort was exerted against a custom-made arm cuff and acquired concurrently with HD-sEMG. The force was acquired using a six-degree-of-freedom (6-DOF) MSA-6 transducer (MC3A, AMTI MA, USA) mounted on a robotic arm (Figure 31B; Motoman Robotics Division, Yaskawa America, USA). All force data were sampled at 1500 Hz and amplified (1000x) using VICON Nexus 1.7.1 software.

8.2.4. Electrocardiography measurement (ECG)

Electrocardiography (ECG) was acquired concurrently with HD-sEMG and force. ECG was collected using silver-silver chloride (Ag-AgCl) disposable electrodes in a monopolar configuration using a wireless telemetered system (Noraxon Telemyo 2400 T G2 Noraxon, Arizona, USA). Before the placement of electrodes, the area was shaved, cleaned with abrasive gel and water. Three electrodes were placed over the left chest at the 6^{th} costal level, approximately along the anterior axillary line, and medially at the sternocostalis junction (Drake and Callaghan, 2006). Raw signals were band-pass filtered from 10-1000 Hz and differentially amplified with a CMRR > 100dB and an input impedance of 100 MΩ. Analog signals were converted to digital using a 16-bit A/D card with a ±10 V range. The sampling frequency was 1500 Hz.

8.2.5. Additional shoulder muscle monitoring

Bipolar EMG was concurrently acquired with HD-sEMG, ECG, and force from six additional shoulder muscles. The muscles included were: upper trapezius, latissimus dorsi, deltoid (anterior, middle, and posterior), and infraspinatus. sEMG activity was recorded using silver-silver chloride (Ag-AgCl) disposable electrodes with a 1 cm diameter and a fixed inter-electrode spacing

of 2 cm in a bipolar configuration. Before the placement of the electrodes, the area overlying the muscle belly was shaved and cleaned with abrasive gel and water. The placement of the sEMG electrodes was confirmed with palpation while the participant exerted a low, submaximal contraction of the muscle in positions described in Supplementary Table 1 (Cram and Kasman, 1998; Kelly et al., 1996). A reference electrode was placed on the acromion. sEMG was collected using a wireless telemetered system (Noraxon Telemyo 2400 T G2 Noraxon, Arizona, USA). Raw signals were band-pass filtered from 10-1000 Hz and differentially amplified with a CMRR > 100dB and an input impedance of 100 MΩ. Analog signals were converted to digital using a 16-bit A/D card with a ±10 V range. The sampling frequency was 1500 Hz.

8.2.6. Experimental protocol

The experimental protocol included eight maximal voluntary efforts (MVE) and six isometric ramped submaximal trials (two trials per effort level) in each of the four tasks. All participants underwent a brief warm-up and training on how to generate MVE in different tasks. Following this, participants practiced exerting effort against an arm-cuff with visual feedback of their force provided on a monitor. This training served to precondition the muscle-tendon unit (Maganaris et al., 2002) and familiarize the participant with the tasks. The participant sat on a chair with the trunk secured to the chair by a padded strap. Additionally, the arm was also secured with padding in the arm cuff to reduce the arm's movement during maximal and submaximal trial performance. Participants performed two task-specific 5-second MVEs against an arm cuff in the following tasks (Figure 31B): a) flexion from 20° of abduction (FLEX); b) horizontal adduction from 90° of abduction and 50° of flexion in the transverse plane (HORADD); c) internal rotation from 90° of abduction and 20° of internal rotation (IR90); and d) extension from 20° of abduction

(EXT). During MVE performance, participants were verbally encouraged. Each MVE was separated by 2 to 3 minutes of rest. MVEs were quantified using a custom-made program in LabVIEW (National Instruments, version 3.1). During MVE performance, off-axis forces were monitored via the LabVIEW program, such that participants were required to achieve above 80% of the total force along the intended transducer axis. If this was not achieved, the participant was provided with verbal feedback, and the trial was repeated. Additionally, if the two MVEs differed by more than 10N, an additional MVE trial was collected. For each task, the mean of two task-specific MVE trials was used to scale all analogous submaximal trials.

Participants performed submaximal ramped isometric efforts scaled to task-specific MVEs. Each task consisted of three effort levels: 15%, 25%, and 50% MVE. Participants performed two trials for each effort, lasting 60 seconds for 15% MVE and 25% MVE and 30 seconds for 50% MVE. Three to four-minute rest breaks were provided between trials, with more time allocated if requested by the participant. Participants were encouraged to report feelings of fatigue and the need for longer rest periods. Submaximal trials consisted of a ramp-up, hold, and ramp-down. At 15% and 25% MVE participants ramped at ~2% MVE/s, while at 50% MVE, the ramp was ~ 3% MVE/s. Tasks were fully randomized between and within participants. Effort levels were randomized within each task, with each submaximal effort performed consecutively within a task. Live intratrial visual feedback provided via a monitor displayed the required effort level and exerted force to facilitate matching.

8.3. Data Analysis

8.3.1. HD-sEMG signal processing

Data analysis involved several pre-processing steps. First, ECG was removed from monopolar HD-sEMG signals. Before removal, ECG was interpolated to 2048 Hz, and the HD-

sEMG signals were cross-correlated with the ECG to match the timing of each heartbeat's peak amplitude. Each trial was visually inspected to make sure the algorithm correctly recognized the ECG peaks. The precise timing of each ECG peak surrounded by 250-millisecond windows before and after the peak was determined and used to avoid the quantification bias of the root mean square (RMS) amplitude.

Following ECG removal, HD-sEMG signals were processed. Raw HD-sEMG data were band-pass filtered with a 3rd order Butterworth filter (20-500 Hz), and the differential derivation was quantified from left to right (i.e., from axilla towards sternum). RMS was quantified for each differential channel. The resultant force was used to focus on the first half of the hold. The most stable part of the hold was selected by dividing the resultant force into 5-second segments and performing EMG analyses on the segment with the lowest coefficient of variation in force. All submaximal data were normalized to maximal trials. Maximal trials were combined for flexion and extension as these tasks were performed at the same arm posture. For each HD-sEMG channel within MVE, the mean of a 3-second segment surrounding the maximal force achieved was extracted. Each channel within a submaximal trial was normalized to the channel-specific maxima. Following EMG normalization, spatial scaling was applied for each participant to account for differences in pectoralis major size by scaling EMG data of each participant to the participant with the largest pectoralis major, according to the clavicle and sternal length. Normalized data was divided into clavicular (rows 1-3), upper sternocostal (rows 4-13), and lower sternocostal (rows 13-16) regions. Subsequently, the regional mean of the two trials within each task and effort level was quantified. This division was based on an anatomical description of regional locations (Fung et al., 2009).

8.3.2. Force

Raw voltage data acquired in submaximal and maximal trials was low pass filtered using a 3rd order Butterworth filter with a cut-off frequency of 15 Hz. Raw voltage was then converted to Newtons using a custom-made program in MATLAB 2019b. The mean force that matched the most stable part of the resultant force (i.e., same as for HD-sEMG analyses) was quantified for all submaximal trials was normalized to the task-specific MVE. Normalized force data was used to confirm that all participants received the same amount of feedback and exerted 15%, 25%, or 50% MVE during submaximal trials.

8.3.3. Bipolar surface electromyography

Bipolar sEMG data for additional shoulder muscles in task-specific maximal MVEs and submaximal trials were analyzed. All sEMG data was band-pass filtered with a 2nd order Butterworth filter (30-500 Hz), and RMS of the signal was quantified across the whole submaximal and maximal trial. Subsequently, RMS for each muscle in the submaximal trial was quantified for the same force segment as for HD-sEMG (i.e., a 5-second segment with the lowest coefficient of variation in force). In maximal trials, the mean of a 3-second window surrounding the maximal force was extracted. Maximal trials were combined for flexion and extension, as these were performed in the same arm posture. Submaximal trials were then normalized to posture specific maxima for each muscle. RMS was normalized to task-specific MVEs to not underestimate EMG activity by normalizing to standard MVEs (Maciukiewicz et al. 2019). Subsequently, the mean for each muscle for each effort level and the task was quantified.

8.3.4.Data removal

The amplitude of HD-sEMG signals across channels was below the noise level in extension at 15% and 25% MVE and internal rotation at 15% MVE in most participants, prompting the removal of these trials from further analyses. In total, ~1% of the trials were removed due to saturation, low skin-electrode contact, or artifacts.

8.4. Statistical Analyses

All statistical analyses were performed using SPSS (IBM, version 21). Before any comparisons, the data were checked for normality and sphericity using the Shapiro-Wilk test and Mauchly's test of sphericity, respectively. Not normally distributed data were ln transformed. Two-way repeated-measures analysis of variance (ANOVA) was performed on EMG amplitude for flexion and horizontal adduction with within-subject factor *Region* (clavicular, upper, and lower sternocostal) and *Effort* (15, 25, 50% MVE). Similarly, for internal rotation, two-way repeated-measures ANOVA was performed on EMG amplitudes with within-subject factor *Region* (clavicular, upper, and lower sternocostal) and *Effort* (25%, 50% MVE). For extension, planned comparisons between regions (clavicular, upper, and lower sternocostal) with Dunn-Bonferonni correction were performed for 50% MVE. If significant interactions between *Region* and *Effort* existed, planned comparisons with Dunn-Bonferonni correction were performed to determine significant differences. EMG amplitudes quantified for additional shoulder muscles were ranked from highest to lowest activity based on the activation level for each task. They were used to determine which additional shoulder muscles contributed highly to the task. Partial eta-squared (ηp^2) assessed the effect size of the significant differences in EMG amplitudes. ηp^2 less than 0.06 was deemed as "small," 0.07-0.14 as "moderate," and greater than 0.14 as "large" (Cohen, 1969). Significance was $p < 0.05$.

8.5. Results

Differential regional activation existed in two out of the four tasks. Specifically, in internal rotation and extension, lower sternocostal regions had high normalized EMG amplitudes. In contrast, in flexion and horizontal adduction, all three regions had similar normalized EMG activity. All participants received the same amount of feedback across tasks and effort levels (Table 11).

Table 11: Mean force in Newtons and as a percent of MVE (± standard deviation) for all tasks and effort levels.

Task	Effort Level	Mean Force (N)	Mean %MVE
Flexion	15%	24.3 ± 5.6	14.5 ± 1.9
	25%	41.1 ± 10.5	24.5 ± 2.9
	50%	86.1 ± 18.7	51.4 ± 3.9
	100%	168.6 ± 40.3	-
Horizontal Adduction	15%	34.3 ± 12.6	15.7 ± 2.2
	25%	57.5 ± 19.1	26.5 ± 1.8
	50%	114.6 ± 37.8	52.8 ± 2.5
	100%	216.6 ± 70.7	-
Internal Rotation	25%	27.9 ± 10	22.9 ± 4
	50%	58.3 ± 20.2	47.9 ± 8.9
	100%	121.6 ± 36.1	-
Extension	50%	103.5 ± 22.2	53 ± 5.7
	100%	198.8 ± 51.5	-

8.5.1. Internal rotation

In internal rotation, significant main effects of *Region* ($F_{(2,18)} = 7.9$, $p = 0.003$, $\eta p^2 = 0.46$; Figure 32A) and *Effort* ($F_{(1,9)} = 24.7$, $p = 0.001$, $\eta p^2 = 0.73$) occurred. Specifically, lower sternocostal region activated 49% more than the clavicular region ($p = 0.012$). No differences existed between upper and lower sternocostal or clavicular and upper sternocostal regions (all $p > 0.025$). EMG amplitudes were 71% higher at 50% MVE in comparison to 25% MVE ($p < 0.0001$).

Other shoulder muscles are also activated highly (Figure 33B; Supplementary Table 5). Specifically, at 25% and 50% MVE, infraspinatus (~23%-47% MVC) and latissimus dorsi (~24%-47% MVC) activated highly.

8.5.2.Extension

Differences in EMG amplitudes between regions existed in extension at 50% MVE (Figure 32B). The abdominal region had ~84% higher EMG amplitudes than sternocostal ($p = 0.001$) and ~376% higher than clavicular ($p = 0.001$). Further, sternocostal region had ~160% higher EMG amplitudes than clavicular region ($p = 0.002$).

Alongside the pectoralis major, an additional shoulder muscle activated highly in this task (Figure 33B; Supplementary Table 5). Specifically, the latissimus dorsi displayed high activity (~41% MVC).

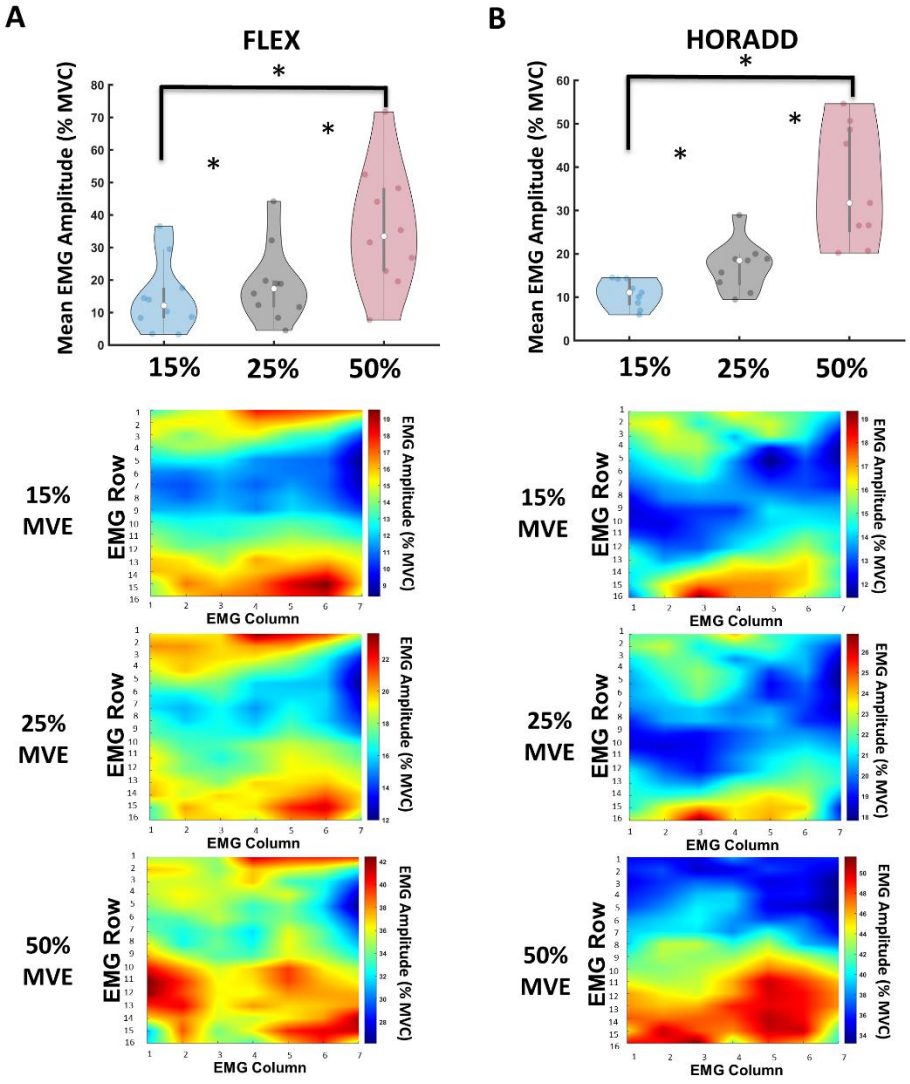

Figure 32: Scaled mean normalized EMG amplitude violin graphs with individual scatter data for clavicular, upper, and lower sternocostal regions with mean normalized (%MVC)spatial topographical maps across the whole sample in 25% and 50% MVE for internal rotation and 50% MVE in extension. In violin graphs, each region is denoted in different shades: clavicular region: blue; upper sternocostal region: grey; lower sternocostal region: red. White dots in the middle of each violin plot are medians. In topographical maps, the red colour indicates high activation, while the blue colour indicates low activation. Asterisk (*) denotes significant differences between regions. **A:** Internal rotation (IR). The lower sternocostal activated more than upper sternocostal and clavicular regions at both efforts. **B:** Extension (EXT). The lower sternocostal region had higher EMG amplitudes than the upper sternocostal and clavicular regions. Additionally, the upper sternocostal region had higher EMG amplitudes than the clavicular region.

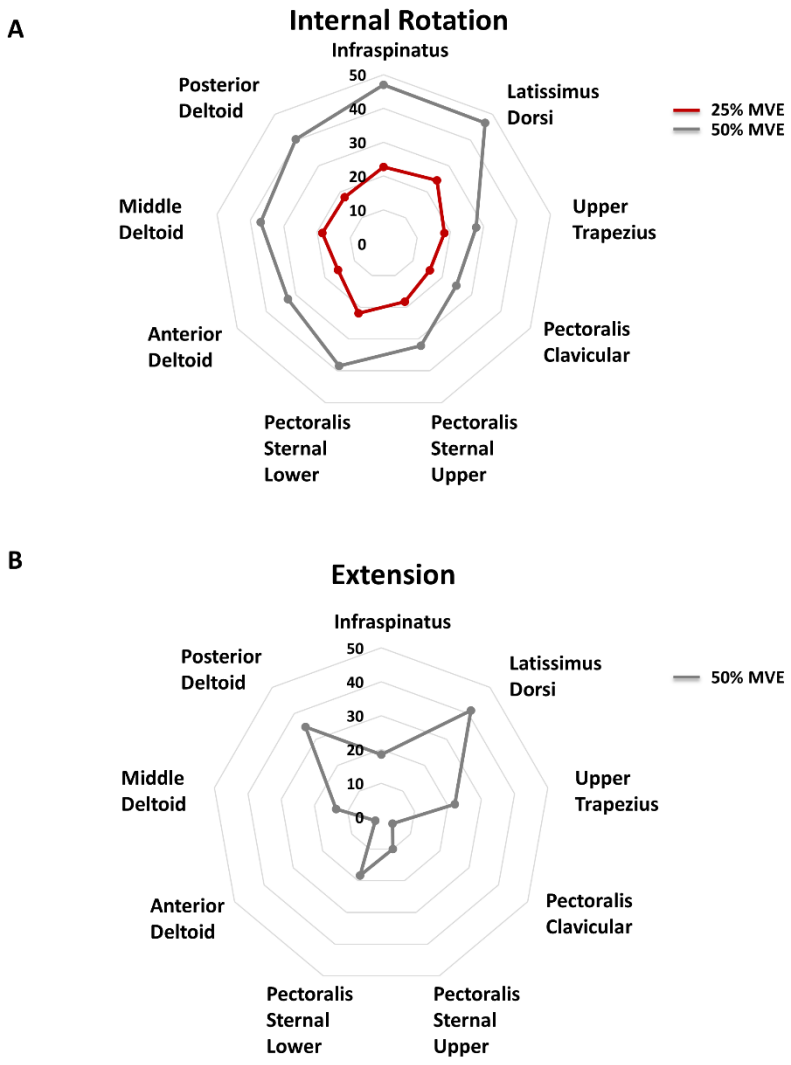

Figure 33: Polar plots depicting mean activation for infraspinatus, latissimus dorsi, upper trapezius, anterior, middle, and posterior deltoid alongside pectoralis major regions in internal rotation (**A**) and extension (**B**). Each coloured line depicts the effort level: blue: 15% MVE; red: 25% MVE; and 50% MVE: grey. The magnitude of activation is represented on the Y-axis, with each additional inner circle representing an increase in 10% MVC.

8.5.3.Flexion

A significant main effect of *Effort* existed in flexion ($F_{(1.12,10.1)} = 58.9$, $p < 0.0001$, $\eta p^2 = 0.86$; Figure 34A). EMG amplitude increased with effort level (all $p < 0.025$). Specifically, EMG

amplitude was ~28% and 147% higher at 25% MVE and 50% MVE in comparison to 15% MVE, respectively, and ~92% higher at 50% MVE in comparison to 25% MVE. There were no differences in EMG amplitude between regions.

In this task, other shoulder muscles are also activated highly (Figure 35A; Supplementary Table 5). Specifically, at 15% MVE, the upper trapezius activated highly (~21% MVC), while at 25% MVE, the upper trapezius (21% MVC) and anterior deltoid (~21% MVC) activated highly. Lastly, at 50% MVE, infraspinatus (~35% MVC), anterior (~40% MVC), and middle deltoid (~40% MVC) activated highly.

8.5.4. Horizontal adduction

A significant main effect of *Effort* emerged ($F_{(1.2,10.9)} = 59.3$, $p < 0.001$, $\eta p^2 = 0.86$; Figure 34B). EMG amplitudes increased with increases in effort (all $p < 0.025$). Specifically, EMG amplitudes were ~44% and ~178% higher at 25% MVE and 50% MVE, respectively, than 15% MVE, and ~94% higher at 50% MVE than 25% MVE. There were no differences in EMG amplitude between regions.

Additional shoulder muscles are activated highly in this task (Figure 35B; Supplementary Table 5). Specifically, at 15% MVE, infraspinatus activated highly (~23% MVC). At 25% MVE, additional muscles had high activations alongside infraspinatus (~21% MVC) and included anterior (~22% MVC) and middle deltoid (~21% MVC). At 50% MVE, latissimus dorsi (~47% MVC) and anterior deltoid (~38% MVC) had high activations.

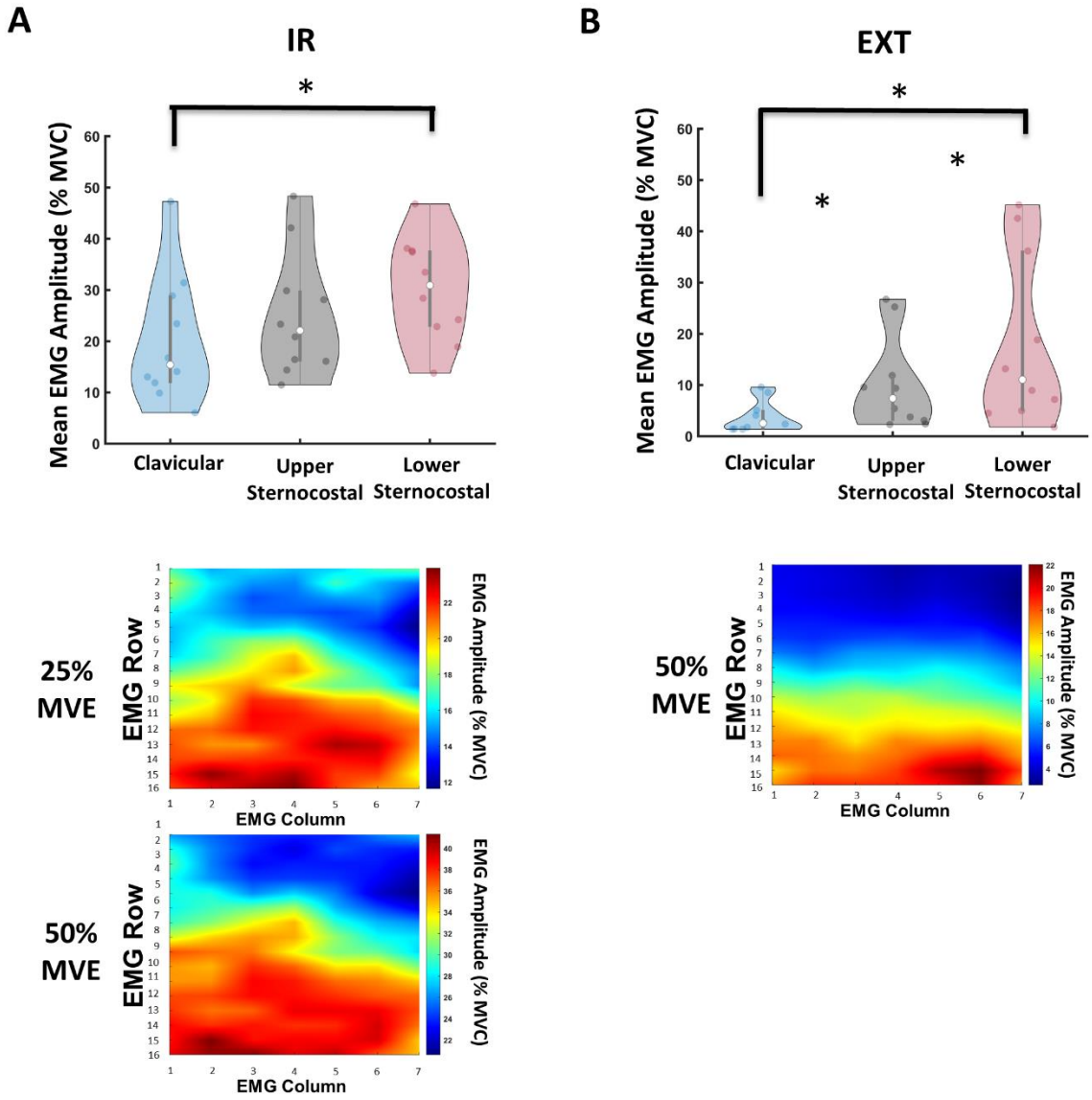

Figure 34: Scaled mean normalized EMG amplitude violin graphs with individual scatter data for clavicular, sternocostal, and abdominal regions with mean normalized (%MVC) spatial topographical maps across the whole sample in 15%, 25%, and 50% MVE in flexion and horizontal adduction. In violin graphs, each region is denoted in different shades: clavicular region: blue; upper sternocostal region: grey; lower sternocostal region: red. White dots in the middle of each violin plot are medians. In topographical maps, the red colour indicates high activation, while the blue colour indicates low activation. Asterisk (*) denotes significant differences between regions. **A:** Flexion (FLEX). All three regions had similar EMG amplitudes across efforts. **B:** Horizontal adduction (HORADD). All three regions had similar EMG amplitudes across efforts.

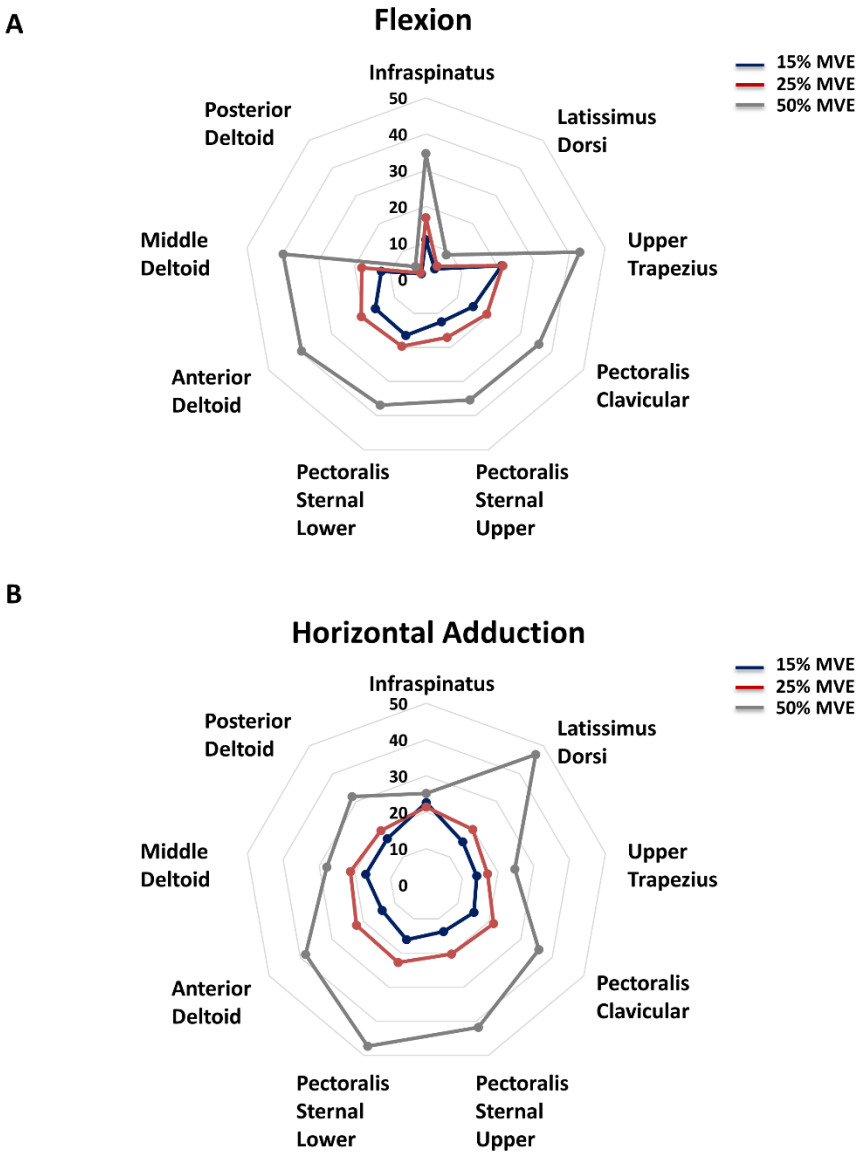

Figure 35: Polar plots depicting mean activation for infraspinatus, latissimus dorsi, upper trapezius, anterior, middle, and posterior deltoid alongside pectoralis major regions in flexion (**A**) and horizontal adduction (**B**). Each coloured line depicts the effort level: blue: 15% MVE; red: 25% MVE; and 50% MVE: grey. The magnitude of activation is represented on the Y-axis, with each additional inner circle representing an increase in 10% MVC.

8.6. Discussion

This study sought to investigate regional pectoralis major activation in four tasks that typically require pectoralis major activation at low to moderate effort levels. While the lower sternocostal region was highly active during internal rotation and extension, all three regions activated to the same magnitude in horizontal adduction and flexion irrespective of the effort level. Present findings provide novel evidence on regional pectoralis major activation, with implications in fundamental and clinical studies.

8.6.1. Relevance of lower sternocostal region in extension and internal rotation

In internal rotation, the lower sternocostal region had higher EMG amplitudes than the clavicular region. Previously, all three regions were implicated in this task (Wolfe et al., 1992; Stegink-Jansen et al., 2011; Leonardis et al., 2019; Marsh et al., 2020; Ackland and Pandy, 2011). The regional contributions to internal rotation depend on arm abduction and flexion angle (Ackland and Pandy, 2011). Specifically, when the arm is at 90° of abduction, the internal rotation moment arms are longer in the lower than upper sternocostal or clavicular region (Ackland and Pandy, 2011).

Similarly, the lower sternocostal region activated more than clavicular and upper sternocostal regions in extension. The role of the pectoralis major in this task was previously examined in mechanical and EMG studies. From both perspectives, this task was solely attributed to lower sternocostal regions (Paton and Brown, 1994; Wolfe et al. 1992), although the pectoralis major is considered a weak extensor. In a simulated bench press, Wolfe et al. demonstrated lengthening of the abdominal muscle fibers in extension between 0° and 30°, with the largest demands placed on the inferior fibers (1992). Greater lateral pennation angles of this region compared to upper sternocostal and clavicular regions (Fung et al. 2009) make the lower

sternocostal regions more likely to contribute to extension, mainly when the arm is closest to the torso.

Anatomically, it is suggested that the lower sternocostal region may have a divergent role compared to the clavicular and upper sternocostal regions. This region receives independent innervation from the medial pectoral nerve (Manktelow et al. 1980; Haladaj et al. 2019) and inserts into the posterior tendon, with the most inferior partitions attaching to the most superior part of the tendon (Fung et al. 2009). This region has greater lateral pennation angles, shorter fiber bundle lengths, and flexor moment arms than sternocostal and clavicular regions (Fung et al. 2009; Brown et al. 2007). The differential localized activity in this region in the current study supports the lower sternocostal region's functional distinction from upper sternocostal and clavicular regions.

8.6.2. Regional pectoralis major activation in flexion and horizontal adduction

Prior studies investigating regional pectoralis major activity using classic EMG in horizontal adduction and flexion tasks reported contrasting findings that may be due to the performance of these tasks in different arm postures or effort levels. For example, pectoralis major regions activated similarly at high effort levels during flexion when the arm was at 20° of abduction (Brown et al. 2007), but clavicular and abdominal regions activated when flexing from 60° of forward flexion (Paton and Brown, 1994). Similarly, for horizontal adduction at 90° of arm abduction, low efforts elicited higher EMG amplitudes in the clavicular, lower sternocostal, and abdominal regions, in comparison to the superior sternocostal regions, while horizontal adduction at 20° of abduction resulted in the high activity of all three regions (Brown et al. 2007; Paton and Brown, 1994). In contrast, the clavicular and the sternocostal regions had similar activations in both isometric (Diefenbach and Lipps, 2019; McDonald et al. 2012; McDonald et al. 2014) and more dynamic tasks, such as bench press (Lauver et al. 2015).

Regional architectural properties estimated from cadavers may provide insights into these activation patterns. Anatomically, regional flexion and horizontal adduction moment arms highly depend on the arm posture (Ackland and Pandy, 2011; Ackland et al. 2008; Brown et al. 2007; Kuechle et al. 1997) and elbow joint angle (Yu et al. 2011). In a cadaver, flexion and horizontal adduction moment arm are longer in the clavicular and superior sternocostal regions than lower sternocostal regions (Ackland et al. 2008; Yu et al. 2011). This data suggests that mechanically, clavicular, and superior sternocostal regions, compared to lower sternocostal regions, have the advantage of producing torque in flexion and horizontal adduction. However, in the current study, the lower sternocostal regions had a similar activation to clavicular and upper sternocostal regions in flexion and horizontal adduction.

The discrepancy between mechanical and activation patterns may be due to the influence of contraction intensity on architectural properties *in vivo*. In a cadaver, clavicular and lower sternocostal regions have the greatest pennation angles, while upper sternocostal regions have the longest fiber bundle length (Fung et al. 2009). However, increases in contraction intensity *in vivo* alter these properties. For example, an increase in contraction intensity increases the pennation angle by ~60-250% and reduces muscle fascicle length by ~30-55% (Herbert and Gandevia, 1995; Hodges et al. 2003; Narici and Maganaris, 2006). The extent of these changes is also influenced by the joint position, such that larger changes are evident when the muscle-tendon unit is more stretched (Narici and Maganaris, 2006). However, these properties were not investigated *in vivo* in pectoralis major, limiting the understanding of the relationship between muscle activity and architecture in this muscle. Indeed, in flexion, clavicular regions and the anterior deltoid act to initiate flexion, activating ~ -47 ms before other regions (Brown et al. 2007). However, EMG

amplitude increases in both sternocostal and abdominal regions once the flexion is initiated. Therefore, all three regions must activate to maintain flexion (Brown et al. 2007).

8.6.3. Practical Implications

The tasks examined in this study are common in the performance of activities of daily living. For example, horizontal adduction and flexion enable reaching for an object on a shelf; extension permits pulling actions, while internal rotation facilitates unbuttoning a bra. Current findings suggest that maintaining effort in flexion or horizontal adduction requires the activation of all three pectoralis major regions. In contrast, abdominal regions activate to maintain internal rotation and extension effort. Therefore, these findings emphasize the importance of acquiring EMG signals from all pectoralis major regions in tasks involving horizontal adduction, flexion, extension, or internal rotation.

Injuries to the pectoralis major typically occur in weightlifters in extension tasks. Injuries typically occurred during a bench press, in the final phase of eccentric contraction, as the athlete transitions to concentric contraction (Petilon et al. 2005; Cordasco et al. 2017). One of the side-effects of such injuries was an inability to extend the arm (Pavlik et al. 1998). Additionally, injuries to the pectoralis major also elicit reductions in horizontal or vertical adduction and internal rotation strength (Pavlik et al. 1998; Schepsis et al., 2000; Provencher et al., 2010; Marsh et al., 2020). Surgical procedures that use pectoralis major as a pedicled flap to reconstruct head and neck following injuries or cancer commonly provoke strength reductions in flexion and extension range of motion (Moukarbel et al. 2010). Collectively, injuries or procedures affecting the pectoralis major may compromise shoulder function or prompt compensatory activity in other shoulder muscles involved in these tasks, particularly in the latissimus dorsi, anterior or posterior deltoid, and subscapularis.

8.7. Limitations

Several limitations must delimit the interpretation of findings. Only young males participated; therefore, findings may not transfer to other cohorts, such as females or aging populations. The data reported may not reflect regional pectoralis major activity for these tasks in other arm postures. In the current study, the pectoralis major had low activation in extension and internal rotation tasks at low efforts. The low activation may be due to a lack of significant involvement of the pectoralis major in this task or arm posture. Future studies should try to acquire EMG signals in these tasks in different arm postures. Additionally, crosstalk from the surrounding muscles, such as the pectoralis minor, serratus anterior, external obliques, or intercostal muscles, may have influenced the patterns of regional activation quantified in this study. Attempts were made to minimize the degree of crosstalk by sampling EMG from many closely spaced electrodes (10 mm interelectrode distance) and quantifying differential derivation in the post-processing steps. Challenges existed in acquiring HD-sEMG signals from the parts located directly underneath the nipple and approximately over the floating ribs. This was mainly due to the HD-sEMG arrays, which were not produced to accommodate the curvature of the chest. Lastly, it is known that the pectoralis major consists of at least two innervation zones (Barbero et al. 2012; Mancebo et al. 2019). Due to the challenges in quantifying innervation zones from motor unit action potentials, the exact location of the innervation zones was challenging to determine. Therefore, this study quantified the mean normalized EMG amplitudes across innervation zones, which may have influenced the findings.

8.8. Conclusions

All three pectoralis major regions worked together to accomplish horizontal adduction and flexion, while the lower sternocostal fibers contribute more so to internal rotation and extension.

These tasks are requisite in daily tasks, such as reaching and pulling, or in exercise tasks such as bench press. Therefore, compromise of pectoralis major regions either in exercise or in surgical procedures that resect pectoralis major may limit the ability to perform these tasks or prompt compensatory activations in surrounding shoulder musculature, potentially predisposing individuals to shoulder injury.

Chapter 9: Inner workings of the pectoralis major: Insights into neural control in isometric efforts

9.0. Abstract

Pectoralis major contributes extensively to shoulder stability and mobility. However, its underlying neuromusculoskeletal control is currently unknown. Two sets of experiments aimed at exploring the pectoralis major neural control were performed in males and females using high-density surface electromyography (HD-sEMG). Participants performed several ramped isometric tasks involving adduction, internal rotation, flexion, and horizontal adduction at three effort levels: 15%, 25%, and 50% scaled to the task-specific maximal voluntary effort (MVE). HD-sEMG signals were decomposed using a convolutive blind source separation algorithm. Motor units were matched between effort levels using a motor unit matching algorithm. For matched motor units in males, the mean discharge rate and coefficient of variation were quantified across the hold and compared between effort levels. Individual two-dimensional motor unit action potentials were extracted using spike trigger averaging. The mean peak-to-peak amplitude was quantified for the clavicular and sternocostal region. In females, motor unit physiology focused on general observation due to low motor unit yield across tasks and effort levels. In males, across all tasks, motor unit discharge rate did not differ between 15% and 25% MVE (all $p > 0.05$) or between 25% and 50% MVE in horizontal adduction ($p = 0.11$). Additionally, motor unit action potential amplitude was not different between regions or effort levels in any task, except for adduction 60. In this task, the peak-to-peak amplitude of motor unit action potentials was larger in the clavicular region at 25% MVE than 15% MVE ($p = 0.016$). For the first time, motor unit physiology in pectoralis major is explored across several tasks, effort levels, and in both sexes. Current findings indicate that the pectoralis major relies heavily on motor unit recruitment for increases in effort

levels. These findings provide insights into the pectoralis major's neural control and lay the groundwork for interpreting healthy aging or clinical case scenarios.

9.1. Introduction

Pectoralis major is a large, multipennate muscle that has a multifunctional role in arm movements. Its regions function to adduct vertically and horizontally, flex, internally rotate and extend the arm against resistance. It is typically divided into clavicular, sternocostal, and abdominal regions (Lewis 1901; Ashley, 1952; Wolfe et al., 1992; Fung et al., 2009). The clavicular region crosses the sternoclavicular, acromioclavicular, and indirectly controls the scapulothoracic joint, while all regions are responsible for controlling the glenohumeral and intercostal joints. However, recent anatomical evidence points to the existence of four and three compartments in sternocostal and abdominal regions, respectively (Fung et al. 2009). Anatomical studies identified differential innervation of pectoralis major muscle fiber bundles. The lateral pectoral nerve innervates the clavicular and superior sternocostal regions, while the medial pectoral nerve innervates the inferior sternocostal regions (Manktelow et al. 1980; Porzionato et al. 2012; Haladaj et al. 2019). Different regional innervation indicates that the pectoralis major may contain neuromuscular compartments (English et al. 1993), increasing the possibility of differential contributions of these compartments to mechanical force production of the whole pectoralis major.

A small number of studies investigated differences in normalized electromyographic (EMG) amplitude between compartments. These studies reported that compartmental EMG amplitude depended on the task, arm posture, and in some instances, effort level (Paton and Brown, 1994; Wickham et al., 2004; Wickham and Brown, 2012). For example, when the arm was abducted at 90°, compartments in the abdominal region had higher EMG amplitudes in isometric adduction (Paton and Brown, 1994). However, all compartments activated similarly when the arm was positioned closer to the trunk (Paton and Brown, 1994).

Differential activation of compartments was attributed to independent control of motor units within each compartment by the central nervous system (Paton and Brown, 1994). While plausible, the sEMG signal depends on many physiological and non-physiological factors (e.g., crosstalk and volume conductor properties) and reflects both central and peripheral properties of motor units (Farina et al. 2004; Martinez-Valdes et al. 2018). Therefore, motor unit behaviour cannot be inferred solely based on normalized EMG amplitudes (Martinez-Valdes et al. 2018). As such, the neuromusculoskeletal control of the pectoralis major remains unclear and understudied. However, this knowledge is critical to delineate the contribution of pectoralis major to typical shoulder function and assess deficits resulting from pectoralis major compromise.

Different techniques exist to discriminate between peripheral and central properties of motor units. One such method is high-density surface electromyography (HD-sEMG), consisting of an array of electrodes that, coupled with a motor unit decomposition algorithm, can provide information on motor unit physiology (Farina et al. 2016). Therefore, this study sought to investigate the neuromusculoskeletal control of pectoralis major in males and females in different tasks suspected to require the muscle in low (15%-25% MVE) to moderate (50% MVE) effort levels. The primary hypothesis was that the motor unit discharge rate will increase with effort level in all tasks, indicating reliance on motor unit rate coding for modulation and an increase in effort level. The secondary hypothesis was that the motor unit action potential amplitude will increase with effort level within a task, indicating the influence of neuromuscular properties on sEMG amplitude.

9.2. Methods

9.2.1. Participants

This study consisted of linked studies. In Study 1, eighteen and twenty healthy, right-hand dominant males and females, respectively, participated (Males: 25 ± 4.7 years; weight: 75.3 ± 8.1 kg; height: 173.5 ± 5 cm; Females: 22.4 ± 2.2 years; weight: 61.7 ± 4.7 kg; height: 164.3 ± 7.5 cm). In Study 2, ten and nine healthy, right hand dominant males and females participated (Males: 25.8 ± 5.3 years; weight: 71.3 ± 10.5 kg; height: 173.07 ± 6.67 cm; Females: 24.5 ± 3.1; weight: 61 ± 8.9 kg; height: 165.6 ± 3.5 cm). The chosen sample size was selected using *a priori* power analyses. Sample size calculations in G*Power 3.1 (Universitat Dusseldorf, Dusseldorf, Germany) indicated that a minimum of 16 participants is required to obtain sufficient power (Cohen, 1988). The effect size chosen ($f^2 = 0.31$) is on the lower end of the observed effect size in previous studies, which reported effect sizes between 0.2 to 0.6 (Paton and Brown, 1994; Brown et al. 2007; Wickham et al. 2004). The second study sample did not satisfy the quantified *a priori* sample calculations as collections were halted due to the COVID-19 pandemic. Males and females were recruited using word-of-mouth or posters advertising the study in the kinesiology, engineering, psychology, and student center buildings. The inclusion criteria included healthy right-hand dominant, young males and females (between 18 and 40 years old). All recruited participants were recreationally active. The inclusion criteria for both sexes in both studies included healthy young (between 18-40 years old), right-hand dominant males, and females. Females who underwent breast reconstruction or augmentation surgeries were not included in the study. Participants reported no history of musculoskeletal injuries to the right arm or low back, including low back pain in the past six months and no neurological disease presence. All participants tested negative for signs of impingement, as screened with Hawkin's impingement and Apley's Scratch test. Participants did not engage in strenuous physical activity at least 24 hours before the session.

Participants were instructed by the investigator not to consume any caffeinated drinks the morning of the session and drink plenty of water the day before the session. This study was reviewed and received ethics clearance from the Institutional Office of Research Ethics and conformed to the Declaration of Helsinki.

9.2.2. High-density surface electromyography

Two 64-channel high-density surface electromyography (HD-sEMG) arrays were used to acquire regional pectoralis major activation in monopolar mode (ELSCH064NM3, OTBioelecttronica, Torino, Italy; Figure 36A). Electrode arrays consisted of channels in an 8 by 8 matrix with a 10 mm inter-electrode distance. Before applying the electrodes, the skin overlying the pectoralis major was cleaned with abrasive paste and water. The electrode arrays were applied on the skin using 1 mm thick two-sided adhesive foam with holes filled with electroconductive gel. The superior array was placed ~ 2 cm inferior to the clavicle, with the middle of the array positioned between the sternum and the axilla and parallel to muscle fibers. The inferior array was placed directly below the superior array. The arrays were fixed with adhesive tape and connected to a 128 channel EMG amplifier (EMGUSB2+, OTBioelecttronica, Torino, Italy). One wet reference band was wrapped around the participant's right wrist, while a reference electrode was placed on the right clavicle. All EMG signals were bandpass filtered with a cut-off frequency between 10 – 500 Hz and sampled at 2048 Hz with a 12-bit A/D converter (5V dynamic range). HD-sEMG signals were amplified by a factor between 100-5000 V/V. Saturation of channels was monitored online in the OTBiolab software (OTBioelecttronica, Torino, Italy). If more than ten channels were saturated, the trial was terminated, gain adjusted, and trial repeated.

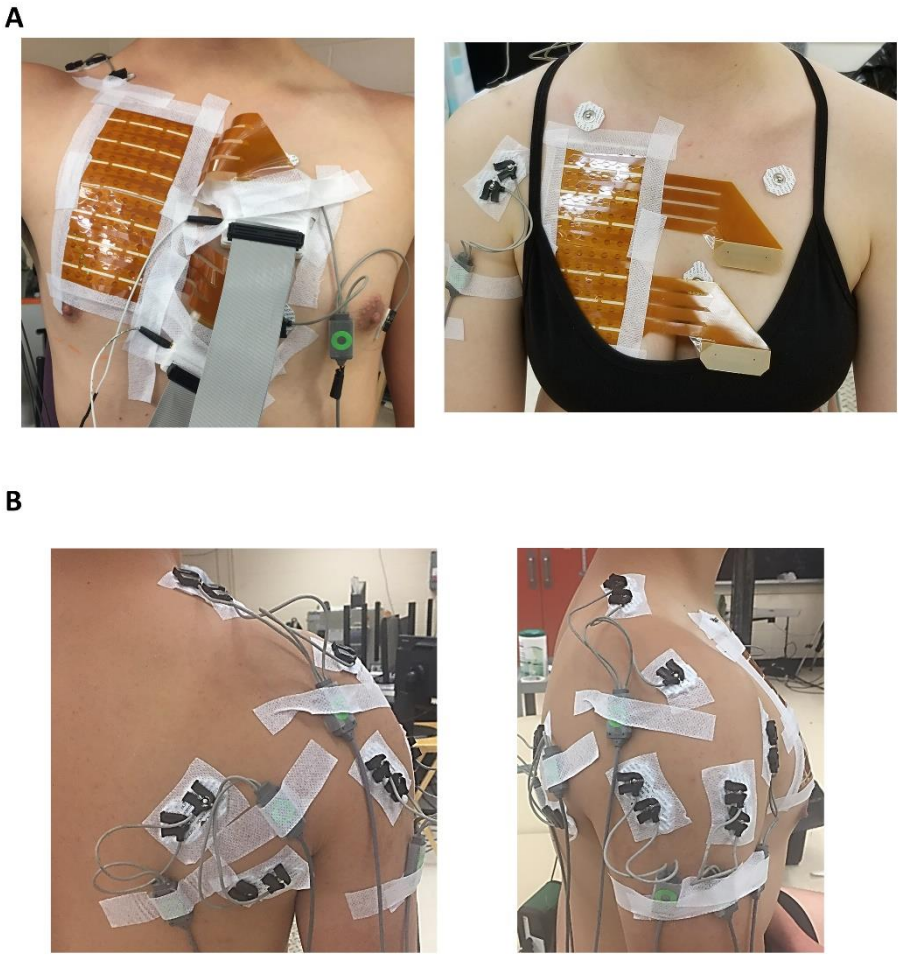

Figure 36: Representative figures of HD-sEMG array location and bipolar sEMG location. **A:** Two HD-sEMG arrays were positioned on the pectoralis major in males and females. The top array represented the superior array and was located ~ 2 cm away from the clavicle. The bottom array represented the inferior array and was located directly below the superior array. **B:** Bipolar sEMG was used to acquire and monitor data from additional shoulder muscles, including anterior, middle, and posterior deltoid; infraspinatus; latissimus dorsi; and upper trapezius.

9.2.3. Force Measurement

Raw voltage was acquired during submaximal and maximal efforts concurrently with HD-sEMG. The effort was exerted against a custom-built arm cuff attached to a six-degree-of-freedom (6-DOF) force transducer (MC3A, AMTI MA, USA) mounted on a robotic arm (Figure 37A and B; Motoman Robotics Division, Yaskawa America, USA). Force was sampled at 1500 Hz and amplified (1000x) using VICON Nexus 1.7.1 software.

9.2.4. Additional shoulder muscle monitoring

The activity of six additional shoulder muscles was acquired with sEMG. Upper trapezius, latissimus dorsi, deltoid (anterior, middle, and posterior), and infraspinatus activity was monitored in the background (Figure 36B). sEMG activity was recorded using silver-silver chloride (Ag-AgCl) disposable electrodes with a 1 cm diameter and a fixed inter-electrode spacing of 2 cm in a bipolar configuration. Before the placement of the electrodes, the area overlying the muscle belly was shaved and cleaned with abrasive gel and water. Placement of the sEMG electrodes was confirmed with palpation while the participant exerted a low, submaximal contraction of the muscle in positions described in Supplementary Table 1 (Cram and Kasman, 1998; Kelly et al., 1996). A reference electrode was placed on the acromion. sEMG was collected using a wireless telemetered system (Noraxon Telemyo 2400 T G2 Noraxon, Arizona, USA). Raw EMG signals were band-pass filtered from 10-1000 Hz, and differentially amplified with a CMRR > 100dB and an input impedance of 100 MΩ. Analog signals were converted to digital using a 16-bit A/D card with a ±10 V range. The sampling frequency was 1500 Hz.

9.2.5. Experimental protocol

Experimental protocol included the performance of several maximal voluntary efforts (MVE) and isometric ramped submaximal trials in five tasks at three effort levels. All participants underwent a brief warm-up and training on how to generate MVE in different tasks. Next, participants practiced exerting an effort against an arm-cuff with visual feedback of their force provided on a monitor. This training served to precondition the muscle-tendon unit (Maganaris et al., 2002) and familiarize the participant with the task. Following training and familiarization, participants performed two trials of task-specific 5-second MVEs against an arm cuff. The

participant sat on a chair with the trunk secured with a padded strap throughout all trials. Additionally, the arm was also secured in the arm-cuff with padding to minimize arm movement during task performance. Participants performed maximal and submaximal trials in the following tasks (Figure 37A and 37B): Study 1: a) adduction and b) internal rotation from 60° of arm abduction; c) adduction from 90° of arm abduction; and d) adduction from 90° of arm abduction and 90° of arm external rotation (adduction external 90), and Study 2: a) flexion from 20° of abduction and b) horizontal adduction from 90° of abduction and 50° of flexion in the transverse plane. During MVE performance, participants were verbally encouraged. Each MVE was separated by 2 minutes of rest. Maximal MVEs were quantified using a custom-made program in LabVIEW (National Instruments, version 3.1). For each task, the mean of two task-specific MVE trials was used to scale all analogous submaximal trials. During MVE performance, off-axis forces were monitored in the LabVIEW program, such that participants were required to achieve above 80% of the total force along the intended transducer axis. Additionally, if the second MVE trial was more than 10 N different than the first, a third MVE trial was performed to ensure consistency in MVEs.

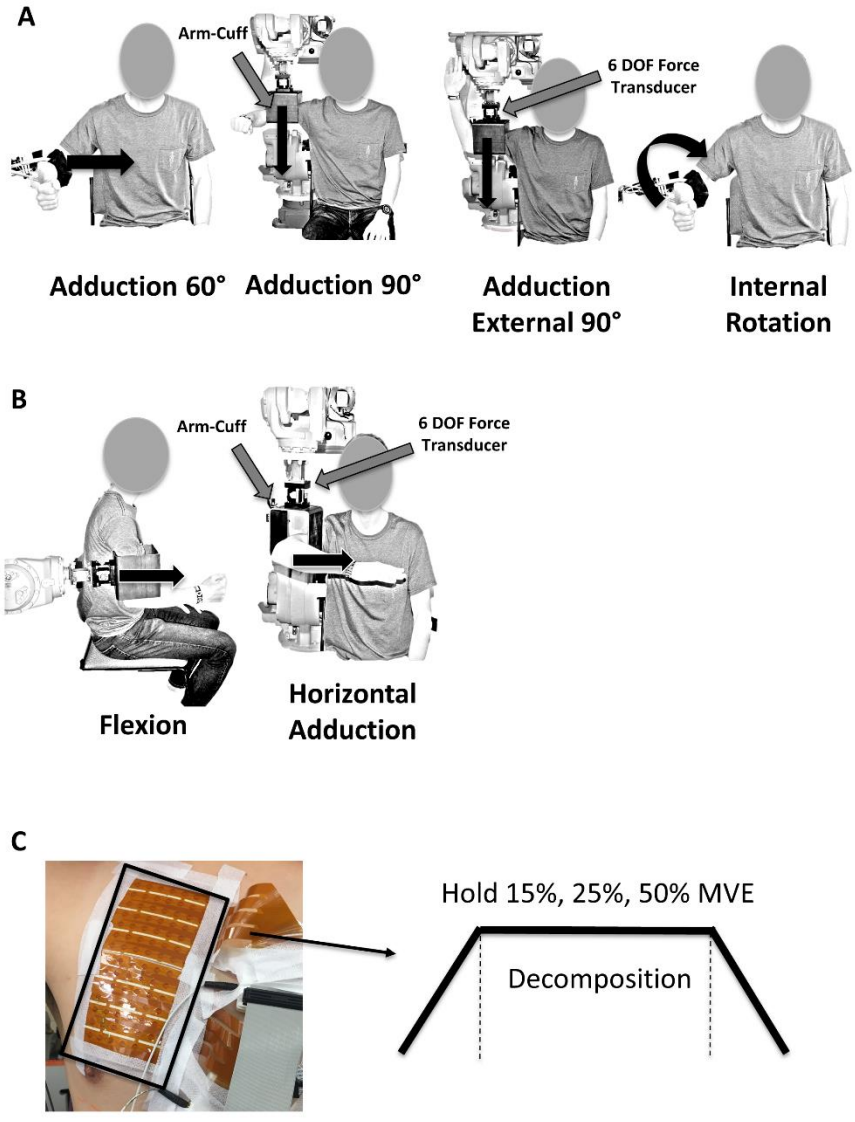

Figure 37: Schematic representation of the tasks and experimental protocol. **A:** Study 1 consisted of four tasks: adduction 60°, which required isometric efforts towards the sternum from 60° of abduction; adduction 90°, which required isometric efforts towards the sternum from 90° of abduction; adduction external 90, which required isometric efforts towards the sternum from 90° of abduction and 90° of external rotation; and internal rotation, which required isometric efforts by medially rotating the arm towards the sternum from 60° of abduction. **B:** Study 2 consisted of two tasks: flexion, which required isometric efforts pushing forward, and horizontal adduction, which required isometric efforts pushing across the body from 90° of elevation. **C:** Schematic of the experimental protocol. HD-sEMG was acquired while participants performed ramped isometric efforts at 15%, 25%, and 50% MVE. The decomposition of the signals was performed on the hold part of the trapezoid.

For each task, participants performed submaximal ramped isometric efforts scaled to task-specific MVE (Figure 37C). The effort levels included: 15%, 25%, and 50% MVE. Participants performed each effort level twice, and trials lasted 60 seconds for 15% and 25% MVE and 30 seconds for 50% MVE with three to five-minute rest breaks between the trials. Participants were encouraged to report feelings of fatigue and the need for longer rest periods, with more time allocated if requested by the participant. Each submaximal trial consisted of a ramp up, hold, and ramp down. For 15% and 25% MVE, participants ramped ~2% MVE/s and at 50% MVE, ~3% MVE/s. Tasks were fully randomized between and within participants. Effort levels were randomized within each task, with each submaximal effort performed consecutively. Intratrial visual feedback was provided on a monitor and displayed the required effort level and live feedback of the effort exerted against the attachment.

9.3. Data Analysis

9.3.1. HD-sEMG decomposition

HD-sEMG processing involved several steps. Before any analyses, HD-sEMG signals were visually inspected in the custom-made program in MATLAB. Any trials that were saturated had an artifact or had insufficient skin contact (i.e., no signal detected) were removed from further analyses. Following this, monopolar HD-sEMG signals were bandpass filtered with a 3rd order Butterworth filter (20-500 Hz). EMG signals in the monopolar mode were decomposed to individual motor unit action potentials using the convolutive blind source separation algorithm. This algorithm was previously validated for a broad range of forces in multiple muscles (Negro et al. 2016; Hyngstrom et al. 2018; Martinez-Valdes et al. 2018; Thompson et al. 2018; Murphy et al. 2018; Kapelner et al., 2019; Pereira et al. 2019; Cogliati et al. 2020; Martinez-Valdes et al.

2020). A trained investigator manually inspected all decomposed motor units, and only those motor units with a reliable discharge pattern were analyzed further (Del Vecchio et al. 2020). The decomposition's accuracy was determined using the silhouette measure (SIL), whose threshold was set to 0.9. SIL is a normalized accuracy index for EMG decomposition [see (Negro et al. 2016) for more details]. Decomposition was performed across the whole hold. Further, for each channel, the individual two-dimensional motor unit action potentials were extracted using spike trigger averaging.

9.3.2. Motor unit matching

In male participants, motor unit tracking was used to match motor units between different effort levels within a task. This method builds on the convolutive blind source separation technique (Negro et al. 2016). It is used to extract motor units with maximally similar motor unit action potential shapes (Martinez-Valdes et al. 2017). Two-dimensional (2D) normalized cross-correlation was used to match motor units between effort levels. Motor units were matched based on similarity using a threshold of 0.8 of 2D cross-correlation. Each match was visually inspected. Only motor units with motor unit action potential waveforms correlated by > 0.8 at the end with respect to the beginning of the two efforts were considered for further analyses. Previously, it was demonstrated that the likelihood of two motor units displaying the same discharge characteristics across days (or in this case, effort levels) is highly unlikely if initial decomposition is performed incorrectly (Martinez-Valdes et al., 2017; Del Vecchio et al. 2020). Once the algorithm successfully matched a motor unit between two effort levels, the mean discharge rate across the hold was evaluated to determine if the motor unit's discharge rate changed with an increase in effort level.

The mean discharge rate and coefficient of variation (CoV) of the inter-spike interval were quantified for 5-second intervals across the hold for the matched motor units. CoV of the inter-spike interval was quantified as the standard deviation of the inter-spike interval divided by the mean inter-spike interval. Peak-to-peak motor unit action potentials were quantified for the clavicular and sternocostal region of matched motor units. The mean peak-to-peak amplitude of motor unit action potentials for the clavicular region was quantified across rows 1 through 3, while for the sternocostal region across rows 4 through 8. These divisions followed anatomically described landmarks by Fung et al. (2009).

9.3.3. Motor unit analyses (Females)

Motor unit analyses in females focused on the superior array due to the declines in surface EMG amplitude in the inferior array because of the breast tissue. For motor units that were successfully decomposed, mean discharge rate and CoV of inter-spike-interval were quantified for 5-second intervals across the hold. Motor unit tracking was implemented to determine if this method may be feasible in females. Since motor units could not be matched due to the low yield in the number of successfully decomposed motor units (as described in Results), all motor unit data was averaged within a trial. The mean across participants is reported.

9.3.4. Force

Raw voltage data obtained in submaximal and maximal trials was processed. Raw voltage in X, Y, and Z directions was filtered using a 3rd order low-pass Butterworth filter with a cut-off frequency of 15 Hz and converted to Newtons using a custom-made program in MATLAB 2019b. Force acquired in submaximal trials was normalized to the mean of the two maximal values

quantified in task-specific MVEs. Normalized force data was used to confirm that all participants exerted similar effort levels at 15%, 25%, or 50% MVE.

9.3.5. Bipolar surface electromyography

Bipolar EMG data in task-specific maximal MVEs and submaximal trials were processed. All sEMG data was band-pass filtered with a 2nd order Butterworth filter (30-500 Hz), and RMS of the signal was quantified. For maximal trials, the mean of 3-second data surrounding the maximal force achieved was extracted. The sEMG signals in submaximal trials were then normalized to muscle-specific maxima. Following normalization, the mean of the two trials and henceforth, mean muscle activation was quantified only for the participants whose decomposition was successful and included in the analyses (see below). Each muscle's mean activity was ranked from highest to lowest to quantify which muscles contributed to the task alongside the pectoralis major.

Statistical Analyses

All statistical analyses were performed using SPSS (IBM, version 21). Before statistical comparisons, the data were checked for normality using the Shapiro-Wilk test. Not normally distributed data were ln transformed. For matched motor units, paired samples, a two-tailed t-test with a Dunn-Bonferonni correction was used to compare if mean discharge rate and coefficient of variation (CoV) differed between 15% and 25% MVE within each task or between 25% and 50% MVE in horizontal adduction. Additionally, a two-way repeated measure analysis of variance (ANOVA) was performed on motor unit action potential peak-to-peak amplitude to determine the

effect of *Region* (clavicular, sternocostal) and *Effort Level* (15%, 25% MVE). Significance was set to $p < 0.05$.

9.5. Results

The number of motor units decomposed across five tasks was 251 at 15% MVE and 173 at 25% MVE in male participants. Total matched motor units across two effort levels in all tasks were 112 (Table 12). Decomposition of 50% MVE was not successful for most tasks due to the increase in the number of superimposed motor unit action potentials in the interference signal. However, in horizontal adduction, 16 motor units that were successfully decomposed at 50% MVE in four male participants were matched to motor units at 25% MVE to evaluate if the discharge rate changed between these effort levels (described below). Further, the adduction external 90 task did not yield any motor units in males and was excluded from further analyses in this cohort. The amount of force feedback was the same in all participants included in the analyses below (Table 13).

Table 12: Summary of motor unit physiology in male participants in adduction 60, internal rotation, adduction 90, flexion, and horizontal adduction at 15% and 25% MVE. 50% MVE is also reported for horizontal adduction. The number of motor units, including the number of participants, successfully decomposed, is included in column 3. The mean discharge rate, CoV inter-spike interval, peak-to-peak motor unit action potential for the clavicular and sternocostal region (with standard deviation) for each task, and effort level is also reported.

Task	Effort Level (%MVE)	Number of Motor Units (Number of Participants)	Discharge Rate (pps)	Coefficient of Variation (CoV)	Clavicular Motor Unit Action Potential Peak-to-Peak (μV)	Sternocostal Motor Unit Action Potential Peak-to-Peak (μV)
Adduction 60	15	11 (N = 8)	13.8 ± 2.4	15.9 ± 2.7	44.2 ± 31.7	39.2 ± 15.8
	25	9 (N = 8)	14.4 ± 1.4	19.1 ± 4	72.7 ± 44	58.4 ± 25.2
Internal Rotation	15	13 (N = 6)	13.9 ± 1.1	18.2 ± 3.4	49.1 ± 23.8	39.6 ± 23.8
	25	11 (N = 6)	14.5 ± 1	19.1 ± 2.4	59.3 ± 20.3	47.6 ± 19.7
Adduction 90	15	12 (N = 7)	12 ± 3.6	21.1 ± 5.7	16 ± 10.8	10.8 ± 8.3
	25	10 (N = 7)	12.3 ± 3.4	19.7 ± 5.7	22 ± 9.6	16.9 ± 12.7
Flexion	15	8 (N = 5)	13.2 ± 1.6	18.5 ± 4	25.4 ± 9.7	22.1 ± 4.1
	25	10 (N = 5)	13.9 ± 1.6	19.4 ± 4.2	31 ± 15.4	28.8 ± 14.7
Horizontal Adduction	15	15 (N = 6)	15 ± 2.6	17 ± 2.5	33.7 ± 21.8	28.7 ± 28.8
	25	13 (N = 6)	13.3 ± 2.7	22.2 ± 5.2	68 ± 42.8	43.9 ± 43.9
	50	16 (N = 4)	15.9 ± 2.8	19.7 ± 2.2	132.7 ± 57.5	99.3 ± 75.5

Table 13: Summary of mean force represented in Newtons and a percentage of MVE exerted by the male participants across tasks and effort levels, including the maximal voluntary effort. The table represents means with standard deviations.

Task	Effort Level	Mean Force (N)	Mean %MVE
Adduction 60	15%	45.7 ± 6.1	15.7 ± 0.75
	25%	75.6 ± 10.3	26.1 ± 1.7
	100%	290.1 ± 38.9	-
Adduction 90	15%	48.4 ± 20.1	15.2 ± 2.2
	25%	79.5 ± 29.9	25 ± 1.6
	100%	314.7 ± 112.5	-
Internal Rotation	15%	44.7 ± 11.7	15.2 ± 1.7
	25%	74.3 ± 17.3	25.5 ± 1.9
	100%	290.7 ± 64.4	-
Flexion	15%	25.4 ± 7.4	13.6 ± 1.1
	25%	45.1 ± 12.4	24.2 ± 1.2
	100%	185.4 ± 45.9	-
Horizontal Adduction	15%	39.1 ± 13.1	16.8 ± 1
	25%	63.4 ± 21.8	27.3 ± 1.6
	50%	110.4 ± 38.7	53.5 ± 1.9
	100%	233.7 ± 86	-

The total number of motor units decomposed across tasks was 33 at 15% MVE and 14 at 25% MVE in females (Table 14). Motor unit decomposition was successful in four females with low breast tissue thickness (range: 3.2-7 cm) and one female with high breast tissue thickness (13.6 cm). All engaged in moderate to high physical activity levels. Motor unit decomposition in females was not successful in Study 2 (i.e., flexion, horizontal adduction), yielding no motor units for any task. Therefore, analyses in females focused on data generated in Study 1.

Table 14: Summary of motor unit physiology in female participants in adduction 90, internal rotation, and adduction external 90 tasks at 15% and 25% MVE. The number of motor units, including the number of participants, successfully decomposed is included in column 3. Mean discharge rate, Coefficient of Variation, peak-to-peak motor unit action potential for the clavicular and sternocostal region (with standard deviation) for each task, and effort level is also reported.

Task	Effort Level (%MVE)	Number of Motor Units (Number of Participants)	Discharge Rate (pps)	Coefficient of Variation (CoV)	Clavicular Motor Unit Action Potential Peak-to-Peak (μV)	Sternocostal Motor Unit Action Potential Peak-to-Peak (μV)
Adduction 90	15	18 (N = 5)	9.4 ± 1.3	17.3 ± 2.1	9.3 ± 7.5	6.7 ± 2.2
	25	4 (N = 3)	9 ± 2.1	19.7 ± 4.1	20.6 ± 13.8	12.9 ± 1.8
Internal Rotation	15	5 (N = 2)	14.8 ± 1.2	14.1 ± 0.8	10.2 ± 1.1	11.9 ± 1.6
	25	1 (N = 1)	12.1	15.9	27.8	12.6
Adduction External 90	15	10 (N = 2)	8.8 ± 0.6	17.9 ± 0.5	11.1 ± 10.2	7.2 ± 3.5
	25	9 (N = 3)	9.9 ± 0.6	17 ± 1.5	14.9 ± 14.8	9.4 ± 6.4

9.5.1. Males

9.5.1.1. Mean discharge rate of the matched motor units

Mean discharge rate did not differ between 15% and 25% MVE in adduction 60 ($p = 0.53$; $d = 0.2$; Figure 38), internal rotation 60 ($p = 0.44$; $d = 0.4$; Figure 39), adduction 90 ($p = 0.71$; $d = 0.14$; Figure 40), flexion ($p = 0.4$; $d = 0.4$; Figure 41A and 42A), or horizontal adduction ($p = 0.058$; $d = 0.9$; Figure 41B and 42B). Further, in horizontal adduction, mean discharge rate was not different between 25% and 50% MVE ($p = 0.11$; $d = 1.01$; Figure 41C and 42C).

9.5.1.2. Mean coefficient of variation (CoV) of inter-spike interval of the matched motor units

Mean CoV of inter-spike interval did not differ between 15% and 25% MVE in adduction 60 ($p = 0.06$; Figure 38), internal rotation 60 ($p = 0.27$; Figure 39), adduction 90 ($p = 0.63$; Figure 40), and flexion ($p = 0.69$; Figure 41A). In horizontal adduction, mean CoV inter-spike interval

was higher at 25% than 15% MVE (p = 0.04; Figure 41B). Further, mean CoV ISI was not different between 25% and 50% MVE in horizontal adduction (p = 0.13; Figure 42C).

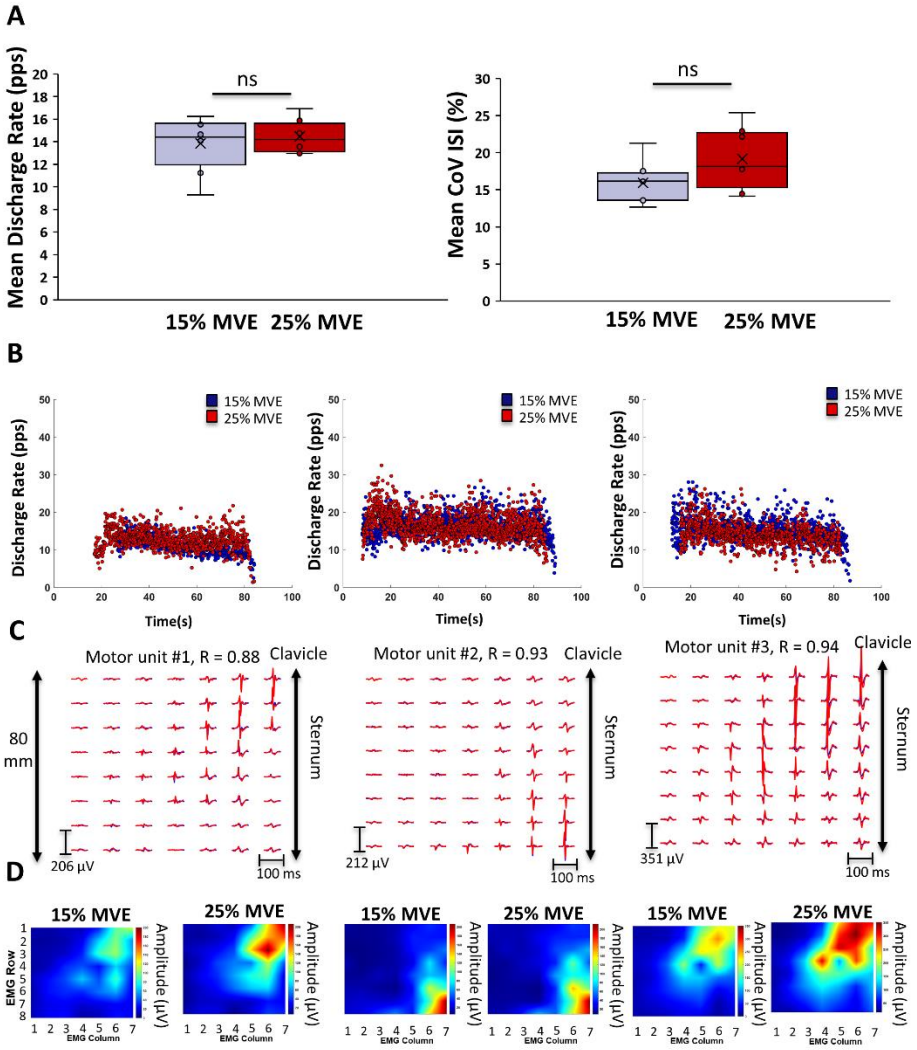

Figure 38: Motor unit behaviour in adduction 60° in males. **A:** Mean discharge rate (top panel left) and mean CoV inter-spike interval (top panel right) between efforts for matched motor units. **B:** Representative examples of three motor units in adduction 60°, showing instantaneous discharge rate across time at 15% and 25% MVE. Each colour represents the discharge rate of the same motor unit in 15% and 25% MVE. Note no change in discharge rate between effort levels in all three motor units. **C:** Motor unit action potentials obtained from high-density sEMG signals corresponding to the motor units displayed in B. The motor unit signatures were extracted using spike-trigger averaging from the discharge times shown in B. **D:** Peak-to-peak motor unit action potential heatmaps corresponding to the motor unit action potential signatures in C for 15% and 25% MVE.

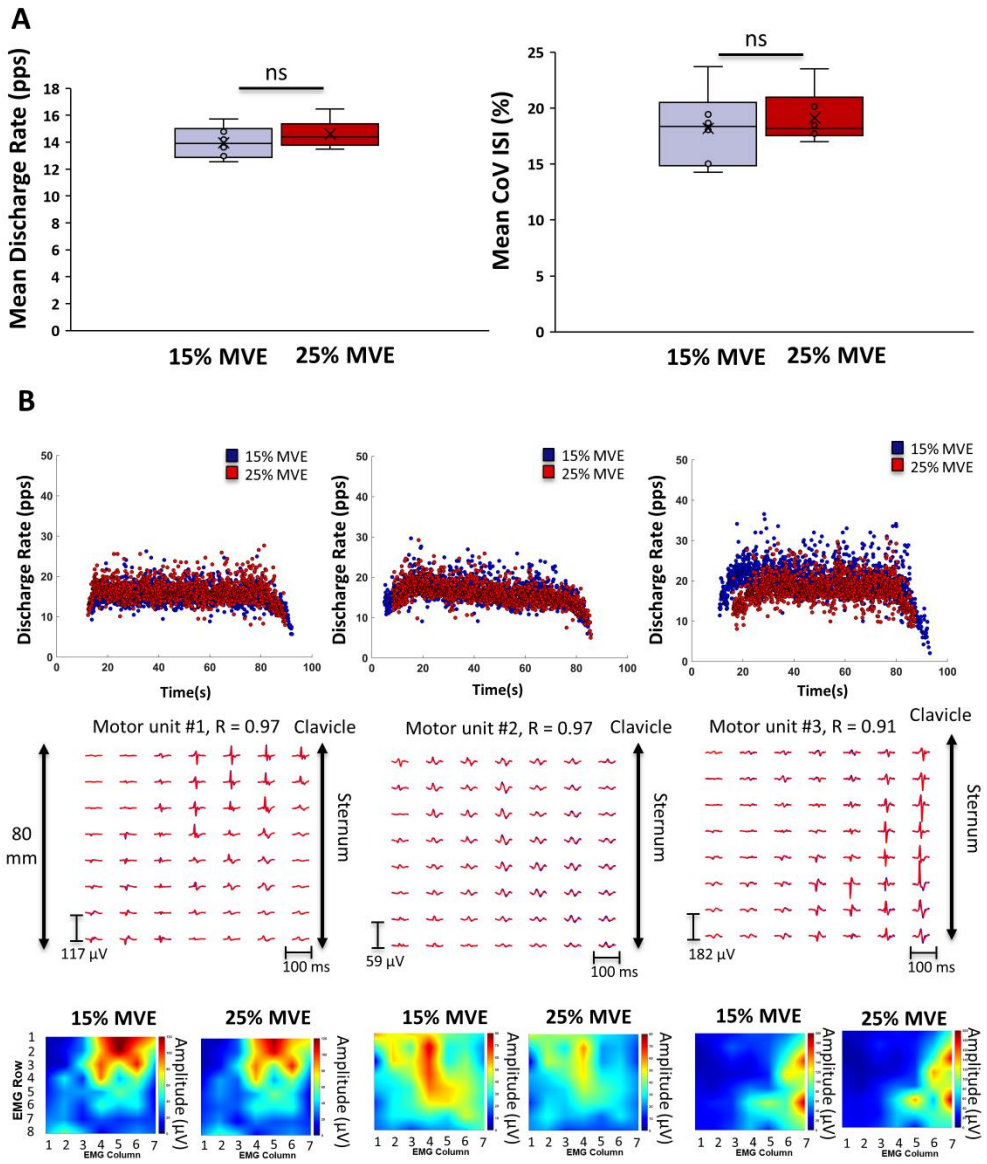

Figure 39: Motor unit behaviour in internal rotation in males. **A:** Mean discharge rate (top panel left) and mean CoV inter-spike interval (top panel right) between efforts for matched motor units. **B:** Representative examples of three motor units in internal rotation, showing instantaneous discharge rate across time at 15% and 25% MVE. Each colour represents the discharge rate of the same motor unit in 15% and 25% MVE. Note no change in discharge rate between effort levels in all three motor units. **C:** Motor unit action potentials obtained from high-density sEMG signals corresponding to the motor units displayed in B. The motor unit signatures were extracted using spike-trigger averaging from the discharge times shown in B. **D:** Peak-to-peak motor unit action potential heatmaps corresponding to the motor unit action potential signatures in C for 15% and 25% MVE.

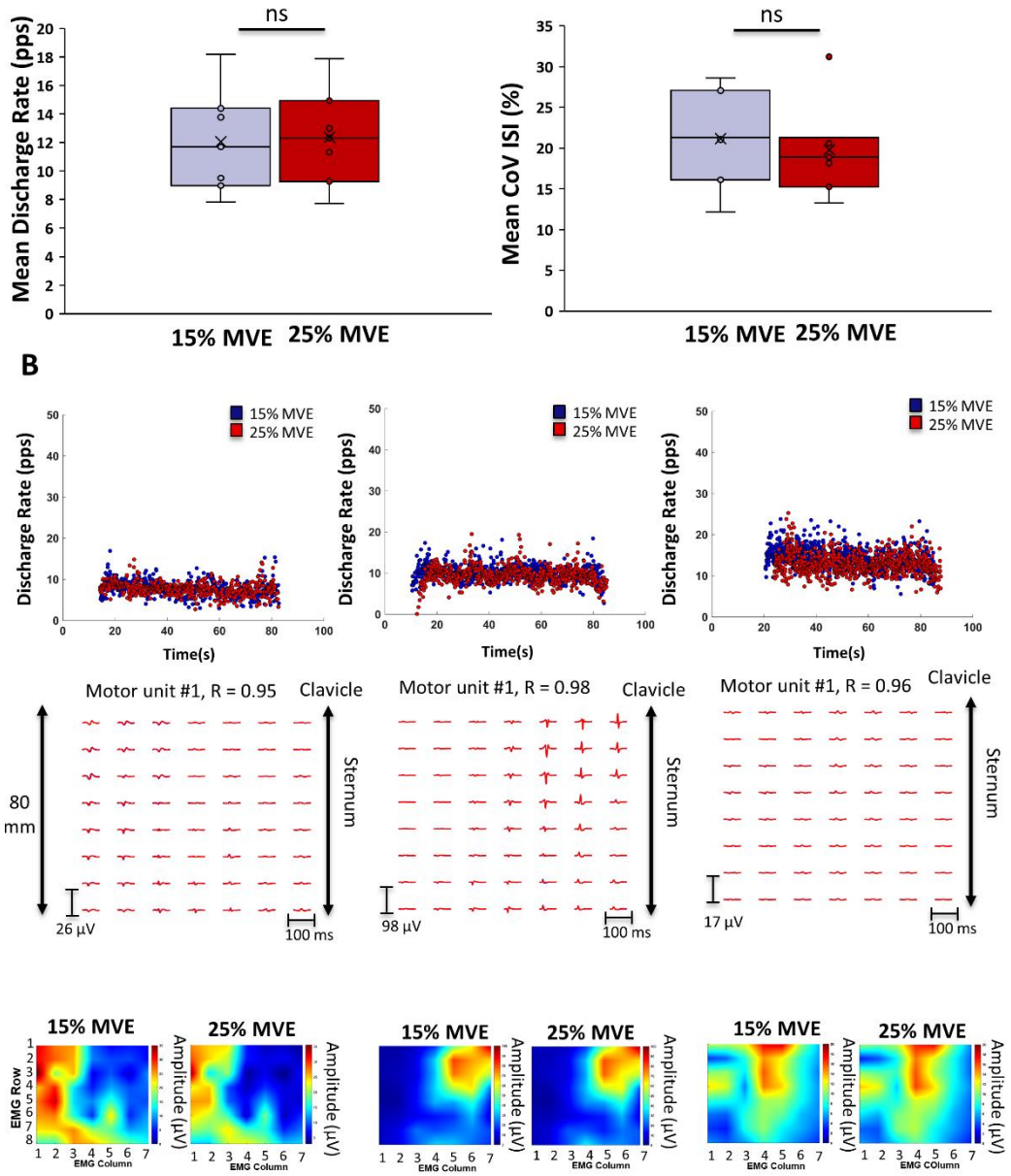

Figure 40: Motor unit behaviour in adduction 90° in males. **A:** Mean discharge rate (top panel left) and mean CoV inter-spike interval (top panel right) between efforts for matched motor units. **B:** Representative examples of three motor units in adduction 90°, showing instantaneous discharge rate across time at 15% and 25% MVE. Each colour represents the discharge rate of the same motor unit in 15% and 25% MVE. Note no change in discharge rate between effort levels in all three motor units. **C:** Motor unit action potentials obtained from high-density sEMG signals corresponding to the motor units displayed in B. The motor unit signatures were extracted using spike-trigger averaging from the discharge times shown in B. **D:** Peak-to-peak motor unit action potential heatmaps corresponding to the motor unit action potential signatures in C for 15% and 25% MVE.

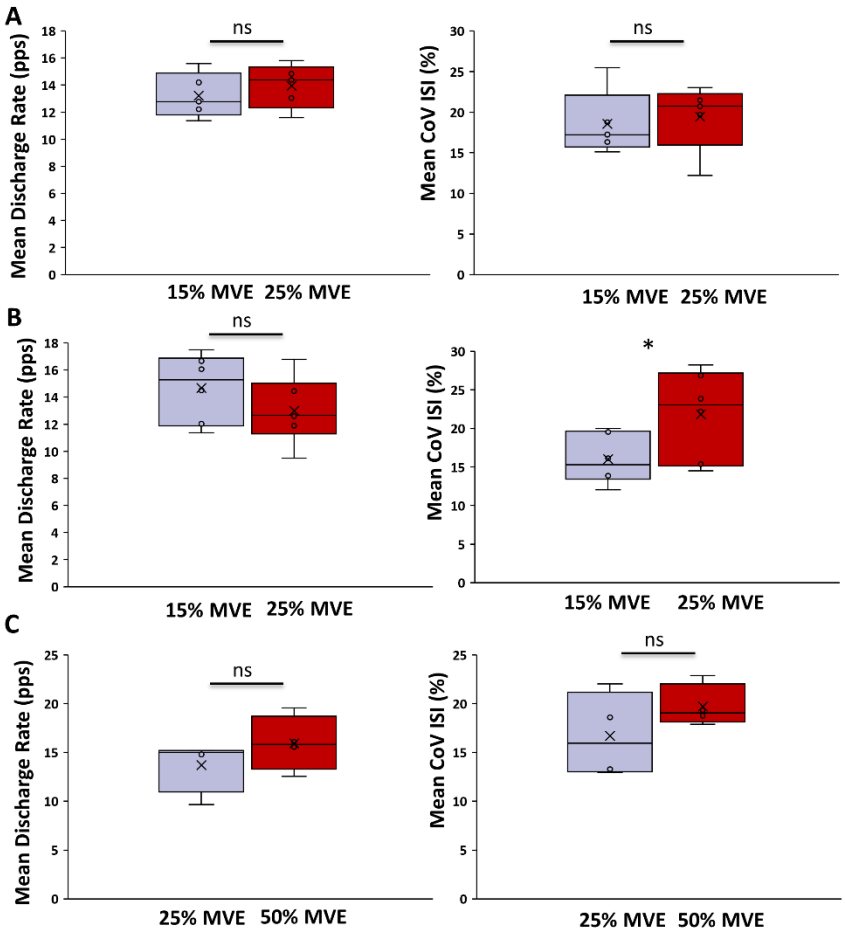

Figure 41: Mean discharge rate and CoV inter-spike-interval in flexion (A), and horizontal adduction (B and C) in males. **A and B:** Mean discharge rate did not differ between 15% and 25% MVE in flexion and horizontal adduction. CoV inter-spike-interval did not differ in flexion but was significantly larger in horizontal adduction. **C:** Mean discharge rate and CoV inter-spike interval did not differ between 25% and 50% MVE in horizontal adduction.

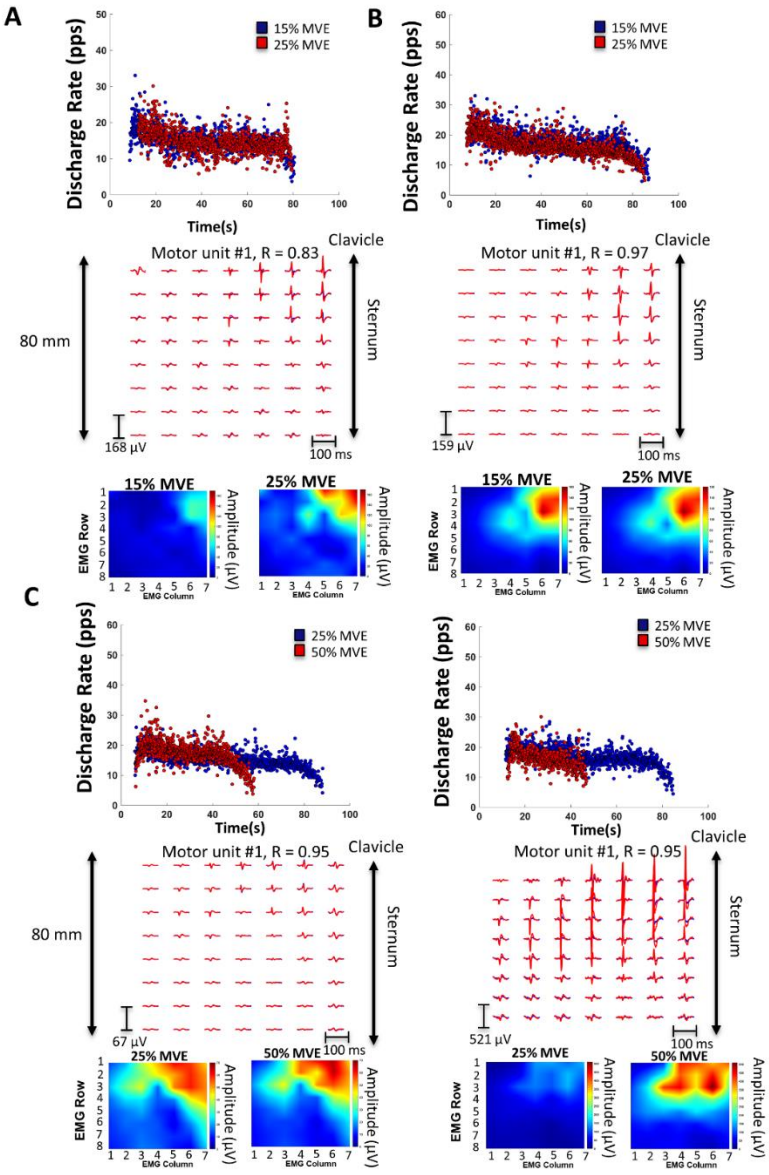

Figure 42: Motor unit behaviour in flexion (A) and horizontal adduction (B and C) in males. **A (top panel):** Representative example of one motor unit in flexion, showing instantaneous discharge rate across time at 15% and 25% MVE. Each colour represents the discharge rate of the same motor unit in 15% and 25% MVE. Note no change in discharge rate between effort levels in the motor unit. **Bottom panel:** Motor unit action potentials obtained from high-density sEMG signals corresponding to the same motor unit displayed in the top panel (A) with peak-to-peak motor unit action potential heatmaps corresponding to 15% and 25% MVE. The motor unit signatures were extracted using spike-trigger averaging from the discharge times shown in A. **B (top panel):** Representative example of one motor unit in horizontal adduction, showing instantaneous discharge rate across time at 15% and 25% MVE. Each colour represents the discharge rate of the same motor unit in 15% and 25% MVE. Note no change in discharge rate between effort levels in the motor unit. **Bottom panel:** Motor unit action potentials obtained from high-density sEMG signals corresponding to the same motor unit displayed in the top panel (B) with peak-to-peak motor unit action potential heatmaps corresponding to 15% and 25% MVE. The

motor unit signatures were extracted using spike-trigger averaging from the discharge times shown in B. **C:** Representative example of two motor units in horizontal adduction, showing instantaneous discharge rate across time at 25% and 50% MVE. Each colour represents the discharge rate of the same motor unit in 25% and 50% MVE. Note no change in discharge rate between effort levels in the two motor units. **Bottom panel:** Motor unit action potentials obtained from high-density sEMG signals corresponding to the same motor unit displayed in the top panel (C) with peak-to-peak motor unit action potential heatmaps corresponding to 25% and 50% MVE. The motor unit signatures were extracted using spike-trigger averaging from the discharge times shown in C.

9.5.1.3. Motor unit action potential amplitude of the matched motor units

No main effects or interactions in peak-to-peak motor unit action potentials existed for adduction 90, internal rotation, flexion, or horizontal adduction (all $p > 0.05$). A region by effort level interaction existed in adduction 60 ($F_{(1,7)} = 7.22$, $p = 0.031$, $\eta p^2 = 0.5$), where the peak to peak amplitude in the clavicular, but not sternocostal region was 65% larger at 25% than 15% MVE ($p = 0.016$; $d = 1.09$). No differences existed between regions in either effort level in this task.

9.5.2. Females

9.5.2.1. General observations on unmatched motor units

Due to the low number of motor units decomposed in females, this section focuses on general motor unit physiology (Table 14). Various spatial distributions of motor unit action potentials occurred in motor units that were successfully decomposed (Figure 43 and Figure 44).

The ability to match motor units between 15% and 25% MVE was explored in adduction 90 and adduction external 90, as two to three participants yielded successfully decomposed motor unit data at both efforts in these tasks (Figure 43). The discharge rate between 15% and 25% MVE in the motor units that were matched did not change (Figure 43A and D), even though the effort level increased as quantified by normalized effort levels (Figure 43B and E). The mean discharge rate was ~9 pps in adduction 90, ~14.8 in internal rotation, and ~8.8 pps in adduction external 90

at 15% MVE (Table 14). Although the ability to match motor units in females was possible in two females in two different tasks, the low number of motor units did not allow for statistical comparisons in motor unit discharge rate and CoV inter-spike-interval.

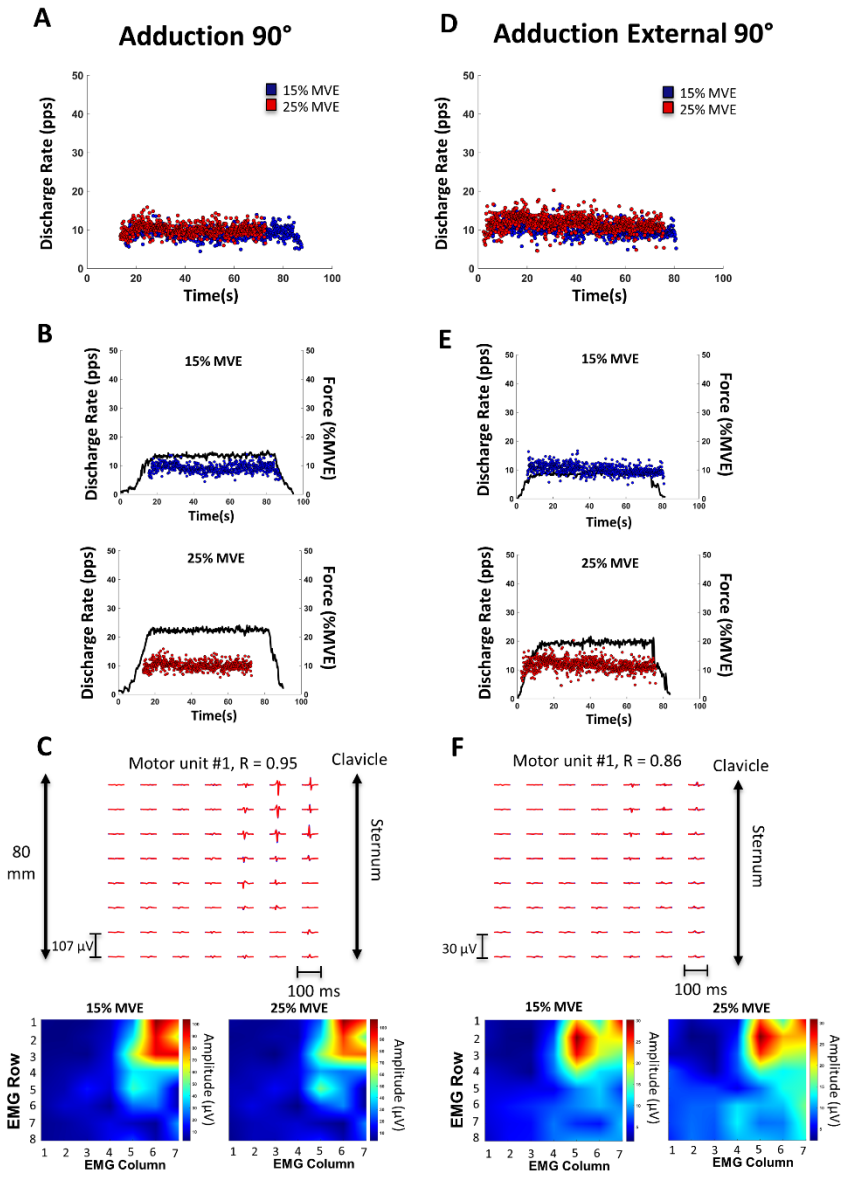

Figure 43: Motor unit behaviour in adduction 90 and adduction external 90 in females with motor unit action potential signatures. **A:** Representative example of one motor unit in adduction 90, showing instantaneous discharge rate across time at 15% and 25% MVE. Each colour represents the discharge rate of the same motor unit in 15% and 25% MVE. Note no change in discharge rate between effort levels in the motor unit. **B:** Same motor unit displayed in A with force overlayed for 15% and 25% MVE. **C:** Motor unit action potentials obtained from high-density sEMG signals corresponding to the same motor unit displayed in the top panel (A) with peak-to-peak motor unit action potential heatmaps corresponding to 15% and 25% MVE. The motor unit signatures were extracted using spike-trigger averaging from the discharge times shown in A. **D:** Representative example of one motor unit in adduction external 90, showing instantaneous discharge rate across time at 15% and 25% MVE. Each colour represents the discharge rate of the same motor unit in 15% and 25% MVE. Note no change in discharge rate between effort levels in the motor unit. **E:** Same motor unit displayed in D with force overlayed for 15% and 25% MVE. **F:** Motor unit action

potentials obtained from high-density sEMG signals corresponding to the same motor unit displayed in the top panel (D) with peak-to-peak motor unit action potential heatmaps corresponding to 15% and 25% MVE. The motor unit signatures were extracted using spike-trigger averaging from the discharge times shown in D.

Motor unit action potential spatial distributions differed within (Figure 44A) and between participants (Figure 44B). Two motor unit action potential distributions depicted within a participant in Figure 44A show a confined motor unit within the clavicular region. In internal rotation, motor units with a diverse distribution of motor unit action potentials between participants were observed (Figure 44B). Based on these examples, it appears that motor unit distributions in tasks at 90° of abduction are more localized towards the sternum. In contrast, in internal rotation, motor unit action potentials are spread out across the muscle and towards the sternum. Additionally, different motor unit action potential distributions occurred between different tasks within a participant (Participant 1 in Figures 44A and 44B).

9.5.3. Global activation of other shoulder muscles in males

Additional shoulder muscles activated alongside the pectoralis major in males. Specifically, in adduction 60, the middle deltoid had high activity in both efforts (~18% -23% MVC; Supplementary Figure 2). At 25% MVE, the latissimus dorsi (~20% MVC) also has high activation. In internal rotation, the latissimus dorsi activated highly at 15% and 25% MVE (15%-19% MVC). In adduction 90, the upper trapezius was highly active at both effort levels (~15% - 18% MVC), while at 25% MVE, the latissimus dorsi and middle deltoid were also highly active (~13% to 15% MVC). In flexion, the upper trapezius and anterior deltoid activated highly in both efforts (19-24% MVC; Supplementary Figure 3). Lastly, in horizontal adduction, anterior deltoid activated highly at both efforts (17% - 23% MVC). Additionally, infraspinatus activated highly at

15% MVE, while at 25% MVE, latissimus dorsi and upper trapezius also had high activations (18% - 20% MVC).

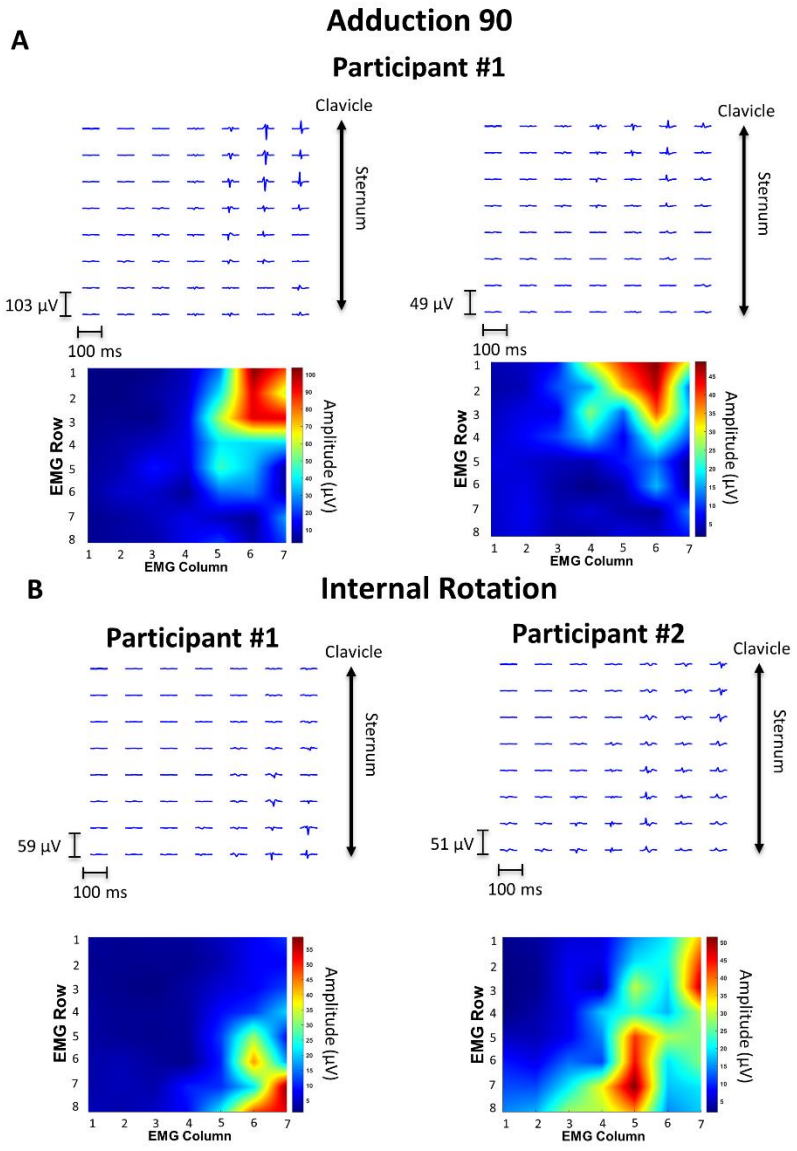

Figure 44: Motor unit action potential signatures in three female participants in adduction 90 and internal rotation. **A:** Examples of two motor units in adduction 90 from a single participant at 15% MVE. Note the spatial distribution of motor unit action potentials. **B:** Examples of two motor units from two participants in internal rotation at 15% MVE. Note the spatial distribution of motor unit action potentials.

9.6. Discussion

Motor units within the pectoralis major behave peculiarly. One striking initial observation was that motor units at *low* effort levels (i.e., 15%-25% MVE) discharged quite highly (~12-15 pps) in comparison to some other commonly investigated muscles, such as vastus lateralis and vastus medialis (~11 pulses per second (pps) at 30% MVE; 15 pps at 75% MVE; Vila-Cha et al. 2010; Martinez-Valdes et al. 2018), or tibialis anterior (~13 pps at 30% MVE; Erim et al. 1996). However, discharge rates approximated reported values for biceps brachii (~16 pps at 10% MVE; Holobar et al. 2009) and upper trapezius (~21.5 at 10% MVE; Holobar et al. 2009). Further, irrespective of the task, the matched motor unit mean discharge rate did not change, despite increased effort level either from 15% to 25% MVE across tasks or 25% to 50% MVE in horizontal adduction. These findings contrast with motor unit findings in other muscles, which demonstrated an increase in discharge rate with increases in effort level (De Luca et al. 1982; Del Vecchio et al. 2017). The current physiological reason and mechanism behind this finding are uncertain, although some hypotheses are proposed and outlined below.

Low-threshold motor units in pectoralis major may reach their saturation level at a relatively low effort level (i.e., <15% MVE). Typically, saturation in motor unit discharge rate occurs at ~20 pps (Fuglevand et al. 2015) as documented for multiple muscles, such as biceps (Mottram et al. 2009; 2014), latissimus dorsi, triceps, brachioradialis, pectoralis major (Bracchi et al. 1966), vastus lateralis (De Luca and Contessa, 2012), deltoid (De Luca et al. 1982), and upper trapezius (Westgaard and De Luca, 2001). An elegant study examining motor unit discharge rates in multiple human and animal muscles demonstrated that the mean discharge rate of single motor units differs between muscle groups and depends on the level of neuraxis the muscle is innervated (Bracchi et al. 1966). For example, motor units in the deltoid, innervated by the motoneurons at

the level of C4 and C5 of the spinal cord discharge at ~17 pps at the maximal effort (Bracchi et al. 1996). In contrast, motor units in the soleus innervated by motoneurons at the level of L5-S2 discharge at ~ ten pps at the maximal effort (Bracchi et al. 1966). At maximal voluntary contractions, motor units in the pectoralis major discharge at ~19.45 ± 2.6 pps (Bracchi et al. 1966). Therefore, low-threshold motor units in the pectoralis major likely modulate discharge rate within a narrow window of effort levels (below 15% MVE). After this, the pectoralis major seems to rely on motor unit recruitment to increase force. Reliance on recruitment is common for large shoulder muscles, as deltoid, trapezius, and biceps rely primarily on motor unit recruitment (De Luca, 1985; De Luca et al., 1982; Westgaard and De Luca, 2001; Kukulka and Clamann, 1981). Since the pectoralis major is involved in powerful contractions and maintaining posture, finely tuned discharge rates existing for incremental modulations of force may not be necessary (De Luca, 1985). Additionally, the pectoralis major consists of predominantly fast, powerful Type II muscle fibers (Johnson et al., 1973; Srinivasan et al., 2007), typically innervated by large high-threshold motoneurons (Burke, 1981; Henneman and Mendell, 1981). Therefore, the recruitment of these units may be enough to increase contractile force without altering the discharge rate substantially.

The contribution of the afferent feedback and descending drive to motoneurons also influences the modulation of the discharge rate in force control (Enoka and Duchateau, 2017). Similar firing rates between effort levels in pectoralis major motor units may be due to a peripheral feedback loop involving muscle receptors (i.e., muscle spindle activity), recurrent inhibition by Renshaw cells, or activation of persistent inward currents (PICs). The density of muscle spindles in the pectoralis major is currently unknown. However, postural muscles, including muscles of the shoulder girdle, have a lower density of muscle fiber spindles than more distal muscles in dogs (Buxton and Peck, 1990) and humans, respectively (Banks, 2006). Alternatively, Renshaw

inhibition may be involved, as it would suppress the activity of active motor units while additional motor units are recruited (De Luca et al. 1982). As such, Renshaw inhibition is generally more pronounced in proximal rather than distal muscles (Katz et al. 1993) and emerges more in low-threshold than in high-threshold motor units (Hultborn et al. 1988). On the other hand, the lack of change in motor unit discharge rate may also be due to persistent inward Ca^{2+} and Na^{+} currents, which modulate motoneuron excitability (Heckman et al. 2008). Previously, it was proposed that these channels are more prominent in postural muscles due to their role in supporting tonic activation (Wilson et al. 2015).

Alternatively, a lack of change in motor unit discharge rate with effort level may originate from the pectoralis major's multi-functional nature. Specifically, not all motor units may act in the primary direction of the external force produced at the arm. Some motor units may enable control of the sternoclavicular or acromioclavicular joints. Multiple matched motor units were located near the sternoclavicular joint, discharging at similar firing rates despite differing effort levels. In addition, in Chapters 7 and 8, the pectoralis major's clavicular region consistently exhibited similar normalized EMG amplitudes in adduction 60, adduction 90, internal rotation, flexion, and horizontal adduction at 15% and 25% MVE, coinciding with these physiological findings.

However, it is essential to recognize that the control of the four articular joints within the shoulder complex requires coordinated activation of over twenty muscles surrounding the shoulder complex. Shoulder muscles act about these joints to produce multidirectional forces and moments, with several muscles having instantaneously similar lines of action (Ackland et al. 2008; Ackland and Pandy, 2011). Hence, the pectoralis major is most likely not the sole contributor to increasing effort in the tasks explored in this study. For example, in adduction and internal rotation, the latissimus dorsi activates as a moment synergist to pectoralis major (Wickham et al. 2004), while

the middle deltoid activates as an antagonist. However, additional muscles, such as the upper trapezius, may also activate at higher arm elevations (e.g., adduction 90) to control the scapulothoracic joint. In tasks such as horizontal adduction and flexion, anterior deltoid, upper trapezius, or infraspinatus may also activate with the pectoralis major. Therefore, these relationships may change depending on the arm posture and task (McDonald et al. 2012; Nadon et al. 2016; Diefenbach and Lipps, 2019; Leonardis et al. 2020). Collectively, the recruitment of different pectoralis major regions and motor units within these regions may be influenced by an increase in the activation of surrounding shoulder musculature, which complicates the interpretation of even the most sophisticated analyses.

9.6.1. Motor unit decomposition in females

Single motor unit decomposition was successful in five females. While statistical analyses were infeasible on a group level, evaluation of motor unit physiology on an individual level provided some insights. Different motor unit action potential distributions occurred between different tasks in the same individual and between individuals within the same task in the current study. While motor unit action potentials are affected by tissue thickness, the HD-sEMG arrays in the current study were located on the pectoralis major's superior regions, diminishing some of these effects. These unique insights into pectoralis major control are relevant, particularly in clinical cohorts, such as breast cancer survivors. The sheer number of individualized surgical and non-surgical breast cancer treatments elicits highly variable side effects in pectoralis major activation and function, and transitively shoulder and whole arm function. The distribution of motor unit action potentials can also provide crucial information regarding newly formed motor units that result from reinnervation of the muscle (Kapelner et al. 2016) or denervation of muscle fibers within a single motor unit. Even though motor unit-specific analyses in females in the current

work are too preliminary to infer differences in motor unit physiology in selected tasks, they provide essential information and a starting point for future work in this area.

9.6.2. Number of decomposed motor units in males and females

The number of correctly identified and decomposed motor units varied between effort levels. In general, fewer motor units were decomposed at 25% than 15% MVE. A smaller number of motor units at 25% MVE does not mean that fewer motor units were recruited. Previously, ~30% reduction in the number of motor units successfully decomposed was quantified in tibialis anterior as the effort level increased (Hassan et al. 2019; Del Vecchio et al. 2020). This is primarily due to challenges in isolating spike trains at higher effort levels, as additional motor units are recruited (Del Vecchio et al. 2020). The number of motor units decomposed also varied between participants, as in some participants, decomposition was not successful. In contrast, in others, five to seven motor units in a single trial were identified. EMG parameters are highly influenced by subcutaneous tissue thickness, muscle architecture, or muscle fiber alignment underneath the electrode (Farina et al. 2002; Holobar et al. 2014). These factors likely influenced the decomposition success in some participants (Del Vecchio et al., 2020). Further, the number of motor units successfully decomposed depends substantially on the muscle (Del Vecchio et al. 2020). Additional challenges, such as breast tissue thickness and composition, disadvantaged decomposition success in females. In previous studies, the total number of motor units decomposed was markedly less in females than males in thenar muscles, first dorsal interosseus, wrist flexors, and biceps (for example, see Pereira et al. 2019; Del Vecchio et al. 2020).

9.7. Limitations

The major limitation of this study is that decomposition was successful only at low efforts. Attempts were made to decompose motor units at 50% MVE. However, difficulties arose in isolating spike trains due to additional motor units contaminating recordings as effort level increased. Improvements in decomposition algorithms for multi-functional muscles, such as pectoralis major in the future, should enable reliable decomposition and tracking of motor units over a broader range of effort levels. Further, decomposition success was relatively low for the inferior array in male participants. The exact reason behind this is unknown but could be due to thicker subcutaneous tissue or deeper localization of motor units. Additionally, the total number of successfully decomposed motor units and the number of participants where decomposition was successful was low due to the decomposition challenges. Therefore, findings in this study should be taken with caution. Future studies should consider recruiting a larger number of participants to increase the probability of successful decomposition and increase the number of motor units decomposed. Only young, healthy males and females participated in this study, and therefore, it is unknown how the current findings transfer onto the aging and clinical cohorts.

9.8. Conclusions

Novel insights emerge from this dataset on the inner workings of a large, multifunctional shoulder muscle, prompting several fascinating discussion points. Initially, it is important to note that the investigation and discovery of pectoralis major neuromusculoskeletal control are feasible at low effort levels, particularly in males. As decomposition algorithms continually improve, similar investigations may be possible in females. Further, the modulation of rate coding and recruitment of motor units in the pectoralis major is unlike that observed in other muscles.

Compared to other muscles, its sophisticated and intricate control appears to rely heavily on motor unit recruitment, starting at very low effort levels.

Chapter 10: General discussion and conclusions

This dissertation's main objective was to establish critical foundational knowledge on regional pectoralis major function in males and females. Within this objective, several methodological and fundamental discoveries emerged. First, several key methodological challenges in investigating pectoralis major in males and females were overcome, leading to the following findings:

1. Current assessment of EMG activity within the sternocostal region using classic EMG electrodes underestimates the activity and contribution of lower pectoralis major regions, especially in adduction, internal rotation, and extension across effort levels.
2. HD-sEMG can be used to acquire EMG from ~ ½ of the pectoralis major in females irrespective of the breast tissue thickness, providing unprecedented insights into pectoralis major activation in this cohort.
3. Specific to males, pairing HD-sEMG with neural decoding can non-invasively quantify neural and neuromuscular properties at low (15-25% MVE) and occasionally, moderate (i.e., horizontal adduction, 50% MVE) effort levels across several tasks. Decomposition at 50% MVE (4/5 tasks) is challenging and currently not feasible. Nonetheless, pairing these two non-invasive methods generates groundbreaking insights into the motor function of this complicated muscle.
4. The decomposition of HD-sEMG signals into neural properties in females is possible, although with low yields in motor unit numbers and high dependency on the task and participant. However, the sole fact that some motor units were decomposed gives me increased confidence that, with improvements in methods, this will be possible in the future.

Secondly, several key foundational discoveries emerged regarding the fundamental neuromusculoskeletal control of pectoralis major in males and females:

1. In females, clavicular, superior, and middle sternocostal regions contribute differentially across tasks and effort levels. The differential activity is more evident at low effort levels than moderate or high efforts. In contrast, moderate or high effort require high activation of all three regions.
2. In males, clavicular, upper, and lower sternocostal regions contribute differentially across tasks, and sometimes, effort levels. Lower sternocostal regions solely assist in tasks involving internal rotation 60 and 90, extension, adduction external 90, and adduction 60 and 90. All three regions activated to the same magnitude in flexion and horizontal adduction (across all efforts), and moderate to high efforts in internal rotation 60, and adduction 60.
3. Motor units in pectoralis major have a strikingly high discharge rate at low effort levels (15-25% MVE), averaging ~14 pps.
4. Pectoralis major relies heavily on motor unit recruitment, rather than motor unit rate coding, to increase effort. This fascinating discovery brings us one step closer to understanding how such a large, postural muscle generates mechanical force.

10.1. Acquisition of EMG signals from pectoralis major in males: Recommendations and considerations

Study 1 findings demonstrated limitations in the current assessment of pectoralis major activation due to the location of classic EMG electrodes on the sternocostal region. Specifically, the lower sternocostal region contribution is underestimated, especially in adduction, internal rotation, and extension across effort levels. Further, in exercise and clinical case scenarios,

quantification of EMG amplitude cannot reveal the exact mechanisms behind observed activity (Martinez-Valdes et al. 2018). Considering this, two critical considerations in EMG acquisition emerged:

1. Acquisition of EMG from at least three pectoralis major locations (i.e., clavicular, upper, and lower sternocostal region) is advised to provide better estimates and avoid mischaracterization of its activation, particularly in studies which examine fundamental shoulder function in daily, occupational, and exercise tasks.
2. Pairing HD-sEMG with a neural decoding algorithm is feasible in pectoralis major. Therefore, clinical and exercise studies should consider pairing HD-sEMG with neural decoding, combining quantifications of the spatial distribution of muscle activity with insights into the motor function to decipher the mechanisms behind any observed alterations in EMG amplitude.

10.2. Regional pectoralis major activation depends on the task in males and females

In females, a complex relationship between task and effort level existed. Clavicular and middle sternocostal regions played a significant role in low efforts, specifically in adduction, internal rotation 60°, flexion, and horizontal adduction. In three tasks, increased effort level resulted in high activation of all three regions, except in internal rotation, where high activity in clavicular and middle sternocostal regions was maintained at high efforts. In contrast, middle sternocostal regions exhibited high activity in adduction external 90, extension, and internal rotation 90°. In adduction, adduction external 90, internal rotation, and extension of other regions of the pectoralis major (i.e., lower sternocostal) may also be involved. However, challenges existed in the acquisition of EMG signals from these regions due to breast tissue thickness. Nonetheless, current findings indicate a potentially middle-to-bottom heavy distribution of activation in

adduction, adduction external 90, internal rotation, and extension. The top-heavy distribution of muscle activity is seen in flexion and horizontal adduction. Thus, resection or disinsertion of the middle sternocostal (or lower) regions may compromise pectoralis major function in adduction, internal rotation, and extension. Since pectoralis major function is compromised, this would prompt compensatory activation of the superior pectoralis major regions or additional shoulder muscles. Considering flexion and horizontal adduction relies heavily on activation of the top regions, resections of the lower pectoralis major region should not influence the performance of these tasks. Indeed, some of these deficits or lack thereof were quantified in breast cancer survivors who underwent subpectoral breast reconstruction (Leonardis et al. 2019).

In males, regional activation depended on the task, and in some instances, on effort level. While low efforts required localized activity in the lower sternocostal regions in internal rotation and adduction at 60°, increased efforts required the recruitment of clavicular and upper sternocostal regions in these tasks. This contrasts with the previous EMG study, which showed no such interactions in adduction at 60° (Paton and Brown, 1994). However, their classic EMG electrodes were located medially (i.e., towards the sternum), close to the defined innervation zone. As such, increases in a muscle contraction may have resulted in the shift of EMG electrodes directly over the innervation zones, suppressing their EMG amplitudes. The exact mechanism behind current findings is unknown but could be due to the interaction between architectural, neural, and biomechanical properties. For example, an increase in effort level may require the recruitment of other regions to increase the sternoclavicular or glenohumeral joint stability. Adduction and internal rotation at higher arm elevations, on the other hand, were not influenced by an increase in effort level, suggesting higher reliance on the lower sternocostal regions in the performance of these tasks at high arm elevations. Lastly, regional activation in flexion, horizontal

adduction, and extension was not influenced by effort level. In both flexion and horizontal adduction, all three regions activated similarly, in contrast to previous suggestions of sole clavicular region involvement in these tasks (Paton and Brown, 1994; Stegink-Jansen et al. 2011). In contrast, extension at moderate efforts requires localized activation generated in the lower sternocostal regions, complementing previous mechanical studies (Wolfe et al. 1992). These findings collectively indicate that compromise to lower sternocostal regions may elicit deficits across the tasks investigated in this dissertation. Indeed, inability to perform or strength reductions across these tasks were reported in male athletes with sternocostal injuries (Pavlik et al. 1998; Schepsis et al. 2000; Hanna et al. 2001; Provencher et al. 2010; de Castro Pochini et al. 2013; Marsh et al., 2020).

10.3. Pectoralis major relies on motor unit recruitment for mechanical force generation

Neural decoding of pectoralis major activity revealed highly sophisticated neural control summarized in three key findings. First, pectoralis major motor units discharge at relatively high rates at low effort levels (i.e., 15% MVE). Second, in males, the pectoralis major does not increase motor unit discharge rate with increases in effort level, unlike most muscles, but instead relies heavily on additional motor unit recruitment. While similar neural control occurs in large muscles, like deltoid, trapezius, and biceps brachii (De Luca, 1985; De Luca et al., 1982; Westgaard and De Luca, 2001; Kukulka and Clamann, 1981), none of these muscles rely on motor unit recruitment at such low effort levels. Pectoralis major is a large, powerful muscle with primary roles in maintaining arm posture and gross motor function. Therefore, it is plausible that rate coding is not a predominant factor in increasing mechanical force in this muscle, as the tasks in which pectoralis major assists do not require fine force modulation. Lastly, motor units decomposed were predominantly located in the superior pectoralis major, close to the sternum and near the

sternoclavicular joint, showing first physiological evidence that the clavicular region may be involved in the stabilization of the sternoclavicular joint. These findings reveal aspects of fundamental pectoralis major control and provide a basis for interpreting healthy aging or clinical case scenarios. Since pectoralis major relies heavily on motor unit recruitment, losses in the number of motor units, by either damage or aging, may reduce mechanical force affecting strategies for tasks that involve the glenohumeral, sternoclavicular, and indirectly, scapulothoracic joints.

10.4. Pectoralis major HD-sEMG signal decomposition: Challenges and limitations

This dissertation presents the first account of HD-sEMG signal decomposition in pectoralis major in males and females. Although signals were decomposed, some specific methodological challenges and limitations should be considered and addressed in the future. Firstly, although decomposition using the blind convolutive separation method was performed across all tasks, effort levels, and in both cohorts, it was not always successful. Specifically, HD-sEMG signals could only be decomposed in 11 out of 19 males in Study 5; 8 out of 10 males in Study 6; 5 out of 20 females in Study 3, and 0 out of 9 females in Study 4. Additionally, the decomposition of signals was not always possible for the inferior array in males. The decomposition's success also depended on the task and effort level, with most motor units successfully decomposed in adduction 60, adduction 90, internal rotation 60, flexion, and horizontal adduction at low effort levels (15-25% MVE). Decomposition of signals at 50% and 75% MVE proved challenging, except in 50% MVE in horizontal adduction, which yielded some motor units, albeit in a limited number of participants (N = 4).

Challenges in the decomposition of HD-sEMG signals exist for other muscles in males (see Del Vecchio et al. 2020), with studies exploring motor unit physiology in females reporting much

lower yields than those in males (Del Vecchio et al. 2020). The reasons behind these limitations are currently unknown. However, they could be due to multiple factors such as subcutaneous tissue thickness (particularly in females), muscle architectural properties, alignment of muscle fibers underneath the array, and potential contamination of EMG recordings (i.e., inability for decomposition algorithm to isolate spike trains due to additional motor unit recruitment) at high effort levels (Farina et al. 2002; Del Vecchio et al. 2020; Holobar et al. 2014). Therefore, it is essential to build on the current findings and investigate whether different tasks, ramps (trapezoidal or triangular), HD-sEMG array position, and alignment with muscle fibers may improve decomposition outcomes at low effort levels in males and females before improvements in the decomposition algorithm are achieved.

10.5. Limitations

Muscle activation and neural properties may be influenced by age, exercise status, or compromise. This dissertation's findings only pertain to healthy young (between 18 to 40 years), recreationally active males and females. It is currently unknown how aging, exercise status, or compromise affect the pectoralis major activation and neural properties. Additionally, data was acquired only from the dominant (right) limb, and it is unknown if handedness may influence the current findings. Further, in females, the bra type may have influenced breast tissue distribution overlying the muscle. All females wore a regular bra (i.e., no sports bra) to mitigate these effects. However, the exact type of bra, band width, or cup was not controlled and may have influenced some of the MNF and EMG amplitude measures in Chapter 4.

The EMG technique is typically influenced by muscle crosstalk, skin-electrode movement, and in the instance of the pectoralis major muscle, ECG artifact. Crosstalk from the pectoralis minor, serratus anterior, intercostal muscles, and external oblique may have influenced some of

the EMG amplitudes reported in this dissertation. However, crosstalk effects were mitigated by using closely spaced electrodes (HD-sEMG array; IED: 10 mm). The effect of the skin-electrode movement was mitigated by evaluating the pectoralis major activation in isometric efforts and only comparing EMG amplitudes within a task and not between tasks. Lastly, pectoralis major EMG signals are typically contaminated by ECG artifact as the muscle is close to the heart. This aspect was considered in the experimental protocol development by referencing the HD-sEMG to the same side of the body (i.e., right side) and collecting ECG in synchrony with HD-sEMG to be removed in post-processing steps.

The thickness of the breast tissue was examined using anthropometric measurements. The type of the ultrasound device available in the department (i.e., clinical as opposed to the research ultrasound) posed difficulties in obtaining high-quality ultrasound images from all breast locations to examine variations in the thickness. Further, the pairing of the ultrasound device with the motion tracking system was not possible due to the lack of a trigger system (i.e., pedal on the ultrasound). Future studies interested in examining the effect of breast tissue thickness on HD-sEMG amplitudes and MNF should consider pairing the two devices to quantify objective measures of breast tissue thickness. Further, the quantification of breast tissue composition using an ultrasound device may also provide invaluable information for further examining the pectoralis major activation in females. Additionally, the effect of age on skin thickness, breast tissue thickness, and breast tissue composition should also be quantified before evaluating pectoralis major activation in older females, as these may influence the HD-sEMG signal quality.

In both cohorts, limitations existed in characterizing either lower sternocostal/abdominal regions (i.e., females) or ½ of the abdominal region (i.e., males). In females, pectoralis major activation was not characterized in the lower sternocostal/abdominal regions due to the current

limitations in HD-sEMG technology. Indwelling EMG was considered, but not used as the needle EMG effects on the breast tissue are presently unknown. Additionally, different needle lengths would have to be designed and individualized depending on the thickness of each participant's breast tissue, which was out of this dissertation's scope. In males, HD-sEMG signals could not be acquired from ~½ of the abdominal region. Attempts were made during piloting to acquire EMG signals from these regions using a third 32-channel HD-sEMG array. However, challenges existed as the HD-sEMG arrays were not designed to accommodate the shape of the chest, resulting in a significant loss in skin-electrode contact during HD-sEMG acquisition. Therefore, future studies should consider using smaller HD-sEMG electrodes, indwelling EMG, or classic EMG to capture the rest of the abdominal region activity.

In males, the inferior HD-sEMG array was not aligned with the lower sternocostal/abdominal region muscle fibers due to the limitations in the technology and time restrictions. Due to the ultrasound device limitations discussed earlier, challenges in quantifying these regions' pennation angle arose during piloting. The quantification of the exact fiber bundle pennation angle was difficult and inaccurate based on the inability to pair ultrasound with the Vicon motion-tracking device consistently. Future studies should consider pairing the ultrasound and motion tracking system to quantify each participant's sternocostal and abdominal region muscle fiber pennation angle and use this data to align the HD-sEMG with muscle fiber pennations. Alternatively, paired HD-sEMG-ultrasound electrodes, as described by Botter et al. (2019), may provide significant improvements in aligning the HD-sEMG arrays with the muscle fiber bundles.

10.6. Future outlook on understanding the intricacies of pectoralis major control

The precise contribution of pectoralis major to typical shoulder function has broad implications in fundamental, exercise, and clinical sciences. Specifically, in clinical sciences, the

pectoralis major's role and contribution to shoulder complex mobility and stability are mostly underestimated, leading to this muscle's frequent resection or disinsertion in various surgical procedures. Experiments in the current dissertation represent the first transformative step in understanding the pectoralis major's neuromusculoskeletal control. However, further work and knowledge are necessary to encourage a change in these protocols. On the fundamental level, a couple of questions arise. For example, does the pectoralis major modulate rate coding below 15% MVE or above 50% MVE? What is the role of neuromuscular partitions in the pectoralis major, and how do they contribute to mechanical force production within the shoulder complex? Does every partition rely on motor unit recruitment, or do motor units in some partitions rely on rate coding? How do motor units in the inferior pectoralis major regions modulate force? What is the effect of aging on pectoralis major control, and how does this influence shoulder complex stability and arm mobility? Additionally, improvements in technology and methodology are required for progress. For example, the pairing of ultrasonography or magnetic resonance imaging with high-density surface electromyography may clarify potential interactions between the neural and architectural properties. Further, improvements in the decomposition algorithms in the future should enable the successful decomposition of many motor units in males and, potentially, females, illuminating the intricate control of this fascinating and crucial muscle. Collectively, the methodological and fundamental breakthroughs in this dissertation lay the groundwork to, for the first time, unravel the intricate control of a powerful and understudied shoulder muscle and advance the development of methodological tools to further explore such large muscles in the future.

References

Abe, T., Kawakami, Y., Suzuki, Y., Gunji, A., Fukunaga, T.J. (1997). Effects of 20 days bed rest on muscle morphology. *Gravit Physiol.,* 4(1)*:* S10-4.

Ackland, D.C., Ponnaren, P., Richardson, M., Pandy, M.G. (2008). Moment arms of the muscles crossing the anatomical shoulder. *Journal of Anatomy*, 213: 383-390.

Ackland, D.C., Pandy, M.G. (2010). Lines of action and stabilizing potential of the shoulder musculature. *Journal of Orthopaedic Research*, 29(5): 658:67.

Akagi, R., Takai, Y., Kato, E., Wakahara, T., Ohta, M., Kanehisa, H., Fukunaga, T., Kawakami, Y. (2010). Development of an equation to predict muscle volume of elbow flexors for men and women with a wide range of age. *European Journal of Applied Physiology*, 108(4): 689-694.

Al Harrach, M., Carriou, V., Boudaoud, S., Laforet, J., Marin, F. (2017). Analysis of the sEMG/force relationship using HD-sEMG technique and data fusion: A simulation study. *Computers in Biology and Medicine*, 83: 34-37.

Alizadeh, S., Rayner, M., Mahmoud, M.M.I., Behm, D.G. (2020). Push-Ups vs. Bench Press Differences in Repetitions and Muscle Activation Between Sexes. *Journal of Sports Science and Medicine*, 19(2): 289-297.

Anders, C., Bretschneider, S., Bernsdorf, A., Erler, K., Schneider, W. (2004). Activation of shoulder muscles in healthy men and women under isometric conditions. *Journal of Electromyography and Kinesiology*, 14(6): 699-707.

Andreassen, S., Arendt-Nielsen, L. (1987). Muscle fibre conduction velocity in motor units of the human anterior tibial muscle: a new size principle parameter. *Journal of Physiology*, 391: 561-571.

Ashley, G.T. (1952). The manner of insertion of the pectoralis major muscle in man. *Anat Rec*, 113: 301-307.

Bak, K., Cameron, E.A., Henderson, I.J.P. (2000). Rupture of the pectoralis major: a meta-analysis of 112 cases. *Knee surgery, sports traumatology, arthroscopy*, 8(2): 113-9.

Banks, R.W. (2006). An allometric analysis of the number of muscle spindles in mammalian skeletal muscles. *Journal of Anatomy*, 208: 753-768.

Barbero M, Merletti R, Rainoldi A. Upper Limb. *Atlas of Muscle Innervation Zones. Understanding Surface Electromyography and Its Applications*. Springer-Verlag Mailand; 2012: 103-120.

Bassett, R.W., Browne, A.O., Morrey, B.F., An, K.N. (1990). Glenohumeral muscle force and moment mechanics in a position of shoulder instability. *Journal of Biomechanics*, 23: 405-15.

Blok, J.H., Stegeman, D.F., Van Oosterom, A. (2002). Three-Layer Volume Conductor Model and Software Package for Applications in Surface Electromyography. *Annals of Biomedical Engineering*, 30: 566-577.

Botter, A, Beltrandi, M., Cerone, G.L., Gazzoni, M., Vieira, T.M.M. (2019). Development and testing of acoustically-matched hydrogel-based electrodes for simultaneous EMG-ultrasound detection. *Medical Engineering & physics*, 64: 74-79.

Bouffard, J., Martinez, R., Plamondon, A., Cote, J.N., Begon, M. (2019). Sex differences in glenohumeral muscle activation and coactivation during a box lifting task. *Ergonomics*, 62(10): 1327-1338.

Boyd, N., Martin, L., Charez, S., Gunasekara, A., Salleh, A., Melnichouk, O. (2009). Breast-tissue Composition and Other Risk Factors for Breast Cancer in Young Women: A Cross-Sectional Study. *The Lancet Oncology*, 10(6): 569-580.

Bracchi, F., Decandia, M., Gualtierotti, T. (1966). Frequency stabilization in the motor centers of spinal cord and caudal brain stem. *Am J Physiol* 210: 1170–1177.

Brisson, J., Morrison, A.S., Kopans, D.B., Sadowsky, N.L., Kalisher, L., Twaddle, J.A., Meyer, J.E., Henschke, C.I., Cole, P. (1984). Height and weight, mammographic features of breast tissue, and breast cancer risk. *American Journal of Epidemiology*, 119(3): 371 – 381.

Brookham, R. L., & Dickerson, C. R. (2016). Comparison of humeral rotation co-activation of breast cancer population and healthy shoulders. Journal of Electromyography and Kinesiology, 29, 100–106.

Brookham, R.L., Cudlip, A.C., Dickerson, C.R. (2018). Quantification of upper limb electromyographic measures and dysfunction of breast cancer survivors during performance of functional dynamic tasks. *Clinical Biomechanics*, 52: 7-13.

Brookham, R.L., Cudlip, A.C., Dickerson, C.R. (2018). Examining upper limb kinematics and dysfunction of breast cancer survivors in functional dynamic tasks. *Clinical Biomechanics*, 55: 86-93.

Brown, J.M.M., Wickham, J.B., McAndrew, D.J., Huang, X.-F. (2007). Muscles within muscles: Coordination of 19 muscle segments within three shoulder muscles during isometric motor tasks. *Journal of Electromyography and Kinesiology*, 17: 57-73.

Brumback, R.J., McBride, M.S., Ortolani, N.C. (1992). Functional Evaluation of the Shoulder after Transfer of the Vascularized Latissimus Dorsi Muscle. *The Journal of Bone and Joint Surgery*, 74(3): 377-382.

Burke RE. *Motor units: anatomy, physiology, and functional organisation*. In Handbook of Physiology, section 3, The Nervous System, ed. Brookhart JM & Mountcastle VB; 1981: pp. 345-422. American Physiological Society, Bethesda, MD.

Butt, U., Mehta, S., Funk, L., Monga, P.(2015). Pectoralis major ruptures: a review of current management. *Journal of Shoulder and Elbow Surgery*, 24(4): 655-662.

Buxton, D.F., Peck, D. (1990). Density of Muscle Spindle Profiles in the Intrinsic Forelimb Muscles of the Dog. *Journal of Morphology*, 203: 345-359.

Carrasco, D.I., Lawrence, J. III., English, A.W. (1999). Neuromuscular Compartments of Cat Lateral Gastrocnemius Produce Difference Torques about the Ankle Joint. *Motor Control*, 3(4): 436-446.

Cemal, Y, Albornoz, C.R., Disa, J.J., McCarthy, C.M., Mehrara, B.J., Pusic, A.L., Cordeiro, P.G., Matros, E. (2013). A paradigm shift in US breast reconstruction: Part 2. The influence of changing mastectomy patterns on reconstructive rate and method. *Plastic Reconst Surg*, 131(3): 320e-326e.

Cescon, C., Rebecchi, P., Merletti, R. (2008). Effect of electrode array position and subcutaneous tissue thickness on conduction velocity estimation in upper trapezius muscle. *Journal of Electromyography and Kinesiology*, 18(4): 628-636.

Chopp-Hurley, J.N., Brookham, R.L., Dickerson, C.R. (2016). Identification of potential compensatory strategies in a breast cancer population: A combined computational and experimental approach. *Clinical Biomechanics*, 40: 63-67.

Cid, M.M., Oliveira, A.B., Januario, L.B., Cote, J.N., de Fatima, R., Moreira, C., Madeleine, P. (2019). Are there sex differences in muscle coordination of the upper girdle during a sustained motor task? *Journal of Electromyography and Kinesiology*, 45: 1-10.

Clark, J., Plonsey, R. (1966). A mathematical evaluation of the core conductor model. *Biophysical journal*, 6(1): 95-112.

Clough, K.B., Kaufman, G.J., Nos, C., Buccimazza, I., Sarfati, I.M. (2010). Improving Breast Cancer Surgery: A Classification and Quadrant per Quadrant Atlas for Oncoplastic Surgery. *Annals of Surgical Oncology*, 17(5): 1375-1391.

Cogliati, M., Cudicio, A., Martinez-Valdes, E., Tarperi, C., Schena, F., Orizio, C., Negro, F. (2020). Half marathon induces changes in central control and peripheral properties of individual motor units in master athletes. *Journal of Electromyography and Kinesiology*, 102472.

Cohen, J. *Statistical power analysis for the behavioural sciences*. New York: Academic Press; 1969.

Coltman, C.E., Steele, J.R., McGhee, D.E. (2018). Effects of age and body mass index on breast characteristics: a cluster analysis. *Journal of Ergonomics*, 61(9): 1232-1245.

Cordasco, F.A., Mahony, G.T., Tsouris, N., Degen, R.M. (2017). Pectoralis Major Tendon Tears: Functional Outcomes and Return to Sport in a Consecutive Series of 40 Athletes. *Journal of Shoulder and Elbow Surgery*, 26(3): 458-463.

Cram, J.R., Kasman, G.S. *The basics of surface electromyography*. Gaithersburg, MD: Aspen; 1998.

David, S., Balaguer, T., Baque, P., de Peretti, F., Valla, M., Lebreton, E., Chignon-Sicard, B. (2012). The anatomy of the pectoral nerves and its significance in breast augmentation, axillary dissection and pectoral muscle flaps. *Journal of Plastic, Reconstructive & Aesthetic Surgery,* 65(9): 1193-1198.

De Castro Pochini, A., Andreoli, C.V., Belangero, P.S., Figueiredo, E.A., Terra, B.B., Cohen, C., Andrade, M.S., Cohen, M., Ejnisman, B. (2013). Clinical Considerations for the Surgical Treatment of Pectoralis Major Muscle Ruptures Based on 60 Cases: A Prospective Study and Literature Review. *The American Journal of Sports Medicine*, 42(1): 95-102.

de Haan, A., Toor, A., Hage, J.J., Veeger, H.E.J., Woerdeman, L.A.E. (2007). Function of the Pectoralis Major Muscle After Combined Skin-Sparing Mastectomy and Immediate Reconstruction by Subpectoral Implantation of a Prosthesis. *Annals of Plastic Surgery,* 59(6): 605-610.

De Luca, C.J. (1979). Physiology and Mathematics of Myoelectric Signals. *IEEE Transactions on Biomedical Engineering*, BME-26(6): 313-325.

De Luca, C.J., LeFever, R.S., McCue, M.P., Xenakis, A.P. (1982). Behaviour of human motor units in different muscles during linearly varying contractions. *J Physiol* 329: 113–128.

De Luca, C.J. (1985). Control Properties of Motor Units. *Journal of Experimental Biology*, 115: 125-136.

De Luca, C.J., Contessa, P. (2012). Hierarchical control of motor units in voluntary contractions. *J Neurophysiol* 107: 178–195.

Del Vecchio, A., Negro, F., Felici, F., Farina, D. (2017). Associations between motor unit action potential parameters and surface EMG features. *Journal of Applied Physiology*, 123: 835-843.

Del Vecchio, A., Holobar, A., Falla, D., Felici, F., Enoka, R.M., Farina, D. (2020). Tutorial: Analysis of motor unit discharge characteristics from high-density surface EMG signals. *Journal of Electromyography and Kinesiology,* 53: 102426.

Dicus, J.R., Holmstrup, M.E., Shuler, K.T., Rice, T.T., Raybuck, S.D., Siddons, C.A. (2018). Stability of Resistance Training Implement Alters EMG Activity During the Overhead Press. *International Journal of Exercise Science*, 11(1): 708-716.

Dickerson, C.R., Chaffin, D.B., Hughes, R.E. (2007). A mathematical musculoskeletal shoulder model for proactive ergonomics analysis. *Computer Methods in Biomechanics and Biomedical Engineering*, 10(6): 389-400.

Diefenbach, B.J., Lipps, D.B. (2019). Postural Differences in Shoulder Dynamics During Pushing and Pulling. *Journal of Biomechanics*, 85: 67-73.

Drake, J.D.M., Callaghan, J.P. (2006). Elimination of electrocardiogram contamination from electromyographic signals: An evaluation of currently used removal techniques. *Journal of Electromyography and Kinesiology*, 16: 175-187.

Duchateau, J., Semmler, J.G., Enoka, R.M. (2006). Training adaptations in the behavior of human motor units. *J Appl Physiol, 101(6):* 1766-1775.

Ebaugh, D., Spinelli, B., Schmitz, K.H. (2011). Shoulder impairments and their association with symptomatic rotator cuff disease in breast cancer survivors. *Medical Hypotheses, 77(4):* 481-487.

Ekholm, J., Arborelius, U., Hillered, L., & Ortqvist, A. (1978). Shoulder muscle EMG and resisting moment during diagonal exercise movements resisted by weight-and-pulleycircuit. *Scandinavian Journal of Rehabilitation Medicine*, 10(4), 179–185.

Ekstedt, J., Stalberg, E. (1973). How the size of the needle electrode leading-off surface influences the shape of the single muscle fibre action potential in electromyography. *Computer Programs in Biomedicine*, 3(4): 204-212.

ElMaraghy, A.W., Devereaux, M.W. (2012). A systematic review and comprehensive classification of pectoralis major tears. *Journal of Shoulder and Elbow Surgery*, 21(3): 412-422.

English, A.W., Wolf, S.L., Segal, R.L. (1993). Compartmentalization of Muscles and Their Motor Nuclei: The Partitioning Hypothesis. *Physical Therapy*, 73(12): 857-867.

Enoka, R.M., Duchateau, J. (2017). Rate Coding and the Control of Muscle Force. *Cold Spring Harbor Perspectives in Medicine*, 7(10): a029702.

Enoka, R.M., Duchateau, J. (2015). Inappropriate interpretation of surface EMG signals and muscle fiber characteristics impedes understanding of the control of neuromuscular function. *J Appl Physiol,* 119: 1516-1518.

Enoka, R.M., Fuglevand, A.J. (2001). Motor unit physiology: some unresolved issues. *Muscle & Nerve*,24(1): 4-17.

Erim, Z., De Luca, C.J., Mineo, K., Aoki, T. (1996). Rank-ordered Regulation of Motor Units. *Muscle Nerve*, 19(5): 563-73.

Fabrizio, P.A., Clemente, F.R. (2014). Anatomical structure and nerve branching pattern of the human infraspinatus muscle. *J. Bodywork Movement Therapies,*18: 228-232.

Farina, D., Rainoldi, A. (1999). Compensation of the effect of sub-cutaneous tissue layers on surface EMG: a simulation study. *Medical engineering & physics*, 21(6-7): 487-497.

Farina, D., Cescon, C., Merletti, R. (2002b). Influence of anatomical, physical, and detection-system parameters on surface EMG. *Biol Cybern*, 86(6): 445-456.

Farina, D., Merletti, R., Enoka, R.M. (2004). The extraction of neural strategies from the surface EMG. *Journal of Applied Physiology*, 96(4): 1486-1495.

Farina, D., Mesin, L., Martina, S., Merletti, R. (2004). A surface EMG generation model with multilayer cylindrical description of the volume conductor. *IEEE Transactions on Biomedical Engineering, 51(3):* 415-426.

Farina, D., Leclerc, F., Arendt-Nielsen, L., Buttelli, O., Pascal, M. (2008). The change in spatial distribution in upper trapezius muscle activity is correlated to contraction duration. *Journal of Electromyography and Kinesiology*, 18:16-25.

Farina, D. (2008). Last Word on Point: Counterpoint: Spectral properties of the surface EMG can characterize/do not provide information about motor unit recruitment and muscle fiber type. *Journal of Applied Physiology*, 105(5): 1683.

Farina, D., Holobar, A. (2016). Characterization of Human Motor Units From Surface EMG Decomposition. *Proceedings of the IEEE,* 104(2): 353-373.

Farina, D., Negro, F., Muceli, S., Enoka, R.M (2016). Principles of motor unit physiology evolve with advances in technology. *Physiology*, 31(2): 83-94.

Forthomme, B., Heymans, O., Jacquemin, D., Klinkenberg, S., Hoffmann, S., Grandjean, F.X., Crielaard, J.M., Croisier, J.L. (2010). Shoulder function after latissimus dorsi transfer in breast reconstruction. *Clin Physiol Funct Imaging*, 30(6): 406-412.

Franchi, M.V., Raiteri, B.J., Longo, S., Sinha, S., Narici, M.V., Csapo, R. (2018). Muscle architecture assessment: Strengths, shortcomings and new frontiers of *in vivo* imaging techniques. *Ultrasound in Med. & Biol.*, 44(12): 2492-2504.

Fuglevand, A.J., Winter, D.A., Patla, A.E., Stashuk, D. (1992). Detection of motor unit action potentials with surface electrodes: influence of electrode size and spacing. *Biol. Cybern*. 67, 143-153.

Fuglevand, A.J., Lester, R.A., Johns, R.K. (2015). Distinguishing intrinsic from extrinsic factors underlying firing rate saturation in human motor units. *Journal of Neurophysiology*, 113(5): 1310-22.

Fukunaga, T., Ichinose, Y., Ito, M., Kawakami, Y., Fukashiro, S. (1997). Determination of fascicle length and pennation in a contracting human muscle in vivo. *J Appl Physiol*, 82:354 - 358.

Fung, L., Wong, B., Ravichandiran, K., Agur, A., Rindlisbacher, T., Elmaraghy, A. (2009). Three-Dimensional Study of Pectoralis Major Muscle and Tendon Architecture. *Clinical Anatomy*, 22: 500-508.

Gans, C., de Vree, F. (1987). Functional bases of fiber length and angulation in muscle. *Journal of Morphology,* 192: 63-85.

Gardetto, A., Thaler, C., Kiechl, S., Maurer, H., Piza-Katzer, H. (2003). Isolated compression of the pectoral nerve resulting in atrophy of the major pectoral muscle. *Muscle Nerve,* 28: 760-763.

Gath, I., Stalberg, E. (1977). On the volume conduction in human skeletal muscle: in situ measurements. *Electroencephalogr Clin Neurophysiol,* 43(1): 106-10.

Gavriilidis, I., Kircher, J., Magosch, P., Lichtenberg, S., Habermeyer, P. (2009). Pectoralis major transfer of irreparable anterosuperior rotator cuff tears. *International Orthopaedics*, 34: 689-694.
Gibson, T.M., Balendra, N., Ustinova, K., Langenderfer, J.E. (2019). Reductions in Kinematics from Brassieres with Varying Breast Support. *Internal Journal of Exercise Science*, 12(1): 402-411.

Glass, S., Armstrong, T. (1997). Electromyographical Activity of the Pectoralis Muscle During Incline and Decline Bench Press. *Journal of Strength and Conditioning Research*, 11(3): 163-167.

Gray's Anatomy. The anatomical basis of medicine and surgery. Sydney: Churchill Livingstone; 1990.

Graham, S.J., Stanchev, P.L., Lloyd-Smith, J.O.A., Bronskill, M.J., Plewes, D.B. Changes in Fibroglandular Volume and Water Content of Breast Tissue During the Menstrual Cycle Observed by MR Imaging at 1.5T. *Journal of Magnetic Resonance Imaging*, 5(6): 695-701.

Hage, J.J., van der Heeden, J.F., Lankhorst, K.M., Romviel, S.M., Vlutters, L.A., Visser, B.,

Veeger, H.E. (2014). Impact of combined skin sparing mastectomy and immediate subpectoral prosthetic reconstruction on the pectoralis major muscle function: a preoperative and postoperative comparative study. *Ann Plast Surg,* 72(6): 631-7.

Haladaj, R., Wysiadecki, G., Clarke, E., Polguj, M., Topol, M. (2019). Anatomical Variations of the Pectoralis Major Muscle: Notes on Their Impact on Pectoral Nerve Innervation Patterns and Discussion on Their Clinical Relevance. *Biomed Research International 2019*; doi: 10.1155/2019/6212039.

Hanna, C.M., Glenny, A.B., Stanley, S.N., Caughey, M.A. (2001). Pectoralis major tears: comparison of surgical and conservative treatment. *British Journal of Sports Medicine*, 35: 202-206.

Hassan, A., Thompson, C.K., Negro, F., Cummings, M., Powers, R.K., Heckman, C.J., Dewald, J.P.A., McPherson, L.M. (2020). Impact of parameter selection on estimates of motoneuron excitability using paired motor unit analysis. *Journal of Neural Engineering*.

Hayes, S.C., Johannson, K., Alfano, C.M., Schmitz, K. (2011). Exercise for breast cancer survivors: bridging the gap between evidence and practice. *Transl Behav Med*, 1: 539-544.

Heckman, C.J., Enoka, R.M. (2012). Motor unit. *Comprehensive physiology*,2(4).

Heckman, C.J., Johnson, M., Mottram, C., Schuster, J. (2008). Persistent inward currents in spinal motoneurons and their influence on human motoneuron firing patterns. *Neuroscientist*, 14: 264-275.

Hemingway, M.A., Biedermann, H.-J., Inglis, J. (1995). Electromyographic Recordings of Paraspinal Muscles: Variations Related to Subcutaneous Tissue Thickness. *Biofeedback and Self-Regulation*, 20(1): 39-49.

Henneman, E., Somjen, G., and Carpenter, D. O. (1965). Functional significance of cell size in spinal motoneurons. *J. Neurophysiol.* 28: 560–580.

Henneman E & Mendell LM. (1981). Functional organisation of motoneuron pool and its inputs. In Handbook of Physiology, section 1, The Nervous System, ed. Brookhart JM & Mountcastle VB, pp. 423-508. American Physiological Society, Bethesda, MD.

Herbert, R.D., Gandevia, S.C. (1995). Changes in pennation with joint angle and muscle torque: In vivo measurements in human brachialis muscle. *Journal of Physiology*, 484: 523-532.

Hermens H.J., Freriks, B., Merletti, R., et al. Recommendations for surface electromyography SENIAM 8: Roessingh Research and Development. Enschede. 1999.

Ho, A.J., Cudlip, A.C., Ribeiro, D.C., Dickerson, C.R. (2019). Examining Upper Extremity Muscle Demand During Selected Push-Up Variants. *Journal of Electromyography and Kinesiology*, 44: 165-172.

Hodges, P.W. Pengel, L.H., Herbert, R.D., Gandevia, S.C. (2003). Measurement of muscle contraction with ultrasound imaging. *Muscle Nerve*, 27: 682-92.

Hoffman, G.W., Elliott, L.F. (1987). The anatomy of pectoral nerves and its significance to the general and plastic surgeon. *Annals of surgery*, 205: 504:507.

Hogfors, C., Sigholm, G., Herberts, P. (1987). Biomechanical model of the human shoulder – I. Elements. *Journal of Biomechanics*, 20(2): 157-166.

Holobar, A., Zazula, D. (2007). Multichannel blind source separation using convolution Kernel compensation. *IEEE Trans Signal Process, 55:* 4487-4496.

Holobar, A., Farina, D., Gazzonni, M., Merletti, R., Zazula, D. (2009). Estimating motor unit discharge patterns from high-density surface electromyogram. *Clinical Neurophysiology*, 120(3): 551-562.

Holobar, A., Minetto, M.A., Farina, D. (2014). Accurate identification of motor unit discharge patterns from high-density surface EMG and validation with a novel signal-based performance metric. *Journal of Neural Engineering*, 11: 016008.

Holtermann, A., Roeleveld, K., Karlsson, J.S. (2005). Inhomogeneities in muscle activation reveal motor unit recruitment. *J Electromyogr Kinesiol*, 15:131–7.

Holtermann, A., Roeleveld, K. (2006). Global muscle activation in sustained contractions. *Acta Physiol (Oxf)*, 186:159–68.

Holtermann, A., Karlsson, J.S., Roeleveld, K. (2008). Spatial distribution of active muscle fibre characteristics in the upper trapezius muscle and its dependency on contraction level and duration. *Journal of Electromyography and Kinesiology*, 18(1): 16-25.

Holzbaur, K.R., Murray, W.M., Gold, G.E., Delp, S.L. (2007). Upper limb muscle volumes in adult subjects. *Journal of Biomechanics,* 40: 742-749.

Huijing, P. A. (1992) Elastic potential of muscle. *In Strength and Power in Sport* (Edited by Komi. P. V.). pp. 151-168. Blackwell Scientific Publications. Oxford.

Hultborn, H., Katz, R., Mackel, R. (1988). Distribution of recurrent inhibition within a motor nucleus. II. Amount of recurrent inhibition in motoneurones to fast and slow units. *Acta Physiol Scand,* 134: 363-374.

Hyngstrom, A.S., Murphy, S.A., Nguyen, J., Schmit, B.D., Negro, F., Gutterman, D.D., Durand, M.J. (2018). Ischemic conditioning increases strength and volitional activation of paretic muscle in chronic stroke: a pilot study. *Journal of Applied Physiology,* 124(5): 1140-1147.

Iceton, J., Harris, W.E. (1987). Results of pectoralis major transfer for winged scapula. *Journal of Bone and Joint Surgery British Volume*, 69(1): 108-10.

Infantolino, B.W., Challis, J.H. (2014). Short communication: Pennation angle variability in human muscle. *J Appl Biomech*, 30:663–7.

Ikegawa, S., Funato, K., Tsunoda, N., Kanehisa, H., Fukunaga, T., Kawakami, Y. (2008). Muscle Force per Cross-sectional Area is Inversely Related with Pennation Angle in Strength Trained Athletes. *J Strength Cond Res*, 22:128–31.

Jagsi, R., Momoh, A.O., Qi, J., Hamill, J.B., Billig, J., Kim, H.M., Pusic, A.L. Wilkins, E.G. (2018). Impact of radiotherapy on complications and patient-reported outcomes after breast reconstruction. *J Nat cancer Inst,* 110(2): 157-165.

Jansen, C.W., Buford, W.L., Patterson, R.M., Gould, L.J. (2005). A model of length increases in pectoralis major muscle to provide rehabilitation precautions for patients after mastectomy. *Conf Proc IEEE Eng Med Biol Soc*, 7: 7692-7694.

Jastifer, J., Gustafson, P., Patel, B., Uggen, C. (2012). Pectoralis major transfer for subscapularis deficiency: a computational study. *Shoulder & Elbow*, 4: 25-29.

Jensen, C., Westgaard, R.H.(1995). Functional subdivision of the upper trapezius muscle during maximal isometric contraction. *J Electromyogr Kinesiol,* 5: 227:237.

Jensen, C., Westgaard, R.H. (1997). Functional subdivision of the upper trapezius muscle during low-level activation. *Eur J Appl Physiol,* 76: 335-339.

Johnson, M.A., Polgar, J., Weightman, D., Appleton, D. (1973). Data on the Distribution of Fibre Types in Thirty-Six Human Muscles An Autopsy Study. *Journal of the neurological Sciences,* 18: 111-129.

Kany, J. (2020). Tendon Transfer for Anterosuperior Cuff: The Pectoralis Major Transfer. *Massive and Irreparable Rotator Cuff Tears*: 237-243.

Kapelner, T., Jiang, N., Holobar, A., Vujaklija, I., Roche, A.D., Farina, D., Aszmann, O.C. (2016). Motor Unit Characteristics after Targeted Muscle Reinnervation. *PLoS ONE*, 11(2): e0149772.

Kapelner, T., Vujaklija, I., Jiang, N., Negro, F., Aszmann, O.C., Principe, J., Farina, D. (2019). Predicting wrist kinematics from motor unit discharge timings for the control of active prostheses. *Journal of NeuroEngineering and Rehabilitation*, 16: 47.

Katz, R., Mazzocchio, R., Penicaud, A., Rossi, A. (1993). Distribution of recurrent inhibition in the human upper limb. *Acta Physiol Scand*, 149: 183-189.

Keenan, K.G., Farina, D., Maluf, K.S., Merletti, R., Enoka, R.M. (2005). Influence of amplitude cancellation on the simulated surface electromyogram. *Journal of Applied Physiology*, 98(1): 120-131.

Kim, S.Y., Boynton, E.L., Ravichandiran, K., Fung, L.Y., Bleakney, R., Agur, A.M. (2007). Three-dimensional study of the musculotendinous architecture of supraspinatus and its functional correlations. *Clin Anat*, 20: 648-655.

Kuechle, D.K., Newman, S.R., Itoi, E., Morrey, B.F., An, K.N. (1997). Shoulder muscle moment arms during horizontal flexion and elevation. *Journal of Shoulder and Elbow Surgery*, 6(5): 429-39.

Kuiken, T.A., Lowery, M.M., Stoykov, N.S. (2003). The effect of subcutaneous fat on myoelectric signal amplitude and cross-talk. *Prosthetics and Orthotics International*, 27(1): 48-54.

Kukulka, C.G., Clamann, H.P. (1981). Comparison of the recruitment and discharge properties of motor units in human brachial biceps and adductor pollicis during isometric contractions. *Brain Research*, 219: 45-55.

Langenderfer, J., Jerabek, S.A., Thangamani, V.B., Kuhn, J.E., Hughes, R.E. (2004). Musculoskeletal parameters of muscles crossing the shoulder and elbow and the effect of sarcomere length sample size on estimation of optimal muscle length. *Clinical Biomechanics*, 19: 664-670.

Lapatki, B.G., Oostenveld, R., Van Dijk, J.P., Jonas, I.E., Zwarts, M.J., Stegeman, D.F. (2006). Topographical Characteristics of Motor Units of the Lower Facial Musculature Revealed by Means of High-Density Surface EMG. *Journal of Neurophysiology*, 95(1): 342-54.

Lauver, J.D., Cayot, T.E., Scheuermann, B.W. (2016). Influence of Bench Angle on Upper Extremity Muscular Activation During Bench Press Exercise. *European Journal of Sport Science*, 16(3): 309-16.

Lee, J., Brookenthal, K.R., Ramsey, M.L., Kneeland, J.B., Herzog, R. (2000). MR imaging assessment of the pectoralis major myotendinous unit: An MR imaging-anatomic correlative study with surgical correlation. *AJR Am J Roentgenol*, 174:1371–1375.

Leonardis, J.M., Desmet, D.M., Lipps, D.B. (2017). Quantifying differences in the material properties of the fiber regions of the pectoralis major using ultrasound shear wave elastography. *Journal of Biomechanics,* 63: 41-46.

Leonardis, J.M., Diefenbach, B.J., Lyons, D.A., Olinger, T.A., Giladi, A.M., Momoh, A.O., Lipps, D.B. (2018). The influence of reconstruction choice and inclusion of radiation therapy on functional shoulder biomechanics in women undergoing mastectomy for breast cancer. *Breast Cancer Res Treat.* doi: 10.1007/s10549-018-5003-8

Leonardis, J.M., Lyons, D.A., Giladi, A.M., Momoh, A.O., Lipps, D.B. (2019). Functional Integrity of the Shoulder Joint and Pectoralis Major Following Subpectoral Implant Breast Reconstruction. *Journal of Orthopaedic Research*, 37(7): 1610:1619.

Leonardis, J.M., Alkayyali, A.A., Lipps, D.B. (2020). Posture-dependent Neuromuscular Contributions to Three-Dimensional Isometric Shoulder Torque Generation. *Journal of Neurophysiology*, 123(4): 1526-1535.

Lewis, W.H. (1901). Observations on the pectoralis major muscle in man. *Bull Johns Hopkins Hosp,* 12: 172-177.

Lieber, R.L. (1992). Skeletal muscle structure and function: implications for physical therapy and sports medicine. Baltimore: Williams & Wilkins; 303 pp.

Lieber, R.L, Friden, J. (2000). Functional and clinical significance of skeletal muscle architecture. *Muscle Nerve, 23*:1647–66.

Lindstrom, L.H., Magnusson, R.I. (1977). Interpretation of myoelectric power spectra: A model and its applications. *Proceedings of the IEEE, 65(5):* 653-662.

Lipps, D.B., Leonardis, J.M., Dess, R.T., McGinnis, G.J., Marsh, R.B., Strauss, J.B., Hayman, J.A., Pierce, L.J., Jagsi, R. (2019). Mechanical properties of the shoulder and pectoralis major in breast cancer patients undergoing breast-conserving surgery with axillary surgery and radiotherapy. *Scientific Reports*, 9(1): 17737.

Liu, R., Gullane, R., Brown, D., Irish, J. (2001). Pectoralis major myocutaneous pedicled flap in head and neck reconstruction: retrospective review of indications and results in 244 consecutive cases at the Toronto General Hospital. *J Otolaryngol,* 30*:* 34-40.

Lowery, M.M., Stoykov, N.S., Taflove, A., Kuiken, T.A. (2002). A Multiple-Layer Finite-Element Model of the Surface EMG Signal. *IEEE Transactions on Biomedical Engineering*, 49(5): 446-454.

Macchi, V., Tiengo, C., Porzionato, A., Parenti, A., Stecco, C., Mazzoleni, F., De Caro, R. (2007). Medial and lateral pectoral nerves: course and branches. *Clin Anat,* 20: 157-162.

Maciukiewicz, J.M., Lulic, T., MacKay, K.L., Meszaros, K.A., Dickerson, C.R. (2019). The influence of posture variation on electromyographic signals in females obtained during maximum voluntary isometric contractions: A shoulder example. *Journal of Electromyography and Kinesiology*, 102319. doi: 10.1016/j.jelekin.2019.05.020

MacLean, K.F.E., Dickerson, C.R. (2019). Kinematic and EMG analysis of horizontal bimanual climbing in humans. *Journal of Biomechanics*, 92: 11-18.

Maganaris, C.N., Baltzopoulos, V., Sargeant, A.J. (2002). Repeated contractions alter the geometry of human skeletal muscle. *Journal of Applied Physiology,* 93(6): 2089-2094.

Mancebo, F., Cabral, H.V., de Souza, L.M.L., de Oliveira, L.F., Vieira, T.M.(2019). Innervation zone locations distribute medially within the pectoralis major muscle during bench press exercise. *Journal of Electromyography and Kinesiology*, 46: 8-13.

Mancebo, F.D., Cabral, H.V., De Souza, L.M.L., Oliveira, L.F. (2019). Is the EMGs Amplitude Distribution Spatially Localizes in the Pectoralis Major Muscle During the Inclined Bench Press? XXVI Brazilian Congress on Biomedical Engineering, 70(2): 299-303.

Mangine, G.T., Hoffman, J.R., Gonzalez, A.M., Townsend, J.R., Wells, A.J., Jajtner, A.R., Beter, K.S., Boone, C.H., Miramonti, A.A., Wang, R., LaMonica, M.B., Fukuda, D.H., Ratamess, N.A., Stout, J.R. (2015). The effect of training volume and intensity on improvements in muscular strength and size in resistance-trained men. *Physiological Reports,* 3(8): e12472.

Mangine, G.T., Gonzalez, A.M., Townsend, J.R., Wells, A.J., Beyer, K.S., Miramonti, A.A., Ratamess, N.A., Stout, J.R., Hoffman, J.R. (2018). Influence of Baseline Muscle Strength and Size Measures on Training Adaptations in Resistance-trained Men. *Int J Exerc Sci*, 11(4): 198-213.

Manktelow, R., McKee, N.H., Vettese, T. (1980). An Anatomical Study of the Pectoralis Major Muscle as Related to Functioning Free Muscle Transplantation. *Plastic and Reconstructive Surgery*, 65(5): 610-5.

Marsh, N.A., Calcei, J.G., Antosh, I.J., Cordasco, F.A. (2020). Isolated tears of the sternocostal head of the pectoralis major muscle: surgical technique, clinical outcomes, and a modification of the Tietjen and Bak classification. *Journal of Shoulder and Elbow Surgery*. doi: 10.1016/j.jse.2019.11.024

Martinez-Valdes, E., Negro, F., Laine, C.M., Falla, D., Mayer, F., Farina, D. (2017). Tracking motor units longitudinally across experimental sessions with high-density electromyography. *The Journal of Physiology*, 595(5): 1479-1496.

Martinez-Valdes, E., Farina, D., Negro, F., Del Vecchio, A., Falla, D. (2018). Early Motor Unit Conduction Velocity Changes to High-Intensity Interval Training versus Continuous Training. *Medicine & Science in Sports & Exercise*, 50(11): 2339-2350.

Martinez-Valdes, E., Negro, F., Falla, D., De Nunzio, A.M., Farina, D. (2018). Surface electromyographic amplitude does not identify differences in neural drive to synergistic muscles. *Journal of Applied Physiology*, 124(4): 1071-1079.

Martinez-Valdes, E., Negro, F., Falla, D., Dideriksen, J.L., Heckman, C.J., Farina, D. (2020). Inability to increase the neural drive to muscle is associated with task failure during submaximal contractions. *Journal of Neurophysiology.*

Masuda, K., Kikuhara, N., Takahashi, H., Yamanaka, K. (2003). The relationship between muscle cross-sectional area and strength in various isokinetic movements among soccer players. *J Sports Sci*, 21:851–8.

McDonald, A., Picco, B.R., Belbeck, A.L., Chow, A.Y., Dickerson, C.R. (2012). Spatial dependency of shoulder muscle demands in horizontal pushing and pulling. *Applied Ergonomics*, 43(6): 971-8.

McDonald, A.C., Brenneman, E.C., Cudlip, A.C., Dickerson, C.R. (2014). The Spatial Dependency of Shoulder Muscle Demands for Seated Lateral Hand Force Exertions. *Journal of Applied Biomechanics*, 30(1): 1-11.

Merletti, R., Holobar, A., Farina, D. (2008). Analysis of motor units with high-density surface electromyography. *Journal of Electromyography and Kinesiology*, 18: 879-890.

Merletti, R., Aventaggiato, M., Botter, A., Holobar, A., Marateb, H., Vieira, T.M.M. (2010). Advances in surface EMG: Recent progress in detection and processing techniques. *Crit Rec Biomed Eng*, 38(4): 305-345.

Minetto, M.A., Botter, A., Sprager, S., Agosti, F., Patrizi, A., Lanfranco, F., Sartorio, A. (2013). Feasibility study of detecting surface electromyograms in severely obese patients. *Journal of Electromyography and Kinesiology*, 23(2): 285-295.

Miyatani, M., Kanehisa, H., Kuno, S., Nishijima, T., Fukunaga, T. (2002). Validity of ultrasonography muscle thickness measurements for estimating muscle volume of knee extensors in humans. *Eur J Appl Physiol.*, 86(3):203-8.

Miyatani, M., Kanehisa, H., Ito, M., Kawakami, Y., Fukunaga, T. (2004). The accuracy of volume estimates using ultrasound muscle thickness measurements in different muscle groups. *European Journal of Applied Physiology*, 91(2-3): 264-272.

Mooers, B.R., Westermann, R.W., Wolf, B.R. (2015). Outcomes Following Suture-Anchor Repair of Pectoralis Major Tears: A Case Series and Review of Literature. *Iowa Orthop J*, 35: 8-12.

Mottram, C.J., Heckman, C.J., Powers, R.K., Rymer, W.Z., Suresh, N.L. (2014). Disturbances of motor unit rate modulation are prevalent in muscles of spastic paretic stroke survivors. *J Neurophysiol*, 111: 2017–2028.

Mottram, C.J., Suresh, N.L., Heckman, C.J., Gorassini, M.A., Rymer, W.Z. (2009). Origins of abnormal excitability in biceps brachii motoneurons of spastic paretic stroke survivors. *J Neurophysiol*, 102: 2026–2038.

Moukarbel, R.V., Fung, K., Franklin, J.H., Leung, A., Rastogi, R., Anderson, C.M., Yoo, J.H. (2010). Neck and Shoulder Disability Following Reconstruction With the Pectoralis Major Pedicled Flap. *The Laryngoscope*, 120: 1129-1134.

Murphy, S.A., Negro, F., Farina, D., Onushko, T., Durand, M., Hunter, S.K., Hunter, S.K., Schmit, B.D., Hyngstrom, A. (2018). Stroke increases ischemia-related decreases in motor unit discharge rates. *Journal of Neurophysiology*, 120(6): 3246-3256.

Muyor, J.M., Rodrígues-Ridao, D., Martín-Fuentes, I., Antequera-Vique, J.A. (2019). Evaluation and Comparison of Electromyographic Activity in Bench Press With Feed on the Ground and Active Hip Flexion. *PLoS One*, 14(6): e0218209.

Nadon, A.L., Vidt, M.E., Chow, A.Y., Dickerson, C.R. (2016). The spatial dependency of shoulder muscular demands during upward and downward exertions. *Ergonomics*, 59(10): 1294-1306.

Narici, M. (1999). Human skeletal muscle architecture studied in vivo by non-invasive imaging techniques: functional significance and applications. *Journal of Electromyography and Kinesiology*, *9*(2): 97-103.

Narici, M., Maganaris, C. (2006). Skeletal Muscle Plasticity in Health and Disease: From Genes to Whole Muscle: Muscle Architecture and Adaptations to Functional Requirements (Roberto Bottinelli and Carlo Reggiani, Ed.): pp. 265.

Negro, F., Muceli, S., Castronovo, A.M., Holobar, A., Farina, D. (2016). Multi-channel intramuscular and surface EMG decomposition by convolutive blind source separation. *Journal of Neural Engineering*, 13(2): 026027.

Nelson, J.A., Lee, I.T., Disa, J.J. (2018). The Functional Impact of Breast Reconstruction: An Overview and Update. *Plast Reconstr Surg Glob Open*, 6(3): e1640.

Nordaner, C., Willner, J., Hansson, G.-A., Larsson, B., Unge, J., Granquist, L., Skerfving, S. (2003). Influence of the subcutaneous fat layer, as measured by ultrasound, skinfold calipers and BMI, on the EMG amplitude. *Eur J Appl Physiol*, 89: 514-519.

Ogawa, M., Mitsukawa, N., Bemben, M.G., Abe, T.J. (2012). Ultrasound assessment of adductor muscle size using muscle thickness of the thigh. *Sport Rehabil.*, 21(3):244-8.

Osu, R., Franklin, D.W., Kato, H., Gomi, H., Domen, K., Yoshioka, T., Kawato, M. (2002). Short- And Long-Term Changes in Joint Co-Contraction Associated With Motor Learning as Revealed From Surface EMG. *Journal of Neurophysiology*, 88(2): 991-1004.

Page, K.A., Steele, J.R. (1999). Breast Motion and Sports Brassiere Design. Implications for Future Research. *Sports Medicine*, 27(4): 205-211.

Paterson, P., Prinsloo, D.J. (2004). The pectoralis major muscle flap – a first choice for shoulder disruption injuries. *Injury, Int. J. Care Injured*, 35: 536-539.

Paton, M.E., Brown, J.M.M. (1994). An Electromyographic Analysis of Functional Differentiation in Human Pectoralis Major Muscle. *Journal of Electromyography and Kinesiology*, 4(3): 161-169.

Pavlik, A., Csepai, D., Berkes, I. (1998). Surgical treatment of pectoralis major rupture in athletes. *Knee Surgery, Sports Traumatology, Arthroscopy*, 6:129-133.

Pereira, H.M., Schlinder-DeLap, B., Keenan, K.G., Negro, F., Farina, D., Hyngstrom, A.S., Nielson, K.A., Hunter, S.K. (2019). Oscillations in neural drive and age-related reductions in force steadiness with a cognitive challenge. *Journal of Applied Physiology*, 126(4): 1056-1065.

Petilon, J., Carr, D.R., Sekiya, J.K., Unger, D.V. (2005). Pectoralis Major Muscle Injuries: Evaluation and Management. *Journal of the American Academy of Orthopaedic Surgeons*, 13(1): 59-68.

Philipp, M., Schulz, E., Mitterer, M., Plachel, F., Resch, H., Lederer, S. (2017). Long-Term Outcome After Pectoralis Major Transfer for Irreparable Anterosuperior Rotator Cuff Tears. *The Journal of Bone & Joint Surgery*, 99(3): 239-245.

Plonsey, R. (1974). The active fiber in a volume conductor. *IEEE transactions on biomedical engineering*, 21(5): 371-381.

Porzionato, A., Macchi, V., Stecco, C., Loukas, M., Tubbs, R.S., De Caro, R. (2012). Surgical Anatomy of the Pectoral Nerves and the Pectoral Musculature. *Clinical Anatomy*, 25: 559-575.

Post, M. (1995). Pectoralis major transfer for winging of the scapula. *Journal of Shoulder and Elbow Surgery*, 4: 1-9.

Powell, P.L, Roy, R.R., Kanim, P., Bello, M.A., Edgerton, V.R. (1984). Predictibility of skeletal muscle tension from architectural determinations in guinea pig hindlimbs. *Journal of Applied Physiology*, 57: 1715-1721.

Provencher, M.T., Handfield, K., Boniquit, N.T., Reiff, S.N., Sekiya, J.K., Romeo, A.A. (2010). Injuries to the Pectoralis Major Muscle. Diagnosis and Management. *The American Journal of Sports Medicine*, 38(8): 1693-1705.

Quittmann, O.J., Meskemper, J., Albracht, K., Abel, T., Foitschik, T., Strüder, H.K. (2020). Normalising Surface EMG of Ten Upper-Extremity Muscles in Handcycling: Manual Resistance vs. Sport-Specific MVICs. *Journal of Electromyography and Kinesiology*, 51: 102402.

Rockwood Jr., C. A. (2009). The Shoulder - Volume 1. (C. A. Rockwood Jr., F. A. Matsen III, M. A. Wirth, S. B. Lippitt, E. V Fehringer, & J. W. Sperling, Eds.) (Fourth). Philadelphia: Saunders Elsevier.

Roeleveld, K., Blok, J.H., Stegeman, D.F., van Oosterom, A. (1997). Volume conduction models for surface EMG; confrontation with measurements. *Journal of Electromyography and Kinesiology*, 7(4): 221-232.

Rosenfalck, P. (1969). Intra-and extracellular potential fields of active nerve and muscle fibres. *Acta Phisiologica Scandinavica*, 321: 1-168.

Roy, R. R. and Edgerton, V. R. (1992). Skeletal muscle architecture and performance. In Strength and Power in Sport (Edited by Komi. P. V.). pp. 115 -129. Blackwell Scientific Publications, Oxford.

Sanchez, A., Ferreri, M.B., Frangiamore, S.J., Sanchez, G., Kruckeberg, B.M., Provencher, M.T. (2017). Pectoralis Major Repair With Unicortical Button Fixation And Suture Tape. *Arthroscopy Techniques, 6(3):* e729-e735.

Sartori, M., Lloyd, D.G., Farina, D. (2016). Neural Data-driven Musculoskeletal Modeling for Personalized Neurorehabilitation Technologies. *IEEE Trans Biomed Eng*, 63: 879-893.

Schepsis, A.A., Grafe, M.W., Jones, H.P., Lemos, M.J., 2000. Rupture of the Pectoralis Major Muscle. Outcome After Repair of Acute and Chronic Injuries. The American Journal of Sports Medicine 28(1): 9-15.

Schwartz, C., Tubez, F., Wang, F.C., Croisier, J.L., Brüls, O., Denoël, V., Forthomme, B. (2017). Normalizing Shoulder EMG: An Optimal Set of Maximum Isometric Voluntary Contraction Tests Considering Reproducibility. *Journal of Electromyography and Kinesiology*, 37: 1-8.

Seth, A., Dong, M., Matias, R., Delp, S. (2019). Muscle Contributions to Upper-Extremity Movement and Work From a Musculoskeletal Model of the Human Shoulder. *Frontiers in Neurorobotics*, 13: 1-9.

Shamley, D.R., Srinaaganathan, R., Weatherall, R., Oskrochi, R., Watson, M., Ostlere, S. et al. (2007). Changes in shoulder muscle size and activity following treatment for breast cancer. *Breast Cancer Res Treat,* 106*:* 19-27.

Shamley, D., Lascurain-Aguirrebena, I., Oskrochi, R., Srinaganathan, R. (2012). Shoulder morbidity after treatment for breast cancer is bilateral and greater after mastectomy. *Acta Oncologica,* 51(8): 1045-1053.

Sherrington, C. (1925). Remarks on some aspects of reflex inhibition. *Proc R Soc Lond B Biol Sci*: 19-45.

Srinivasan, R.C., Lungren, M.P., Langenderfer, J.E., Hughes, R.E. (2007). Fiber Type Composition and Maximum Shortening Velocity of Muscles Crossing the Human Shoulder. *Clinical Anatomy*, 20: 144-149.

Staudenmann, D., Kingma, I., Daffertshofer, A., Stegeman, D.F., van Dieen, J.H. (2009). Heterogeneity of muscle activation in relation to force direction: A multi-channel surface electromyography study on the triceps surae muscle. *Journal of Electormyography and Kinesiology*, 19(5): 882:895.

Staudenmann, D., Roeleveld, K., Stegeman, D.F., van Dieen, J.H. (2010). Methodological aspects of SEMG recordings for force estimation – A tutorial and review. *Journal of Electromyography and Kinesiology*, 20(3): 375-387.

Stegink-Jansen, C.W., Buford, W.L., Patterson, R.M., Gould, L.J. (2011). Computer Simulation of Pectoralis Major Muscle Strain to Guide Exercise Protocols for Patients After Breast Cancer Surgery. *J Orthop Sports Phys Ther*, 41(6): 417-426.

Steinmann, S.P., Wood, M.B. (2003). Pectoralis major transfer for serratus anterior paralysis. *Journal of shoulder and elbow surgery*, 12(6): 555-560.

Stout, N.L., Binkley, J.M., Schmitz, K.H., Andrews, K., Hayes, S.C., Campbell, K.L., McNeely, M.L. et al. (2012). A Prospective Suverillance Model for Rehabilitation for Women With Breast Cancer. *Cancer*, 118: 2191-2200.

Takai, Y., Katsumata, Y., Kawakami, Y., Kanehisa, H., Fukunaga, T. (2011). Ultrasound method for estimating the cross-sectional area of the psoas major muscle. *Med Sci Sports Exerc.*, 43(10): 2000-2004.

Thompson, C.K., Negro, F., Johnson, M.D., Holmes, M.R., McPherson, L.M., Powers, R.K., Farina, D., Heckman, C.J. (2018). Robust and accurate decoding of motoneuron behavior and prediction of the resulting force output. *Journal of Physiology*, 596(14): 2643-2659.

Tobin, G.R. (1985). Pectoralis major segmental anatomy and segmentally split pectoralis major flaps. *Plast Reconstr Surg*, 75: 814-824.

Vandeweyer, E., Hertens, D. (2002). Quantification of Glands and Fat in Breast Tissue: An Experimental Determination. *Annals of Anatomy*, 184(2): 181-184.

Vidt, M.E., Potochny, J., Dodge, D., Green, M., Sturgeon, K., Kass, R., Schmitz, K.H. (2020). The influence of mastectomy and reconstruction on residual upper limb function in breast cancer survivors. *Breast Cancer Research and Treatment*, https://doi.org/10.1007/s10549-020-05717-z

Vila-Cha, C., Falla, D., Farina, D. (2010). Motor unit behaviour during submaximal contractions following six weeks of either endurance or strength training. *Journal of Applied Physiology*, 109: 1455-1466.

von Tscharner, V., Nigg, B.M. (2008). Point: Spectral properties of the surface EMG can characterize motor unit recruitment strategies and muscle fiber type. *Journal of Applied Physiology.*

Warden, J.M., Roberts, S.L., Chang, Y., Baker, R., Boulias, C., Ismail, F., Agur, A.M. (2014). Neuromuscular Partitioning of Subscapularis Based on Intramuscular Nerve Distribution Patterns: Implications for Botulum Toxin Injections. *Archives of Physical Medicine and Rehabilitation, 95(7):* 1408-1415.

Watanabe, K., Kouzaki, M., Moritani, T. (2011). Task-dependent spatial distribution of neural activation pattern in human rectus femoris muscle. *Journal of Electromyography and Kinesiology*, 22(2): 251-258.

Westgaard. R.H., De Luca, C.J. (2001). Motor Control of Low-Threshold Motor Units in the Human Trapezius Muscle. *Journal of Neurophysiology*, 85(4): 1777-1781.

Wickham, J.B., Brown, J.M.M. (1998). Muscles within muscles: the neuromotor control of intra-muscular segments. *European Journal of Applied Physiology and Occupational Physiology*, 78: 219-225.

Wickham, J.B., Brown, J.M.M., McAndrew, D.J.(2004). Muscles within muscles: Anatomical and functional segmentation of selected shoulder joint musculature. *Journal of Musculoskeletal Research*, 8(1): 57-73.

Wickham, J.B., Brown, J.M. (2012). The function of neuromuscular compartments in human shoulder muscles. *Journal of Neurophysiology*, 107(1): 336-45.

Wickiewiz, T.L., Roy, R.R., Powell, P.L., Edgerton, V.R. (1983). Muscle architecture of the human lower limb. *Clinical Orthopaedics*, 179: 275-283.

Wilson, J.M., Thompson, C.K., Miller, L.C. Heckman, C.J. (2015). Intrinsic excitability of human motoneurons in biceps brachii versus triceps brachii. *Journal of Neuroscience*, 113(10): 3692-3699.

Wolfe, S.W., Wickiewicz, T.L., Cavanaugh, J.T. (1992). Rupture of the pectoralis major muscle. An anatomic and clinical analysis. *Am J Sports Med,* 20: 587-593.

Yasuda, T., Fujita, S., Ogasawara, R., Sato, Y., Abe, T. (2010). Effects of low-intensity bench press training with restricted arm muscle blood flow on chest muscle hypertrophy: a pilot study. *Clinical Physiology and Functional Imaging,* 30(5): 338-343.

Yi, T., Han, I.S., Kim, J.S., Jin, J.R., Han, J.S. (2012). Reliability of supraspinatus muscle thickness measurement by ultrasonography. *Ann Rehabil Med,* 36(4): 488-95.

Yu, J., Ackland, D.C., Pandy, M.G. (2011). Shoulder muscle function depends on elbow joint position: An illustration of dynamic coupling in the upper limb. *Journal of Biomechanics*, 44: 1859-1868.

Zajac, F.E. (1989). Muscle and tendon: properties, models, scaling, and application to biomechanics and motor control. *Crit Rev Biomed Eng*: 359–411.

Appendix: Supplementary Information

Supplementary Table 1: Description of EMG electrode placement for each shoulder muscle monitored in the background alongside a pectoralis major.

Muscle	**Electrode Placement**
Anterior Deltoid	3.5 cm below the anterior angle of the acromion, parallel to muscle fibers
Middle Deltoid	Lateral aspect of the upper arm, and approximately 3 cm below the acromion, parallel to the muscle fibers
Posterior Deltoid	2 cm below the posterior lateral surface of the acromion, parallel to muscle fibers
Infraspinatus	4 cm below, and parallel to the spine of the scapula, on the lateral aspect of the infrascapular fossa
Upper Trapezius	Along the ridge of the shoulder, slightly lateral to one half the distance between C7 and the acromion
Latissimus Dorsi	Approximately 4 cm below the inferior angle of the scapula, half the distance between the spine and the lateral edge of the torso, oriented in a slightly oblique angle of approximately 25 degrees

Supplementary Table 2: Mean normalized sEMG amplitude ± standard deviation across tasks and effort levels for infraspinatus, latissimus dorsi, upper trapezius, anterior, middle, and posterior deltoid. (1) denotes the first rank in terms of highest EMG activation.

Task	Effort Level	Infraspinatus (%MVE)	Latissimus Dorsi (%MVE)	Upper Trapezius (%MVE)	Anterior Deltoid (%MVE)	Middle Deltoid (%MVE)	Posterior Deltoid (%MVE)
Adduction 60	15%	11.2 ± 6.7	15.2 ± 8.9	16.2 ± 8.6(1)	10.5 ± 8.7	17.3 ± 8.5(1)	16.9 ± 6.7(1)
	25%	17.3 ± 10.6	26 ± 9.5(1)	16.3 ± 8.1	17.3 ± 13.6	27 ± 13(1)	25.6 ± 7.5(1)
	50%	30.5 ± 15.1	54.6 ± 18.5(1)	28 ± 17.3	33.5 ± 16.9	50.1 ± 15(1)	53.9 ± 13.1(1)
Adduction 90	15%	10.5 ± 3.8	10.2 ± 5.5	22.6 ± 9.4(1)	11.4 ± 9.3	15.4 ± 8.2	10.8 ± 6.4
	25%	12.6 ± 5	14.6 ± 7.2	18.7 ± 7.3(1)	15.1 ± 8.5	17.3 ± 8.7	13.1 ± 5.5
	50%	23 ± 8.5	34.4 ± 12.4(1)	29.2 ± 8.2	35.9 ± 14.9(1)	34.6 ± 16.4(1)	26.4 ± 8.1
Adduction External 90	15%	18.3 ± 5.7	15 ± 7.2	21.5 ± 6.9(1)	9.7 ± 6.1	12.1 ± 6.5	13.5 ± 7
	25%	22.6 ± 6.5(1)	20 ± 7.8	22.4 ± 5.5(1)	14.5 ± 6.8	17 ± 9.6	18.6 ± 8
	50%	42.4 ± 11.8(1)	42.4 ± 17.5(1)	36.8 ± 10.4	34.6 ± 16.9	38.7 ± 17.6	39.8 ± 13.8
Internal Rotation	15%	6.1 ± 3.3	10.5 ± 7.1	15.2 ± 12(1)	9.1 ± 6.8	11.4 ± 4.7	11 ± 4.5
	25%	9.9 ± 5.8	18.2 ± 8.4(1)	15.9 ± 9.7	13.3 ± 7.6	16.3 ± 6.6	16.9 ± 5.8
	50%	21.6 ± 14	37.5 ± 13.4(1)	26.5 ± 18.4	28.6 ± 15.7	33.2 ± 12.5(1)	32 ± 10.7(1)

Supplementary Table 3: Mean normalized sEMG amplitude ± standard deviation across tasks and effort levels for infraspinatus, latissimus dorsi, upper trapezius, anterior, middle, and posterior deltoid. (1) denotes the first rank in terms of highest EMG activation.

Task	Effort Level	Infraspinatus (%MVE)	Latissimus Dorsi (%MVE)	Upper Trapezius (%MVE)	Anterior Deltoid (%MVE)	Middle Deltoid (%MVE)	Posterior Deltoid (%MVE)
Flexion	15%	18.9 ± 10.4**(1)**	4.8 ± 2.5	17.4 ± 13.2**(1)**	19.9 ± 3.5**(1)**	19 ± 9**(1)**	4.6 ± 2
	25%	29.6 ± 18.5**(1)**	7.5 ± 4.4	22.7 ± 11.3	29.5 ± 6.1**(1)**	28.4 ± 13.8**(1)**	8.7 ± 5.6
	50%	47.3 ± 18.5**(1)**	11.3 ± 5.8	44.1 ± 15.3	56.8 ± 13.9**(1)**	50.5 ± 11.3**(1)**	13.6 ± 6.1
	75%	66.8 ± 20.7**(1)**	16.9 ± 9.1	64.2 ± 23**(1)**	77.8 ± 15.6**(1)**	71.8 ± 16.3**(1)**	23.1 ± 9.3
Horizontal Adduction	15%	25.5 ± 12.3**(1)**	20.5 ± 7.6	25.3 ± 11.5**(1)**	19.4 ± 9.2	28.1 ± 14.2**(1)**	23.7 ± 10.6
	25%	26.9 ± 13.5	24.9 ± 9.9	28.6 ± 17.1**(1)**	23 ± 13.5	30.1 ± 19.3**(1)**	28.6 ± 12.2**(1)**
	50%	36.4 ± 19	40.3 ± 16.2**(1)**	48 ± 22.3**(1)**	40.7 ± 14.7(1)	35.8 ± 19.2	39.7 ± 15.3
	75%	42.1 ± 16.8	53.6 ± 12.9	61.6 ± 24**(1)**	55.5 ± 18.5	41.8 ± 21.4	54.2 ± 21
Extension	25%	12.6 ± 4.8	20.9 ± 13.4**(1)**	12.3 ± 8	1.3 ± 0.8	5.7 ± 3.7	20.8 ± 11.9**(1)**
	50%	29.9 ± 12	44.7 ± 17.2**(1)**	24.2 ± 17.2	4 ± 3.1	15.6 ± 6.8	46.5 ± 13.6**(1)**
	75%	44.2 ± 9.3	71.6 ± 19.5**(1)**	40.6 ± 26.6	6.2 ± 2.9	30.2 ± 13.1	78.4 ± 27.3**(1)**
Internal Rotation	25%	23.4 ± 9.2	24.4 ± 8.6	21.1 ± 11.2	23.2 ± 8.1	24.6 ± 23.1	23.3 ± 18
	50%	54.3 ± 23.8**(1)**	45.3 ± 12.2	40.8 ± 22.7	50.2 ± 22.4	37.4 ± 25.6	40.2 ± 19.9
	75%	59.4 ± 32.1	72.7 ± 14.8**(1)**	61.2 ± 24	66.5 ± 19.1	44 ± 21.4	51.1 ± 11.4

Supplementary Table 4: Mean normalized sEMG amplitude ± standard deviation across tasks and effort levels for infraspinatus, latissimus dorsi, upper trapezius, anterior, middle, and posterior deltoid. (1) denotes the first rank in terms of highest EMG activation.

Task	Effort Level	Infraspinatus (%MVE)	Latissimus Dorsi (%MVE)	Upper Trapezius (%MVE)	Anterior Deltoid (%MVE)	Middle Deltoid (%MVE)	Posterior Deltoid (%MVE)
Adduction 60	15%	10.3 ± 6.6	14.2 ± 9.4(1)	12.7 ± 9	8.4 ± 11.6	15.7 ± 6.9 (1)	12.9 ± 4.6
	25%	12.4 ± 6.6	22.1 ± 15.2(1)	13.8 ± 8.9	10.9 ± 9.4	22.8 ± 44(1)	20.3 ± 9.6
	50%	25.7 ± 12	40.7 ± 21.5(1)	28.1 ± 16.8	25.1 ± 14.7	46.2 ± 18.9(1)	42.5 ± 17.7
	75%	50.2 ± 16	62.9 ± 21.9(1)	51 ± 19.9	41.9 ± 18	69.4 ± 23.3(1)	69.3 ± 22.1(1)
Adduction 90	15%	6.8 ± 2.5	10.1 ± 6.9	19.1 ± 15.6(1)	10.2 ± 7.7	11.2 ± 6.1	5.8 ± 5.8
	25%	7.6 ± 3.4	14.2 ± 9(1)	14.2 ± 6.8(1)	15 ± 9.2(1)	15 ± 7.9(1)	6.6 ± 5.1
	50%	16.1 ± 7.1	40.8 ± 25.7(1)	28 ± 16	42.8 ± 27.5(1)	33.6 ± 20.1	16.1 ± 11.8
	75%	28.9 ± 12.2	52.5 ± 24.7(1)	42.4 ± 21	53.7 ± 19(1)	48.3 ± 28.7	32.1 ± 20.5
Adduction External 90	15%	17.4 ± 11.7(1)	10.5 ± 4.7	21.3 ± 14.2(1)	9.3 ± 7.8	11.2 ± 7.7	10.4 ± 6
	25%	23.3 ± 13.3(1)	16.4 ± 6	21.6 ± 9.7(1)	15 ± 11.4	13.7 ± 6.6	15.8 ± 14
	50%	43 ± 15.2	43.2 ± 16.2	38.3 ± 17.2	42.1 ± 24.9	41 ± 25.6	32.9 ± 19.8
	75%	66.8 ± 18.2	74.9 ± 18.4	55.8 ± 19.2	58.2 ± 27.9	55.3 ± 27.6	58.8 ± 24.1
Internal Rotation	15%	4.2 ± 2.9	15.8 ± 8.5(1)	12.8 ± 9.8(1)	4.8 ± 3.4	10.1 ± 4.5	9.5 ± 4.2
	25%	6 ± 4	23.1 ± 11.6(1)	13.5 ± 9.2	8.7 ± 8.4	15.3 ± 8.6	13.8 ± 6.2
	50%	13.3 ± 8.1	46.5 ± 17.7(1)	25.5 ± 17.7	19.9 ± 17.7	33.9 ± 19.3	31.2 ± 14.8
	75%	24.6 ± 18.2	70.1 ± 25.2(1)	43.7 ± 28.3	29.1 ± 23.2	50.1 ± 25.5	51.8 ± 27.3

Supplementary Table 5: Mean normalized sEMG amplitude ± standard deviation across tasks and effort levels for infraspinatus, latissimus dorsi, upper trapezius, anterior, middle, and posterior deltoid. (1) denotes the first rank in terms of highest EMG activation.

Task	Effort Level	Infraspinatus (%MVE)	Latissimus Dorsi (%MVE)	Upper Trapezius (%MVE)	Anterior Deltoid (%MVE)	Middle Deltoid (%MVE)	Posterior Deltoid (%MVE)
Flexion	15%	10.8 ± 7.4	3.7 ± 5.3	21.1 ± 13**(1)**	16.1 ± 9.5	12.4 ± 6.5	1.9 ± 2.2
	25%	16.9 ± 10.1	4.6 ± 6.1	21.4 ± 13.1**(1)**	20.5 ± 11.1**(1)**	18 ± 9.4	2.2 ± 1.9
	50%	34.6 ± 16.9**(1)**	8.7 ± 11	43 ± 21	39.6 ± 19.8**(1)**	39.8 ± 21.4**(1)**	4.5 ± 3.4
Horizontal Adduction	15%	22.5 ± 13.4**(1)**	15.4 ± 13.2	14 ± 13.8	14 ± 14.7	16.9 ± 14.5	16.6 ± 8.9
	25%	21.4 ± 16.8**(1)**	19.8 ± 10.3	17 ± 24.7	22.1 ± 26.2**(1)**	21.2 ± 19.9**(1)**	19.4 ± 8.1
	50%	25.5 ± 15.9	46.8 ± 28.9**(1)**	24.7 ± 15	38.3 ± 21.4**(1)**	27.8 ± 17.4	31.7 ± 17
Internal Rotation	25%	22.6 ± 10.7**(1)**	24.4 ± 15**(1)**	18.2 ± 12.4	15.6 ± 5.7	18.4 ± 7.7	17.9 ± 11.9
	50%	47 ± 21.6**(1)**	46.5 ± 24.9**(1)**	27.7 ± 25.5	32.6 ± 14.9	36.8 ± 18.6	40.3 ± 28
Extension	50%	18.5 ± 5.7	41.1 ± 18.3**(1)**	22.1 ± 16.3	2 ± 1	13.5 ± 8.2	34.8 ± 15.7

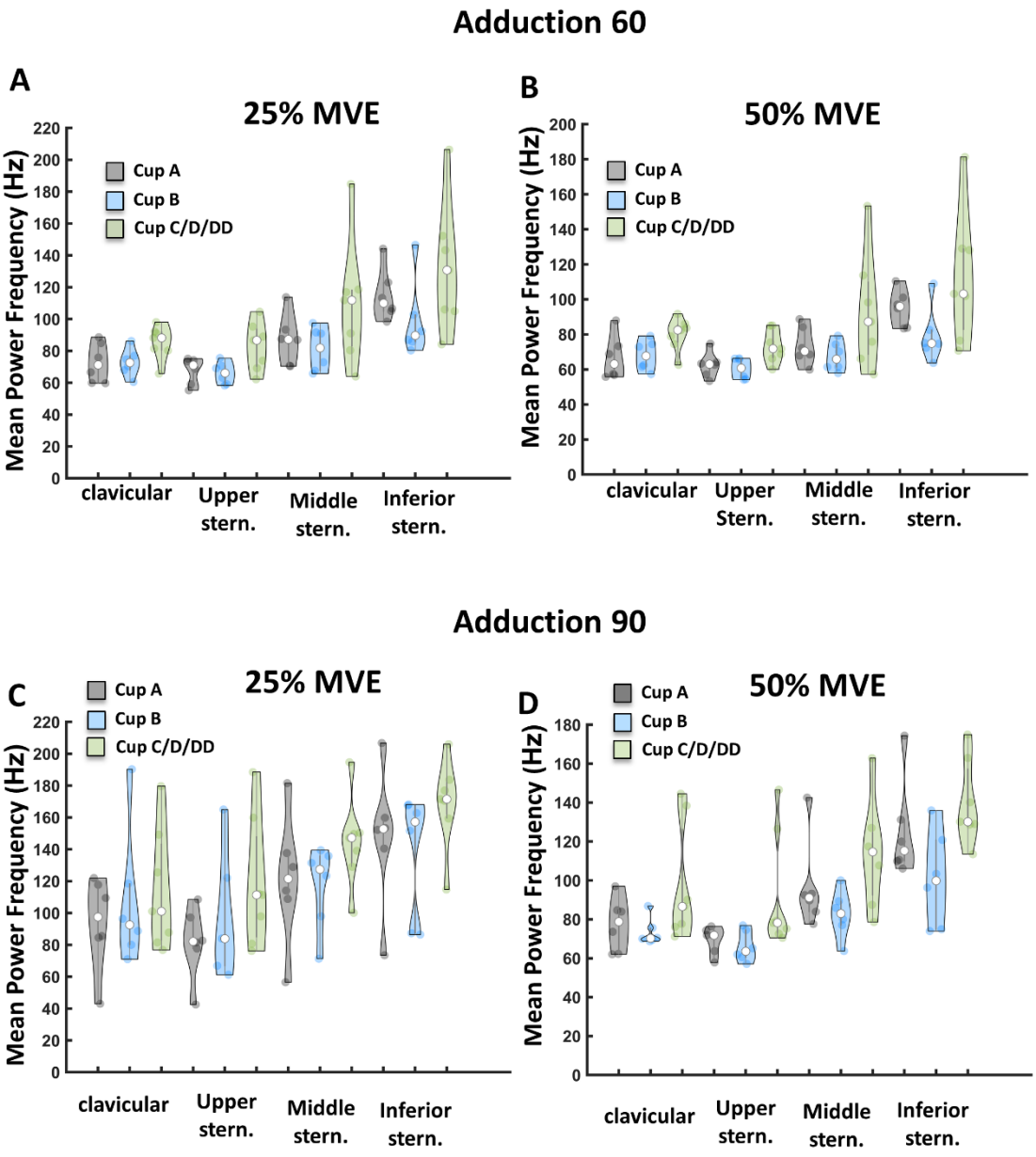

Supplementary Figure 1: Violin plots of mean power frequency in each task and effort level across groups and regions. Note the increase in mean power frequency for the inferior array, as well as in Cup C/D/DD.

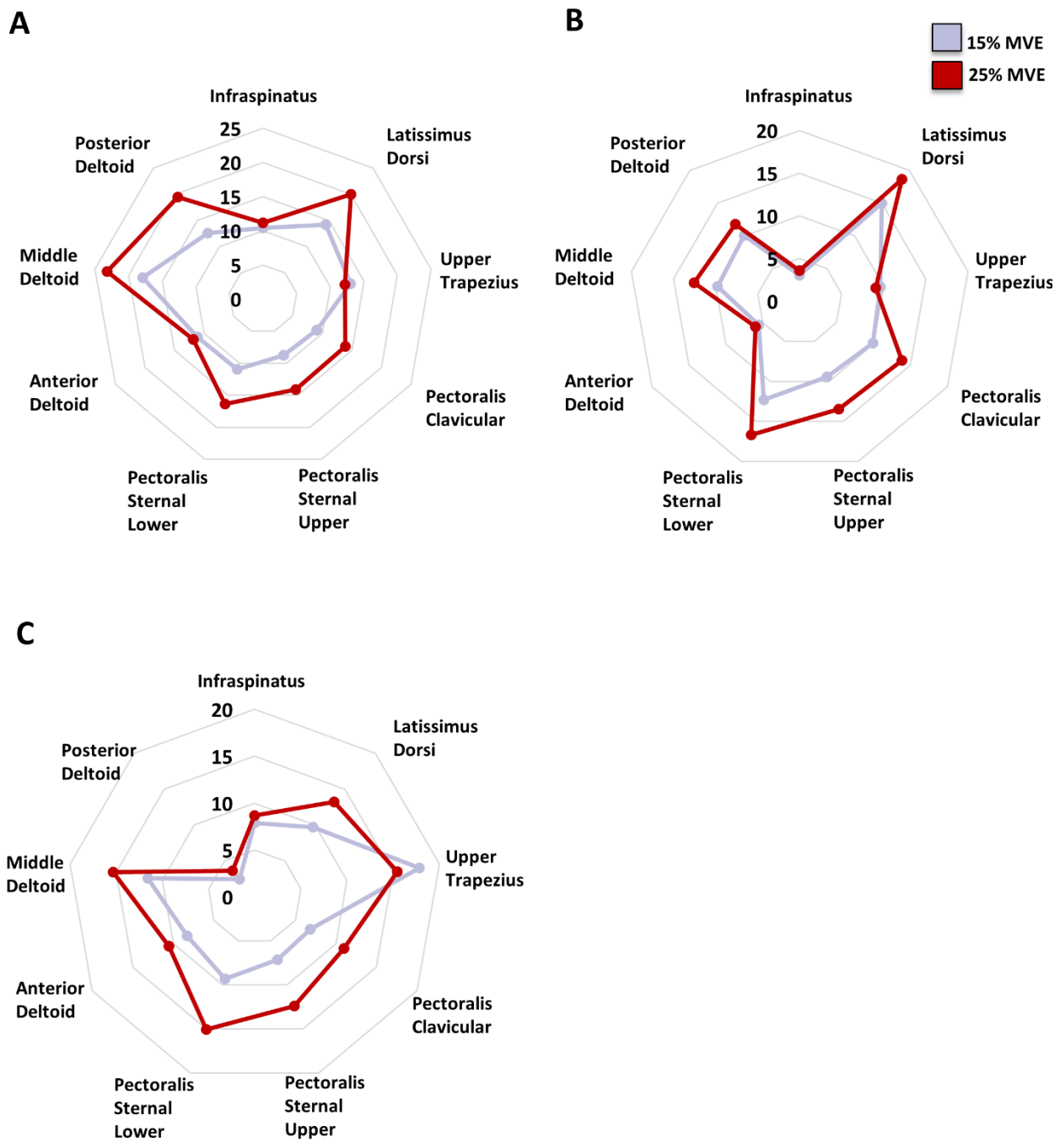

Supplementary Figure 2: Representative polar plots of muscle activity distribution across shoulder muscles in adduction 60, internal rotation, and adduction 90 in males. **A:** Muscle activity distribution in adduction 60°, showing high activation of middle deltoid and latissimus dorsi. **B:** Muscle activity distribution in internal rotation, showing high activity in latissimus dorsi. **C:** Muscle activity distribution in adduction 90°, showing high activity in the upper trapezius and middle deltoid.

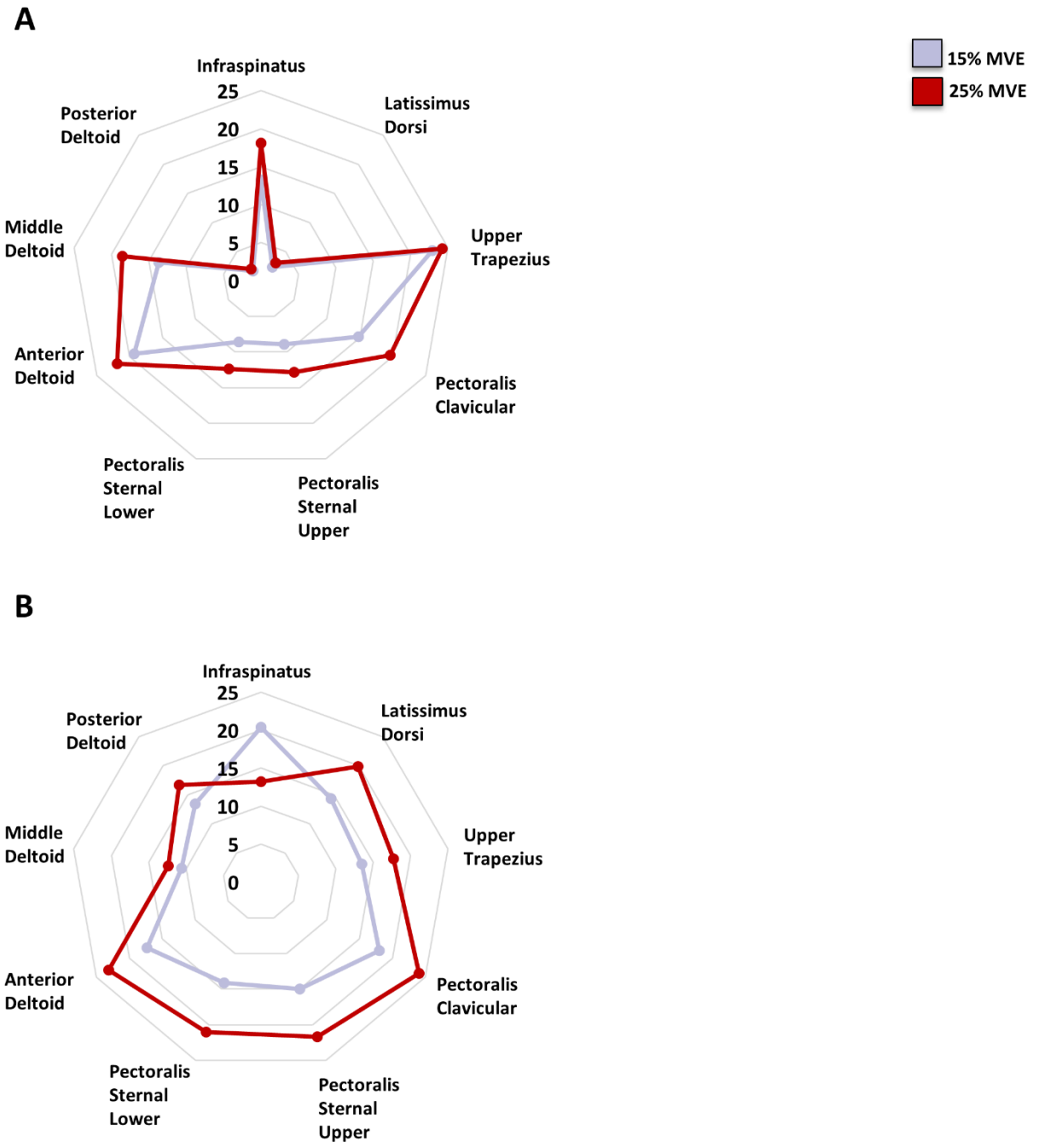

Supplementary Figure 3: Representative polar plots of muscle activity distribution across shoulder muscles in flexion and horizontal adduction in males. **A:** Muscle activity distribution in flexion, showing high activation of the anterior deltoid and upper trapezius. **B:** Muscle activity distribution in horizontal adduction, showing high activity in anterior deltoid and pectoralis major.